UNIVERSITÀ DEGLI STUDI DI MILANO
FACOLTÀ DI SCIENZE MATEMATICHE FISICHE E NATURALI
DOTTORATO DI RICERCA IN
FISICA, ASTROFISICA E FISICA APPLICATA

Investigation of morphological and structural properties of ionic liquid thin layers on solid surfaces by Scanning Probe Microscopy

Settore Scientifico disciplinare FIS/03

Coordinatore: Prof. Marco Bersanelli
Tutore: Dott. Alessandro Podestà
Cotutore: Prof. Pietro Ballone

Tesi di Dottorato di:
Simone Bovio
Ciclo XXIV

Anno Accademico 2010-2011

Extended abstract

Molten salts attracted the attention of the scientific community several times during the last century. This interest is motivated by the physico–chemical properties of these systems. In fact, usually molten salts show chemical and thermal stability, i.e. they do not easily decompose or react. Furthermore, these compounds remain liquid over an extended range of temperatures, in which they show also a remarkably low volatility. The fact that molten salts are composed solely by ions, and can have a quite wide electrochemical window, make them very interesting as electrolytes[15].

The main disadvantage in the usage of molten salts in any practical process, is their high melting point (for example as high as 800°C for NaCl), which severely limits the number of reactions that can be done in these media and reduces the possibility of industrial scaling, due to the high energy required to maintain those high temperatures. Since the '70s lower temperature molten salts has been synthesised, like chloroaluminate eutectic mixtures, having melting points around 100°C or even lower, but the real turning point that boosted the research field has been the development of the first water–stable low melting point molten salts, that is what are now usually named room temperature ionic liquids, or simply ionic liquids.

Ionic liquids are usually composed by a big organic cation and a bulky inorganic, water stable, anion: the bulkiness and the complex asymmetric structure of the ions prevent an efficient packaging, leading to a lowering of the coulombic cohesive energy and so of the melting point.

Ionic liquids maintain all the characteristics of the high temperature molten salts, but they are usually liquid at room temperature. This fact induced a renewed interest in the field, as is proved by the several thousand papers published on the topic in 2011.

The community of chemists devoted a great effort to the study of ionic liquids, because of the potential use of those liquids as solvents. Ionic liquids are complex systems, that usually are organised in polar and apolar domains, and can dissolve both polar and apolar species. In addition, there are virtually unlimited choices of ions, and each choice changes the physico–

chemical characteristics of the systems: this allows to tailor the properties of the ionic liquids (like miscibility, density, viscosity...), in order to match specific tasks. The characteristics of ionic liquids, last but not least their low vapour pressure, promote them as good solvents for the growing field of the Green Chemistry, in substitution of the volatile organic compounds.

Ionic liquids are also promising as lubricants, in particular in micro– and nano– –electromechanical devices (NEMSs and NEMSs)[39, 40] as well as electrolytes in photoelectrochemical devices used for energy storage and energy production such as supercapacitors[60, 50] or Grätzel solar cells[51].

In all these cases, the most relevant processes determining the performance of the devices, take place at the liquid/solid interface between ILs and solid surfaces: this is a region only a few nanometers thick where the properties of ILs can be significantly different from those of the bulk. The investigation of the interfacial properties of ILs is therefore of primary importance for their technological exploitation. To date, the (bulk)liquid–vapour and solid–(bulk)liquid ILs interfaces have been studied, mostly by sum–frequency generation spectroscopy[65, 68] and by X–ray photoemission spectroscopy[69]. For imidazolium–based ILs, ordering of the ions at the solid/liquid or liquid/vapour interface has been inferred from vibrational spectroscopy data. For example Mezger et al.[70] performed a study of the (bulk)liquid/solid interface between a negatively charged sapphire substrate and imidazolium and pyrrolidinium–based ILs. They found strong interfacial layering, with repeated spacing of 0.7–0.8 nm, decaying exponentially into the bulk liquid. Recently the ionic liquid/solid interface has been studied with the surface force apparatus (SFA)[94, 95, 96]. In those experiments thin layers of ionic liquids are compressed between two approaching sheets of mica, while the normal force is recorded. The force vs. distance curves show a characteristic oscillatory profile, extending for few nanometers from the interface and exponentially decaying into the bulk.

Only very recently, in order to explore in details the ionic liquid/solid interfaces, more local approaches has been used, i.e. scanning probe microscopies and numerical simulations. Layering at the solid/(bulk)liquid have been found by Atkin[77, 76] performing force spectroscopy with atomic force microscope (AFM). In these kind of measurements, in which the AFM tip is ramped against the interface while measuring the force acting on it, as in SFA experiments, subsequent ruptures of solvation layers are seen, beginning few nanometers above the surface. The group of Atkin, in collaboration with other groups, performed also scanning tunneling microscopy (STM)/ AFM study on ionic liquid/Au(111) interface, finding a dependence of the behaviour of the solvation layers upon potential changes[78].

In simulation studies is again evidenced the formation of strong interfa-

cial layering on different surfaces[100, 101], where moreover, the preferential orientation of the ions at the interface can be analysed.

The studies previously cited about the interfacial behaviour of the ionic liquids, are mainly focused to the analysis of the bulk ionic liquid/solid interface. To date, a little effort has been devoted to what happens when thin layers of an ionic liquid are put in contact with a solid substrate. In those kind of situations, where the surface/volume ratio is high, it can been argued that the interaction with the surface can greatly change the physico–chemical and structural properties of the ionic liquid. The study of systems with high surface/volume ratio is directly relevant in all those applications in which a thin film of ionic liquid is used, e.g. in tribological applications, as well as in photoelectrochemical devices, where the liquid is soaked into a nanoporous matrix: a change of the properties of the ionic liquid in this case can heavily modify the final performance of the devices.

My PhD work has been devoted to improving further extend the understanding of the behaviour of thin films of ionic liquids in contact with solid surfaces. At the time when I begun my work, very few studies regarding such systems were published. A pioneering study on thin film of [Bmim][PF_6] on mica has been published in 2006 by Liu et al.[79]. In this work, performed using an AFM, the ionic liquid has been found to structure in two different ways on substrate: as droplets and as flat layers, qualitatively referred to as solid layers. Inspired by the approach of Liu, I decided to study more quantitatively the thin–layer/solid interface, in particular using atomic force microscopy, because this instrument can acquire morphologies with vertical sub–nanometer and lateral nanometric resolution, so giving access to very localised information. Furthermore other kind of maps regarding different physico–chemical properties can be acquired simultaneously to the topography and moreover, force spectroscopy studies can be performed ramping the AFM tip against the surface.

In particular I focused my investigation on the interaction of [Bmim][Tf_2N], a hydrophobic and almost water–stable liquid, with different substrates, i.e. mica, amorphous silica, single crystal silicon covered by its native oxide, and HOPG graphite. The main part of the work has been performed on those test substrates, because their properties are well known and because they are flat, so very suitable for an accurate AFM investigation. With the experience gained on those systems and the results obtained, on the last part of my PhD, the attention has been moved to surfaces more relevant for applications, as the nanostructured silicon oxide, directly synthesised in our lab with supersonic cluster beam deposition (SCBD).

In order to perform my investigation, I first obtained very thin ionic

liquid layers on the surface, diluting the liquid into a solvent, (methanol, ethanol, chloroform), and then drop–casting few μl of the solution onto a freshly cleaned substrate, letting the evaporation to proceed in air. On all the insulating surfaces studied, the [Bmim][Tf_2N] coexists in 2 forms: as liquid micro- and nano- -droplets and in flat ordered domains. The melting temperature of this particular ionic liquid is $\sim$-4°C, so a fundamental role in the liquid to solid transition has to be played by the interaction with the solid surface. The solid–like terraces appear as flat layers, often growing one on top of the other. The hypothesis is that each layer is composed by several layers of cations and anions. By a statistical analysis of the morphological maps acquired, I extrapolated that the height of the best sub–multiple of the solid–like terraces is δ=0.6nm, in good agreement with the result of the simulations.

The AFM has also been used to study the mechanical behaviour of the solid–like structures. If imaged in contact mode, the layers tend to be eroded after repeated scans, and in some cases the terraces are removed one by one, as in a lamellar solid. Investigating the resistance to normal loads, saw tooth profiles in force vs. separation curves have been found, highlighting a sequence of ruptures, separated by 1.8–2nm, where the average rupture pressure is $\sim$2–3KBar, very similar to the maximum pressure found in a MD simulation of a tip penetrating in 4nm of [Bmim][Tf_2N] on silica[99]. Moreover, the observation that supported IL islands were not disrupted by intense electric fields up to 10^8-10^9V/m (applied biasing the AFM with respect to sample during imaging) and that Scanning Nanoscale Impedance Microscopy[14] measurements highlighted a dielectric insulating character of the ordered domains (ε_r = 3–5 was measured[83]) is consistent with the idea that IL ordered domains behave as solid materials in which the ions are tightly bound.

To understand what is the influence of the nanostructure on the formation of the solid–like layers, I realised [Bmim][Tf_2N] depositions on nanostructured silica deposited on oxidised silicon by SCBD in our lab. Of particular interest is the case of IL coating on a sub–monolayer deposition of silica nanoparticles. The preliminary results show that the presence of a dense distribution of nanoparticles on the surface of oxidised silicon actually doesn't prevent the growth of multilayered solid–like domains, that are as thick as on flat surfaces and densely distributed. The liquid part of the deposition is pinned to the silica clusters, fact that evidences the strong affinity of [Bmim][Tf_2N] with silica. The results suggest that the formation of immobilised, possibly solid–like, layers of ionic liquids in contact with nanoporous matrices, is not unlikely and such structures and can strongly affect the properties of the devices in which those interfaces are present. This possibility is also supported by the

fact that a small percentage of silica nanoparticles (5 wt%) is enough to induce the gelation in an IL–based electrolyte used for dye sensitised solar cells[52].

The findings of my PhD work highlight the potentialities of scanning probe techniques for the quantitative investigation of the interfacial properties of thin ionic liquid films. My AFM investigation highlights how heterogeneous can be the IL/solid interfaces and so how is of fundamental importance to deal with local and not with average properties. The results of my work show that the behaviour of thin layers of ionic liquid is greatly modified by the influence of the substrate. In particular, I found a coexistence of liquid domains and terraces with elevated structural order. The formation of those structures, not present in the bulk liquid, is clearly induced by the contact with the solid surface. The solid–like terraces are very resistant to normal loads and to intense electric fields and, differently from the bulk, they tend to behave as insulating layers: the development of those structures can then have a crucial influence in the performances of photoelectrochemical devices.

The importance of this field of research and the validity of my work, are witnessed by the increasing number of papers studying thin ionic liquid layers appeared just before, but especially during the course of my PhD[71, 72, 84, 80, 85, 76, 78]; in many of these works, the AFM is the instrument of choice for the interfacial investigation because it allows to access to the physico–chemical properties of the system with nanometric or sub–nanometric resolution in all the three dimensions.

In the next future the structural behaviour of the ionic liquids in contact with nanostructured surfaces will be further studied, making use of the experience of our group in synthesise the nanostructured oxides and metals. Moreover, we will explore in more details the dielectric properties of thin film of ionic liquids, in particular selecting those ILs directly used in supercapacitors and solar cells. Another interesting field that to date is still poorly explored is the interaction of ionic liquids with biological tissue. For this reason, we are going to begin to study the effects of ionic liquids on supported lipid bilayers.

Contents

Chapter 1

Ionic liquids

In this chapter I'm going to briefly describe the compounds called ionic liquids and their applications. I will begin with a short history and a view on the properties of ionic liquids. Then I will speak about their field application, focusing in particular on the areas where the ionic liquids are in contact with solid surfaces.

In the end of the chapter I will describe the principal techniques used to investigate the physico–chemical and structural properties of ionic–liquid/ solid interfaces.

1.1 Brief history of ionic liquids

Molten salts attracted the attention of the scientific community several times during the last century. This interest is motivated by the physico–chemical properties of these systems. In fact, usually molten salts show chemical and thermal stability, i.e. they do not easily decompose or react. Furthermore, these compounds remain liquid over an extended range of temperatures, in which they show also a remarkably low volatility. For example, ethanol, one of the most used solvents, has a liquidus range of about 200°C, while the range of sodium chloride overcomes 650°. Moreover molten salts are composed solely by ions, and they can have a quite wide electrochemical window, so they can be useful as electrolytes.

There are some processes that cannot be performed in conventional solvents or in water. For example, the Hall–Héroult process, for the production of aluminium from aluminium oxide, is performed in molten cryolite, (sodium hexafluoroaluminate), i.e. a molten salt, at ∼1000°C. The main disadvantage in the usage of molten salts is their high melting point, which severely limits the number of reactions that can be done in these media and reduces the

possibility of industrial scaling, due to the high energy required to maintain those high temperatures.

In the early sixties, the U.S. Air Force Academy begun a research program on low temperature molten salts, aimed at substituting the eutectic LiCl/KCl, whos melting point is 355°C, in thermal batteries, used as power supplies on rockets. Those batteries are active only when the electrolyte is liquid, so with LiCl/KCl electrolyte, over 355°C, inducing a series of problems for the material of the electrodes and for everything surrounding the device. Lower melting point salts have been found in chloroaluminate eutectic mixtures, having melting points around 100°C or lower. In the paper published in 1978 by Gale et al.[17], it is reported the characterisation of 1–butylpyridinium chloride/$AlCl_3$, a molten salt liquid at room temperature: this was one of the first compounds of the class of the now commonly known as room temperature ionic liquids[15]. Because the cation 1–butylpyridinium is easily reducible, it has been replaced by dialkylimidazolium. Wilkis et al. in the early eighties, synthesised and characterised many 1-alkyl-3-methylimidazolium chloride ([EMIM][Cl])/$AlCl_3$ mixtures, having melting points below room temperature[18]. Some of the ionic liquids synthesised by Wilkis had melting points below 0°C: never before had been obtained such low temperature molten salts.

The only problem with those ionic liquids, was their hygroscopic nature. Those compounds were extremely sensitive to water contamination, which decomposes the ions forming HCl, so limiting their range of application.

The real turning point in the field of ionic liquids, especially for their application as solvents and electrolytes, has been at the beginning of the 90s, when Zaworotko synthesised liquids with dialkylimidazolium cations, but more water–stable anions, like tetrafluoroborate, hexafluorophosphate, etc...

Since those early works, the number of available ionic liquids growth exponentially, together with the interest of the scientific community, as witnessed by the number of papers published on the field (see Figure1.1).

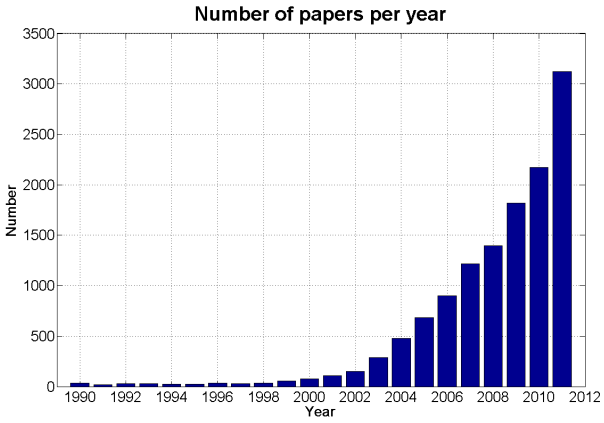

Figure 1.1: *Number of papers published on ionic liquids between 1990 and 2011. Font: Scirus. Research tips: Ionic liquids or ionic liquid*

1.2 Properties and applications of ionic liquids

As pointed out at the end of the previous section, what are now commonly know as room–temperature ionic liquids, or simply ionic liquids, are compounds usually composed by a large cation and a bulky inorganic, water–stable, anion: the bulkiness and the complex asymmetric structure of the ions prevent an efficient packaging, leading to a lowering of the coulombic cohesive energy and so of the melting point.

One of the major source of interest about ionic liquids, is their use as solvents. In ionic liquids can be performed processes of organic synthesis (see for example Chapter. 5 of the reference [16]), biocatalysis[23] biphasic extraction of metal ions and aggregates from waste water[27, 29], synthesis of metallic (or metallic alloys) nanoparticles[30, 31, 32] and metal electrodeposition[33]. A very interesting characteristics is also the ability of some ionic liquids to dissolve complex sugars like cellulose in [Bmim][Cl][26].

In the last twenty years a always greater effort has been devoted to the development of a less environmentally harmful chemistry, i.e. what is now called Green Chemistry[24]. The aim of Green Chemistry, (that is summarised in 12 points, see for example ref [24]), is to try to find more efficient processes of synthesis, especially at industrial scale, using as few as possible toxic solvents, or no solvents at all. To this regard, a useful tool providing a qualitative scale of the "goodness"of a process is the E factor, introduced by R. Sheldon[22], that is the amount of waste produced in the process [Kg] di-

vided by the amount of the desired product(s) produced in the process [Kg], where in the waste also the amount of energy spent in the whole process is considered.

In order to address the 12 principles of Green Chemistry, four main ways are under study:

- developing solvent–free synthesis[111];
- using water as solvent[112];
- using of supercritical fluids[110];
- using ionic liquids.

Ionic liquids are good candidates especially for the following reasons:

1. they are non volatile in the whole liquidus range;
2. their ions can be tailored ad–hoc for the specific application.

In fact the volatility of organic compounds is dangerous for the environment and is costly, because the solvent that evaporates cannot be reused any more. Furthermore sometimes the extraction of the products of a reaction is obtained by solvent evaporation, or by distillation, that wastes at least a 10% of the solvent itself.

The low vapour pressure of ionic liquids is due to their nature of ionic compounds. In these systems the coulombic interaction is limited by the size and structure of the ions, and differently respect to molten salts, it is not energetically favourable to evaporate ion couples. If the temperature is raised, the ions in an ionic liquid will generally decompose before undergoing to evaporation. Anyway it will be quite ingenuous to assert that ionic liquids are "green"just because they do not evaporate. In fact, in order to be considered green, the synthesis and also the disposal of that compound should be green too. In a study conducted by Deetlefs and Seddon[20], the environmental impact of the laboratory production of imidazolium–based ionic liquids is performed. In the study is evidenced the fact that in the synthesis as well as in the purification or decolourisation of the ILs, several volatile solvents can be used, and also that a quite high amount of energy is usually necessary. Furthermore, common ionic liquids are usually not designed to be biodegradable, so the study concludes with the statement that ionic liquids are green, (if compared to ordinary compounds used in synthesis), but not green enough. The replacement in industrial processes of volatile solvents

with ionic liquids needs to be careful and should be motivated and sustained by a proper life cycle assessment study (see for example the Ref. [21]).

One important aspect in favour of the greenness of ionic liquids is the second statement of the list above, i.e. the possibility of tailoring the properties of those compound by the ad–hoc synthesis of the ions. In fact, given the limited number of available organic solvents, some processes are not efficient at all, are just as much efficient as they can. The possibility of a targeted synthesis of an ionic liquid will then take care of this issue.

The number of possible ionic liquids available is huge, approximatively one trillion (10^{18})[19], but in order to design an ionic liquid that have some specific properties, it is necessary to know how those properties are modified by the modification of the ions. Unfortunately, not many properties of ionic liquids are so easy to predict, that is, it is difficult to find general rules telling scientists how a modification of an ion will influence the behaviour of the IL. An example is the melting point of the ionic liquids. In an ionic liquid the dominant force is the coulombic attraction between the ions. Increasing the size of an ion, in particular adding non–polar groups surrounding the charged site and increasing charge delocalisation will decrease the melting point. This is generally true, but looking for example at ionic liquids having [Emim] cation with different anions, shows that with a [Cl] anion a melting point the compound melts at 87°C, whereas with the bulkier [CB_11H_12] the melting point raises to 122°C (see Chapter. 3 of the reference [16]).

This tells that ions cannot be considered as isolated, because not only the coulombic interaction is present, but also Van Der Waals and hydrogen bonding are there.

Van Der Waals interaction becomes more important increasing the length of the alkyl chain of the cation. In fact, if the melting point of a series of ionic liquids with increasing number of carbons in the alkyl chain and with the same anion is monitored, it can be seen that this property has a minimum around 6–8 carbons and then increasing again. This phenomenon is induced by the chain–chain interaction that in some cases leads to liquid crystal phases[16, 19].

As previously stated, ionic liquids have hydrogen bonding ability: usually the cation is an hydrogen bonding donor, while the anion can be hydrogen bonding acceptor. In particular anions such as Cl are strong H–bond acceptors and this characteristic appeared fundamental for the dissolution of cellulose and for the interaction with biological materials[23, 26]. The influence of the degree of H–bonding ability on the physico–chemical properties of the ionic liquids is still not clear. An interesting and counterintuitive example is that reported by Fumino et al., where they found that suppressing the

H–bonding ability of the [C_2mim] cation in the ionic liquid [C_2mim][Tf_2N] by methylating the C(2) position on the ring, the melting point increases from -3°C to 20°C[25].

In the prospect of the use of ionic liquids as solvents, in analogy with molecular solvents, it is important to know how these compounds mix (or solubilise) polar and apolar materials. An intuitive reasoning will drive to the idea that, because composed by ions, ionic liquids will dissolve polar species. Actually the internal structure of an ionic liquid is quite complex. The complexity of a bulk of ionic liquids is well shown in studies performed by Lopes et al.[108] and Triolo et al.[106, 107], showing how a pure IL has to be considered nanostructured, due to the formation of networks composed by the polar parts of the ions and the induced apolar domains composed by the segregated apolar parts. The nanostructured nature of ionic liquids can be an explanation of their ability to dissolve both polar and apolar materials: polar molecules will be solvated in the polar domains while the apolar will be solvated into apolar domains.

The peculiar structure of ionic liquids offers the possibility to develop many processes impossible in conventional media and in particular in volatile organic compounds: nevertheless a lot of effort has still to be devoted to the study of their bulk properties in order to find general rules that allow the scientists to specifically choice or design an ionic liquid that fits their purposes.

1.2.1 Application of ILs in lubrication and in photoelectrochemical devices

In the last fifteen–twenty years applications of ionic liquids in chemical industry have been extensively studied (e.g. ILs are already used in some industrial processes like Basil™process, or the dissolution of cellulose that is the subject of a collaboration between R. Rogers, at University of Alabama and BASF). Instead, a field that attracted the attention of the scientific community only since the last ten years, regards the application of ionic liquids as lubricants and in photoelectrochemical devices.

In many machines and apparatus developed after the industrial revolution, there are mechanical part involved in rotating or reciprocating movements. These parts, usually metallic, experience friction and need to be lubricated in order to lower friction and wear and so increasing there lifetime and reducing also the arising noise.

Both solid and liquid lubricants can be used. A solid lubricant have the advantage of being insensitive to leakage problems, but suffers of increased noise during the operation, reduced lifetime and low thermal and electrical conductivity. The most widely used lubricants are then liquids, usually divided in mineral (petroleum–derived) or synthetic (ester, or perfluoropolyether PFPE) oils, possibly doped with a series of additives used to fit to specific tasks and to form protective anti–wear layers.

Since the first paper appeared in 2001[48], ionic liquids have shown good performances as lubricants. As already pointed out, even in this case the possibility to design ionic liquids, makes them very appealing. Furthermore, ILs show good thermal stability and lower flammability respect to ordinary lubricating fluids, so they are promising for those applications in which extreme temperatures or very low pressures are involved, like in the aerospace field[46].

Several studies performed, allow to depict some trends in the properties of different ionic liquids used as lubricants. First of all, it appears that if an imidazolium cation is used, an increase in the alkyl chain length, that increase viscosity, induces a reduction in both friction and wear[42, 43, 45]. In contrast, it appears that cations with longer alkyl chains are less thermally stable and also more susceptible to tribochemical reactions, especially in presence of moisture: it seems that the cation loses its longer side chain, with the formation of N–Methylimidazole[44], testified also by the browning of the ionic liquid.

The influence of the anion on the tribological behaviour of the ionic liquid, is more complex. Opposite to the case of the cation, if a replacement of the anion leads to an increased viscosity, this usually don't provide an improvement in trobological performances. In fact, best performances are shown by $[Tf_2N]$ and the family of [PFA] anions, which provides lower viscous liquids as compared to $[BF_4]$ and $[PF_6]$. $[BF_4]$- and $[PF_6]$- -containing ionic liquids are the most extensively studied in tribology. These anions are not particularly suitable for tribological applications, because they are hydrophilic and they easily degrade forming HF: ionic liquids containing those anions are simply the most widespread and easily available on the market. In fact XPS[46] and TOF–SIMS[47] studies show that, especially in presence of moisture, but even in high vaccum conditions, on steel–steel contacts tribochemical reactions induce the formation of FeF_2 in the case of $[BF_4]$ and also $FePO_4$ in the case of $[PF_6]$ inside the wear scar. Even if more stable, also the $[Tf_2N]$ anion can undergo to degradation with the formation of fluorine compounds on surface[41] (see figure 1.2 for a scheme of the relationships between structure and lubricant properties). These compounds cannot be

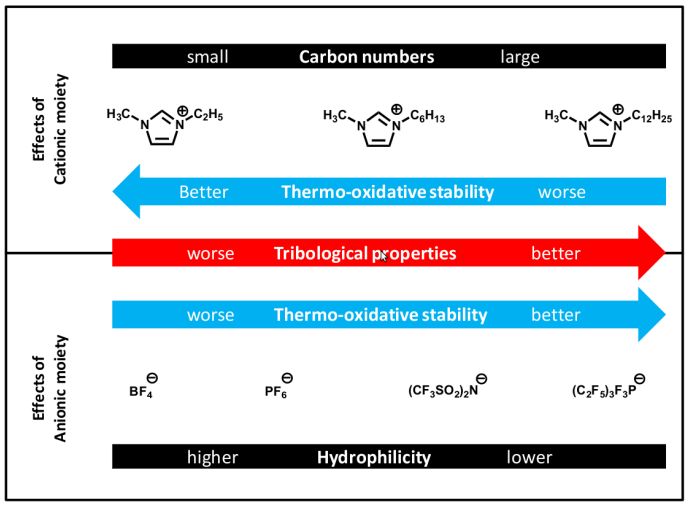

Figure 1.2: *The relation between structure and lubricant properties. Figure reproduced from the reference [43].*

found outside the scar produced during the friction tests, so their formation seems to be induced by slicing bodies, that can be high temperatures, high pressure, catalysing effect of a freshly exposed metallic surface, etc, and need to be further studied. Depending on the type of material, the formation of a surface layer can provide a reduction of wear. This can be a possible explanation of the better performances of ILs when used as additives instead of neat lubricating fluids: the presence of a bulk ionic liquid can further induce the surface corrosion by the tribochemical reactions, whereas a small amount of it can be only enough to form a protective layer but not a subsequent corrosion.

ILs can be effectively used as additives because of their good miscibility with oil, that can be tuned modifying the ions. It has been shown that adding few percent of an IL to mineral or synthetic oils reduces friction and wear as compared to the neat oil and usually also respect to the neat IL. Interestingly, in the case of mineral oil it seems that the increase of the alkyl chain length in imidazolium–based ILs leads to a worsening in tribological performances, contrary to the case of pure ILs[42]. Further studies regard the development of additives for the neat ILs in order to improve their performances. In particluar a study by Ye et al.[49], shows how a salt containing carboxyl acid can be dissolved in [Bmim][Tf_2N], reducing friction coefficient and wear respect to neat IL in steel-steel contact. The mechanism proposed is the absorption of the anion containing carboxyl group on metal surface, forming an immobilised layer. By coulombic interaction, the ions of the ionic liquids

tend to form a layered structure on top of the first linked layer. The first bound layer works as an anti–wear layer while the mobile ionic liquid layers on top of it reduces friction.

An explanation similar to that provided by Ye, has been proposed also by Bhushan et al.[40] in a paper where an ultrathin (few nanometers–thick) ionic liquid layer is deposited on top of Si(100). The behaviour of ultrathin layers is of direct importance for the application of ILs in MEMS/NEMS lubrication. The lubrication of micro- and nano- -electromechanical devices is a difficult task, because the mechanical components involved are very thin and delicate and the separation distances between moving part is reduced even to few nanometers. In these conditions a lack in lubrication can bring to immediate damaging of the device. Furthermore, an efficient lubricating fluid should provide good thermal and charge dissipation.

In MEMS and NEMS the behaviour of the lubricant layer can change respect to the case in which bulk quantities of liquid contact a solid surface. In fact, in a nanometer–thick layer the surface to volume ratio is very high, and the interaction with the solid surface plays a fundamental role. In the work previously cited, Bhushan compares the behaviour [Bmim][PF_6] and [Bmim][$OctSO_4$] with the reference Z–Tetraol (a PFPE lubricant). The comparison is performed both with a standard ball on disk tribometer and with an AFM using a diamond tip. [Bmim][PF_6] shows comparable or better performances than the reference and it is more able to dissipate or screen the charges produced during the friction. In all the cases, the coatings of ionic liquid prepared annealing the samples just after deposition at 150°C for 30 minutes have the best durability and low friction coefficient. The authors ascribe this behaviour to an immobilised layer formed by the reaction of the anions with OH groups on the surface, covered by a mobile fraction composed by the rest of the liquid. If the mobile fraction is removed by washing with isopropanol, the performances worsen.

Surface–induced effects at liquid/solid interfaces are expected to became more important when the surface to volume ratio at the increases. This is the case in all those applications in which the solid material is nanoporous or nanostructured.

Due to the nature of ionic liquids, they are appealing candidates for the substitution of canonical electrolytes in electrochemistry and photoelectrochemistry.

Two categories of those devices that are gaining considerable attention in the last years, are double–layer capacitors, also called ultra– or super– –capacitor or also electrochemical capacitors (ECs), and Dye Sensitised Solar Cells (DSSCs).

ECs are devices composed by electrodes with high specific surface area (SSA), filled with an electrolyte. In an electrochemical capacitor the reversible adsorption of the ions of the electrolyte at electrodes is exploited for energy storage. Compared to traditional capacitors, their capacitances are huge: capacitors of thousands of Farads are already available, with specific capacitances also exceeding 300 F/g. Differently respect to batteries, no reactions take place at the electrodes, only the physical accumulation of charges from the electrolyte: this leads to faster times of charge/discharge of ECs, that can be of the order of few seconds or less. Furthermore, batteries, even the most performing Lithium ion batteries available, can sustain at maximum few thousand cycles of fully charge/discharge, whereas supercapacitor durability is measured in hundred thousand or even million of cycles. In the other hand, batteries can store greater amounts of energy respect to ECs, but their specific power is an oredr of magnitude lower[59].

Supercapacitors are then suitable for those applications in which high power and short time of charging/discharging are needed, coupled with high durability[59].

The working principle of the EC was first described by Helmoltz in 1853 and relates to the formation of a double layer of charge at the surface of the electrode once a potential is applied, that is responsible for the capacitance of the device:

$$C = \frac{\varepsilon_0 \varepsilon_r \Sigma}{d} \tag{1.1}$$

where ε_0 is the dielectric constant of the vacuum, ε_r is the dielectric constant of the electrolyte, Σ is the surface area of the electrode and d is the thickness of the double layer. The theory was further developed by Gouy and Chapman, who introduced a contribution to the capacitance due by a diffuse layer of accumulated ions close to the electrode, induced by a non–perfect screening of the ions in the double layer.

In ECs electrodes with high SSA are used because the capacitance increases linearly with the surface area since a larger surface is avaible for charge storage. Usually the choice is to use graphitic carbon electrodes, because they are highly conductive and electrochemically stable. Different structures of the electrodes can be used[61], like nanofibers, nanotubes or carbide derived carbons (CDCs) and activated carbons: this materials can have surface areas exceeding 2000 m^2g^{-1}. A fundamental ingredient for an efficient operation of a supercapacitor is the electrolyte. Usually, organic electrolytes, i.e. electrolytic solutions in an organic solvent, are used in ECs, because even if higher capacitances can be generally achieved in aqueous solutions, organic solvents have a wider electrochemical window. Since the energy stored in a capacitor is $E = \frac{1}{2}CV^2$, the largest is the electrochemi-

cal window, the greater the specific energy that can be hold in the device. This choice is driven by the fact that water is not electrochemically stable as some organic solvents like acetonitrile. The problem is that usually organic solvents have high vapour pressure, so the sealing of ECs using organic electrolytes is crucial and anyway can lead to a shortened life of the devices and furthermore some of the solvents used are toxics.

The use of ionic liquids as electrolytes in ECs seems promising, because their vapour pressure is very low, but also more important, because they can have electrochemical windows exceeding 5 V, that is almost twice wider than that of an organic electrolyte. A problem in using ILs as electrolytes is related to their high viscosity and low conductivity. The conductivity of an ionic liquid is usually just few milliSiemens per centimetre and this directly affect the equivalent series resistance (ESR), and so the specific power, calculated as $P = \frac{V^2}{4R}$. Furthermore, also the details of the dynamics of the ionic liquid inside the pores affects the ESR, as well as the wetting properties of the liquid on the electrode surface[62].

A more local and accurate behaviour of ILs in high surface/volume ratio configuration is necessary for further improve the performances of these devices, along with the developing of new well suited ionic liquids.

Dye sensitised solar cells, belonging to the third generation of solar cells. This kind of cells, at least in the current design, have been developed by Grätzel at the end of the eighties, and the first paper on the topic has been published in 1991 on Nature[56].

The are several reasons suggesting that these devices may go to replace conventional solar cells in next future. In fact, DSSC reached efficiencies close to that of commercial silicon–based devices[58], furthermore the reduced cost of the materials compared to e.g. silicon or GaAs, the possibility of printing the cells over large areas, also on flexible substrates and their transparency make them very appealing.

The working principle of a DSSC is represented in the Figure1.3

The cell is composed by a transparent anode (conducting glass like ITO or FTO), on which is deposited a nanostructured wide gap semiconductor (from now on I will refer to TiO_2 because is the most diffused, even if also ZnO and other oxides can be used) few tens of nanometers thick. The surface of the nanostructured material is covered by a monolayer of the sensitizer, called dye, the component responsible for the light harvesting. The cell is then filled with an electrolyte containing a redox couple (the most common is I^-/I^-_3). In contrast with conventional silicon cells, where light conversion and charge carrier transport are both performed by the semiconductor, here the light is absorbed by the dye, whereas the photo–generated electrons flow

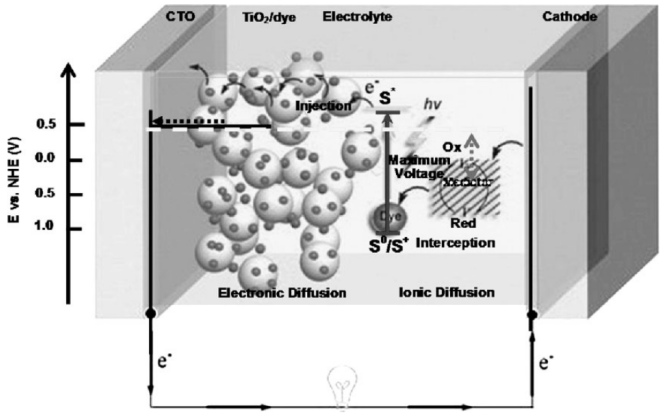

Figure 1.3: *Dye sensitised solar cell: scheme of the working principle. Figure reproduced from the reference [54].*

into the nanostructured oxide. The dye is carefully chosen in such a way that the energy of its excited states matches the energy of the conduction band of the TiO_2: the electrons can then jump into the conduction band and flow into the nanostructured matrix to the anode. The oxidised dye molecules are then regenerated by the oxidation of redox couple and the circuit is closed once the redox couple reduces at the counter electrode.

Here again, as in the case of ECs, the nanostructure is used in order to increase the active area. In fact, it has been seen that the better performances are obtained when a single layer of dye molecules is absorbed onto the surface, but the light capture by a such monolayer on a flat surface would be very low. Instead, on a nanostructured material this single layer allow to reach efficiencies higher then 12%.

One of the crucial ingredients for the efficiency of the device is the electrolyte. In fact, the electrolyte should provide sufficient mobility to the redox couple, needs to maintain its performances for a long time (corresponding to at least 15–20 years of operation) and to don't be corrosive or toxic. Electrolytes based on organic solvents allow to have good diffusion coefficients for the redox couple, but their usage requires that the cell is perfectly sealed, even because some of them are toxic, so making difficult their application in flexible devices and furthermore they can permeate plastics in time.

Ionic liquids offer a valid alternative to ordinary solvents. As already mentioned, ILs have a low vapour pressure and furthermore they do not tend to permeate plastics. Moreover ILs can be carefully chosen in order to dissolve the redox couple and to properly wet the nanoporous matrix.

Different ILs have been tried in DSSC[54] since the first usage of [Hmim]-[I][57]. ILs like [Emim][I] and [Pmim][I] with the addition of I_2 have been tried, because of their lower viscosity compared to [Hmim], and the same liquids have been used with the addition of [Emim][DCA] or [Emim][Tf_2N] or in eutectic mixtures, (e.g. [Dmim][I]/[Emim][I]/[Amim][I]/I2 (8:8:8:1)), in order to further reduce their viscosity and increase the mobility of the redox couple. Actually the mobility is not as low as expected at such high viscosities, because this diffusion is the sum of physical diffusion and a Grotthus–type diffusion, in which triiodide encounters iodide from one end, and triiodide is released from the other end. In this way, triiodide, i.e. the ion that is reduced by the ionised dye, travels a distance of one I–I bond (~ 2.9Å) without having to overcome it.

A good mobility of the redox couple is fundamental, because the sensitiser molecules, once ionised, need to be regenerated as fast as possible. First of all, a faster regeneration of the dye allows a greater photoelectron density injection in the TiO_2, second, ionised dyes are centres of positive charge, so they can induce recombination of the electrons and slow down their diffusion and third, even more important, an ionised dye molecule can undergo to degradation[55]. Thus, it is extremely important to know how the ionic liquid electrolyte behave at the nanostructured–solid/liquid interface.

In fact, as we actually observed, if an oxide surface can induce a structural change when the surface to volume ratio is high, as it is the case in the nanoporous structure of a DSSC, and especially if compact insulating layers are formed, the regeneration of the dye can be slowed, and also the mobility, because of the narrowing of the pores.

1.3 Techniques for the investigation of ionic liquid–solid interfaces

The previous section highlight how the study of the ionic liquid/solid interface can be of fundamental importance in a series of applications. Nonetheless the systematic study of those interfaces is more recent than the investigation of the bulk properties of the ILs.

Among the studies of the IL/solid interfaces present in the literature, the major part has been conducted by electromagnetic spectroscopic techniques.

The interface between a bulk of an ionic liquid and a solid surface has been studied by sum frequency generation spectroscopy (SFG)[68, 67, 66], a technique sensitive only the first ions in contact with the solid. In these studies are evidenced ordering phenomena of the ions at the interface and is

capable to monitor how this orientation depends on both the nature of the ionic liquid and the solid surface. Also X–Ray reflectivity has been used to study the same kind of interface. A study conducted by Mezger et al.[70] on the surface of sapphire (0001) highlights the presence of electron density oscillations at the solid surface, decaying exponentially into the bulk with a decay length of the order of 2nm. This oscillations have been interpreted as the signature of the formation of stacked double layers of anions and cations. The authors guess that this kind of interfacial order may be induced by the charged sapphire surface. Some interesting studies have been performed by X–Ray photoelectron spectroscopy (XPS) on thin evaporated ionic liquid films[71, 72], that again show the development of ordering phenomena of the ions in contact with solid surface. Furthermore the authors in their work performed on gold surface[72] indicate that the ions maintain an organised ordered structure until to a film thickness of 9nm.

Generally the spectroscopic techniques are extremely sensitive to the first layers at the IL/solid interface, meaning that they have a resolution along the direction normal to the surface of fraction of nm or below, such that the orientation of the molecules at the interface can be detected. Spectroscopic techniques anyway, usually collect to the detector information coming from macroscopic or quasi–macroscopic areas of the sample. That means that, even if they are very sensitive the the first layers at the interface, the measured quantities are averaged over large areas, so they suffer of a poor lateral resolution.

For this reason in recent times the interest has grown in using scanning probe techniques in the study of ionic liquid/solid interfaces. Scanning probe microscopies (SPMs) use a probe with a radius of curvature that is usually around few nanometers in order to be sensistive to the local properties of the sample surface. The surplus value of SPMs respect the the spectroscopic techniques is the possibility of investigating the properties of the sample surface with a high lateral resolution. In fact, using these techniques is possible to acquire topographic map of the surface with resolution normal to the surface below 1Åand lateral resolution of few nanometers, related to the size of the probe used. Furthermore other type of maps (surface potential mpas, friction maps, phase maps...) sensitive to different physico–chemical properties of the sample. Among the SPMs the atomic force microscope (AFM) is the most versatile because it can be used equivalently on insulating or conducting sample (of course some maps related o electrical properties will be sensitive to the type of material), it doesn't require ultra high vacuum, in fact it is normally operated in air and it can work in liquids.

Very recently, in the last 5–6 years, few studies have been published in which SPMs, and manly AFM, have been used to investigate the ionic liquid/

solid interfaces. Atkin and co–workers studied several bulk IL/solid interfaces using the atomic force microscope[76, 77]. In these works the AFM has been used to perform force vs. distance curves in order to sense the different forces experienced by the AFM tip approaching the surface. Different ILs on different surfaces have been used; the studies evidence that the ionic liquids tend to structure under the influence of the surface, forming solvation layers, that are subsequently broken by the tip. The layering can extend few nanometers far from the surface and the intesity of the force needed to break the layers increases moving toward the substrate. The same authors performed also a study where they couple the AFM spectroscopy described above with electrochemical STM, were they see the reconstruction of gold surface immersed in an ionic liquid once the potential difference between the tip and the sample is changed[78]. In this study it is also shown how an electrified interface influences the solvation layers; upon the application of a negative potential on the surface of gold, the number of detectable layers increases as well as the forces required to breakup. In these AFM studies the local strcturing of the ionic liquids in contact with solid surfaces is probed, differently respect with electromagnetic spectroscopies. Anyway the authors don't make use of the high lateral resolution of the AFM in order to explore the topography of the IL/interface. In fact it can be expected that the interface can be unven, displaying different morphological and physico–chemical properties in different areas.

Other groups actually performed AFM imaging of the bulk ionic liquid/solid interface. Yokota et al.[84] performed AFM imaging in bulk of [Bmim][Tf_2N] and [Bmim][BF_4] in contact with mica and HOPG surfaces, showing the presence of layered structures unevenly distributed. In two other works performed by the same group[79, 80], the morphology of a thin film of [Bmim][PF_6] on mica and HOPG is investigated by AFM, showing the tendency of the IL, more pronucned on mica, to coexist in a liquid and highly ordered form. This systems can be expected to show a different behaviour than those systems in which a bulk of ionic liquid is in contact with a solid surfaces, since here the reduction of the volume means an increased surface to volume ratio and so the IL would be more influenced by the interaction with the substrate.

In the field of the study of IL/solid interfaces, numerical simulations works have been performed. Pietro Ballone et al.[98] performed a molecular dynamics simulation of a thin slab (∼4nm) of [Bmim][TF_2N] on a silica surface. The study evidences the formation of a density oscillation having a periodicity of 0.6nm and extending for ∼2.5nm from the silica at 300K, whose amplitude decays moving away from the surface. If the silica surface is removeddensity oscillations disappear, restoring the symmetry of the slab

and its fluid–like state, highlighting that the role of the substrate is responsible for the layering formation. In another study Ballone et al.[99] performed a force spectroscopy experiment on the same thin IL slab indenting the liquid with a nanometric hard sphere (2 spheres with radius of 1.6nm and 2nm have been used). During indentation the dependence of the normal force F_z on Z is not monotonic, but displays both localised irregularities and longer–wavelength small–amplitude oscillations: the longer wavelength oscillations reflect the defective layering at the interface. The same kind of features are reproduced in another simulation study performed on the same slab of IL supported on a mica surface[103], confirming that local mechanical properties at the interface are different for thin and thick [Bmim][TF_2N]layers on a solid support.

Another simulation study analyses the behaviour of various ILs in contact with a quartz surface[100], showing ordering phenomena can occour due to hydrogen bonding between the surface and the anion.

At the beginning of my PhD only few works about the study of IL/solid interfaces were available. Furthermore, only in one work[79] the behaviour of thin ionic liquid films onto solid surfaces was investigated by atomic force microscopy, despite the great potentiality of this technique for the study of these kind of systems.

The findings of that study motivated my work on the AFM characterisation of supported thin ionic liquid films. In the important qualitative observation of a coexistence of liquid and ordered phases at ambient temperature (named solid–like by the authors) it is vary interesting for a compound that is liquid in its bulk form at the same conditions. This fact can have important consequences for the applications. In particular, as reported before, when a nanoporous matrix is impregnated by an ionic liquid if mechanically–resistent ordered domains are formed on the surface can strongly influence electrical properties (since immobilised ions are likely to behave like electrical insulators) and flow properties since they can shrink or even block the nanopores.

The aim of my work has been devoted to study in further details the behaviour of thin IL films on solid surfaces using the atomic force microscope, since itss versatility in the study of this kind of systems. In particular I used the ionic liquid [Bmim][TF_2N] because it is hydrophobic and water stable its bulk properties have been well characterised and because this IL or ILs very similar, are used in applications, in particular in photoelectrochemical devices.

The study has first been conducted on the morphological investigation of [Bmim][TF_2N] thin films on different test solid surfaces (amorphous silica,

silicon covered by its native oxide, mica, HOPG and preliminarly on MgO, TiO_2 and NaCl), chosen because they are smooth (some of them atomically flat) and so very suitable for an high–resolution AFM study. The thin films have been realised by drop casting droplets of few μl of a IL/solvent solution in air.

On all the substrates checked but HOPG, the ionic liquid coexists in the form of micro- and nano- -droplets and flat ordered domains behaving like solids under the AFM tip. Ordered flat layers can have an in–plane extension of several microns or even tens of microns and can be more than 50nm thick. Those structures are usually composed by superimposed terraces, in a ziggurat–like arrangement. The thickness of each single terrace ranges from fractions of nanometer to about 10 nanometers. Layer thickness of 2–6nm is typical. On top of layers it is possible to find nano–droplets; also interfacial layers located at the bottom boundary between a droplet and the solid substrate are somtimes found.

A quantitative statistical analysis of the heigths of the terraces as been performed by using histogram of the heigths. The internal stucture of each terrace is interpreted using a simple model as the stacking of fundamental layers of thickness δ. A $\delta = 0.6$nm has been found for all the set of data collected on different substrates (mica, amorphous silica and oxidised silicon) and using different solvents (methanol, ethanol and chloroform), suggesting that the internal structure of the IL ordered domains is not strongly influenced by the kind of substrate and also that the solvent acts only as a fluidising agent that allow the IL to reconstruct under the influence of surface forces. This value is in agreement with the period of density oscillations found in a molecular dynamics simulation of a thin slab of [Bmim][TF_2N] on silica[98]

The mechanical resistance of the ordered domains has then been examined by nano–mechanical tests performed with the AFM. Under the influence of forces parallel to the substrate surface by contact mode scanning, the ordered domains are not easily removed and tend to be eroded as lamellar solids, since a terrace–by–terrace erosion can be observed. Investigating the resistance to normal loads, saw tooth profiles in force vs. tip–substrate distance curves have been found, highlighting a sequence of ruptures, separated by 1.8–2nm, where the average rupture pressure is $\sim$2–3KBar, very similar to the maximum pressure found in a MD simulation of a tip penetrating in 4nm of [Bmim][Tf_2N] on silica[99]. The first part of the sawtooth profile shows a compression that has been treated as an elastic compression of the domain. A simple Hertz model has been applied to fit the compression, leading to Young modulus E^* $\sim$1.8GPa, similar to that of some plastic material like nylon. Moreover, the observation that supported IL islands were not

disrupted by intense electric fields up to 10^8-10^9V/m (applied biasing the AFM with respect to sample during imaging) and that Scanning Nanoscale Impedance Microscopy[14] measurements highlighted a dielectric insulating character of the ordered domains (ε_r = 3–5 was measured[83]) is consistent with the idea that IL ordered domains behave as solid materials in which the ions are tightly bound. From this observations we concluded that the ordered domains are actually solid–like structures.

Finally, some preliminary studies have been conducted on nanostructured substrates. Even if in principle the roughening of the substrate could lead to an increased difficulty in the formation of ordered domains, on a sub–monolayer of silica nanoparticles on oxidised silicon (deposited by supersonic cluster beam deposition directly in the lab), a dense distribution of multy-layered solid–like domains has been found. The roughening of the interface doesn't prevent the formation of ordered domains. The reason for this behaviour could lie in the fact that in a nanostructured deposition the surface area is greatly increased respect to a flat substrate and if the affinity between the ionic liquid and the material composing of the nanoparticles is high, the formation of solid–like structures couldn't be inhibited.

This results of my thesis is extremely important for photoelectrochemical devices since its suggest the possibility that inside the nanoporous matrices, where the surface to volume ratio is high, solid–like layers can still develop. This idea is in accordance with a paper in which a small amount (5% wt) of silica nanoparticles is enough to induce gelation in an ionic liquid–based electrolyte[52].

The findings of my PhD work highlight the potentialities of scanning probe techniques for the quantitative investigation of the interfacial properties of thin ionic liquid films. In fact my AFM investigation highlights how heterogeneous can be the IL/solid interfaces and so how is of fundamental importance to deal with local and not with average properties.

My work shows that the behaviour of thin layers of ionic liquid is greatly modified by the influence of the substrate. In particular, I found a coexistence of liquid domains and terraces with elevated structural order. The formation of those structures, not present in the bulk liquid, is clearly induced by the contact with the solid surface. The solid–like terraces are very resistant to normal loads and to intense electric fields and, (differently with respect to liquid droplets), they tend to behave as insulating layers. Furthemore the that fact solid–like layers can still form on rough and nanostructured surfaces tells that those structures can then have a crucial influence in the performances of photoelectrochemical devices. Further reseacrh effort would be devotet to a systematic study of different nanostructured materials, in

particular focussing the attention to those used in applications. An important parallel investigation would be that on different ILs in order to understand if the behaviour found is a general feature to be awared of when working with ionic liquids.

The importance of this field of research and the validity of my work, are witnessed by the increasing number of papers studying thin ionic liquid layers appeared just before, but especially during the course of my PhD[71, 72, 84, 80, 85, 76, 78]; in many of these works, the AFM is the instrument of choice for the interfacial investigation because it allows to access to the physico–chemical properties of the system with nanometric or sub–nanometric resolution in all the three dimensions.

Chapter 2

Experimental apparatus and protocols for data analysis

2.1 Atomic force microscopy

A detailed description of the basic principles of the AFM is beyond the scope of this thesis. The interested reader can refer to the studies in the Refs.[2, 3]. The atomic force microscope belongs to the family of scanning probe microscopies (SPMs), whose progenitor is the scanning tunneling microscope (STM)[1]. The AFM working principle is based on the measurement of the interaction force between a probe and the sample surface. The probe used in an AFM is a sharp tip, typically less than 10μm tall and having a nanometric radius of curvature. The tip is located at the free end of an elastic cantilever that is usually 100–500μm long. Typically, during the scanning opf the surface the force of interaction between the tip and the surface is monitored by a feedback loop that drives the piezoelectric actuators responsible for the vertical movement of the tip with respect to the sample surface, in order to keep it to a constant value (see Figure 2.1). I summarize here the basic properties and characteristic of an AFM:

- high lateral resolution (down to few nanometers in air), whose lower limit is determined by the size of the tip, and vertical resolution below 1Å;

- possibility of operating on insulating samples, on delicate samples like biological material or ionic liquid;

- the AFM microscope can be operated in air, in ultra high vacuum and in solutions, and measurements can be done on very different length scales, from few nanometers to few hundreds of microns.

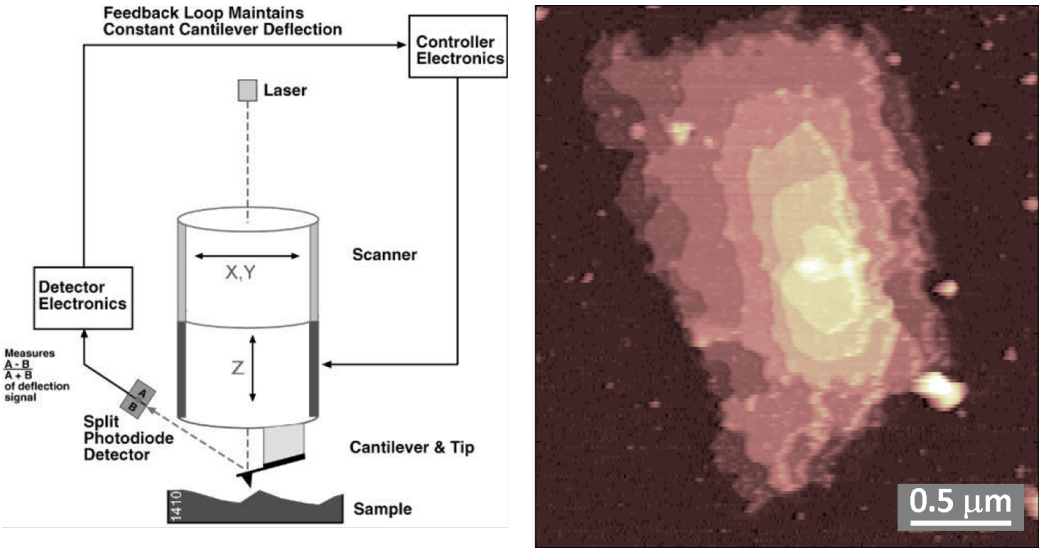

Figure 2.1: *Scheme of the working principle of an AFM operated for the acquisition of a topographic map. On the left–hand side an example of a morphology output. The image has been acquired in tapping mode (see below in the text) on an ionic liquid ordered layer (vertical scale 50nm).*

The topographies acquired by an AFM are truly 3D morphologies, and the instrument output consists of numerical matrices ready to be processed via numerical algorithms that can be developed ad–hoc for specific purposes. The availability of 3D data allows to perform reliable measurements of volumetric quantities, for example for evaluating the volume of a globular protein onto a flat substrate, or to calculate the contact angle of nanodroplets[82]. The part of my work devoted to the quantitative statistical analysis of the heights of ionic liquid terraces, has been possible thanks to this important characteristic of the atomic force microscope.

Usually the acquisition of morphological maps can be performed in two modalities: contact mode (CM) or tapping mode (TM). Briefly, in CM, that has been the first modality developed, usually cantilevers with low force constant are used (0.01–0.2N/m). The tip is brought into contact with the sample surface and the surface is scanned with constant applied force. That means that a permanent contact between the tip and the sample surface is maintained during the scan, so subjecting the surface features to lateral forces, whose entity is related to the finite response time of the feedback loop. Lateral forces, as well as friction forces experienced during contact mode operation, can be very hazardous for delicate surfaces, like biological materials or ionic liquid depositions, but also for loosely bound coatings as

some nanostructured materials.

To overcome this limitation tapping mode has been developed. In tapping mode cantilevers with higher force constants are used (30–60N/m). The cantilevers are oscillated near to their resonance frequency (usually around 200-400KHz) and, instead of the cantilever deflection (i.e. of the constant applied force), the amplitude of oscillation is monitored by the feedback loop. In this way the time in which the tip contacts the surface during the movement of the sample for the scan is very limited, so greatly reducing the problematic lateral forces. Even though normal loads can be high even in this modality (pressures can be of the order of 0.2KBar), the high reduction of friction forces allows the acquisition of high resolution maps on fragile samples like lipid bilayers, proteins and even liquid droplets, as can be seen in the left–hand part of Figure 2.1.

During the same scan performed for the acquisition of morphological data, other maps can be acquires (phase map, surface potential, friction...), in order to evaluate different physico–chemical properties of the sample surface (visco–elasticity, electrical character, adhesion...). Particularly interesting is the possibility of using the AFM as a force sensor and force transductor for performing nanoscale force spectroscopy and nano–mechanical tests: these aspects will be described in the following sections.

2.2 Sample preparation procedures

During my PhD work, the major part of the depositions have been carried out using the method of the drop–casting of a dilute solution of an ionic liquid into a volatile solvent. The reason is that in this way very thin coverages can be obtained, suitable for an AFM investigation of the behaviour of the first layers of IL in contact with a solid surface. As will be discussed in a section of the next chapter3.2.1, the dissolution of the ionic liquid into a solvent, allows to deposit very small quantities of the IL on the substrate during the evaporation procedure. This gives the possibility to observe the effect of substrate–IL interactions that will be suppressed increasing the amount of liquid, but that are extremely important in the optics of understanding the behaviour of ILs in confined geometries, like in nanoporous matrices.

The deposition by drop coating has been performed on different substrates, principally smooth flat surfaces. The most studied substrates have been amorphous silica coverslips, single crystal silicon covered by its native oxide layer, mica, highly oriented pyrolityc graphite (HOPG). Those substrates have been chosen because they are smooth surface, even atomically flat as mica and HOPG, so particularly suitable for an AFM investigation

of the behaviour of thin layers of ionic liquids. Furthermore oxidised silicon is used in NEMS/MEMS devices, in which ionic liquids could be used as lubricants. Preliminary depositions have been performed on MgO, TiO_2 and NaCl single crystal in order to see the behaviour of [Bmim][Tf_2N] on other oxide surfaces. Some preliminary study have been conducted on corrugated or nanostructured surfaces, in particular gold and nanostructured silica films.

On most of the substrates checked, the ionic liquid coexist in the form of micro- and nano- -droplets and flat ordered domains behaving like solids, as will be shown in the next chapter.

Usually [Bmim][Tf_2N] thin films depositions consist in spotting a droplet of few microliters (on the order of 3–10μl) of [Bmim][Tf_2N]–solvent solution on the substrate of choice and allowing the volatile solvent to completely evaporate in air. Using solutions in which the IL concentration is typically kept below $1 \cdot 10^{-3}$ mg/ml. thin ionic liquids films can be deposited. The typical morphology of the thin films show the coexistence of ordered layers and/micro- to nano- -droplets.

In order to reduce water contamination, all the ILs used have been kept in a desiccator under mild vacuum condition (around 10^{-2} mbar). For the last solutions prepared, the ILs have been kept in ultra high vacuum ($1 \cdot 10^{-6}$ mbar) for several days prior to use. All the solvent used, (methanol, ethanol and chloroform), originally HPLC purity grade, were distilleld twice prior the preparation of the solutions, in order to decrease the amount of non volatile contaminants as well as water content. After the distillation, test samples were prepared by spotting the solvents onto a cleaned substrate and then were characterised both visually and by the AFM. The distillation step usually leads to solvents that do not form any visible halo on the substrate surface, and the investigation with AFM does not show any trace of structures similar to what is found after the deposition of IL/solvent solutions. The IL concentration in the deposition solution is typically kept below $1 \cdot 10^{-3}$mg/ml. Substrates were freshly prepared immediately before deposition of the [Bmim][Tf_2N] solution. Mica and HOPG were stripped with adhesive tape in order to obtain atomically smooth, cleaned surfaces. Discs (13 mm-diameter) of amorphous silica (glass coverslips) and squared specimens of polished, oxidized Si(110) were cured in aqua–regia solution (HCl–HNO_3 from, respectively, 37% and 69.5% solutions at ratio 3:1) before use, to remove organic contaminants and rehydroxilyse the surface. After aqua–regia the substrates are usually rinsed copiously with distilled water or with the solvent used for the deposition and then dried under nitrogen flux.

Some samples have been produced depositing a pure ionic liquid micro–droplet directly onto the substrate. In this case the excess of IL have been

removed by spinning the substrate at high speed (2000–4000rpm). This method of deposition anyway, is not capable to separate the ionic liquid into volumes small enough to allow a restructuring of the IL from its bulk–stable form (i.e. liquid) to the ordered phase promoted by the interaction with the substrate.

2.3 Statistical structural characterisation

On all substrates used but HOPG, ionic liquid has been found to coexist in liquid and ordered domains. A statistical analysis of the heights of this domains has been performed.

The morphological survey has been performed with both the atomic force microscopes available in our lab, a Bioscope II–Nanoscope V and a Nanoscope IV Multimode, both provided by Veeco. The last measurements have been collected on the upgraded instrument Bioscope Catalyst, provided by Bruker.

The main part of the statistical study has been performed on images collected in tapping mode that is less invasive, although also images acquired in contact mode have been analysed to check the hardness of layered domains.

Tapping mode images were usually collected using standard silicon cantilever holding silicon tips with a nominal radius of curvature lower than 10nm. The cantilever have force constants of the order of 40N/m and resonance frequencies between 200 and 300KHz. Normally AFM maps have been collected with 2048 points x 512 lines or 4096 points x 1024 lines on areas ranging between 500x500nm^2 and 30x30μm^2 and using scan rates between 0.5 and 1Hz per line.

For contact mode scans, standard contact Si_3N_4 tips (Veeco Probes) have been used, with a radius of curvature ranging between 20 to 60nm (four cantilevers are available for each chip, with nominal spring constants between 0.07 and 0.35N/m) and sharpened contact silicon tips (Vista probes), with a nominal radius of curvature below 10nm and a typical spring constant of 0.1N/m. The typical scan areas and scan rates are the same used for tapping mode images.

This analysis is based on the study of height histograms (see Figure 2.2). This approach allows to consider in the analysis a huge amount of topographic data (order of 10^6–10^7 data points), that are not influenced by an arbitrary choice by the user, as in the case of the selection of few profiles (sections). AFM topographic maps are first flattened by line–by–line subtraction of 0^{th} to 3^{rd} order polynomials evaluated on flat substrate regions, in order to get rid of distortions introduced by the scanning piezos and of the tilt of the sample. Terraces, that on flat surfaces are constant–height regions, produce sharp

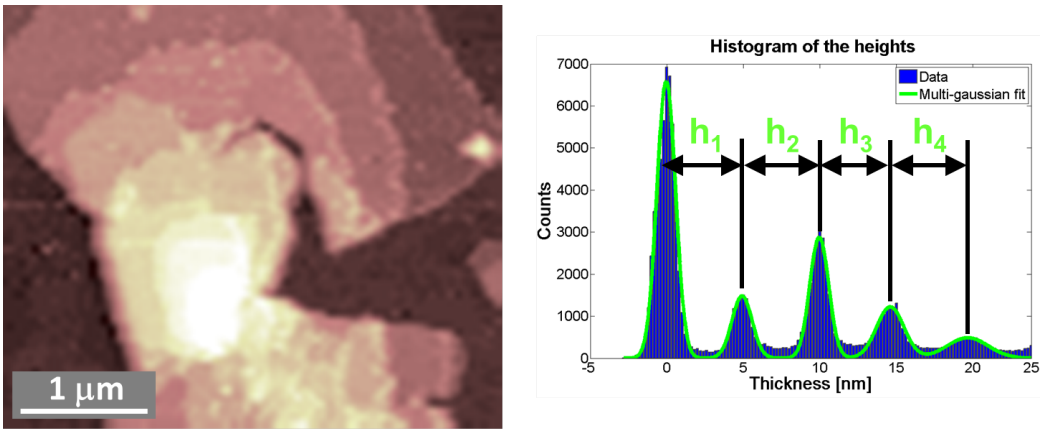

Figure 2.2: *Example of a typical AFM topographic map of [Bmim][Tf_2N] deposition on silicon with its relative histogram of the heights. The envelope of the histogram is the multi–Gaussian fit.*

peaks in the height histograms. Peak–to–peak distances represent terrace heights h_i. From a multi–Gaussian fit of the histogram the peak positions, the corresponding widths and the number of counts below each peak can be extracted. The error associated to the height of a terrace is calculated summing in quadrature the statistical error, and an instrumental error that reflects the accuracy of the calibration of the vertical piezo ($\sim$2% of average terrace height for each value). The statistical part of the error σ'_h associated of each terrace height is calculated as:

$$\sigma'_h = \sqrt{{\sigma_{m,1}}^2 + {\sigma_{m,2}}^2}$$

where $\sigma_{m(1,2)}$ are the standard deviation of the mean of the single peaks of subsequent terraces, calculated as $\sigma_{m(1,2)} = \frac{\sigma_{1,2}}{\sqrt{N_{1,2}}}$, where $\sigma_{1,2}$ is the standard deviation of the peak as extracted by the multi–Gaussian fit, and $N_{1,2}$ represent the number of counts under the peaks. The overall statistical error is typically small compared to the systematic one, thanks to the large number of points in each image. This may not be true in standard section analysis.

The most simple guess about the internal structure of an ordered ionic liquid island, is that each terrace is composed by a superposition of molecular layers having a fundamental height δ. Each height h_i is then supposed to be an integer multiple of this basic monolayer height δ, as schematically shown in Figure 2.3.

In order to find the best divider of terrace heights, and the series of best

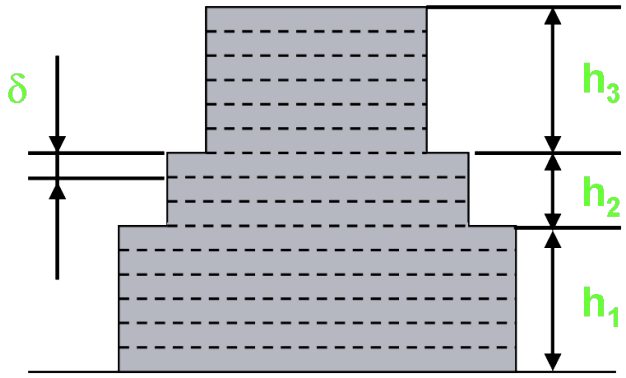

Figure 2.3: *Example of an histogram of the height of a typical topographic map of [Bmim][Tf_2N] deposition on silicon. The envelope of the histogram is the multi–Gaussian fit.*

integers, we minimise the following chi–squared function with respect to δ:

$$\chi^2 = \frac{1}{M}\sum_{i=1}^{M} w_i \left(\frac{h_i}{\delta} - \left[\frac{h_i}{\delta}\right]\right)^2 \tag{2.1}$$

where $w_i = (\sigma_i^2)^{-1}$, where σ_i is the error associated with h_i, $\left[\frac{h_i}{\delta}\right]$ represents the closest integer N_i such that $\delta N_i \sim h_i$ and M is the number of elements of the specific dataset. For each set of data usually a great number of images were analysed. According to the simple model proposed, in each set of data the heights tend to cluster around specific values, that we identify as the integer multiple of the fundamental thickness δ. In order to remove from the data set some spurious values coming from an incorrect Gaussian fit, possibly due to the superposition of different peaks in the histogram because of close terrace heights or to the presence of droplets, the data are filtered using a recursive procedure. Knowing an approximate value of δ estimated from the data set, the heights are separated in intervals centred around each integer multiple of δ. Within each interval an average and a standard deviation of the average is calculated, and data far from the average for more than $n * \sigma$ where n can be specified by the user, are excluded from the average (but can still fall in other intervals when they are overlapping). The same procedure is then repeated recursively until no more data will be excluded. The output of the recursive procedure is than used as input of the Matlab routine that calculates χ^2 as shown in Eq. 2.1. The range of the spanned δ can be chosen based on physical considerations. In fact, the results of numerical simulations [98] show density oscillations in a slab of [Bmim][Tf_2N] on silica

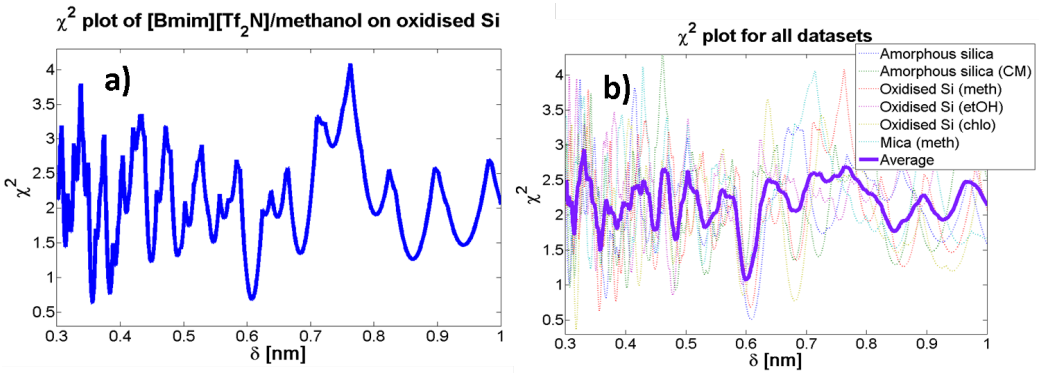

Figure 2.4: *a)* χ^2 *calculated for the data collected depositing [Bmim][Tf*$_2$*N]/ methanol on oxidised silicon. b) Plot of the single* χ^2 *calculated from all the datasets. The average* χ^2 *superimposed shows that the minimum around 0.6nm occours for all the datasets.*

with a periodicity of 0.6nm, that is compatible with the ion sizes (around 0.78nm the cube root of the molecular volume calculated from the known density and the molecular weight). Considering the simple model of a stack of fundamental layers proposed, we looked for χ^2 minima for values of δ ranging between 0.3 and 1nm. The upper limit is motivated by the fact that height below 1nm have been measured several times.

Each set of data, relative to terrace heights measured on the different substrates (amorphous silica, oxidised silicon and mica), and using different solvents (methanol, ethanol, chloroform), has been analysed independently, because in principle each data set could lead to a different fundamental layer thickness. A plot of χ^2 as a function of δ usually does not show a single deep minimum, but instead a series of minima, as can be seen in Figure 2.4 a). The presence of many minima is due to several reasons. First of all, the heights in each dataset usually go from one to few times δ to 10*δ or more. Furthermore the data do not cover all the possible integer multiples of delta densely, meaning that some multiples are missing. This implies that within each dataset some subsets could be integer multiples of other dividers, and the number of heigth values belonging to each subset vary depending on the heights measured. Furthermore, it cannot be discarded the possibility that the terraces can be composed by a stacking of layers having different thicknesses.

Nonetheless, in all the χ^2 there is usually a deeper minimum around 0.6nm (see Figure 2.4 b)). This fact is evidenced when the χ^2 are averaged together, is can be seen in Figure 2.4 b): while all the other minima are almost averaged out, the minimum at $\delta = 0.6$nm becomes clearly evident. This observation

suggests that the structural organisation of the islands does not substantially change on different substrates, and also that the use of different solvents does not lead to detectable changes.

2.4 Mechanical characterisation

Along with the operation with the scanning modalities, it as to be remembered that AFM is one of the most sensitive dynamometers existent (along with optical and magnetic tweezers). For this reason AFM can be used to perform force spectroscopy measurements, by ramping the AFM tip against the sample surface and monitoring the interaction force between them as a funtion of the tip–sample distance[7]. It is important to underline that atomic force spectroscopy can be coupled to the imaging, so allowing to find the area of interest and then to perform measurements on specific positions located from the morphological map. The basic output obtained performing a standard force spectroscopy measurement with an AFM, is a force curve. A force curve is a curve acquired recording the variation of a quantity of interest (deflection, TM deflection, amplitude of oscillation, lateral force...), as a function of the distance travelled by the piezo driving the tip (or the sample depending on the instrument). A typical force curve, in the specific case a deflection vs. distance curve, is shown in Figure 2.5. A force curve is performed ramping the tip against the surface of the sample, or the sample against the tip, depending on the type of instrument used, along the vertical axis (z axis) (from now on we will refer to a system in which is the tip that moves along the vertical axis). In the absence of long–range forces, during the first part of the approaching the deflection remains constant (point A in Figure 2.5). At point B there is the jump–in, i.e. the tip jumps to contact under the action of surface attractive force (capillary meniscus formation, vdW); the region C is the contact region, in which a strong repulsion atcs between the tip and the surface. Normally, when performing force spectroscopy, a threshold on the deflection is fixed, the trigger deflection: once the trigger is reached, the motion of the tip is reversed, increasing the tip–sample distance. The region D in Figure 2.5 extends from the trigger to the point E, where there is the jump–off, i.e. the tip leaves the surface and comes back to the non–interaction part and returns to the starting position. As can be noticed, point B and point E are not located at the same tip–sample distance, because of the interaction with the sample that traps the tip until a certain deflection, and so a certain force, necessary to free it is reached: this force is the adhesion or pull–off force, and is related to the details of the interaction between the tip and the sample. Differences in adhesion force can be

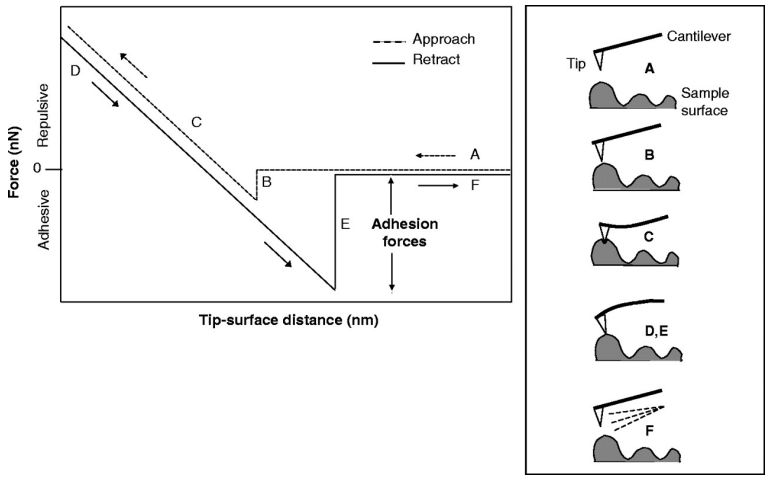

Figure 2.5: *Scheme of a complete (approaching and retracting) force curve. Point E is the jump–off position. The force necessary to detach the tip from the sample is the pull-off or adhesion force. The 2 curves have been slightly shifted for a better visibility. Some sketches of the tip in the various point along the force curve are shown on the right–hand side.*

used during a force volume (see below) to qualitatively or also quantitatively distinguish materials having different physico–chemical properties.

At this stage, what I have called a force curve, has in abscissa the distance travelled by the piezo during the ramping, that is set by the user while in ordinate doesn't reports a force, but a deflection signal in Volts. In order to get a real force curve, i.e. reporting a force, for example in nanonewtons, versus the distance between the tip and the sample, two operations have to be done: first, it has to be measured the deflection sensitivity ($zsens$) and then the cantilever force constant has to be calibrated. The $zsens$ is necessary to convert from V to nm the deflection signal. In order to perform a correct conversion one proceeds to the acquisition of a force curve (usually more than one to measure an average) on a cleaned rigid substrate, whose Young modulus provides very small deformations compared to the deflection on the cantilever in the range of forces applied. The contact part of this force curve in nm units, is expected to be linear with slope 1, because the only contribution is due to the cantilever bending and the amount of deflection in volts is equal to the distance travelled by the piezo driving the chip holding the tip: the correction factor, i.e. the $zsens$, is the inverse of the slope of the contact part of the force curve.

At this stage what we have is a deflection in nm vs. the distance travelled by the piezo. Anyway it would be more physically meaningful to have the

deflection as a function of the tip–sample distance. To this purpose the z axis needs to be rescaled in such a way that the 0 corresponds to the point of contact (jump–in, point B in Figure 2.5). If there is no indentation (see below for details about indentation), all the points of the part of the force curve should lie on a vertical line at deflection = 0.

The tip–sample distance is calculated as $z = (z_p - z_0) + d$, where z_p is the distance travelled by the piezo, d is the deflection in nm, and z_0 is the offset to shift the contact point (jump–in) at $d = 0$.

At this point a force vs. tip–sample distance curve can be obtained multiplying the deflection by the k of the cantilever. Among several methods that can be used for the calibration of a cantilever (see Ref. [4] for a review on the argument), we chose the thermal noise[5, 6]. Thermal noise is a non invasive method for the calibration of the force constant based on the measurement of the free oscillation of the cantilever due to thermal energy, that is based on the equipartition theorem. For the k calibration it is only necessary to measure the temperature of the room, perform some force curves in order to calculate the *zsens* and then acquire the thermal spectrum. If standard rectangular cantilevers without coatings are used, the force constant can be calculated with an accuracy of 10%.

In order to obtain from force curves the applied pressures, a parameter more meaningful then force to compare different AFM data among them and with data from other techniques, including molecular dynamics simulations, the tip apex profile has to be characterised.

An AFM topographic image is always the result of the convolution of the tip shape with that of the object scanned (see Figure 2.6 left). Actually the distortion caused to the data obtained is not related to Fourier convolution, which is linear and invertible, but is related to the dilation algorithm, also called Minkowsky addition[8]. We can see the dilation as a translation of the structuring element T: the structuring element T is drag over the image S (see Figure 2.6 right). The more the object S decreases in size, the more the result of the convolution will approximate the real shape of T. The same is true when an AFM tip scans the surface of a sharp object having an high aspect ratio: in this case the resulting image will be the more close to the reverse image of the tip the more the feature is sharp and with an high aspect ratio.

For tip radius calibration then, topographic scans have been performed on a TGG01 sample, a silicon calibration grating provided by MikroMasch, which is composed by a 1–D array of triangular steps with sharp ridges and high aspect ratio. The radius of the apexes of the structures is below 10nm, with an aperture angle of $\sim 70°$. The measurements were all executed with fast scan axis (x axis) normal to the edge of the triangular structures, because

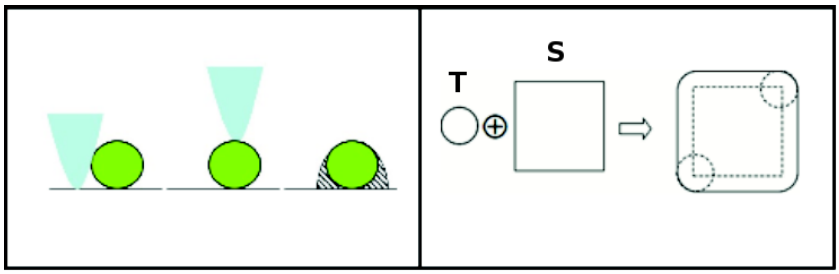

Figure 2.6: *Left, apparent image is a convolution of the tip geometry and the true sample geometry. Right: example of dilation between a circle (T) and a square (S).*

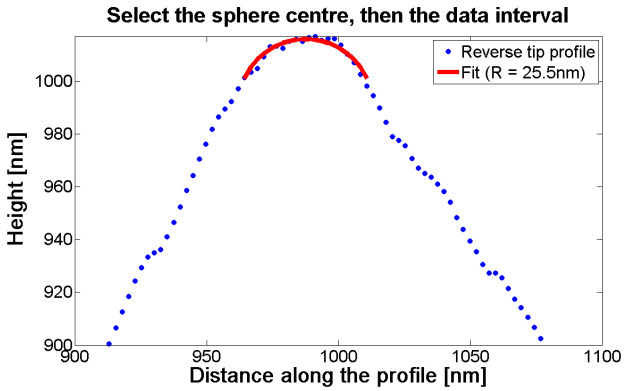

Figure 2.7: *Particular of a reversed tip profile extracted from an image acquired on TGG01. On the last 20nm near the apex have been performed a fit to a circle in order to measure the radius of curvature of the AFM tip.*

the slow scan axis (y axis), is more subjected to distortions introduced by the piezo movements. For every tip to be calibrated, two scans have been performed, in order to collect the tip profile along two perpendicular axis: in the first scan the fast scan axis is aligned with the cantilever main axis, and so the edges of the grating are perpendicular to the cantilever; in the second scan, the fast scan axis is perpendicular to the cantilever axis, and the grating has been rotated by 90°.

From the two images collected some line profiles have been extracted and then, for both profiles, the topmost part is fitted with an arc of circumference in order to extract the radius of curvature of the probe (see Figure 2.7). The average radius of curvature (i.e. the inverse of the average curvature) is calculated as $R = 2(R_1R_2)/(R1 + R2)$, where $R_{1,2}$ are the radius measured

on the two perpendicular profiles.

Standard AFM tips can be conical or pyramidal in shape, so it could appear that the previous measure of the tip radius couldn't provide accurate results. Anyway, in the case of characterisations like indentation measurements, so where an AFM probe indents a film for only a few nanometers, the only part of the probe that contacts the sample is the very apex, and this is well approximated by a spherical object, as witnessed also by the fact that the radii measured on orthogonal profiles where always very close to each other.

For indentation measurements (see below), all the tip radii have been calculated has described above.

All the rescaling procedures of the force curves described, as well as all the data analysis on them, has been performed in Matlab environment, using routines developed in our lab. New routines have also been developed by my self in order to match specific tasks in data manipulation. The procedures described in this section have been adopted in treating the data acquired in the two modalities of force spectroscopy described in the following: force volume and point and shoot.

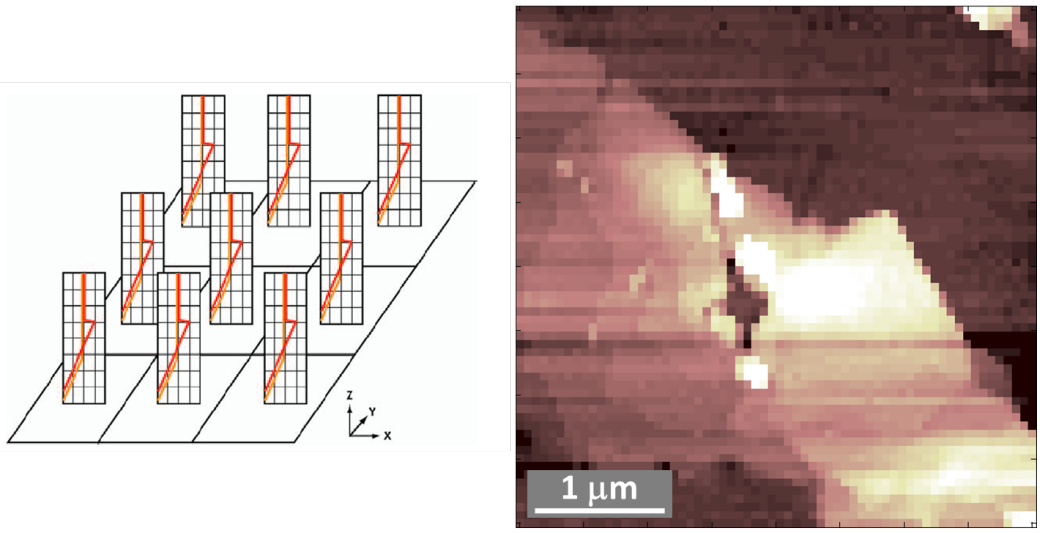

Figure 2.8: *Left: Scheme showing the principle of FV measurement. A force curve is acquired in every point on a matrix defined on an area of the sample. Right: example of a topographic image acquired in FV mode (vertical scale 70nm).*

2.4.1 Force volume

Force volume (FV) is force spectroscopy methodology in which, a force curve is made on every point of a regular matrix defined on that area[9] (see Figure 2.8). In order to perform a FV, first of all an area of interest has to be selected. The area is then scanned in FV mode, cllectin force curves by ramping the tip until a common maximum force (deflection) is reached. The morphology is reconstructed from the ensemble of FC by recording the absolute vertical positions at which the trigger deflection is reached, for each point defined in the matrix. The morphology in a FV is then always acquired at a force corresponding to the trigger force (see Figure 2.8).

In a typical force volume 64x64 or 128x128 force curves can be collected. Force curves, in the specific case of my work, are usually performed using ramps 300 to 500nm long (for both approaching and retracting paths) with a number of point between 512 and 2048. Ramp rates usually ranges between 1 and 6Hz.

During all the experiments performed in force volume, the same standard contact mode tips used for the acquisition of topographies, described above (see Sec. 2.3) have been used.

The measurements were generally performed in air even if few FV have been collected in dry nitrogen atmosphere.

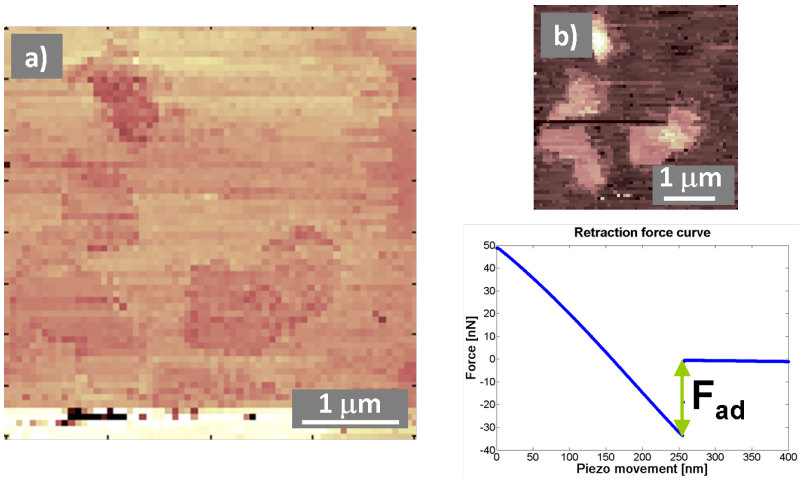

Figure 2.9: *a) Adhesion map calculated from a force volume (vertical scale 60nN). b) Force volume topography (vertical scale 27nm). The force curve below b) is an example of a retraction curve, where the adhesion force F_{ad} is indicated.*

The output of a FV consists of a 3D matrix containing, for each position defined along the scan area, a force curve. The output of a force volume is analysed by using specific routines developed in Matlab environment. In order to acquire reliable data, the scan are have to be chosen in such a way that always a reference part, i.e. the substrate, is available. On the topography acquired in FV, a mask can be defined in order to mask out all the points that don't belong to the substrate. The mask is then passed in input to a routine that selects only those curves corresponding to the point not excluded by the mask. If the curves have been acquired on the rigid substrate, from their slope the deflection sensitivity can be calculated and successively used to convert the deflection signals from Volts to nanometers, as described in the previous section.

From a FV output the adhesion map can be calculated. Adhesion map (an example can be seen in Figure 2.9) is a map reporting, for each point, the vertical distance (in force units), between the non–interaction part of the force curve (at high distances) and the pull–off point, immediately before tip detachment. The force of adhesion, that is mainly related in air to capillary forces[], can reveal heterogeneities on the surface that are not evidenced in the topography or, on the contrary, can show how different domains visible in the topography can have compatible physico–chemical properties.

There are several drawbacks working in force volume. First of all, the number of points in the morphological map is limited, because for each point a

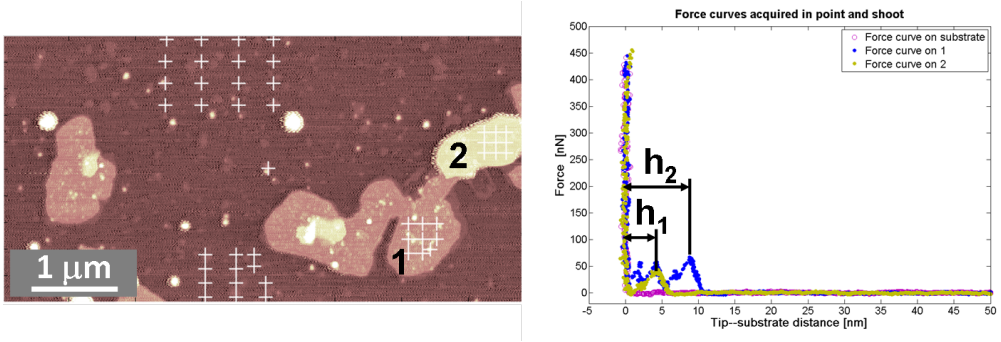

Figure 2.10: *Typical point and shoot output. On the left–hand side the morphology, in this case acquired in tapping mode, is reported (vertical scale 15nm). Each white cross on the image represent a point where a force curve has been acquired. On the right–hand side, there is a plot reporting 2 force curves acquired on islands with different thickness, together with another one acquired on the substrate as a reference.*

force curve is acquired too, and memory limits don't allow more than 512x512 points. Furthermore the FV is a technique intrinsically slow: for example the acquisition of 128x128 curves with a ramping rate of 5Hz, will take about one hour. As already mentioned, the acquisition of the topography to locate the area of interest prior to the force volume, can be performed only in contact mode, so as it will be discussed in the next chapter 3, potentially eroding the ordered domains, especially if cantilevers having high force constants, necessary to look for indentation, are used. The area of interested can also be located directly in force volume, but the topographic map is built during the ramping, so it is slow, limiting an extensive exploration of the sample surface needed to locate an area of interest. Furthermore the way in which the topography is built, prevents the acquisition of high–resolution maps.

2.4.2 Point and shoot

Due to the rigidity of the structures found, no indentation could be induced using standard contact levers. If the AFM operates in FV mode the only contact mode is allowed to be used to locate the area of interest, that considering the high lateral forces, is potentially harmful for the sample. The only alternative that avoids the use of CM is to directly look for a good area on the surface through the FV topographic map, that anyway is very time–consuming. For this reasons force volumes with more rigid levers are very difficult to perform. For these reasons, I used another spectroscopic technique: the point and shoot (PS). In a general PS measure, after the ac-

quisition of a morphology, several points on the map can be marked by the user, as the cross in Figure 2.10 show. For each point specified by a cross one (or multiple), force curve is acquired. This technique has several advantages compared to FV.

The main advantage, especially on the specific system studied during my work, is the possibility to locate the area of interest in tapping mode, and then using the same tip to perform standard deflection vs. distance curves, zeroing the oscillation amplitude. The tapping modality is more gentle with the deposition than the CM, and allows the acquisition of high–resolution maps, useful to carefully choose the places where to perform the force curves and also for looking to the effect of the spectroscopy on the area of interest by a subsequent morphology acquisition. Furthermore, the k of the cantilevers used for tapping mode is high enough (as will be shown in Chapter 3), to indent the ionic liquid ordered layers.

A second important advantage respect to FV is that the acquisition times are greatly reduced, because the high–resolution map permits to carefully select the points of interest where to acquire force curves. In the case of the system I have studied, i.e. flat islands on flat substrates, a limited number of curves (30–100) is usually enough to have a good statistics, since usually curves on the substrate and on an island are, respectively well overlapping. In the time needed to acquire an FV, several PS can be acquired moving on different areas of the sample.

When the microscope is operated in tapping mode, curves reporting the tapping mode deflection (TM deflection) as a function of the distance travelled by the piezo are acquired. After the acquisition of the image, before the beginning of the ramping, the drive frequency, i.e. the frequency of the electrical signal driving the oscillation of the cantilever, is moved out of resonance, in order to reduce as much as possible the oscillation amplitude (it actually goes nearly to zero), that can be monitored on a separate channel. The TM deflection vs. z piezo curves are then equivalent to the deflection vs. z piezo curves acquired in contact mode but in this case are performed with more rigid cantilever.

In order to quantitatively characterise the nano–mechanical properties of IL solid–like layers probed in PS measurements, all the tips used for this kind of force spectroscopy have been fully characterised, both with thermal noise (to calculate k) and performing scans on the TGG01 grating (to calculate the tip radius R).

The force curves acquired on solid–like islands show a sawtooth profile (see Figure 2.10) led us to think about a compression (indentation) and a subsequent rupture of one or more solid layers, whose number depends on the

thickness of the island. The thickness of the solid–like terraces, as measured in tapping mode, is compatible with the total length of the indentation profile, as highlighted in Figure 2.10. The first curved part of the contact part of the force curve is the indentation part. Analysing a PS output, the force curves acquired on the rigid area (substrate) arond the IL island are used to calculate the *zsens* in order to rescale the curves performed on the island. Once these curves have been rescaled, the first part does not appear as a straight vertical line, but shows a residual curvature typical of deformable materials: this deformation is called indentation. As shown in Figure 2.10 the indentation is followed by the rupture of the terrace when a threshold pressure is reached.

The indentation part of the profile has been interpreted as an elastic compression of the solid–like layers. This compression has then be modeled by a simple Hertz model of a rigid sphere pressing an elastic flat plane. The application of this model is justified by the fact that:

- the very apex of the tip can be effectively modelled as a sphere, as discussed previously;
- the surface of the layers is usually flat and the force curves are acquired far from the edges;
- the indentation is smaller than the sphere radius;

More complex models, like DMT or JKR, that consider accurately the effect of adhesion, completely neglected in the Hertz model, are not thought to provide noticeable improvements in the calculated Young modulus values, since other factors are probably preponderant respect to the differences between the models, first of all the fact that we don't actually know if the behaviour during compression is purely elastic or it is more of a visco–elastic type (for a comprehensive review on interpretation of force curves and contact mechanics, refer to Ref. [7]).

The Hertz model provides the following expression for the force as a function of the indentation:

$$F = E_{tot}\sqrt{R}d^{3/2} \tag{2.2}$$

where d is the indentation and E^* is the total reduced Young modulus:

$$\frac{1}{E_{tot}} = \frac{3}{4}\left(\frac{(1-\nu_t^2)}{E_t} + \frac{(1-\nu_s^2)}{E_s}\right) \tag{2.3}$$

where $E_{t,s}$ and $\nu_{t,s}$ are the Young modulus and the Poisson ratio of the tip and of the substrate respectively. The previous expression simplifies if we

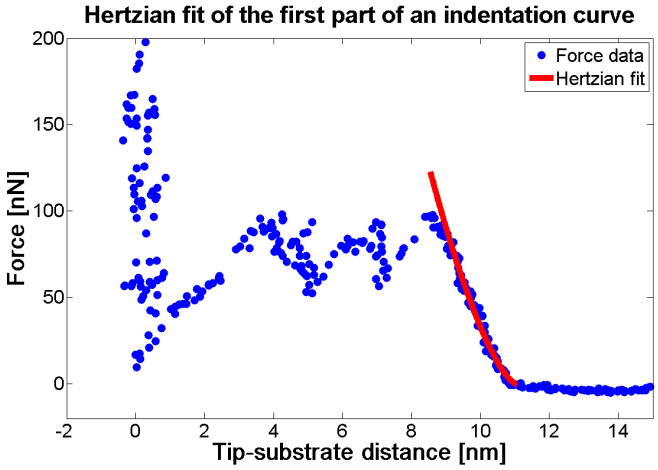

Figure 2.11: *Example of a fit performed using the Hertz model on first part of the contact in a force curves on a solid–like island.*

assume that tip is much stiffer than the sample (silicon Young modulus is of the order of 100GPa), as it is the case in my measures, and becomes:

$$F = \frac{4}{3} E^* \sqrt{R} d^{3/2} \tag{2.4}$$

where $E^* = E_s/(1-\nu_s^2)$ is called reduced Young modulus. Once a force curves is rescaled in force vs. tip–substrate distance, and this can be done with the procedures described above, the expression 2.4 can be used to fit the first part of the indentation profile, (an example of the fit is shown in Figure 2.11). From the fit what it can be calculated is not the actual Young modulus, since ν cannot be determined by this kind of measures. Anyway, Poisson ratios, except for peculiar cases, have values between 0 and 0.5, so the reduced Young modulus can be effectively compared with Young modulus of known materials, in order to have an idea of the rigidity of the ionic liquid layers, with a possible error less the one order of magnitude.

2.4.3 Force curves in bulk ILs

The interfacial behaviour of a bulk of the ionic liquids [Bmim][Tf_2N] and [Bmim][PF_6] in contact with solid surface has been studied.

The measurements have been performed using the Nanoscope IV Multimode quartz fluid cell, carefully washed in ethanol and methanol and dried under nitrogen flux just before the use. Standard contact mode silicon probes with sharpened tips have been used, and washed in methanol immediately

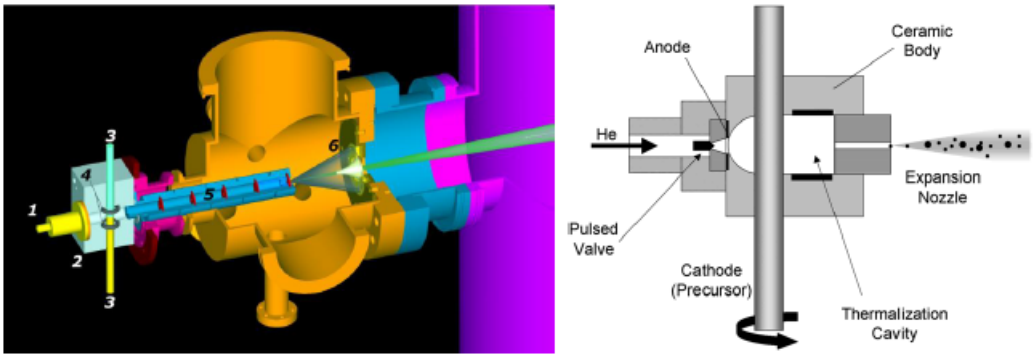

Figure 2.12: *Scheme of the pulsed microplasma cluster source and of the expansion chamber (left–hand side) and detail of the PMC source (right–hand side).*

before the use. We wanted to replicate all the experimental details of the measurements of Atkin et al.[77, 76, 78]. All the force constants of the tips used in the experiments reported in this thesis work have been calibrated by thermal noise revealing $k \sim 0.2N/m$.

Prior to those measurements the ionic liquids have been kept in ultra high vacuum ($1 \cdot 10^{-6}$mbar) for some days. The measurements have been performed dropping a microlitre drop of the pure ionic liquid onto the freshly cleaned solid substrate (mica or silicon, cleaned as described previously). Before the beginning of the measurements, usually the system is left to thermalise for at least half an hour.

In this kind of investigation force curves have been performed approaching the substrate with the tip into the bulk of ionic liquid. Normally, the force curves are acquired in different point along the surface and for each point 10 to 50 curves are performed. The length of the ramp is typically between 50nm and 400nm, and the approaching velocity ranges between 5nm/s and 80nm/s, while the retracting velocity is usually 2 to 3 times higher in order to reduce the acquisition times.

2.5 Supersonic cluster beam deposition

Some very important preliminary measurements have been carried out depositing [Bmim][Tf_2N] onto nanostructured silica (sn–SiO_x). In particular two depositions, one sub–monolayer deposition on oxidised silicon and a complete nanostructured film with thickness of 32±2nm have been used as substrates. Those films have been deposited with use of an Supersonic Cluster Beam Deposition (SCBD) apparatus equipped with a pulsed microplasma

cluster source (PMCS) as described in detail in Refs [10, 11, 12] (the scheme of the apparatus is reproduced in Figure 2.12). The PMCS operation principle is based on the ablation of a conductive rod (in this case highly doped silicon) by a helium or argon plasma jet, ignited by a pulsed electric discharge[10, 12]. After the ablation, Si ions thermalise with helium or argon and condense to form clusters. The mixture of clusters and inert gas is then extracted in vacuum through a nozzle to form a seeded supersonic beam, which is collected on the surface of the oxidised silicon pieces intercepting the beam. The clusters kinetic energy is low enough to avoid fragmentation and hence a nanostructured film is grown. Cluster mass distribution is affected by the carrier gas: typical mass distribution with He as carrier gas is log–normal and it peaks at several hundreds atom per cluster, corresponding to a diameter of roughly 1nm. The use of Ar shifts the distribution toward larger masses[11]. The as–deposited material is poor of oxygen; however, it is oxidized very quickly as soon as it is exposed to air.

Chapter 3

Results and discussion

In this chapter the results obtained during the study of ionic liquid/solid interfaces will be exposed. First of all a survey of the morphologies found in the different depositions on the various substrates is presented, and then the qualitative differences among samples produced on different substrates and/or with different solvents will be highlighted. Then the results of the quantitative morphological and mechanical analysis will be reported. At the end of the section first results obtained by using Scanning Electron Microscopy (SEM) are shown.

The second section will be devoted to the discussion of the results and their comparison with the available literature. Results of numerical simulations performed by Pietro Ballone et al. in collaboration with our group will be presented and compared with experimental results. Some preliminary results on ionic liquid depositions onto nanostructured surfaces will be discussed.

At the end of the chapter some perspectives are reported.

3.1 Presentation of the results

3.1.1 Overview on AFM morphological images

During my PhD work I devoted particular attention to 4 main substrates: silicon/doped silicon covered by its native oxide, amorphous silica, mica and HOPG graphite. Few preliminary depositions have also been realised on other substrates, i.e. on gold and on TiO_2, MgO and NaCl single crystals. The first four substrates are typical substrates suitable for an AFM investigation because they are smooth over extended areas and chemically inert. Furthermore, silicon is a material whose used is very diffused in applications

in which ionic liquids can be used, like in micro or nano electromechanical devices. Gold is an interesting substrate because it is a non reactive material and furthermore some studies on the IL/gold interface have already been performed[72, 76], so can be the subject of useful comparison. For the moment on this surface have been performed only preliminary tests. TiO_2, MgO and NaCl single crystals are other examples of insulating flat substrates. In particular TiO_2 is of direct interest because it allows to see the behaviour of the ionic liquids on the surface of the material that is currently used in DSSCs. The flat surface of this TiO_2 allow an easy AFM investigation and furthermore can be used to have a reference for looking at the role of the substrate roughness on the morphology of the deposition, because nanostructured TiO_2 can be directly synthesised in our lab by supersonic cluster beam deposition.

My work is based on the AFM investigation of thin IL films, so a great part of the work, especially in the beginning, has been devoted to the extensive exploration of samples via the acquisition of morphological maps. Some maps resulting from that investigation are reported in order to show how [Bmim][Tf_2N] thin films re–structures in contact with the different substrates.

Figure 3.1 shows a collection of the typical morphologies that can be found on amorphous silica. Amorphous silica, in my experiments used in the form of thin coverslips, is a smooth substrate having roughness lower than 0.3nm over some μ^2. The silica surface, as the surface of the oxides in general, it is covered by OH groups and at ambient conditions, so in the presence of water, some OH groups dissociate leading a neat negative charge (1 charged site per $20nm^2$ in water at neutral pH[77]).

As it can be noticed in the image a) the structure of the ionic liquid is not homogeneous, in the sense that flat layers coexist with nano- and mciro--droplets (white rounded features). In the images b), c) and d) it is possible to see how ordered structures composed by a superposition of flat terraces, can grow to remarkable thicknesses, sometimes exceeding 50nm.

The oxidised silicon is the substrate where the highest number of depositions and characterisations have been performed (Figure 3.2). The characteristics of oxidised silicon are fundamentally the same than those of amorphous silica. The difference is that single crystal silicon is almost an atomically flat surface. The native oxide layer, that is just 1–2nm thick is likely to grow in an ordered fashion, so leading to a more uniform surface compared to the surface of a coverslip. Furthermore silicon is more versatile because can be directly cut from wafer in pieces with the desired dimension. In this way can be used substrates big enough to avoid the pinning of the drop of solution at

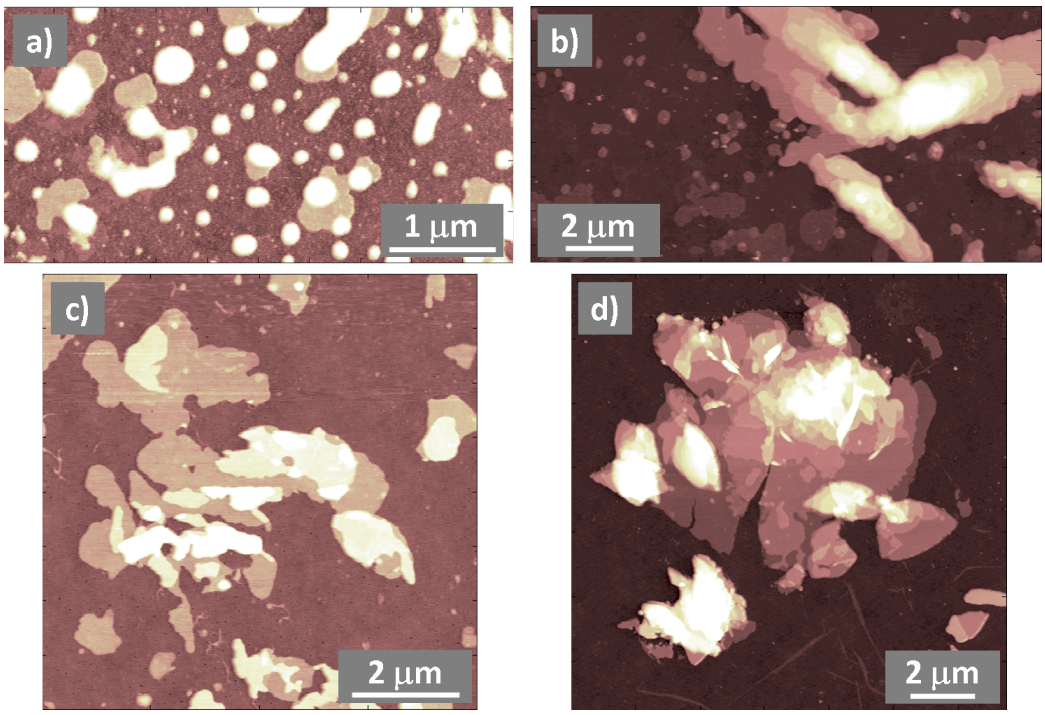

Figure 3.1: *AFM morphological maps of [Bmim][Tf_2N] on amorphous silica. Vertical scales: a) 10nm, b) 55nm, c) 15nm and d) 50nm.*

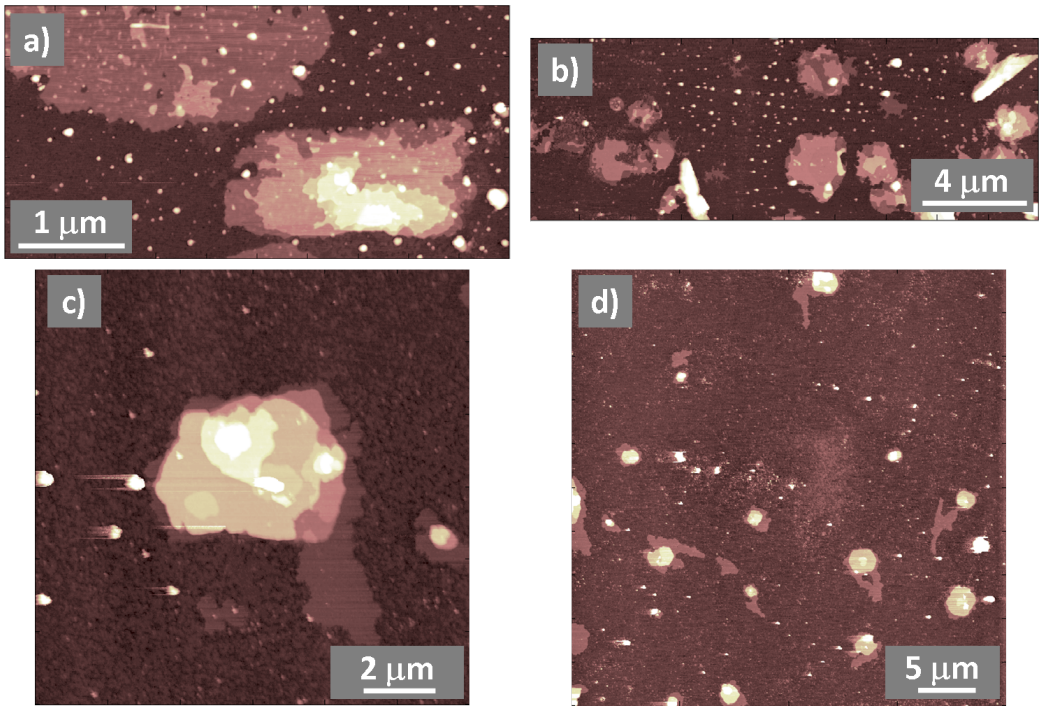

Figure 3.2: *AFM morphological maps of [Bmim][Tf_2N] on oxidised silicon. Vertical scales: a) 25nm, b) 35nm, c) 10nm and d) 10nm.*

the borders and obtain more reproducible depositions.

Also on this surface, even if usually area with more terraces than liquid domains are selected for the imaging, liquid droplets appear to coexist with highly ordered lamellar structures. The ordered structures can have diverse lateral and vertical sizes, and have different shapes.

Figure 3.3 reports the results of [Bmim][Tf_2N] deposition on mica. Mica (in particular I used muscovite mica) is a mineral formed by superimposed lamellas. Tetrahedral layers of $(SiAl)_2O_5$ surround a layer of $Al_2(OH)_2$. Successive layers composed in this way are separated by a single layer of K^+ cations. The process of stripping breaks the structure on the plane of K^+ cations, leading to extended atomically flat regions. In the presence of water some potassium ion can dissociate, leaving a neat negative charge on the surface. This charge density on mica is greater than on silica surface 1 charged site per 0.48nm^2 in water at neutral pH[77]).

As can be noticed, even this substrate is covered by the ionic liquid structured in two different phases, i.e. liquid phase and highly ordered phase. In particular, from Figure 3.3 it is clear how the liquid droplets can form on

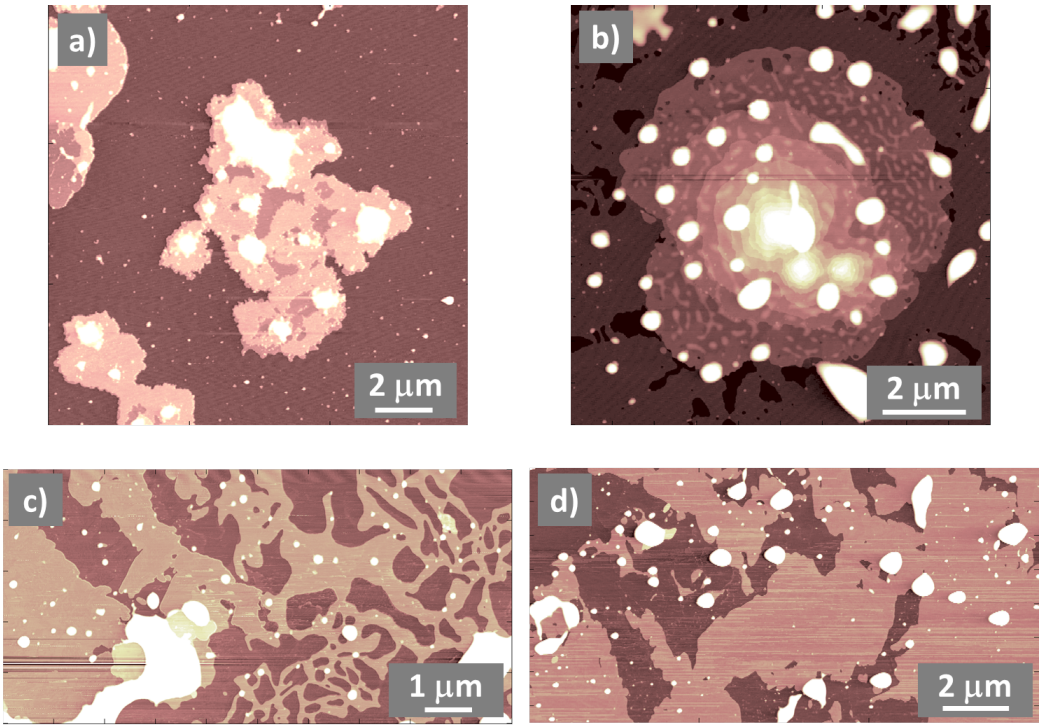

Figure 3.3: *AFM morphological maps of [Bmim][Tf_2N] on mica. Vertical scales: a) 25nm and b) 55nm.*

both the substrate, or on top of ordered layers. On mica the lateral extension of the layers can be higher than on all the other substrates checked, exceeding 50μm, as will be further remarked later in the text. Similarly to what found on glass and oxidised silicon, even on mica very thick ordered structures can form (see Figure 3.3 b)), although on mica there is a propension to form extended single terraces.

Graphite is one of the most common forms of carbon and is composed by superimposed atomic layers heaving an hexagonal structure. Usually graphite is composed by small domains with random orientation. Highly ordered pyrolityc graphite (HOPG) show extended ordered domains. As in the case of mica, stripping leads to the exposure of cleaned and extended atomically flat domains, very suitable for an AFM investigation. The single planes of the graphite are electrically conductive (graphite is a semi–metal), so the ions of the ionic liquid will induce image charges on the surface, but no fixed charges will reasonably sit on it. For this reason it is reasonable to expect a different behaviour of the ionic liquids on graphite respect to insulating surfaces.

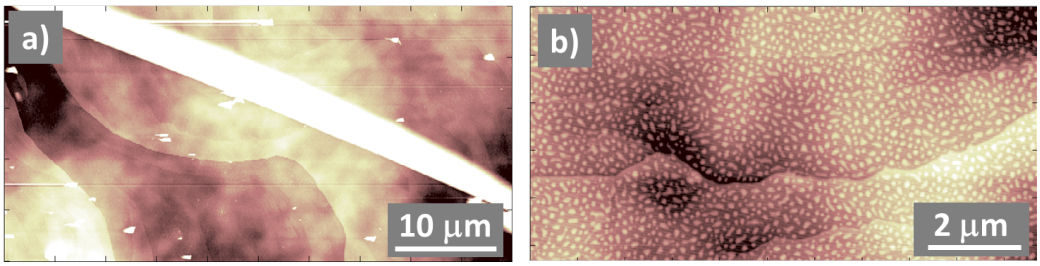

Figure 3.4: *AFM morphological maps of [Bmim][Tf_2N] on HOPG graphite. Vertical scales: a) 80nm and b) 20nm.*

Figure 3.4 a) shows a wide scan of a deposition of [Bmim][Tf_2N] on graphite. Differently with respect to previous cases, nothing but graphite planes and nanometric rounded domains can be found. In b), a magnified view of the surface shows how nothing resembling the ordered layers found on the other surfaces can be clearly detected, while only very small droplets cover the substrate surface.

The images shown before evidence how the general behaviour of thin layers of [Bmim][Tf_2N] on solid surfaces is to develop two coexisting phases, a liquid phase in which the IL forms micro–/nano– –droplets, and a more structured phase, where the IL molecules show an high degree of ordering, at least in the direction perpendicular to the surface. The only substrate, on which the ionic liquid doesn't form ordered domains is HOPG.

In what follows I will enter in more details about similarities and differences of the morphology of ionic liquid depositions on different substrates, and then also using different solvents. I will manly focus the attention to the highly ordered domains.

3.1.2 Morphological study of highly ordered layers

As seen in the previous images, due to method of deposition, i.e. the drop casting technique, even on the same substrate, different topographies can develop. Nonetheless, due to the extensive AFM morphological characterisation performed, it is possible to understand which are the typical morphologies to expect for on the different substrates, as shown in In Figure 3.5.

First of all, it has to be underlined that in the morphological maps, it is possible to distinguish clearly the liquid and highly ordered domains. At the first order, the liquid domains are identifiable because of their shape, as can be understood looking at 3D morphology in Figure 3.6. Furthermore, those identified as liquid domains often look noisy when scanned in tapping mode:

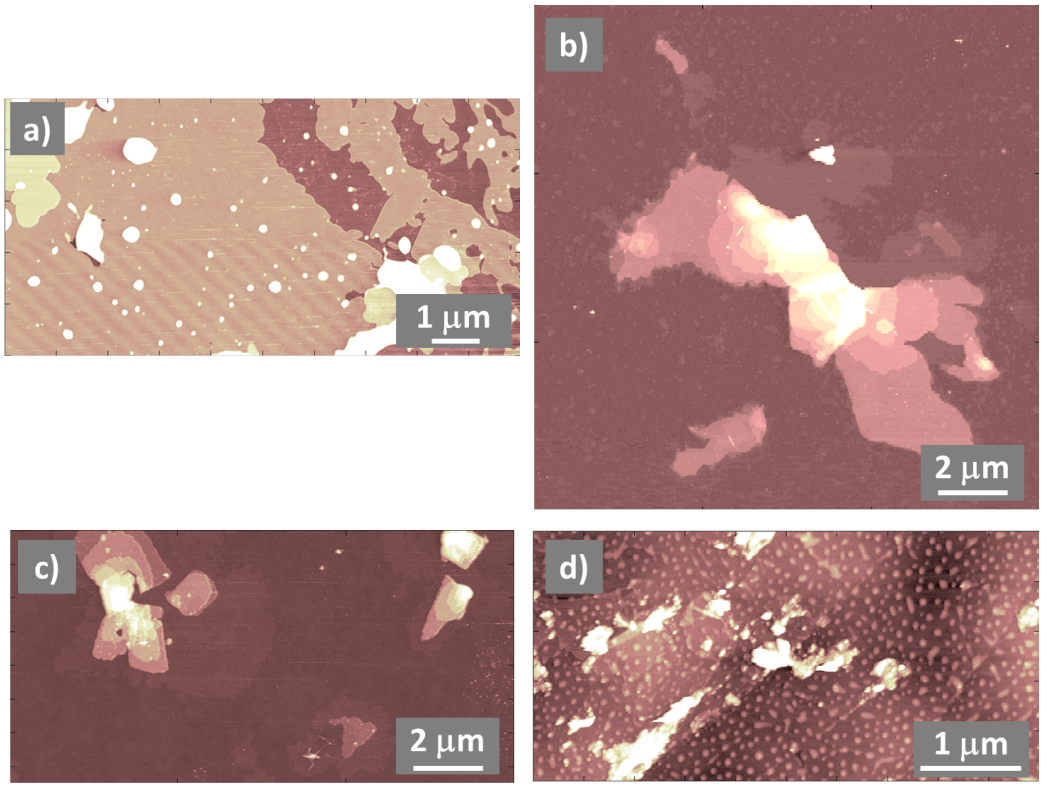

Figure 3.5: *AFM morphological maps of a) mica (vertical scale 20nm); b) oxidised silicon (vertical scale 70nm); c) amorphous silica (vertical scale 40nm); d) HOPG graphite (vertical scale 25nm).*

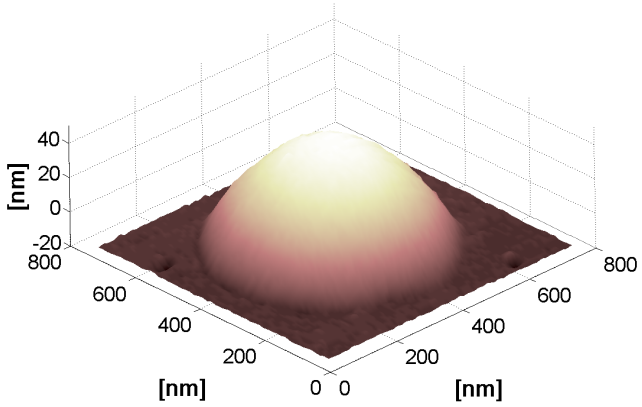

Figure 3.6: *3D morphology of a nanodroplet of [Bmim][Tf_2N] on amorphous silica drop casted with methanol.*

this happens because of a strong interaction between the tip and the liquid, often causing the formation of liquid necks bridging the tip to the droplet.

The other phase found appears in the form of flat layers, following the morphology of the substrate, and their surface is typically uniform, featureless. The edges of those ordered domains are steep and usually their profile is uneven, even if sometimes layers with more defined geometries have been observed (see Figure 3.10 below in the text). Ordered flat layers can have an in–plane extension of several microns or even tens of microns and can be more than 50nm thick. Those structures are usually composed by superimposed terraces, in a ziggurat–like arrangement. The thickness of each single terrace ranges from fractions of nanometer to about 10 nanometers. Layer thickness of 2–6nm is typical. On top of layers it is possible to find nano–droplets; also interfacial layers located at the bottom boundary between a droplet and the solid substrate are somtimes found.

The ordered structures are quite tightly bound to the substrate, in fact they are stable against repeated scanning. If scanned in tapping mode, the islands show only slight erosion at the borders after many scans, whereas in contact mode, where higher lateral forces are applied, the structures can undergo to delamination. Furthermore even if the pressure applied in tapping mode is increased changing the amplitude of oscillation, or the trigger force is increased in force volume mode, there is no evidence of any change in thickness measured: the layers behave like solid under the AFM tip.

Another remarkable aspect of the thin ionic liquid depositions, is their stability in time. In fact, qualitatively the morphology doesn't change in time, keeping the coexistence of the liquid and ordered phases for more than

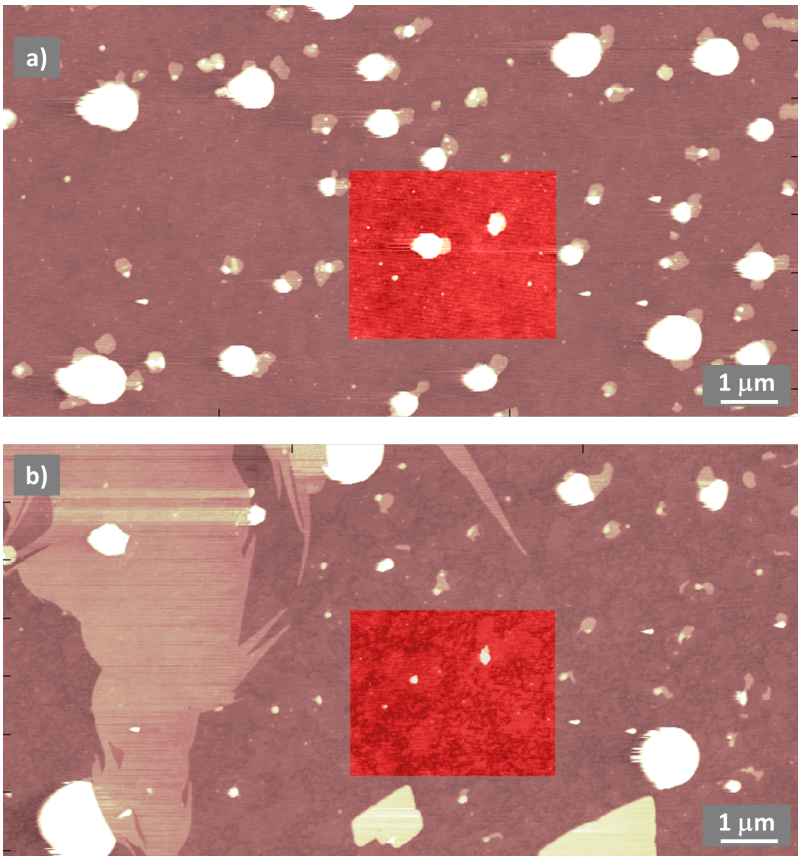

Figure 3.7: *[Bmim][Tf_2N]/methanol on amorphous silica. The top topography has been acquired 5 days after the one at the bottom. A decrease in the number and size of droplets and an increasing in lateral extension of ordered domains is clearly recognisable. Vertical scales 20nm.*

several months. If the same region of the sample is monitored for few days, generally an increase in lateral size of the ordered domains and a reduction of the size of the droplets can be observed. The bottom image in Figure 3.7 has been acquired5 days after the top one. It can be noticed that there have been a clear reduction of the volume of the droplets; in particular the reduction in the volume of the 4 bigger droplets on the left is compatible with the volume of the ordered layer grown. Moreover, the regions around the islands, i.e. what is believed to be the exposed substrate surface, became more textured, as can be seen in the highlighted regions of Figure 3.7. Despite relatively short–time evolution of the interfacial domanis, the same ordered structures can be seen after several months if not years, the upper limit being the duration of a PhD.

Despite their durability and mechanical stability, if samples are rinsed with the same solvent used in the deposition (and probably also with others solvents), usually the deposit is removed. If the rinsed surfaces are scanned with AFM. no traces of any chemical erosion by the liquid can be noticed. The chemical inertness of [Bmim][Tf_2N] on silicon is further confirmed by XPS analysis performed on a silicon substrate washed in methanol after that a bulk of IL was kept in contact with its surface for few days.

Qualitative differences among different substrates and solvents

Drop casting is a deposition technique that allows to realise very thin depositions, but details like the rate of evaporation, the pinning of the drop of solution to the edges of the substrate and many others, are difficult to control and to reproduce identically every time. Moreover, it is also difficult, if not impossible, to clean the substrate perfectly (contamination can determine pinning of solution droplets and/or inhibition of domain formation). As reported before, on every insulating surface checked, it is possible to identify liquid and highly ordered phases, but the distribution of the features and the morphology of the terraces can vary from sample to sample. Anyway, this doesn't prevent to draw some general considerations about differences that can be observed on different materials or if the media in which IL is dissolved is changed (in what follows the attention will be devoted only to those substrates where ordered structures and not only liquid IL droplets could be clearly identified).

The first thing that can be noticed is that the more regular and flat the surface is, the more regular and uniform will be the deposition. In fact, usually the samples produced on coverslips (amorphous silica), show the same features as on oxidised silicon, but they are more randomly distributed.

Figure 3.8 shows the topography of two depositions realised on oxidised silicon and mica. Nothing like the very extended layers developing on mica can be obtained on silicon, no matter the concentration of IL in the solution: on mica some layers can extend for more than 50μm. Moreover, the shape of the ordered domains on oxidised and amorphous silicon appear more regular than on mica, where the layers look more branched.

In order to clarify the possible role of the solvent used in the formation of the ordered domains, in addition to methanol, the first solvent used, ethanol and chloroform have been tried. Since oxidised silicon has been the most extensively studied surface, because it is easier to cut it in the size desired and its surface is very smooth, different samples have been deposited on this substrate, with both ethanol and chloroform, and to representative images can be seen in Figure 3.9. With both solvents there is still the development

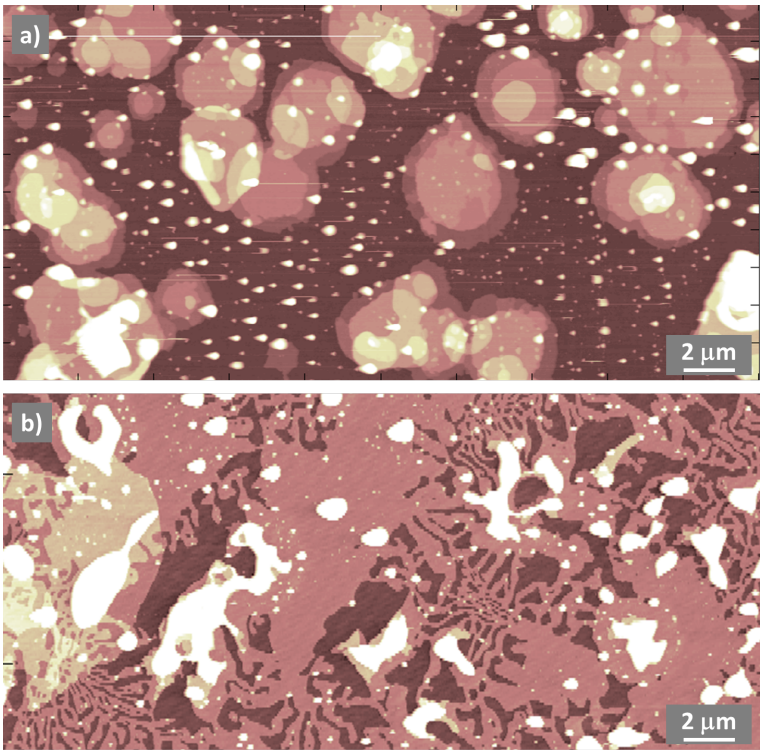

Figure 3.8: *[Bmim][Tf_2N]/methanol on a) oxidised silicon (vertical scale 35nm); b) mica (vertical scale 25nm).*

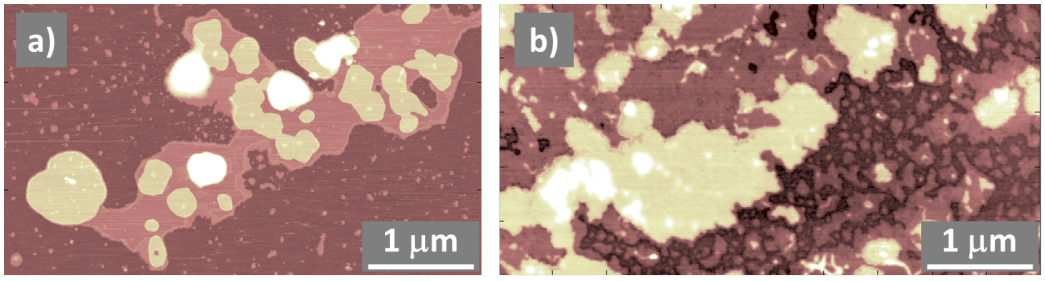

Figure 3.9: *a) [Bmim][Tf_2N]/ethanol on oxidised Si; b) [Bmim][Tf_2N]/chloroform on oxidised Si.Both vertical scales are of 10nm.*

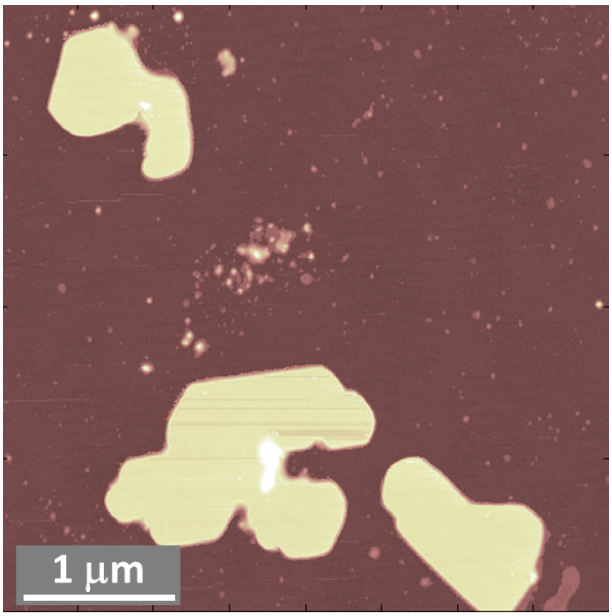

Figure 3.10: *[Bmim][Tf_2N]/ethanol on oxidised Si. Vertical scale 15nm.*

of the liquid and highly ordered phases, as with methanol. What it has been observed, is that in general not many thick islands can be grown using chloroform, whereas ethanol develops almost the same features than methanol. One peculiar aspect of ethanol, is that often it provides islands more regular in shape, as can be appreciated in Figure 3.10

Some preliminary depositions has been performed also on TiO_2, MgO, gold and NaCl. The fact that on all those very different surfaces, both morphologically and chemically, ordered layers are formed, allows to appreciate that terraced structures are quite ubiquitous. Furthermore, looking to Figure 3.11, it can be noticed the capability of the ordered layers to adapt their morphology to that of the substrate. On TiO_2 it is possible to see how an edge of the island follows the profile of a scratch produced by the surface polishing. The same behaviour can be seen also on MgO, where the track of the scratches can be seen under the islands also. Whereas on TiO_2 the typical features are similar to what can be found on silicon or amorphous silica, on MgO some vermicular structures appear together with droplets and flat layers. Furthermore, the surface of some terraces is not flat, but some elongated flat strips sit on top of them. The only deposition performed on NaCl shows how even on this surface, ordered layers can be formed. Here it is more troublesome to distinguish ionic liquid ordered layers, because the NaCl surface has a layered aspect too. The ionic liquid layers have been

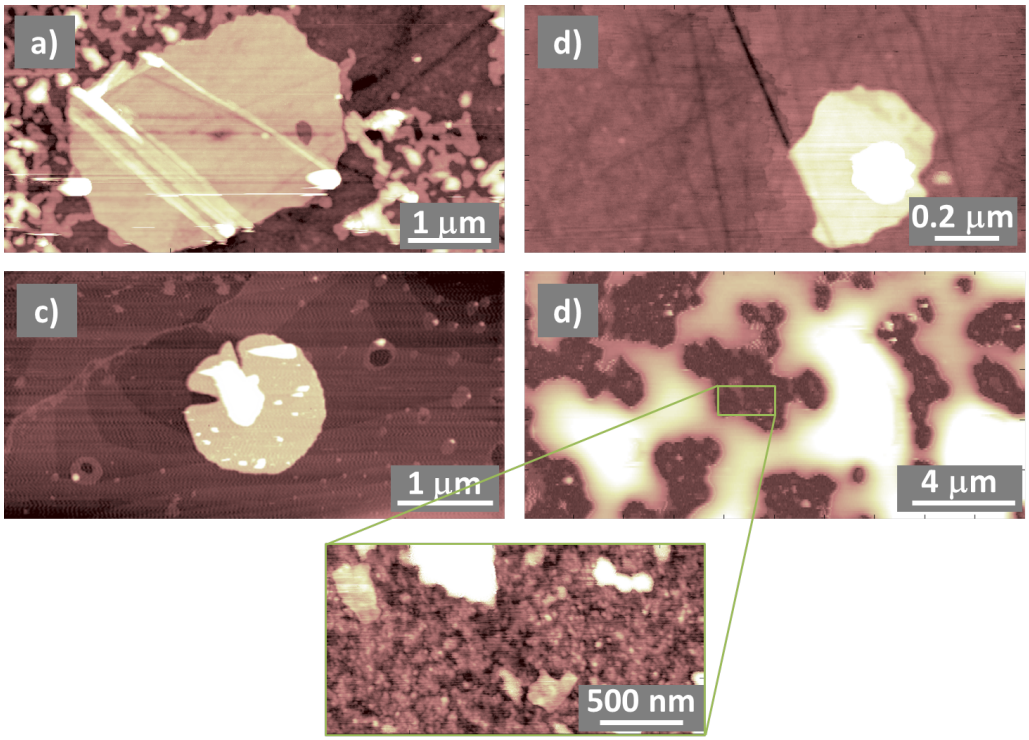

Figure 3.11: *Surface morphology of [Bmim][Tf_2N] on a) single crystal polished MgO (ethanol solution, vertical scale 20nm); b) single crystal polished TiO_2 rutile (methanol solution, vertical scale 10nm); c) single crystal NaCl (ethanol solution, vertical scale 10nm); d) gold (methanol solution, vertical scale 100nm). The magnification shows ordered layers between liquid domains on gold (vertical scale 10nm.*

identified by force curves, as only the curves acquired in the centre of Figure 3.11 c) show indentation.

The gold used as substrate for deposition has a nanostructured surface. This surface looks very wettable by [Bmim][Tf_2N], as witnessed by the fingered shape of the droplets in Figure 3.11 and by the fact that they are quite flat. In the inset of Figure 3.11 it can be seen how, even in this case, structures qualitatively similar to those found on the other substrates develop, and how they follow the morphology of the surface below them. It is interesting to notice that the nanostructured character of the gold surface doesn't prevent the formation of the ordered domains; we will see later that this is also true on other nanostructured surfaces.

The study of the role of the substrate roughness is important in order to understand how surface topography affects the morphology of the first

interfacial layers of ionic liquid. Flat surfaces are fundamental to understand the behaviour of thin IL layers because they are easier to study by the great part of experimental techniques as well as theoretically, but textured surfaces are used in devices like Grätzel cells or electrochemical capacitors. For those reasons, preliminary studies of the interaction of ILs with nanostructured surfaces have been done. It has been decided to deposit nanoparticles of SiO_x on oxidised silicon, because it gives the possibility to see the effect of the roughening of an already studied substrate. On the first substrate a sub–

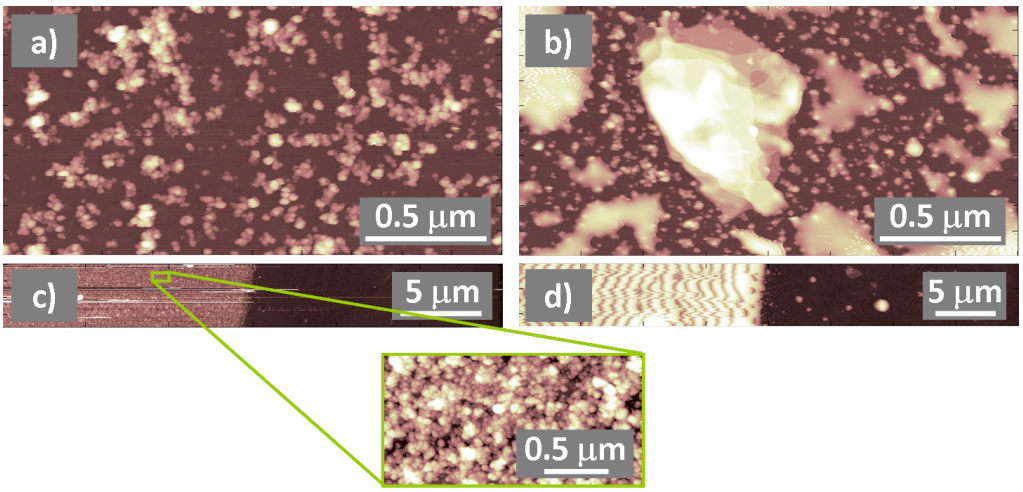

Figure 3.12: *a) Sub–monolayer deposition of silicon oxide nanoparticles on silicon (vertical scale 50nm); b) [Bmim][Tf_2N]/methanol on the sample represented in a), (vertical scale 50nm); c) Step in a 32nm thick deposition of Ns-SiOx on silicon (vertical scale 155nm); d) [Bmim][Tf_2N]/methanol on the sample imaged in c): the regular pattern in the left of the image is due to an unstable imaging induced by the ionic liquid that permeate completely the nanostructured film. (Vertical scale 155nm).*

monolayer of SiO_x particles has been deposited, whereas another sample has been covered for an half by a 32 ± 2nm thick nanostructured film. As it can be seen in Figure 3.12 a) and b), the presence of nanoparticles on the surface of silicon doesn't prevent the formation of highly ordered structures, that are found to be quite densely distributed on the surface. Looking at the liquid part of the deposition, it can be noticed that the shape of the droplets is very uneven and determined (pinned) by the silica nanoparticles distribution. This is not surprising because the [Bmim][Tf_2N] wets very well the silica surface (direct measurements of contact angle of [Bmim][Tf_2N] on different substrates by AFM imaging have been performed, see App. B); for the same reason the samples where few monolayers of silica nanoparticles

Data set	**Silica (met)**	**Silica (met, CM)**	**Si (met)**
δ **[nm]**	0.61 ± 0.01	0.59 ± 0.01	0.61 ± 0.01
Data set	**Si (etOH)**	**Si (chloro)**	**Mica (met)**
δ **[nm]**	0.60 ± 0.01	0.59 ± 0.01	0.60 ± 0.01

Table 3.1: *Fundamental multiples δ calculated for each data set. All the set of data have been collected from maps acquired in tapping mode, a part the one in the second column (Silica (met, CM)), where the microscope was operated in contact mode (CM). The abbreviations met, etOH and chloro has been used respectively for methanol, ethanol and chloroform.*

has been deposited, it is not possible to acquire meaningful AFM images. In Figure 3.12 c) it is possible to see the nanoparticle film on the left and the substrate on the right and in Figure 3.12 d) the same sample has been observed after IL deposition: the nanoporous matrix is completely permeated by the IL, and the strong interaction between the IL and the tip impede a stable acquisition, as evidenced by the regular noise in the left part of the image, whereas on the right side is possible to observe the usual morphology.

Quantitative structural analysis

AFM three–dimensional topographies allow to extract quantitative information about the structure of [Bmim][Tf_2N] films. From AFM morphologies it is possible to hypothesise that every terrace composing a layered structure could be the result of the regular vertical arrangement of a molecular fundamental layer having thickness δ, as shown in the scheme in Figure 3.13. For each of the most studied surfaces where ordered layers develop, (amorphous silica, oxidised silicon and mica), and for each of the three solvents used, (methanol, ethanol and chloroform), terrace heights have been measured by using a statistical approach, based on the analysis of the height histograms. Figure 3.13 shows a 3D AFM morphology of an ordered structure with its histogram of the heights. As described before, on flat substrates the terraces which compose the layered structures are also flat, so they give rise to sharp peaks in the histogram. The best submultiples δ found for each set of data are reported in Table 3.1.2. Figure 3.14 reports the correlation between average terrace heights for all the datasets and the number of basic steps in each terrace, obtained by fitting structural data. The values in Table 3.1.2 are all very close to each other, even if substrate or solvent are changed. This means that the ordered structures, that have been seen to grow on the great part of the substrates and with different solvents, keep the same structure, at

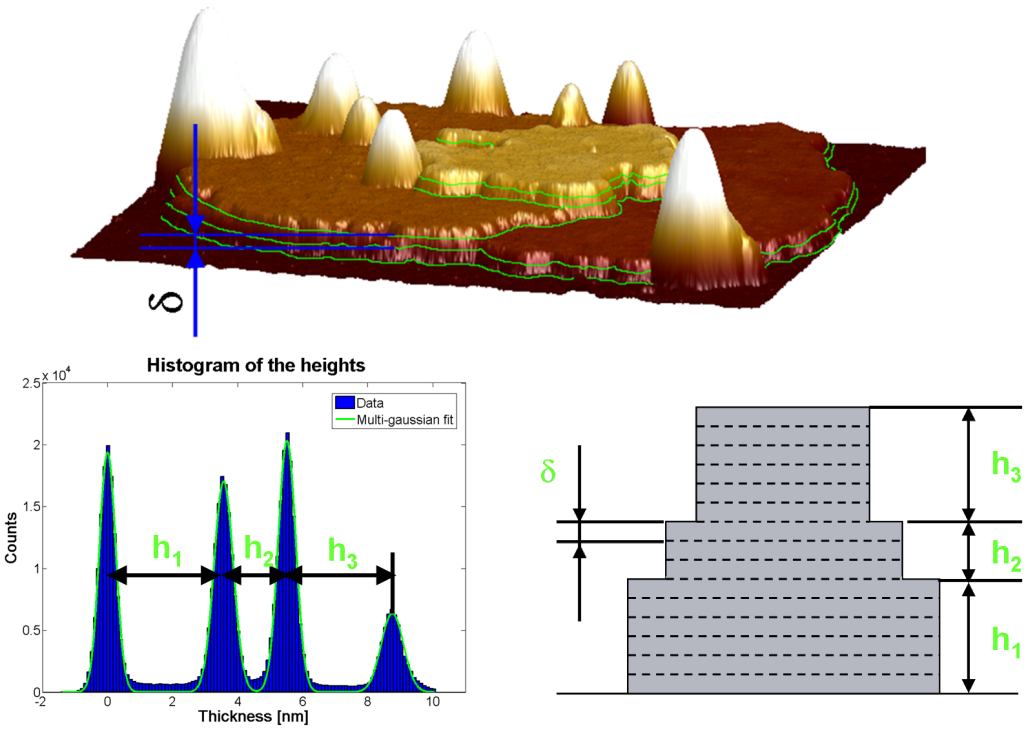

Figure 3.13: *3D AFM morphology of a layered structure on oxidised Si (2.2 μm, vertical scale 35nm) and the corresponding histogram of the heights. On the AFM image the green lines are drawn in order to show the supposed internal structure of each layer, composed by vertically superimposed fundamental layers of thickness δ. At the bottom rigth is shown a scheme of the presumed structure of a generic ordered terrace.*

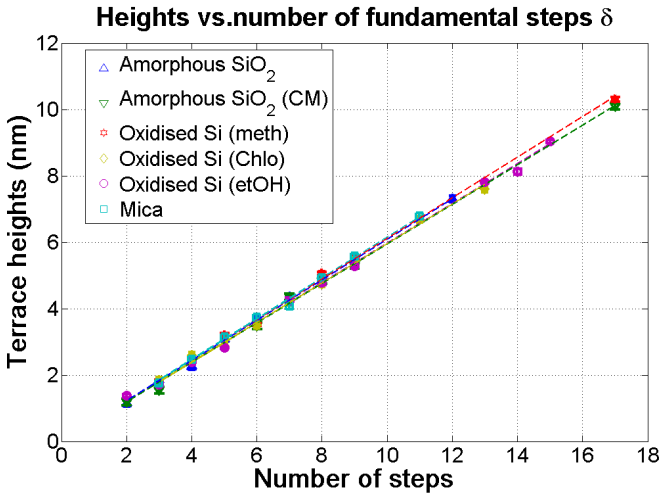

Figure 3.14: *Correlation between average terrace heights measured on different surfaces and the number of basic steps in each terrace, obtained by fitting structural data (error bars are comparable to marker size).*

least in the direction perpendicular to the surface. The fact that compatible δ are found for each solvent used, suggests that probably the solvent has not a structural role in the formation of the ordered layers, i.e. it doens't act as a networking agent. Furthermore, it is important to underline how the value of δ found on silica in contact mode, is compatible with all the others, calculated from data extracted from images acquired in tapping mode. This was not necessarily to be expected because the forces applied to the islands by the tip in the two modes are very different. Furthermore, this again show that those islands are quite stiff, and behave as solid–like entities.

The most probable fundamental step common to all the set of data, is $\delta = 0.6nm$ (see Sec. 3.2 below). This value is in very good agreement with the results of a numerical simulation performed by Prof. Pietro Ballone[98] (the paper is reported in App. B). In that simulation a slab of ∼4nm of [Bmim][Tf_2N] was placed in contact with a silica surface, showing strong density oscillations whose intensity decrease moving away from the substrate and whose periodicity, that doesn't depend on the temperature in the range 300K–400K, is $\delta = 0.6nm$.

3.1.3 Mechanical tests on highly ordered layers

Besides appearing very regulary ordered in the vertical direction, IL islands respond during imaging in both TM and CM like stiff undeformable structures. In order to further check the surprising mechanical stiffness of

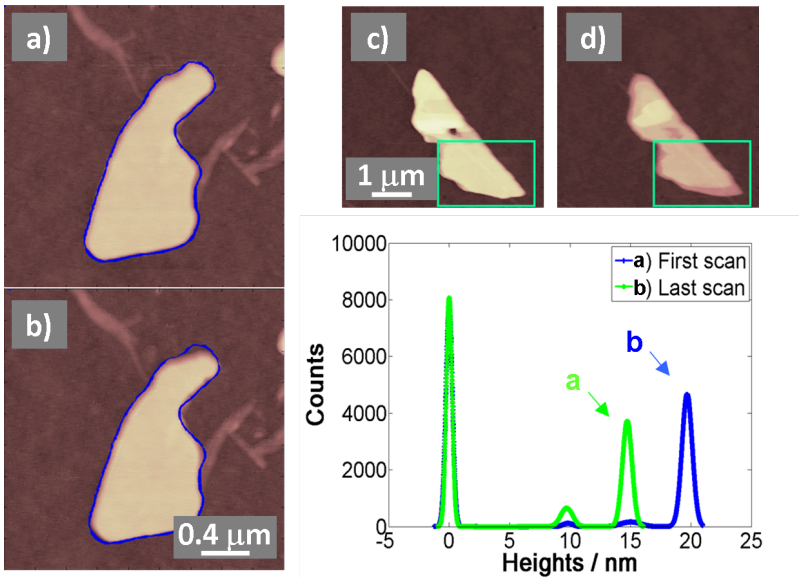

Figure 3.15: ***Left–hand side**: effect of 10 repeated scans in tapping mode on an ordered layer: only a very small erosion has been produces (vertical scales 20nm). **Right hand side**: repeated scanning in contact mode (4 scans, vertical scales 35nm), induces an evident consumption by eroding the borders and removing the top layers from the island, as is evidenced by the envelopes of the histograms of the heights of the 2 images.*

the highly ordered structures, several nano–mechanical tests have been performed.

Resistance to in–plane forces

When ordered layers are imaged in tapping mode, i.e. the modality that I generally used in my work, they are stable against repeated scanning. If the same area is scanned for several times, nothing but a limited erosion at the edges of the terraces can be seen (see left hand–side of Figure 3.15). The edges of those terraces are usually very steep, so due to finite response time of the AFM feedback loop, they are the part subjected to the action of the highest lateral forces, and furthermore the edges are also the most fragile regions. Observation of little erosion, mostly concentrated at the edges of IL domains, is consistent with the picture of a rather stiff structure.

Even when the microscope is operated in contact mode, highly ordered layers are not easily destroyed. However Figure 3.15, shows that their erosion proceeds by delamination, i.e. by removing each subsequent terrace, as could be expected for a lamellar solid.

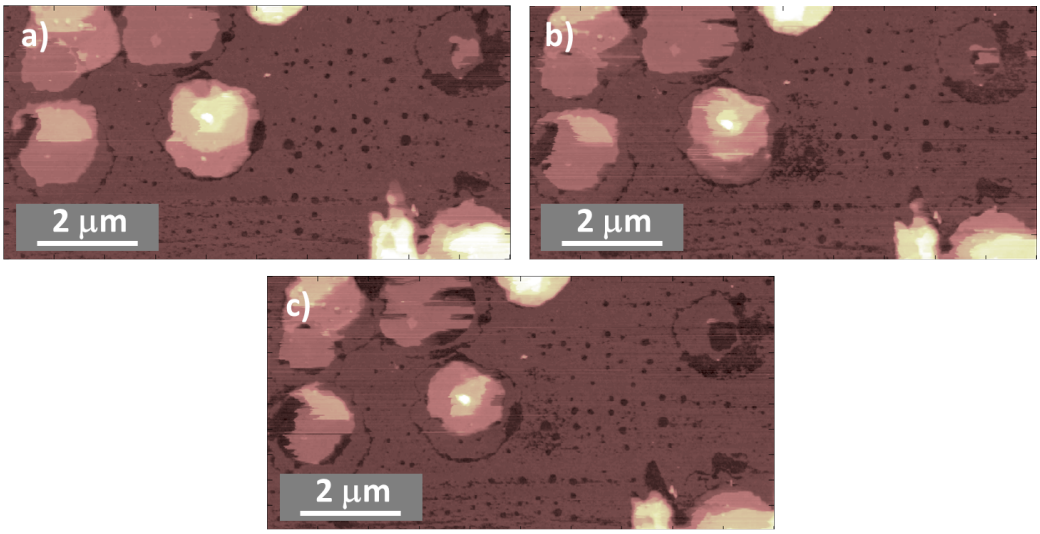

Figure 3.16: *AFM morphologies acquired in contact mode on [Bmim][Tf_2N] on oxidised silicon. The scanning tip erodes the structure starting from the most delicate edges and removing terrace by terrace. It is interesting to note how in the part of the images between the islands seems to sit a very extended bottom layer with a thickness of ∼2–3δ. Vertical scales 25nm.*

The evolution of the structures under the effect of subsequent scans in CM can be appreciated in Figure 3.16. From a) to c) it is evident how the lateral size of the ordered domains decreases under the action of the scanning tip, but also how terraces on top of other layers are peeled off and the erosion proceeds removing lamella by lamella. It is interesting to note, as it will be further discussed in the following section, that between the individual islands and after the erosion also around and below them, there are some holes whose depth is compatible with 2–3 molecular layers. The rounded holes are probably liquid droplets in which the scanning tip pass through, and could be in principle accounted for as artefacts induce by the different environment felt by the tip inside and outside them. Anyway, the other irregular scratches formed by the tip action have the same depth. This seems to indicate that when a sample is deposited by drop casting, diffused layers with a thickness of few δ, can be formed on the surface and that they can be very extended. Furthermore the Figure 3.16 shows also, as will be seen in the next section too, how many droplets are not sitting on the top of the diffused layer but on what can reasonably be the substrate. This can indicate that both the layer was already formed but once the droplets stack on it they melt the ionic liquid below till the substrate, or that the bottom layer growth after the deposition of the droplets, and from them by means

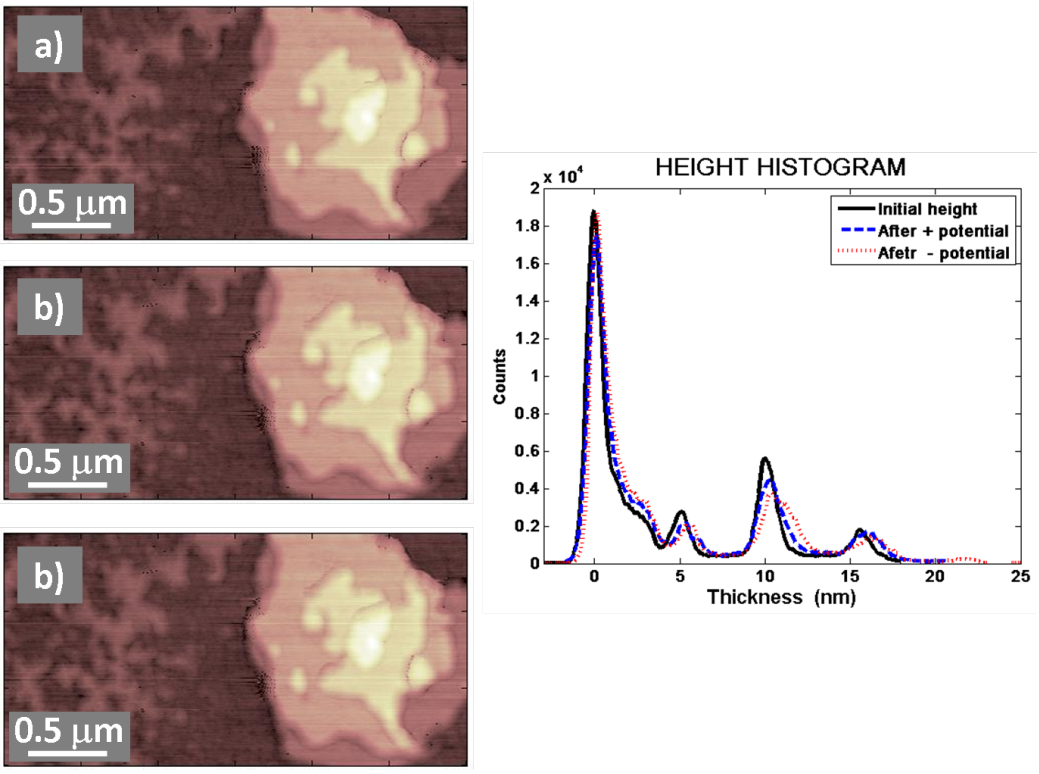

Figure 3.17: *Effect of strong electric fields on a thin [Bmim][Tf_2N] deposition. All the images have been acquired in neutrality conditions. Image a) is the first image. Image b) it has been acquired after 1 scan in applying ΔV=+8V. Image c) has been acquired after a scan at ΔV=-8V, (vertical scales 26nm). On the right–hand side the envelopes of the histogram of the heights of the images show that no quantitative changes in the structure of the ordered layers took place.*

of diffusion of the ions along the surface.

Resistance to strong electric fields

Beyond normal topographic maps, some areas of the samples have been scanned for several times applying a potential difference between the tip and the substrate. The small distance between the 2 electrodes, leads to the development of very strong electric fields, E$\sim 10^9$V/m. If the ions in the ordered layers, as suggest by their behaviour under imaging, were more tightly bound than in the liquid droplets, a different behaviour under the action of the electrostatic field is expected, as will be shown in the following. The study of the effect of strong electrostatic fields on the ionic liquid deposition, was usually performed in this way: first both the tip and the sample were

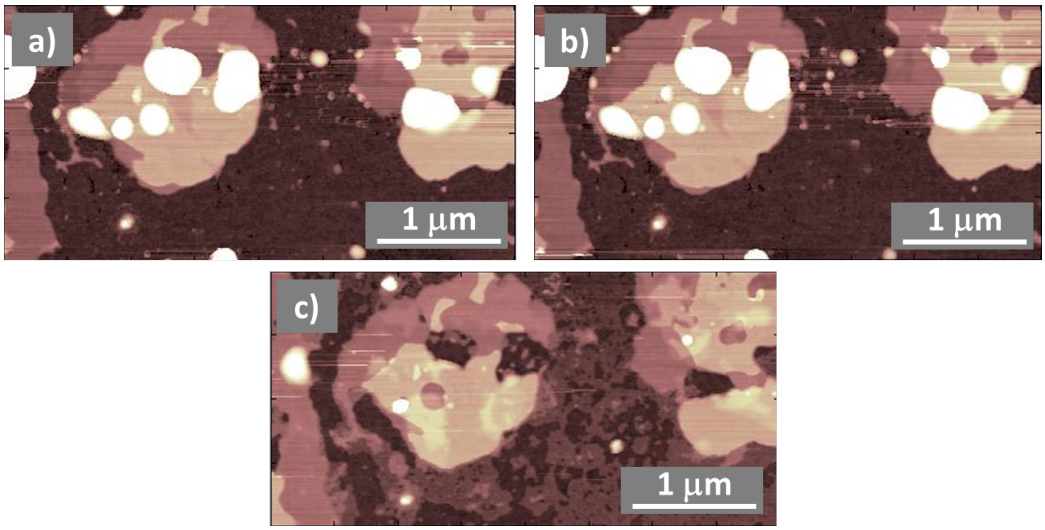

Figure 3.18: *Effect of strong electric fields on a thin [Bmim][Tf_2N] deposition. All the images have been acquired in neutrality conditions. Image a) is the first image. Image b) has been acquired after 3 scans in neutrality conditions. Image c) has been acquired after a scan at +8V, (vertical scales 20nm). The images evidence the stability of the ordered layers compared to the liquid droplets.*

grounded and one or more topographic maps were acquired, then a scan was performed applying a potential difference and a subsequent scan was acquired again with both electrodes grounded, and the cycle could be iterated using different potential. A scan with the tip and the sample grounded is usually performed after the application of the potential, because for high potentials the long–range electrostatic force between the tip and the sample leads to a decrease in the lateral resolution that doesn't allow to fully appreciate any possible modification in the morphology.

In Figure 3.17 3 topographic maps show the behaviour of ordered ionic liquid layers under the influence of a strong electrostatic field. The map a) is the first of the series and has been acquired with both the tip and the sample grounded. The second image has been again acquired with tip and sample grounded, but after a previous scan performed applying a ΔV=+8V between the tip and the sample. In the same way, image c) has been acquired after a scan at ΔV=-8V. The 3 histograms of the heights reported in Figure 3.17 show that, a part from a small broadening of some peaks, possibly due to a slight decrease in the quality of the morphologies because of a dirtier tip, the envelopes overlap, meaning that the structure of the ordered layers has not been substantially modified by the electrostatic field.

In Figure 3.18 3 AFM topographies acquired in tapping mode using a

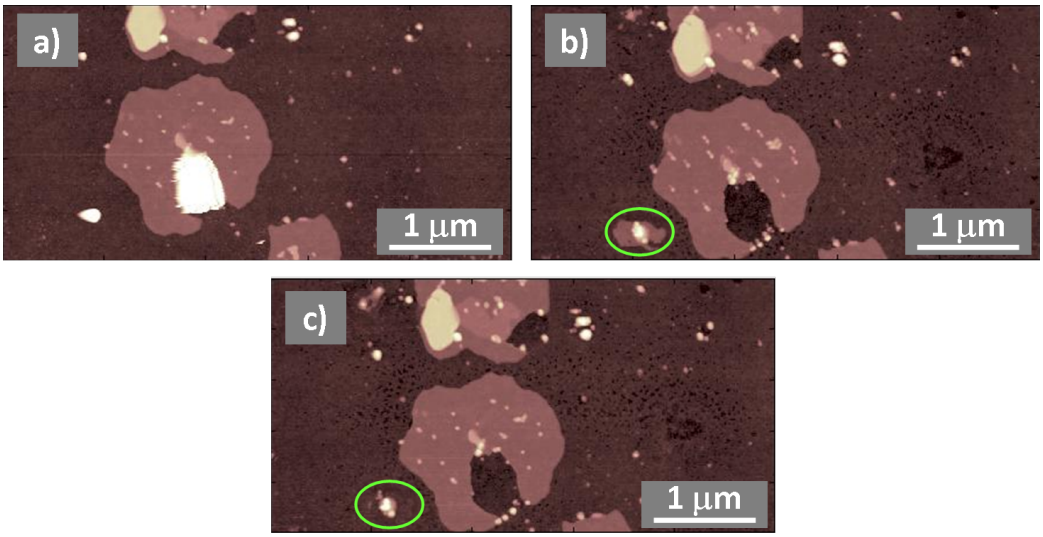

Figure 3.19: *Effect of strong electric fields on thin IL deposition. a) is the first image acquired in neutrality conditions. b) Has been acquired after 4 more scans without electric field and 2 scans at +8V and -8V. c) is the morphology after another scan at +8V (vertical scales 20nm). The application of a potential difference between a conductive tip and the substrate, can lead to the uptake and subsequent deposition of small quantities of ionic liquid. Such small quantities can rearrange as ordered layers, even if they don't appear as stable as the others.*

conductive tip (the conductive coating is Cr–Pt and typical tip radius is around 25nm) on a sample deposited on doped silicon are shown. The image a) has been acquired in neutrality conditions and show an area where the IL is structured in both liquid and highly ordered form. The image b) is the third image after a) acquired in neutrality conditions, and illustrates how the ordered layers, but also the droplets are stable against scanning. After acquisition of b), has been performed a scan applying a ΔV of 4V between the tip and the substrate and another one in neutrality conditions. The image c) of Figure 3.18 has been acquired, again in neutrality conditions, after a scan performed applying a ΔV=8V. Has can be noticed, there is a clear difference in the behaviour of ordered layers and liquid droplets. In fact, while the layers, even if damaged, are still there and kept their shapes, the droplets disappeared almost completed from the scanned area. Another interesting feature to note, is the texturing of the areas of the sample between the terraces, where evidently there was a uniformly distributed sublayer, exactly as observed in the case of contact mode images. In Figure 3.19 it is interesting to note that passing from picture a) to b), i.e. after 4 scans in neutrality conditions and 1 scan applying -8V and another applying +8V, the droplets

disappeared again, but furthermore a small flat layer has been grown: this growing was probably due to a deposition of a very small quantity of ionic liquid that was on the tip from previous scans, and shows how a quantity small enough can spontaneously rearrange in the form of an ordered layer instead than in a droplet. Anyway that grown layer was not as stable as the rest of the islands in the scanned area, because it disappeared after a subsequent scan at +8V, as can been seen in Figure 3.19 c).

The stability of the ordered domains under strong electric fields evidences how the ions of the ionic liquids are tightly bound in a stable structure. This is a further indication of the fact that IL islands are not only structurally ordered in the vertical direction, but also possess a solid–like mechanical character. Beside, this observation suggests that ordered [Bmim][Tf_2N] domains may possess electric/dielectric properties analogous to those of standard solid salts, i.e they may be insulators and dielectrics. Experimental results support strongly this hypothesis [83].

Resistance to normal forces

It is then interesting to see how the IL islands behave when subjected to normal loads, i.e. to forces acting perpendicularly to the interface. In fact, while usually the in–plane shape of the ordered structures in very uneven, and there is no evident crystalline ordering, along the z direction their is a clear and strong regular arrangement.

In order to perform a study of the response of the layered structures to normal loads, different force spectroscopic techniques has been used. The first of those techniques is the force volume (FV). During the acquisition of a force volume, once a area has been selected during a previous scan in contact mode, a force curve is performed on every point of a regular matrix defined on the scan area. During the acquisition of a force volume, a topographic map is simultaneously acquired together with the acquisition of the force curves. In order to perform the measure, a trigger deflection (that can be converted to a trigger force once the cantilever has been calibrated) is set: for each point on the matrix the tip approaches the surface and when the trigger is reached, the motion of the piezo is reversed increasing the tip–surface distance. Monitoring the height the tip needed to reach the trigger at each point, allows to record the topographic map of the sample surface at the trigger force used. If acquiring subsequent force volumes at increasing trigger force, a lowering in the height of a feature is observed, it is representative of the compression/indentation of the object under the applied load. In Figure 3.20, 2 typical topographic maps acquired in force volume are shown. These two maps are the first and the last of a series of 4 FV maps acquired on

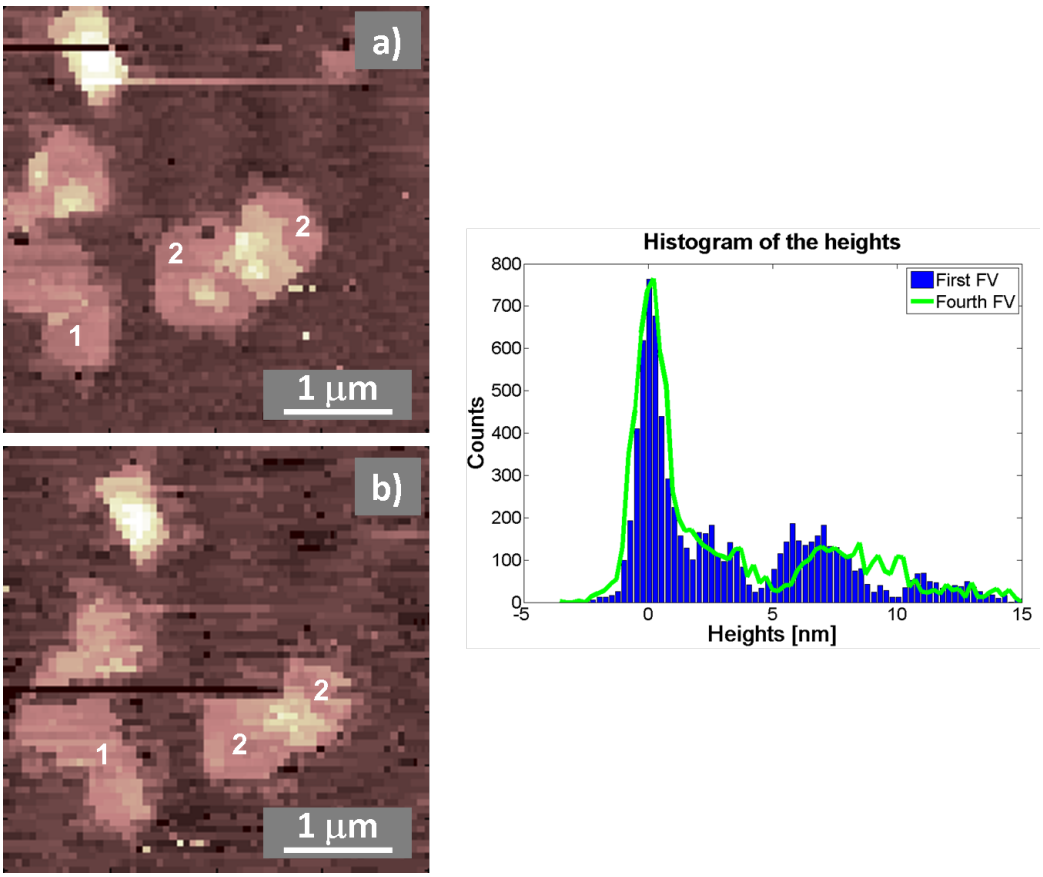

Figure 3.20: *Force volume images of [Bmim][Tf_2N] on oxidised silicon. a) is the first force volume map acquired, with a trigger force ∼4nN (vertical scale 27nm). b) is the 4th force volume performed on the same area, applying a trigger force of ∼50nN (vertical scale 27nm). On the right–hand side, the envelope of the histogram of the heights of b) is plot superimposed to that of a).*

the same islands: starting from the first, the trigger force has been increased from 4nN to 48nN. Considering the presence of the adhesion force between the tip and the sample, that acts as an additional load, the highest force applied by the tip was around 80nN. The tip radius range for the tip used is between 20nm and 60nm, so the pressures corresponding to 80nN ranges between 0.07KBar and 0.6KBar. In the second map the islands look a bit shrunk than in the first. This effect could be ascribed to an erosion of the edges, as happens during the imaging in contact mode, due to a greater fragility respect to the internal part of the terraces. The same effect could account for the disappearance of the small island in the top–right corner of Figure 3.20 a). The pressure exerted by the tip can in principle induce indentation or compression of the ordered layers and this should first of all appear in the topographic maps. As can be noticed looking at the histogram of the heights in Figure 3.20 there is no evidence of any compression varying the trigger force from 4nN to 48nN, instead there is something like a slight shift and widening of the third peak, corresponding to the parts **1** and **2** of the structures in the image. This increase in thickness, opposite to the expected behaviour, can be the result of a light damage of the flat surface of the ordered layers by the repeated action of the tip, also through pulling due to adhesion, as the peak widening lets to suppose.

Even if there is no evidence of penetration of the ordered layers by the tip, in this and in all the other force volumes performed, the whole set of approaching force curves has been analysed, in order to find any trace of indentation. Specifically, in the force volume corresponding to the map b) of Figure 3.20, steps in few force curves have been found, but if the positions corresponding to those curves are reported on the topographic map, it can be clearly seen that they sit on the edges, so these steps probably correspond to slips of the tip or erosion of the border: anyway those steps are absent in almost all the curves acquired on the flat parts of the ordered terraces, for this specific force volume and also for the others performed (see Figure 3.21).

There are several drawbacks working in force volume. First of all, the number of points in the morphological map is limited, because for each point a force curve is acquired too, and memory limits don't allow more than 512x512 points. Furthermore the FV is a technique intrinsically slow: for example the acquisition of 128x128 curves with a ramping rate of 5Hz, (usually ramp rates of 2Hz or less are used), will take about one hour. Another drawback is related the acquisition of the topography. First of all, prior to the force volume, the sample surface needs to be scanned in contact mode, so as it has been shown, potentially eroding the ordered domains, especially if

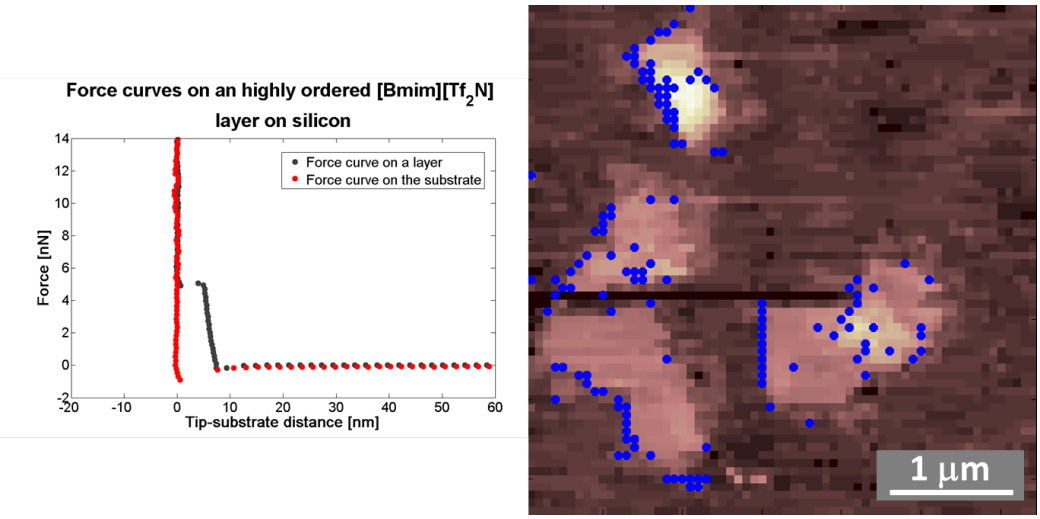

Figure 3.21: *Trace of indentation in a force curve extracted from a force volume. In the morphological map on the right blue dots mark the positions where indentation events have been found.*

cantilevers having high force constants, necessary for looking for indentation, are used. The area of interested can also be located directly in force volume, but the topographic map is built during the ramping, so it is slow, limiting an extensive exploration of the sample surface needed to locate an area of interest. Furthermore the way in which the topography is built, prevents the acquisition of high–resolution maps.

For these reasons another approach has been used, i.e. the point and shoot technique, in which the sample can be scanned in tapping mode using high force constant cantilevers and then force curves in specific points can be acquired but with this more rigid cantilevers. With this approach, the acquisition time is greatly shortened, the resolution of the morphological map can be higher the positioning of the curves can be selected in order to avoid edges or droplets or other uninteresting or possibly misleading features. Because high pressures are applied during the acquisition of the force curves, usually tapping mode images acquired after one or more point and shoots can contain some bad lines and be noisier respect to the usual tapping mode morphologies seen at the beginning of this chapter.

In Figure 3.22 a typical point and shoot is shown. On the left–hand side is shown the morphology acquired in tapping mode, where each cross represents a point where a force curve is acquired; on the right–hand side there are 2 the force vs. distance curves acquired on ordered layers and one curve on the substrate as a reference. As in force volume, the force

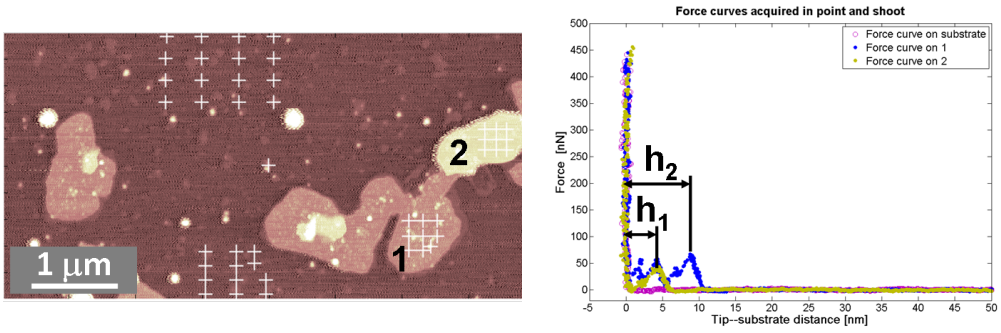

Figure 3.22: *Typical point and shoot output. On the left–hand side the morphology, in this case acquired in tapping mode, is reported (vertical scale 15nm). Each white cross on the image represent a point where a force curve has been acquired. On the right–hand side, there is a plot reporting 2 force curves acquired on islands with different thickness, together with another one acquired on the substrate as a reference.*

constant K of each cantilever used has been calibrated with thermal noise method; additionally the radius of curvature of each tip has been measured by scanning the a calibration grating (Mikromasch TGG01) composed by a 1–D array of triangular steps with sharp tips and high aspect ratio. An AFM topographic image is always the result of the convolution of the shape of the tip and the object scanned. When a sharp feature having an high aspect ratio is scanned by the tip, the resulting convolution approaches the reverse image of the tip.

With respect to force curves seen in force volumes, where the only discontinuities were in the curves acquired on the edges of the terraces (see Figure 3.21), here for forces high enough, each single curve acquired on an island shows a clear structured indentation. The force curves on the islands have a characteristic sawtooth profile, whose extension is compatible with the thickness of the island measured from the topography. Once the tip approaches the top surface of the terrace, there is an increase in the force applied, together with a decrease in the tip–substrate distance. This means that an indentation occurs, whose extension is, for example for 10nm thick island, around 1.6nm and 2nm. A simple Hertz model of an hard sphere on an elastic plane applied to this part of the force curves, leads to an estimation of the reduced Young modulus of E*∼1.8GPa, compatible with the values of some plastics like Nylon and PET (see Figure 3.23). After this first part, when a pressure of about 200–300MPa is reached , there is a breakthrough of the tip into the layer. At this point, depending on the thickness of the film, the

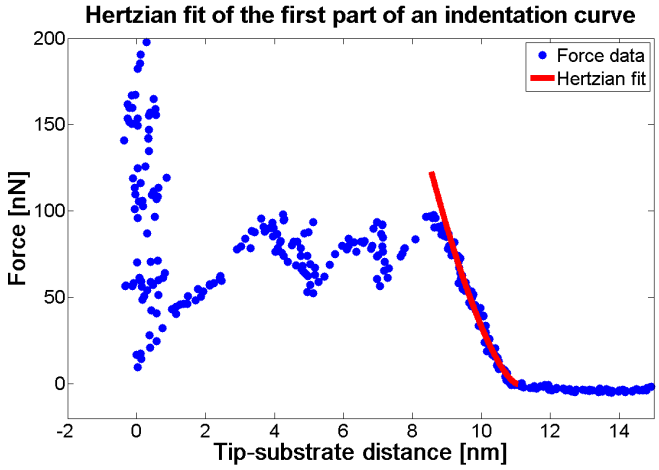

Figure 3.23: *Example of a fit performed using the Hertz model on first part of the contact in a force curves on a solid–like island.*

tip can directly reach the substrate or it can repeat the same profile again, giving rise to the same kind of structure. The pattern of peaks show one or more well defined peaks having the same heigth (i.e. the same peak force). After each peak there is a descending part, meaning that the force on the tip decreases, where secondary structures are usually visible. The distance between the main peaks is usually around 4–5nm, whereas the distance between subsequent peaks measured considering also the secondary structures, is around 2nm. Interestingly, as can be seen in Figure 3.24, the distance between the peaks doesn't change performing force curves on different ordered structures having the same thickness.

The values of the breakthrough pressure are in good agreement with the maximum pressures achieved in a simulation study performed by Pietro Ballone et al.[99], where a nanometric hard sphere is moved toward the substrate in a slab of ∼4nm of [Bmim][Tf_2N] on silica, in which pressure values are around 500MPa. Different curves acquired on the same island are almost perfectly overlapping (Figure 3.24 a)) and not only the main peaks but also the fine structure is reproduced. Moreover very often, even if different islands are explored and different tips are used, the curves found show the same profile, as can be seen in the Figure 3.24 b). The differences in the force are partially accounted for by the different tip radius resulting in a different pressure applied by the tip, even if not completely, probably due the detailed structure of the tip apex and on its contamination by ionic liquid molecules. Probably the same reasons are at the base of the behaviour found in a point and shoot performed on [Bmim][Tf_2N] deposited using ethanol. In fact, as

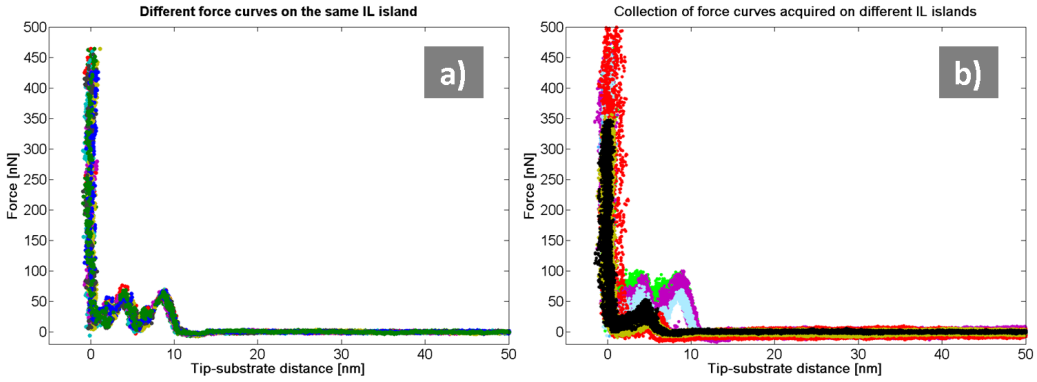

Figure 3.24: *In a) are reported different force curves acquired on the same island in the same point and shoot measurements, while in b) many sets of force curves acquired with different tips on different samples are plotted together, showing a remarkable reproducibility.*

can be seen in Figure 3.25, while the profile of the force curves is almost the same as on samples deposited using methanol, the scale of the force is higher in this case. The tip radius, as measured by TGG01, seems to be the same in this set of curves as in curves shown in Figure 3.24 a), so the breakthrough pressure seems to be greater. Anyway this result is preliminary, since only one measurement has been performed on ethanol at the moment.

The great part of the point and shoot studies has been performed with standard silicon tips on an oxidised silicon substrate, but the same qualitative behaviour has been found using a conductive tip coated with Cr–Pt, as shown in Figure 3.26. As it can be noticed, in this case the force curves don't have perfectly the same profile as those in Figures 3.22 or 3.24: this effect is due to the fact that the tip surface was not regular, as shown in Figure 3.26, where a sketch of the shape of the tip fpund from the calibration grating scan is reported. In this case, the tip profile shows at least 2 different apexes close enough in hight to interact both with the surface of the terrace during the indentation, as can be noticed also by the replicated features in the topography. The dynamic of the penetration is then more complex and accounts for the lack of overlapping between the force curves.

It is very interesting to note that, even if there is a strong electrostatic noise probably due to the charged surface of the substrate, if a point and shoot is performed on an IL island on NaCl, characteristic peaks are again visible (see Figure 3.27), showing how the structure of the terraces seems to be similar even on very different surfaces.

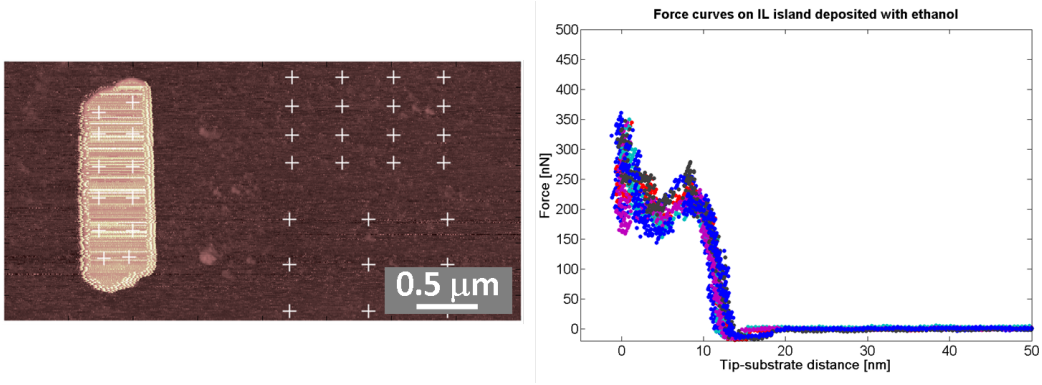

Figure 3.25: *Output of a point and shoot performed on a sample deposited with ethanol on oxidised silicon. The force curves evidence the already seen behaviour, but the breakthrough pressure is greater than in the previously shown point and shoots. Vertical scale of the image 30nm.*

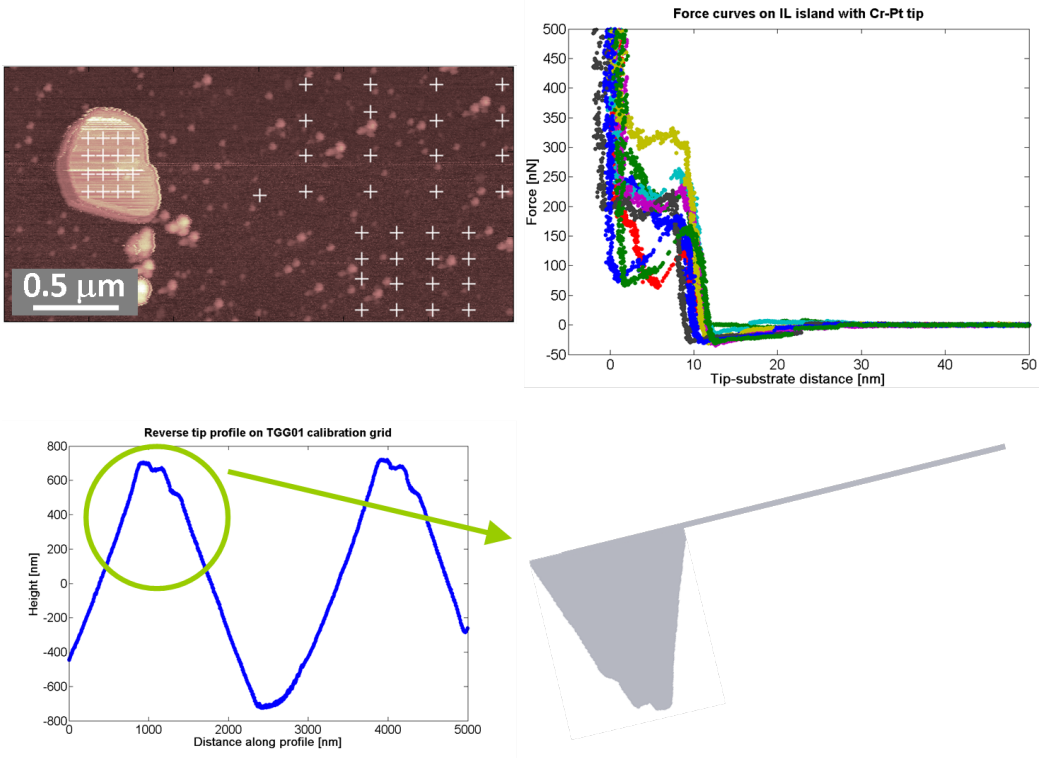

Figure 3.26: *Output of point and shoot on IL island on silicon performed with a Cr-Pt coated tip (image vertical scale 20nm). At the bottom–left of the figure, a profile of a scan on TGG01 is shown, in order to evidance the bad shape of the tip used. At the bottom–right a is a cheme representing the shape of the tip.*

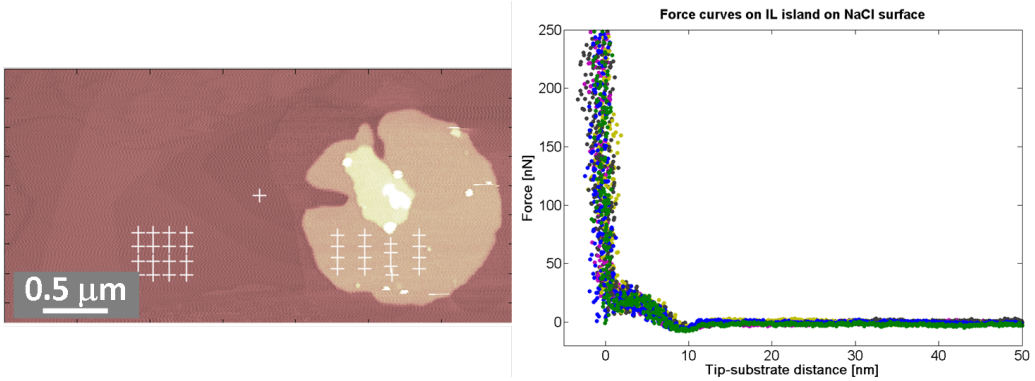

Figure 3.27: *Output of point and shoot on IL island on NaCl single crystal surface (image vertical scale 30nm). The freshly broken surface of NaCl was probably charged, inducing regular noise in the force curves.*

As a last observation on these indentation measurements on ionic liquid islands, it is worth to notice how these layers show a self–healing behaviour. In fact, as can be seen in Figure 3.28, comparing the images acquired before and after a point and shoot performed standard AFM tips, only small traces of tip penetration are visible. If a tip with a Cr–Pt coating is used, the traces of indentation are more clear. This is probably due to the different interaction between the tip surface and the ionic liquid as well as to the greater dimension of the latter tip respect to the former. Furthermore, in other point and shoot measures performed with conductive tips, even using trigger forces well below the breaking pressure, so where no indentation could be found in approaching curves, some holes could be produced in the solid–like islands. It is believed that this effect is due to a stronger interaction between diamond coated or Cr–Pt coated tips with respect to silicon tips, that can lead to the rapture of the surface of the island during the retraction curve. This effect could be further enhanced because coated tips can be easily pick up small IL droplets that can increase the tip–sample interaction as well as induce a phase change from solid to liquid at the contact point. Anyway, in many cases not a single trace of puncturing of the island surface by the tip can be found: this can mean after the tip that broke the surface of the IL terrace has left, the ions can rearrange in order to fill the hole and restore the surface morphology. It is possible in fact that the action of the tip that pushes against the layer can induce a sort of phase change, especially if, as said before, the tip surface is contaminated by traces of ionic liquid. In the case of standard tips then, given a lower contact area and a lower interaction force acting during the retraction part of the force curve, the final visible damage to the islands appear minimum compared to the conductive tips

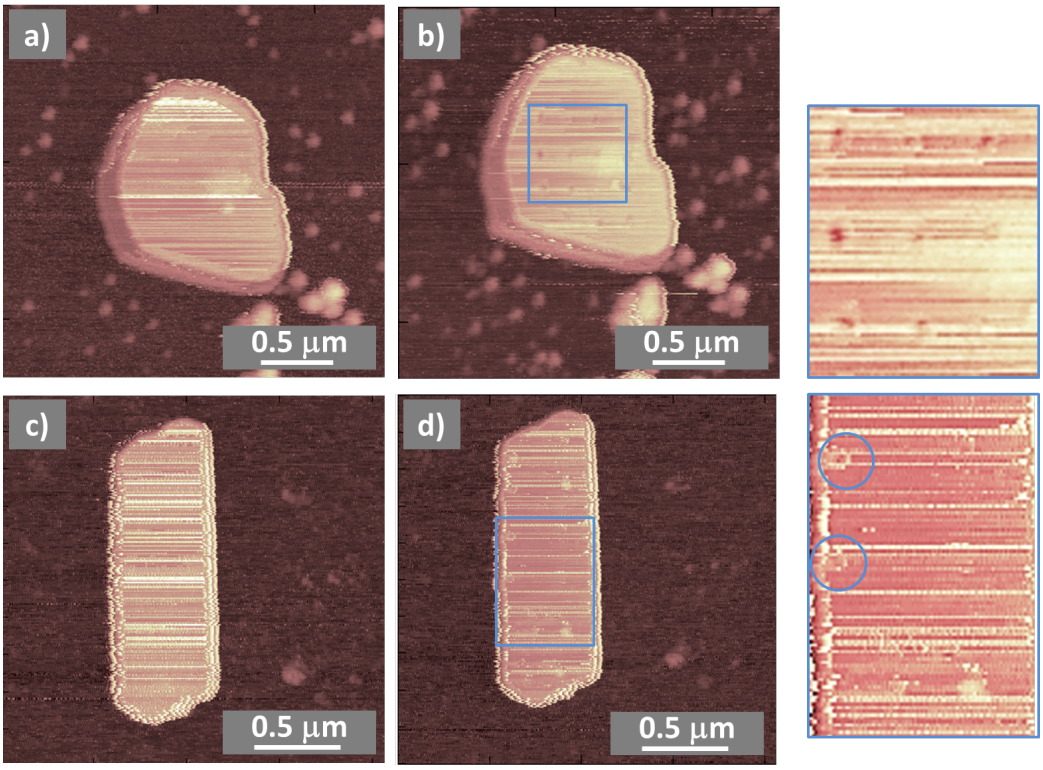

Figure 3.28: *2 examples of morphologies acquired before and after a point and shoot. a) and b) have been collected with a Cr–Pt covered tip (vertical scale 20nm); c) and d) with a standard silicon tip (vertical scale 30nm). Maps a) and c) has been acquired before performing the force curves: b) and d) just after. Figure b) clearly reveals the traces of the positions where force curves have been acquired, (see inset on the right). In c) only slight traces of the penetration of the tip can be noticed, as evidenced in the inset.*

used.

Even if the ordered layers possess this sort of self-healing ability that is typical of liquids, all the mechanical tests and in particular the indentation curves, lead us to the conclusion that the highly ordered layers developed by [Bmim][Tf_2N] on several substrates are solid–like in nature.

3.1.4 Force curves in bulk ionic liquids

In the literature there are several recent studies in which two surfaces immersed in a bulk of ionic liquid are approached and possibly brought into contact and where the forces between those surfaces are measured. Some of the studies[94, 95, 97], have been conducted with the surface force appara-

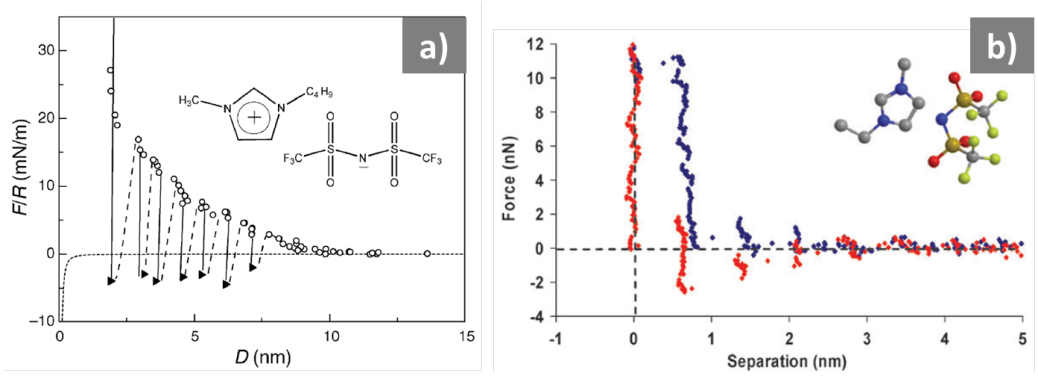

Figure 3.29: *a) Output of an SFA measurement performed in a bulk of [Bmim][Tf_2N] between 2 silica surfaces. Layering at the surface can be clearly detected as oscillation in the force between the surfaces (reproduced from reference [94]. b) Force curve acquired with an AFM in a bulk of [Emim][Tf_2N] with a silicon nitride tip on a mica substrate. As in SFA measurement, solvation layers are clearly visible in the force profile starting around 4nm from the substrate (reproduced from reference [76]).*

tus (SFA). In its typical set–up an SFA consist of two smooth cylindrically curved surfaces whose cylindrical axes are positioned at 90°to each other are made to approach each other in a direction normal to the axes. The distance between the cylinders is measured by optical interferometry and one of them is held by a cantilever spring in order to sense the interaction forces. The surface of the cylinders, normally made of mica, can be covered with the material of choice in order to match specific purposes. Figure 3.29 a), reproduced from the work of Ueno et al.[94], reports the results of a measurement performed on a bulk of [Bmim][Tf_2N] (one of the 2 ILs studied in the paper), between to silica surfaces. An oscillatory profile of the force with an amplitude exponentially decreasing with the distance can be clearly seen. The oscillations are ascribed to the rupture of solvation layers formed by the ionic liquid in contact with the silica surface and the thickness of each layer is about 0.8–0.9nm.

Other studies, performed by Atkin and co–workers, utilise the atomic force microscope tip as one of the approaching surfaces[77, 76, 78], and show qualitatively similar results to the works performed with SFA. Figure 3.29 b), reports the a force curve acquired with a standard contact silicon nitride tip and a mica substrate. Even in this case a strong layering is seen, starting from around 4nm above the substrate.

The systems I investigated during my PhD are qualitatively different from those studies in SFA and AFM measurements previously cited, first of

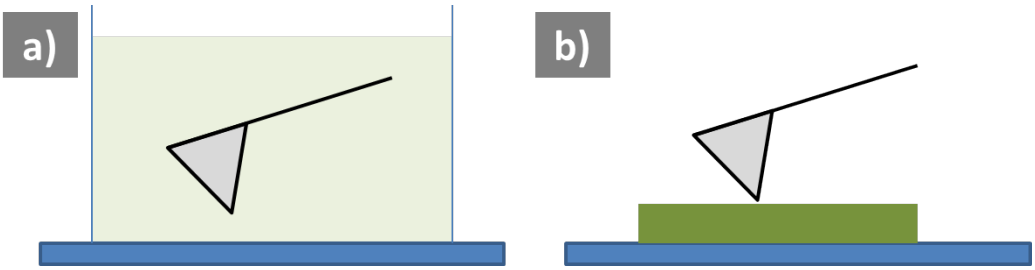

Figure 3.30: *Representative schemes of the two kind of measurements performed with the AFM. a) shows how in bulk measurements the tip is completely immersed in the liquid along with the substrate, while in b) the tip contacts a solid–like layer of ionic liquid supported in the surface and surrounded by the environment.*

all because in my case I don't work in a bulk of ionic liquid but in a thin film configuration, as schematised in Figure 3.30. Furthermore, the ordered structures I found during my work appear to possess a solid–like character and extends for tens of nanometers in the direction perpendicular to the interface, while the layers found in studies conducted in bulk ILs can sustain only moderate pressures and cannot be detected few nanometers far from the surfaces.

In order to show that these two systems are also quantitatively different, I would like to replicate the experiments performed by Atkin, to check I if can obtain results in agreement with his works, and so quantitatively different to what I found on the solid–like terraces.

In order to have a direct comparison with the measures of Atkin, [Bmim]-[PF_6] on mica has been used. Although Atkin and co–workers adoperated many different ionic liquids, to date they never used [Bmim][Tf_2N], that is the liquid of interest in my work, so measurements have been performed in this liquid on oxidised silicon and mica.

Force curves in bulk of ionic liquids have been performed using standard contact silicon sharpened tips, with scan sizes between 50nm and 400nm. The approaching velocity were between 2.5nm/s and 80nm/s. It could be expected that a lower velocity leads to more overlapping or reproducible curves, but this is not the case. In fact, often the decreasing in the velocity gives rise to an increase in the degree of dispersion of the first part of the contact in the force curves. Figure 3.31 shows a force–distance curve acquired in a bulk of [Bmim][Tf_2N] on oxidised silicon substrate. In the main figure and in particular in the inset, are marked the positions where a signature of a rupture event can be identified. Many of the ruptures, ascribed to as breakthroughs into solvation layers, take place for very low forces, at fraction

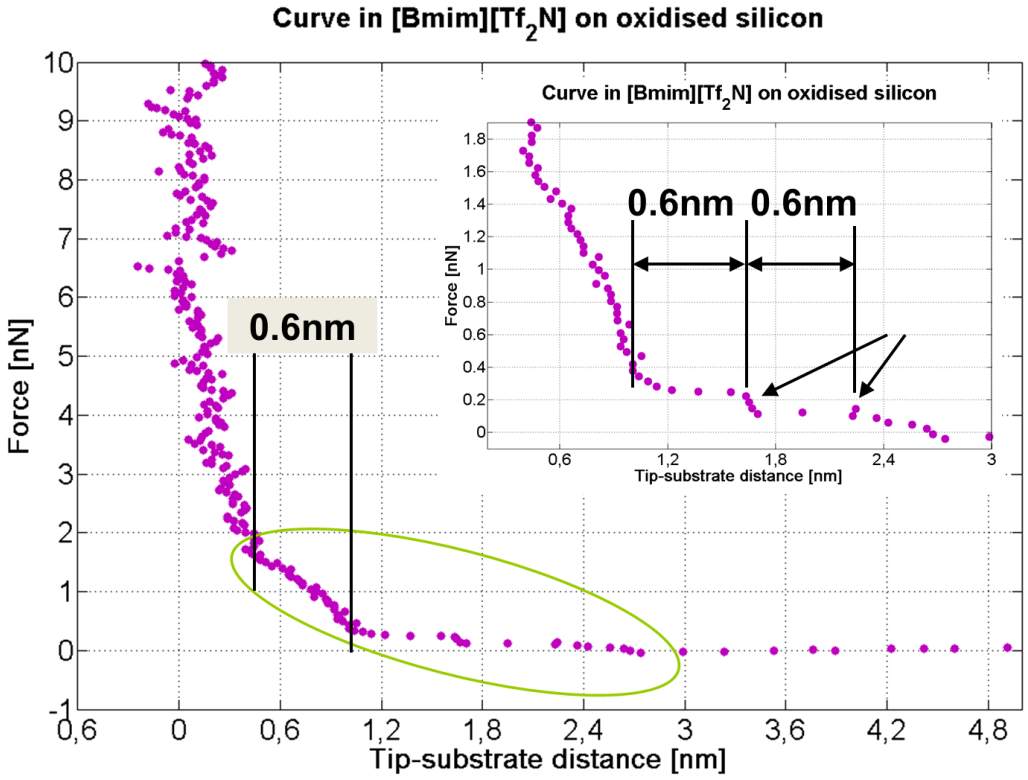

Figure 3.31: *Example of a force curve acquired in bulk [Bmim][Tf_2N] on silicon. The curve shows a series of smooth discontinuities, i.e. traces of the possible breakthroughs into solvation layers. The distance between subsequent events is around 0.6nm.*

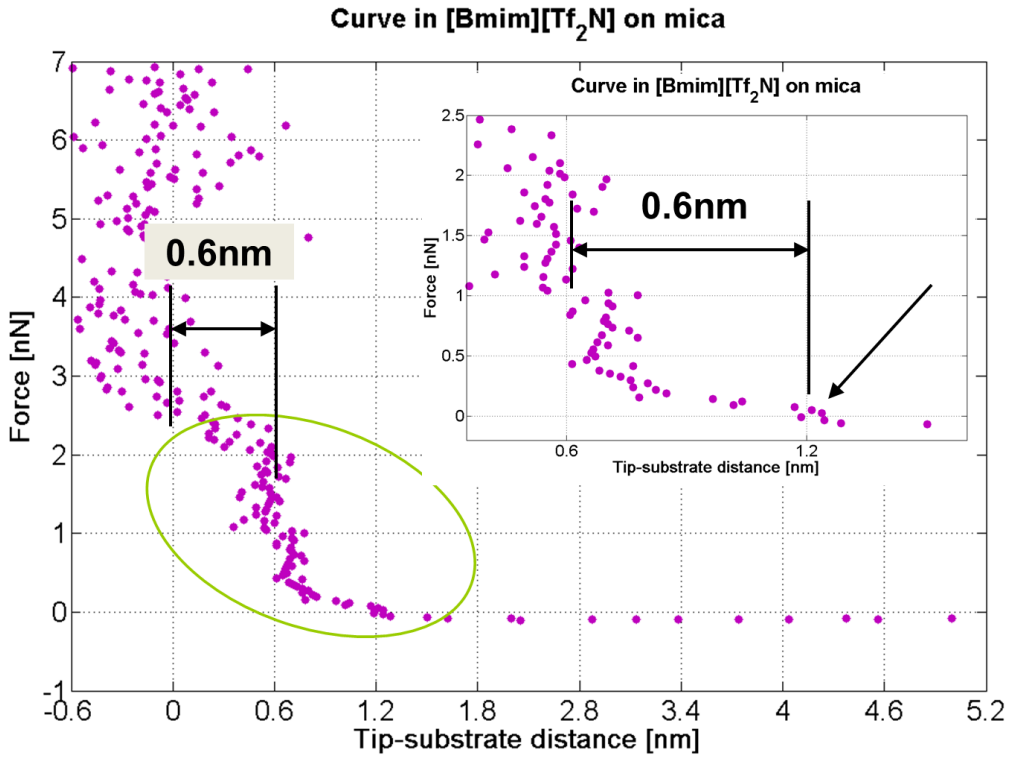

Figure 3.32: *Example of a force curve acquired in bulk [Bmim][Tf_2N] on mica. Ruptures of the solvation layers are evidenced in the inset. The distance between subsequent events is around 0.6nm.*

of nanonewtons, while the last steps is around 1,5nN. The spaceing between the ruptures is around 0,6nm, in agreement with what found from structural analysis on solid–like terraces.

Almost the same features with the same distance between subsequent rupture events, can be found on force curves acquired in bulk [Bmim][Tf_2N] on freshly cleaved mica. In Figure 3.32 can be noticed a lower extension of the contact region moving away from the substrate, but since, as said before, the length of this part of the curve can change even in the same set of measures. Also on mica, some layering can be found, as in the previous case and the separation between the traces of ruptures is around 0.6nm.

The measurements in bulk of [Bmim][PF_6] on mica, as displayed in Figure 3.33 show some more pronounced traces of indentation due to a slight increase in the breakthrough forces respect to those found in [Bmim][Tf_2N]. In fact, for example the first identified layer, breaks at around 0.5nN. Those differences can anyway be due to a different radius of curvature of the tips used in the

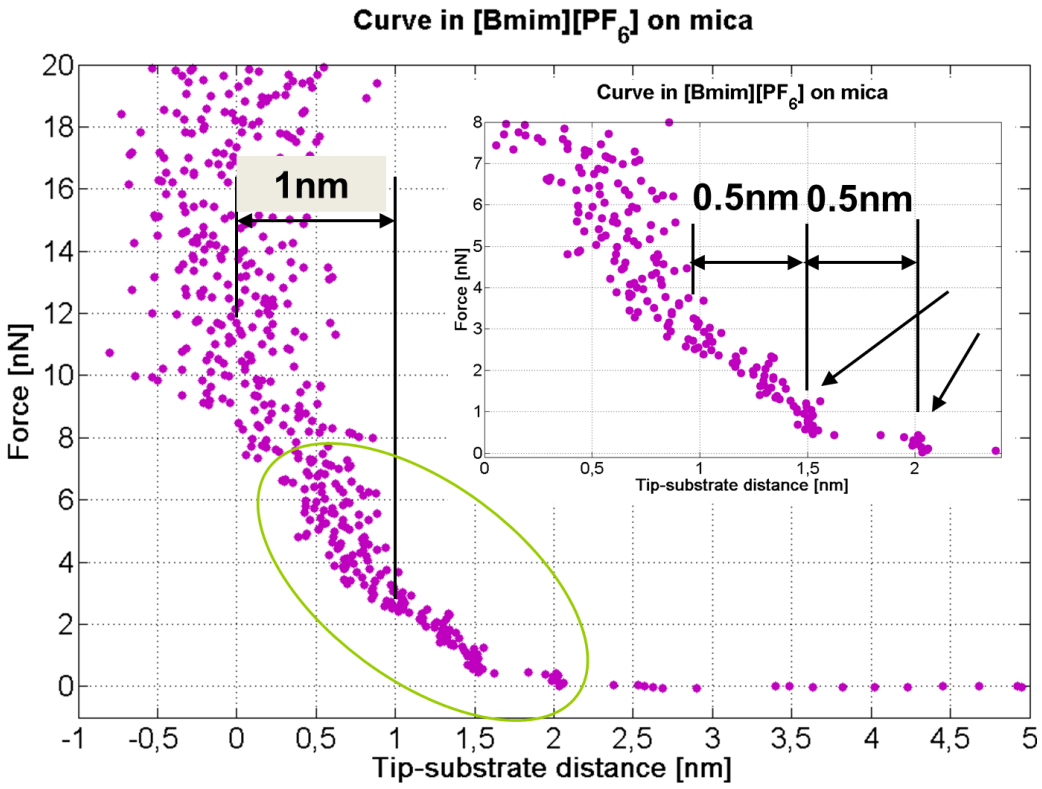

Figure 3.33: *Example of a force curve acquired in bulk [Bmim][PF_6] on mica. Ruptures are somewhat more evident, due to higher loadings the solvation layers can resist. The measured distance between 2 next layers is around 0.5nm.*

different experiments performed. In the case of [Bmim][PF_6] the separation between subsequent ruptures appears to be about 0.5nm, less than with the other ionic liquid, fact that could be reasonable if considering the smaller size of the anion.

In force curves performed in a bulk of ionic liquid, a sort of evidence of subsequent breaking of solvation layers has been found, in agreement with the work of Atkin. The force curves I acquired look noisier than those reported by Atkin in the publications, especially when the force increases and a good contact with the sample is realised. The low rupture forces involved and the difficulty in obtaining well overlapping reproducible curves, didn't allow to give very precise values of the separation distances between solvation layers.

3.1.5 Scanning electron microscopy investigation

The investigation with another imaging tool is interesting because, first of all it gives the opportunity to study different properties of the deposition, but also because it allows to check that the islands are not artefacts induced by the action of the scanning AFM tip and also that they are not formed by some dip–pen lithographic effect. Solid–like structure are usually very thin, so they cannot be observed by standard optical microscopy. Instead an investigation with scanning electron microscope (SEM) can be performed.

SEM is a fast imaging technique, and gives the opportunity to image larger areas of the sample then AFM. Furthermore SEM can be used on those samples where an AFM study is difficult; for example it can be a very useful tool in the study of ionic liquid thin films on nanostructured surfaces, where, as seen in Figure 3.12, AFM imaging could be very difficult. Another example is a deposition of [Bmim][Tf_2N] realised on a very smooth nickel film produced by ion–gun sputtering. On this sample, only small droplets or extended liquid domains where visible with AFM, but given the fact the even with multiple scans the area investigated with AFM is quite limited, some rare structures may be lost. In the specific case, several SEM scans confirmed the absence of anything but liquid domains, with nothing resembling solid–like islands or other peculiar structures, (see Figure 3.34).

Figure 3.35 shows two large scale views of a deposition of [Bmim][Tf_2N] on oxidised silicon, showing a regular pattern of droplets. This gives some insights on the way the solvent (methanol in this case) typically evaporates, i.e. the original drop splits up into many smaller and smaller droplets. The brighter parts visible between the droplets are the solid–like layers seen with AFM. Due to the electrically insulating character of the layers, as revealed by nanoscale impedance spectroscopy measurements performed by Galluzzi[83],

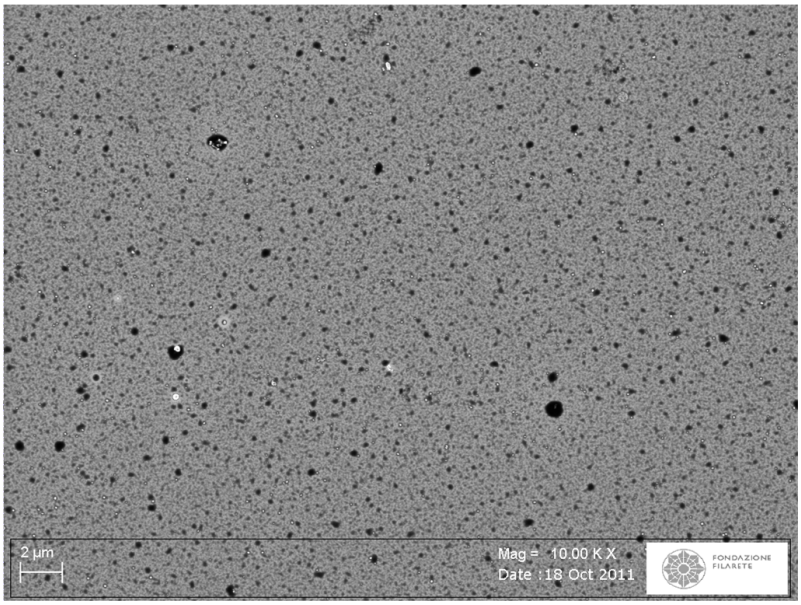

Figure 3.34: *SEM morphology of [Bmim][Tf_2N] on Nickel deposited with ion–gun.*

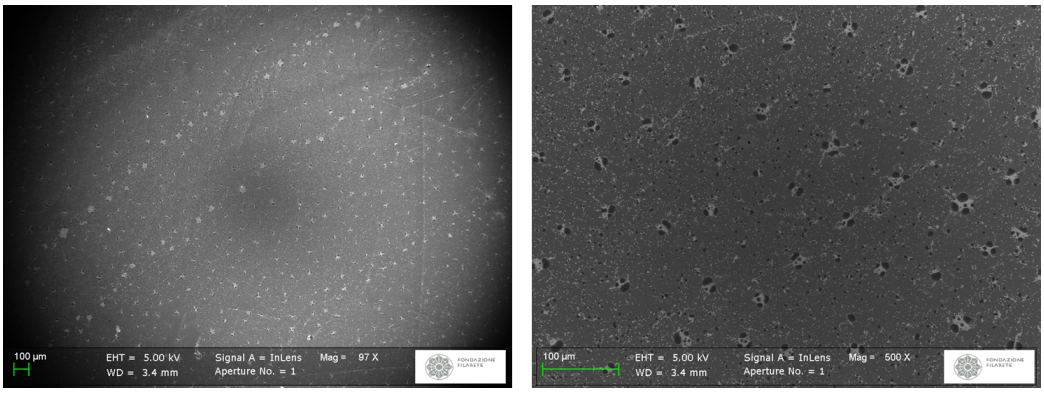

Figure 3.35: *SEM morphology of [Bmim][Tf_2N] oxidised silicon. In the images, the darker rounded features are the ionic liquid droplets, whereas the lighter areas are the same solid–like layers found with AFM.*

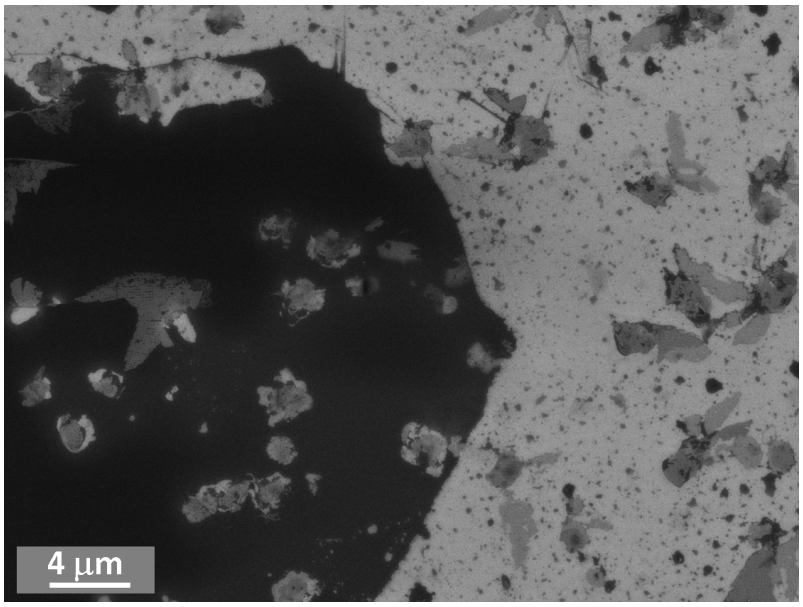

Figure 3.36: *SEM morphology of [Bmim][Tf_2N] oxidised silicon. Nicely branched solid like structures are visible, and some multilayer can be recognised because some parts of the images appear darker than others. Unespectidely, some islands can form also on IL liquid domains (darker part of the image, on the left).*

a clear contrast can be seen between the islands and the substrate, even if they are very thin.

Exposure to electrons has been shown to be very harmful for ILs[75]. In particular, in the case of ordered domains, that are only few nanometers thick, the stability under the electron beam is greatly reduced respect to the bulk. Ionic liquid terraces in fact, can be scanned only for few tens of seconds before they disappear. Nonetheless, as shown in Figure 3.36, nicely resolved images can be obtained, where traces of the superimposed terraces can be distinguished. The darker region located at the left part of the image, is an ionic liquid microdrop. Interestingy some structures appear to sit on top of this liquid domain, and if the electron beam is focused on the droplet, heating induces convective movements and some island are found to move around on the surface.

Images a) and b) of Figure 3.37 show, as AFM investigation evidenced, that solid–like domains can form even if a flat surface is covered by a sub–monolayer layer of nanometric silica nanoparticles. Something similar can be observed even on a thicker deposition of silica nanoparticles, as shown in Figure 3.37 c), where the with spots are solid–like layers. Figure 3.37 d) has been collected on the same sample as c). Beautiful flower–like structures are

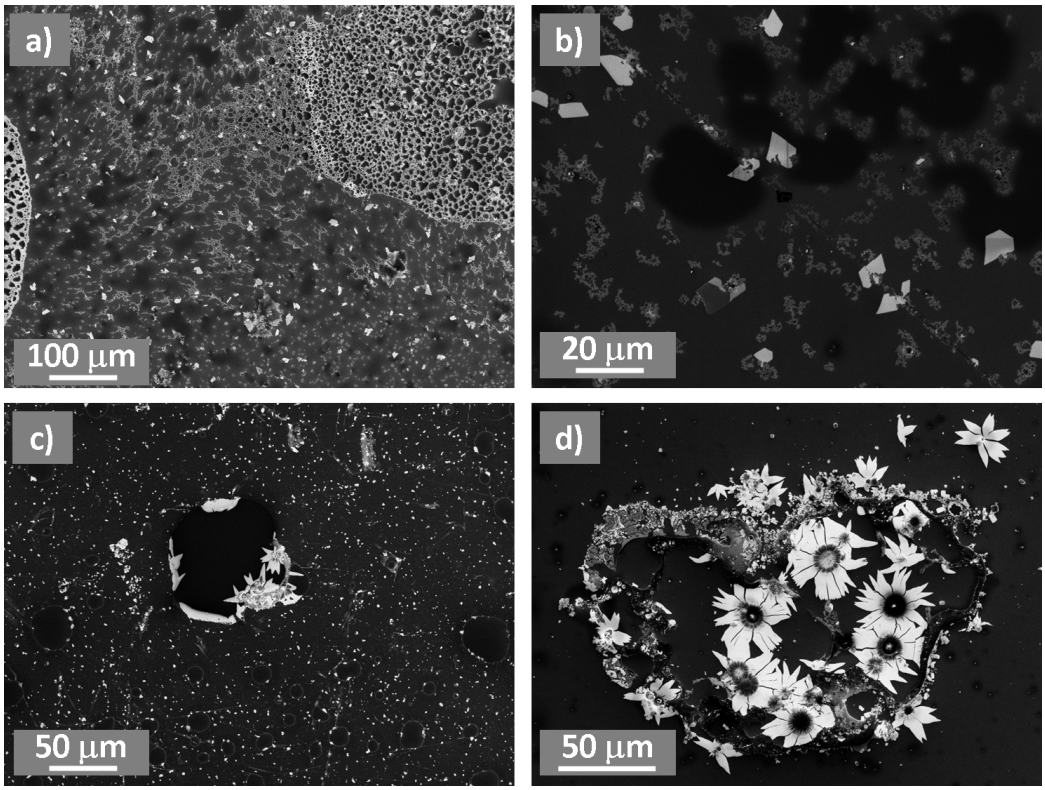

Figure 3.37: *SEM morphology of [Bmim][Tf_2N] nanostructured silica on oxidised silicon. Images a) and b) are relative to IL deposited on a sub–monolayer of silica nanoparticles. In images c) and the IL was on top of a 32nm thick layer of Ns-silica. In the last image can be noticed beautiful flower–like structures, whose origin is still unclear.*

found to sit on top of the 32nm thick nanostructured film of silica. Those structures could be another form of the solid–like terraces, but can also be formed by the aggregation of silica particles detached from the substrate by action of the ionic liquid. In fact, due to the high affinity of [Bmim][Tf_2N] with silica and to the possible solvation effect of the particles in ionic liquid (as it has been actually seen in colloidal suspesion of silica particles in ionic liquids[88]), silica clusters can detach and aggregate at the surface. Those structures are still not fully understood and a more detailed investigation is required.

This section was to underline that, even if no studies on supported ionic liquid thin layers have been performed with SEM so far, this microscopy technique can be a useful tool for the investigation of those systems, has probably, if samples may be realised on TEM grids, can be the TEM, that

can allow to elucidate the details of the internal structure of the ions inside solid–like terraces.

3.2 Discussion of the results

The results reported in the previous part of the chapter, show how the first interface of an ionic liquid with a solid surface is not as simple as it could be thought. In particular the study of the solid–like layers developing on many of the substrates used has been the main part of my PhD activity.

The development of solid–like layers when an ionic liquid contacts a solid surface, can have a considerable impact on applications. The formation of such sort of highly resistant structures may be positive when ionic liquids are used as lubricants, but it can decrease the performances of those devices in which liquid flow in a nanoporous matrix is necessary, as well as where the presence of an electrically insulating layer is undesirable, like in Grätzel cells.

Solid–like terraced structures found, are a metastable phase of the ionic liquid, that coexist with its liquid phase. Nanometer–sized heterogeneities have been observed in the bulk liquid phase of imidazolium-based ILs by both experimental[106, 107] and simulation studies[108] and interpreted as the result of the segregation of the non–polar alkyl chains, separated by thin layers of cations paired to anions. The size of these locally ordered domains turned out to be roughly twice the length of the alkyl tail plus the cation–anion pair, scaling linearly with the number of CH_2 units in the alkyl chain. The same behaviour has been found in a simulation performed by Manini et al.[109], where [C_{12}mim][Tf_2N] film of nanometric thickness was squeezed at kbar pressure by a piecewise parabolic confining potential. In this case, in–plane modulation in the density similar to the 3D structures found in the studied cited above where found. Interestingly nothing similar could be found without an external pressure applied on the ions or decreasing the lateral chain length to 4 carbon atoms.

Anyway this picture seems not to be fully compatible our case, where the interaction with the substrate is likely to play a fundamental role. In fact, it has to be considered that the melting point of [Bmim][Tf_2N] is around -4°C and the terraces are stable even for months at ambient temperature.

3.2.1 Role of the solvent

In order to state that the formation of solid–like islands and multilayered structures is a pure surface–induced effect, an important question to be answered is about the role played by the solvent used for the deposition of the samples. The choice of using an ionic liquid diluted into a solvent, has already mentioned, is due to the necessity of depositing only very small quantities

of the IL onto the surface, in order to produce very thin films. The issue of the role of the solvent has been studied in 2 different ways. First of all an X-Ray photoelectron spectroscopy (XPS) analysis has been performed on a sample of [Bmim][Tf_2N] previously mixed with methanol, in order to see if any modification in the structure of the ions could be detected (see App A for further details and for beam effects on the ionic liquids). The second approach has been to use two more solvents, i.e. ethanol and chloroform. The results of different depositions have been studied by AFM in order to find if the solvent influences qualitatively or quantitatively the structure of the IL thin layer.

For the XPS analysis first of all, a sample of the pure liquid has been loaded in order to acquire some reference spectra and to verify the stoichiometry. The top spectrum in Figure 3.38 is the wide scan spectrum collected on a droplet of pure [Bmim][Tf_2N] completely covering an oxidised silicon substrate, and shows the elements expected for this IL. The bottom spectrum has been collected on a silicon substrate densely covered by micro–droplets of [Bmim][Tf_2N], realised by drop–casting a highly concentrated solution of the IL in methanol. The spectrum again shows the peaks of the elements of the ions, plus the peak of Si, coming from the substrate partially exposed. From high–resolution spectra acquired on both the samples (see Figure 3.39), the stoichiometry has been calculated, giving the ratios F:O:N:C:S = 6:4:3.5:11.2:2 for the pure liquid and F:O:N:C:S = 6:4:3:11:2 for the one mixed with methanol, both in agreement with the nominal stoichiometry of [Bmim][Tf_2N] F:O:N:C:S = 6:4:3:10:2 and with data reported in the literature[73, 74].

XPS analysis doesn't highlight any modification in the structure of the ions and also any strong interaction with methanol: the binding energy of the elements in ionic liquid molecules is not modified respect to the pure bulk, at least up to the energy resolution of the instrument (0.3–0.4eV should be detected as shoulders on the peaks).

The XPS study shows that at least the major part of the ionic liquid molecules into the micro–droplets, is not influenced by the mixing with methanol, so meaning that presumably the formation of solid–like domains is not related to a chemical modification of the structure of the ions. Anyway, XPS cannot exclude that a structural change happened only for a small fraction of the ions composing the liquid. This small fraction can then be responsible for the formation of the solid–like terraces.

In order to try to get rid of it, we used 2 more solvents, i.e. ethanol and chloroform. The use of ethanol is related to the fact that it has the same chemical composition of methanol, but one carbon more in the lateral

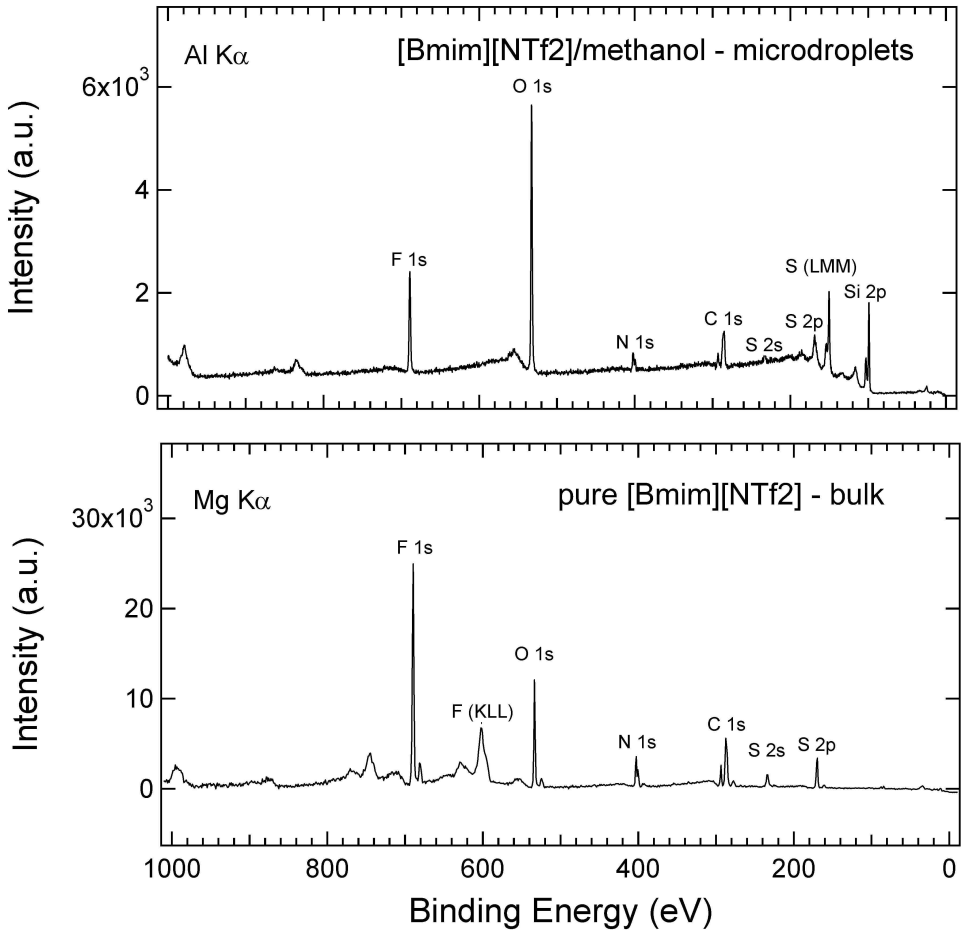

Figure 3.38: *Comparison between low resolution XPS wide–scans of [Bmim][Tf_2N] micro–droplets on silicon deposited from a [Bmim][Tf_2N]/methanol solution (top panel) and pure bulk [Bmim][Tf_2N] (bottom panel).*

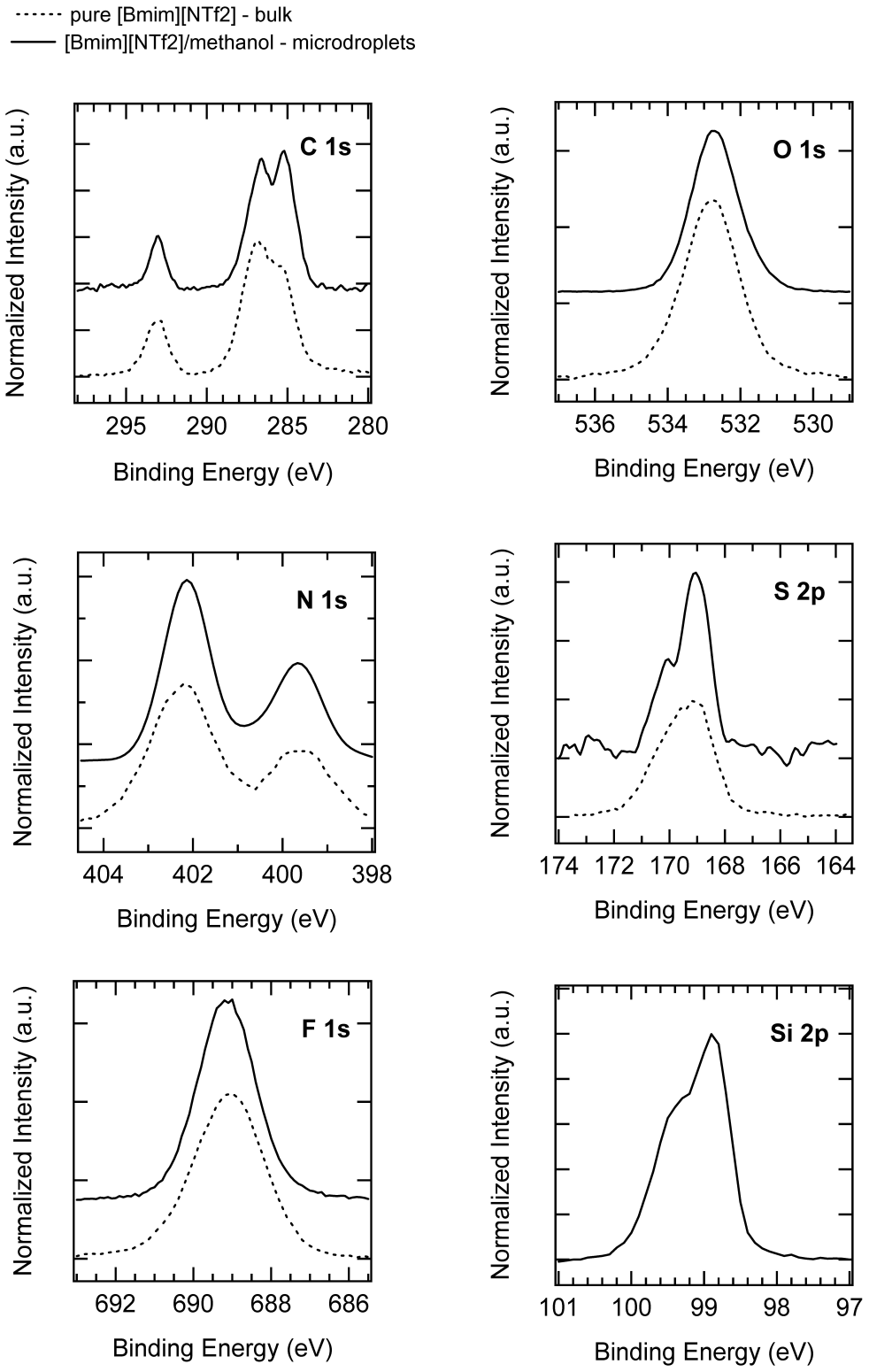

Figure 3.39: *High resolution core level photoemission spectra of [Bmim][Tf_2N] micro–droplets on silicon deposited from a [Bmim][Tf_2N]/methanol solution (solid line) and of pure bulk [Bmim][Tf_2N] (dashed line).*

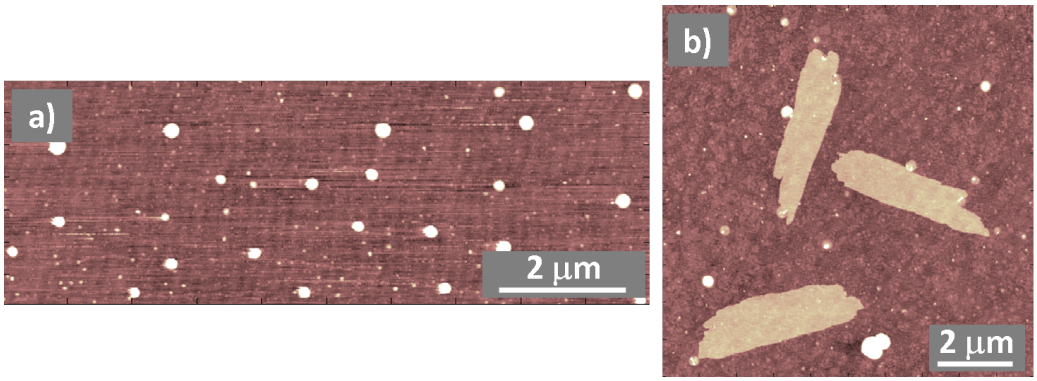

Figure 3.40: *AFM morphologies of pure [Bmim][Tf_2N] on amorphous silica. a) Topographys acquired on as deposited sample (vertical scale 10nm). b) Topography, acquired on the same sample, after a thermal treatment at 150°C for 2 hours, evidencing the formation of few ordered layers (vertical scale 10nm).*

chain. It would be checked if there could be an increased affinity of this molecule with the lateral butyl chain of the cation and if this can affect the structure formation. Chloroform has been chosen because it has completely different characteristics respect to the other 2 solvents, having a different chemical structure and being apolar, so it is not suppose to realise the same interaction with IL ions.

As seen in Figure 3.9 qualitatively similar morphologies than by using methanol, have been obtained. Furthermore, as described in section 3.1.2, the statistical analysis of the heights of the solid–like layers evidenced also that the structures formed by using the 3 solvent are also quantitatively similar, all of them being compatible with a fundamental layer thickness of 0.6nm.

To further elucidate the role, if any, of the solvent in the formation of the solid–like terraces, solvent–free depositions has been tried. Solvent–free depositions of thin ionic liquid layers are quite difficult to perform. In fact, the easiest way to realise them is by using spin–coating technique: a micro–droplet of pure ionic liquid is casted onto the substrate of choice and the excess is removed by rotating it at high speed. The morphological map in Figure 3.40 a) represents the typical morphology obtained depositing pure [Bmim][Tf_2N] by spin coating. AFM map shows a collection of small droplets, but nothing like solid–like layers can be found. Nonetheless, if the sample is annealed for 2 hours at 150°C (in the case of the sample reported in Figure 3.40 b)), some ordered terraces develop. Figure 3.41 further evidences the possible way in which liquid phase transforms into solid–like. In the topogra-

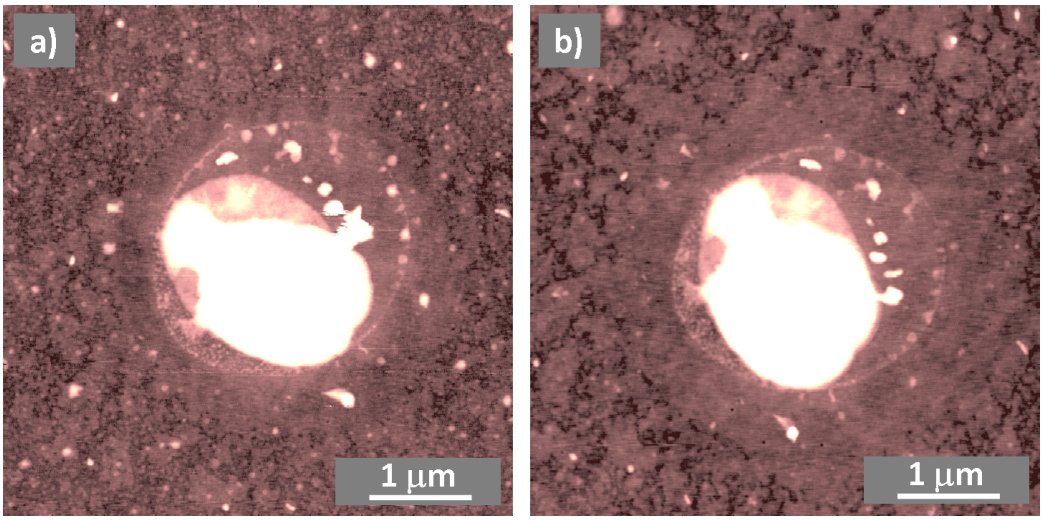

Figure 3.41: *AFM morphologies acquired on pure [Bmim][Tf_2N] annealed at 150°C for 2 hours. The a) map has been acquired just after thermal treatment, while b) shows the aging effect occoured to the sample after 4 days in ambient conditions. Vertical scales 16nm.*

phy a) in fact, it is possible to see a droplet surrounded by a circular ring, as if the droplet volume reduced during the annealing and a flat ordered layer, rounded in shape, developed around the drop. The morphology reported in Figure 3.41 b) has been collected 4 days after a). In b) is evident an increase in the size of the ordered underlayer surrounding the droplet. The same effect, reported as a visible texturing of the background, has been often seen in samples produced by drop–casting (an example is shown in Figure 3.7).

This behaviour may be explained supposing that there is some energy barrier separating the energy minima corresponding to the two phases, liquid and solid–like. If pure ionic liquid is deposited, the potential barrier needs to be overcome. Given that the surface of the substrate is not chemically and morphologically uniform, there could be some places where the interaction with the ionic liquid can modify and lower this barrier respect to other areas. This could explain why with the annealing the formation of solid–like layers can be induced, but only in some area of the sample. In fact, around the sample imaged in Figure 3.41, only in few areas the transition from liquid to solid–like occurred: around many other droplets nothing noticeable happened. When drop casting method from solvent/IL solution is used, the extra–energy needed to overcome the barrier can be easily provided by the driving forces of the evaporating solvent (see later for more details).

The Figure 3.41 shows also that once a layer is developed, it can increase

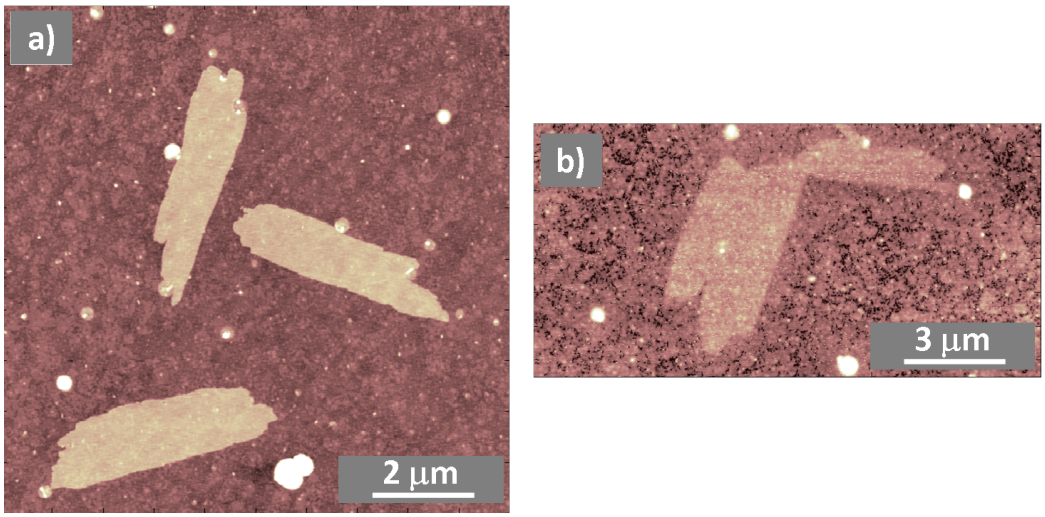

Figure 3.42: *AFM topographies of pure [Bmim][Tf_2N] deposition after annealing. a), as shown above, is the result of an annealing at 150° C. b) has been acquired presumably in the same area as a), and shows the result of a further annealing at 250° C. Vertical scales 10nm.*

it lateral size slowly in time. Figure 3.41 a) has been acquired immediately after the annealing of the sample at 150°C, whereas the b) shows the same area after 4 days in which the sample has been kept at ambient conditions. This aging effect is also evident in Figure 3.7, where the droplets decrease in volume and the lateral size of the solid–like domains increase. This behaviour means the ionic liquid, in the form of ion couples or clusters, can diffuse on the substrate surface and that once it finds an ordered layer can stick on it. Looking to Figure 3.7 the solid–like phase seems to be the most stable one at room temperature, but when some few month–old samples have been imaged by AFM, still a coexistence of solid–like and liquid domains has been noticed. It has to be underlined anyway, that the dynamic of the diffusion is very slow, and also that the volume of the ionic liquid in the liquid phase is quite high usually respect to that in solid–like form, so a complete transition can take a longer time. In fact, it has not been possible to acquire AFM images exactly in the same position to look for long time evolution, so it wouldn't be possible to asses if the IL in the solid–like phase increased respect to that in the liquid one.

Another possibility is that the two phases have almost the same stability and so in time transitions from liquid to solid–like form and back can occur. This idea is in some way supported by the observation that a further annealing cycle at 250°C for 4 hours, didn't produced any further ordered

domain formation, and also roughen the already grown terraces, as shown in Figure 3.42. Anyway, the observation of solid–like domains even in solvent–free depositions, further suggests that the solvent has only a structural role in the formation of the structures, easing their formation. The results of the solvent–free deposition are very different respect to those obtained in a drop casting deposition. It is possible that several factors contribute to this difference. First of all, as already mentioned, the solvent decreases the strong interaction between the ions in the ionic liquid so increasing the number of available conformations. During a deposition by drop casting, the ionic liquid is added to the surface in very tiny amounts since it comes from a solution. This means that the influence of the substrate, that is clearly the key factor in the formation of solid–like domains, becomes very important because the surface to volume ratio of small amounts of IL is very high. An interesting phenomenon supporting the previous idea can be observed if a sufficiently small drop of ionic liquid is deposited onto the substrate: in this case, an ordered layer can develop, even in the absence of any solvent. This effect can be seen in Figure 3.19, where a small quantity of IL, adsorbed on the tip in a previous scan of the sample, has been redeposited onto the silicon surface, leading to a small flat terrace. A further support to the idea that the solvent acts only as an agent helping in structure formation, is given by an interesting work performed by Kaisei et al.[85]. In this study small droplets, containing few thousands of ion couples, of [Bmim][BF_4] are inkjet–printed onto a Pt substrate by applying a potential difference between an hollow AFM tip filled by pure IL and the substrate. The IL is deposited on several points laying on a grid and tends spontaneously to form flat terraces, that coalesce forming a complete layer with thickness of about 4nm if the deposition time at each site is increased. This study shows that, if a sufficiently small quantity of IL is deposited onto a solid support, doesn't structure itself in the phase stable for the bulk, i.e. the liquid phase, but instead it forms ordered planar structures.

In the solvent–free deposition it is very difficult to attain the small volumes necessary to nucleate the solid–like phase and so ordered domains cannot easily growth.

The density and size of solid–like domains found in solvent–free depositions of ionic liquid, are small respect to what found in drop–casting depositions. A possible explanation may be that the already cited potential barrier between liquid and solid–like phases can be lowered by the action of the solvent. In fact the solvent decreases the ion–ion interaction, so the relative weight of the interaction with the substrate increases, promoting the formation of the ordered structures.

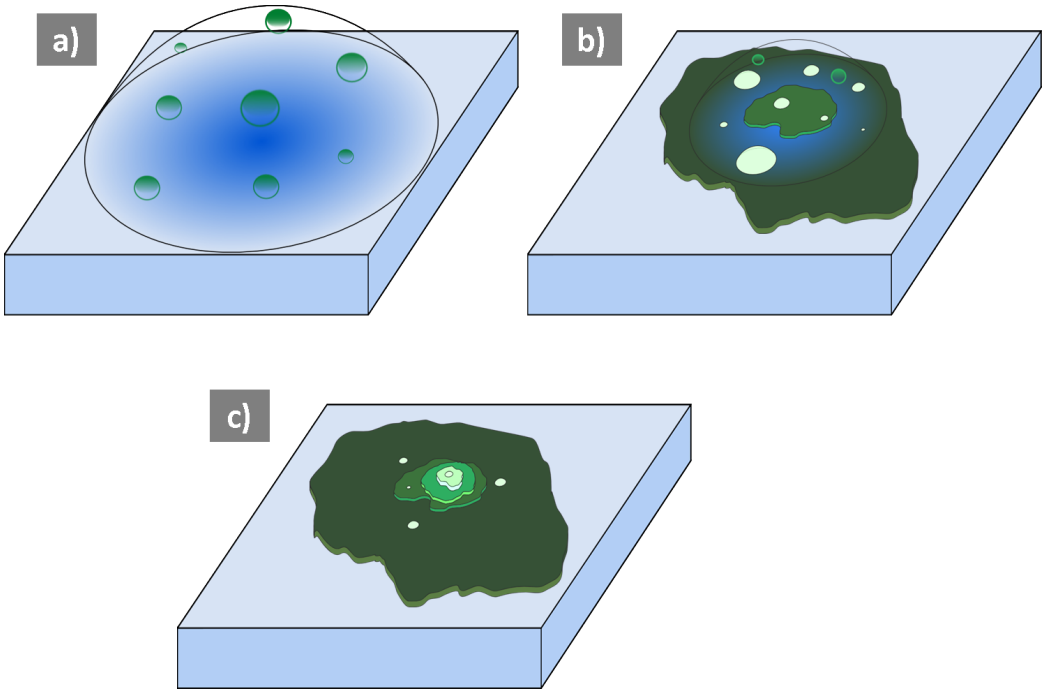

Figure 3.43: *Scheme of the proposed mechanism for 3D growth of solid–like layers. Moving from a) to c), the solution droplet decreases in size and capillary forces pull the IL in solution toward the centre and upward.*

Furthermore, what have never been found in samples produced with pure ionic liquids, are multilayered terraces. As seen at the beginning of the previous section, ziggurat–like structures can grow to considerable thickness, even more than 50nm. Those structures are formed as lamellar structures, showing a pronounced ordering in the direction perpendicular to the surface. A formation composed by terraces stacked one on top of the other, is likely to be induce by some driving force that pulls the ionic liquid molecules along the z direction. Such driving force could be provided by the evaporating solvent dragging ionic liquid molecules along with it. In fact, during the drying of a droplet of the solution on the substrate, even if the evaporation proceeds uniformly with the droplet front moving smoothly toward the centre, at the border the drop fragments and smaller droplets form. If within the area covered by these small droplets there is a nucleation site, a first ordered layer can develop on the substrate. As the solvent still evaporates, with its ionic liquid content, the droplet reduces in size and can lead to the formation of further terraces on top of the first, as schematised in Figure 3.43. The detailed behaviour of the moving front of the evaporating droplet, depend on the nature of the solvent, and in particular by its contact angle on the

surface. In the case of silicon, where all the 3 solvent have been used, it can be observed a complete wetting by methanol, an almost complete wetting by ethanol a non–zero contact angle, appreciable by eyes, of chloroform. The wettability of the substrate by different solvents can influence the solid–like structure. In sample produced by using chloroform, usually Ziggurat–like structures cannot be found, and this is possibly due to a lower formation of small droplets at the front evaporation of the main drop of solution.

Actually the dynamics of an evaporating droplet and in particular the deposition of a solute from such system, is a complex problem, still subjected to study nowdays[93, 92]. The evaporation of the solvent induces cooling and temperature gradients develop in the droplets. Since surface tension is dependent on temperature, surface tension gradients develop and these gradients induce Marangoni vortices. Those vortices carries the solute parts that are near the free liquid surface of the droplet inward toward the top of the droplet and then plunges them downward where they can either adsorb onto the substrate near the centre of the droplet, or be carried along the substrate to the edge, where they are recirculated along the free surface back toward the top of the droplet. The Marangoni vortices inside small drops of solution, may provide driving forces along the directions proper for allowing the 2D and 3D growth of the solid–like layers, in the same way sketched in Figure 3.43.

Anyway, the picture is complicated by the fact that during the evaporation the volume of the drop of solution decreases and so the concentration of the ionic liquid can be increased, possibly change bulk properties of the solution as well as the surface tension and so modifying fluxes inside the drop.

At the moment, a precise picture of the mechanism leading to the formation of ionic liquid ordered layers by drop–casting is not known and further investigation will be necessary, in order to obtain more reproducible depositions and possibly to control the morphology of the sample.

The last comment about a possible foreign molecule acting as a networking agent, is about water. In fact, even if [Bmim][Tf_2N] is an hydrophobic ionic liquid, it can hold up to 2% (w/w) of water at saturation[28], is quite hygroscopic. First of all it has to be considered that all the solvents used have a lower water content than those from the original bottles (for example less than 0.05% (w/w) for HPLC purity grade methanol), since all the solvents are distilled twice prior to the preparation of the solutions. In particular on silicon, that is cleaned in aqua regia prior the deposition, different depositions have been performed. Usually the substrates are rinsed with distilled water, than dried under nitrogen flux before the deposition. In order to avoid water contamination of the surface, the substrates have also been

rinsed in bi–distilled methanol and then, before methanol leaves the surface, the deposition is performed. The formation of the islands has been found in both cases, noticing no differences. As a further attempt, the samples, after aqua regia cleaning and rinsing, have been annealed for few hours in nitrogen atmosphere at 250°C, in order to remove any water on the surface, and then, after cooling in nitrogen atmosphere, have been immediately deposited, again noticing no differences.

Moreover in samples produced with pure [Bmim][Tf_2N], no structures have been observed, even if also in this case the samples were deposited in air on amorphous silica, with the ordinary cleaning procedure. It has to be said that, as already discussed, the absence of the driving force provided by the evaporating solvent, could play a major role in the formation of solid–like structures. In the course of a molecular dynamics simulation performed by Pietro Ballone et. al[98], some water molecules have been added to a thin slab of [Bmim][Tf_2N], but no substantial differences in the arrangement of the ions have been noticed.

Even if these tests gave equivalent samples, the water role cannot be completely ruled out since the depositions are performed in air, and water uptake of solvent or substrate may be quite fast, and furthermore maybe fraction of water molecules per ion couples may be enough to provide structuring effect. In fact, in some cases some samples evidencing no structures, even if produced in the same experimental conditions, have been obtained. The differences with the usually obtained samples may be related to a slightly different temperature as well as to different relative humidity of the environment. In fact, water is known to have a strong effect on both density and viscosity of the ionic liquids[38], and this can of course influence the output of the depositions.

The last comment about the role of the solvent regards the qualitative difference sometimes observed using ethanol respect to the other solvents. In fact, as shown in Figure3.10, some solid–like terrace produced using this solvent show a certain degree of crystalline order along the plane of the surface. The discussion of the results of the study of the role of the solvent let us argue that the difference in the structures has not to be search in a modification of the ionic liquid by the solvent, but more in a different solvation of the [Bmim][Tf_2N] in ethanol. Even if the arguments needs to be further studied, some ideas for the different behaviour can be sketched. It is possible that ethanol fluidise better the IL than the other two solvents, or also that increases the mobility of the ions along the substrate, favouring ions migration and aggregation. Moreover, in IL/solvent solutions small aggregates can be present and the dimension of these aggregates can depend

on the solvent use: given that the size of the domains of IL reaching the substrate is possibly of critical importance in the nucleation and growth of solid–like layers, if in ethanol only small or none aggregates are formed, the development of the ordered layers can be easier because of the increased mobility of the ions, leading to more 3D–ordered structures.

3.2.2 Role of the substrate

From the study performed, it looks evident that the formation of the ordered terraces is an effect due to the interaction with the substrate. In fact this formations are not already present in the bulk liquid, but neither in the solutions. For example, the same solution used for depositions on oxidised silicon has been used on nickel, where nothing structured could be found (see Figure 3.34).

The interaction of ionic liquid with solid surfaces is known to induce orientation and self–assembly of ionic liquid molecules, and to promote the formation of solvation layers. Second frequency generation (SFG) is a spectroscopic technique sensitive only to the very first layer at the liquid/solid interface. Rollins, Fitchett and Coboy[68] studied the orientation of the imidazolium cations on a silica surface, as a function of the alkyl chain length. They found that the alkyl tails orient almost perpendicularly to the surface, whereas the imidazolium rings tend to lie the more parallel the shorter the lateral chain. Furthermore they found that the orientation of the cation ring is related with the different surface charge induced by the contact with the different ionic liquids: a higher negative surface charge, induces the ring to lie more parallel. The authors report a very little influence of the anion on the orientation of the cation at the interface.

SFG has been used also for studying the interfacial behaviour of [Bmim]-[BF_4] and [Bmim][PF_6] on the surface of quartz by Romero and Baldelli[66]. The authors found that in this case the imidazolium ring can form an angle between 45°and 90°with surface normal in the case of [Bmim]–[BF_4], while in [Bmim][PF_6] this angle is reduced to 38°–58°, evidencing an influence of the anion on the cation orientation, even if also in this study, only the resonances of the cation were monitored.

Cremer et al.[71] deposited, by means of physical vapour deposition (PVD), [Emim][Tf_2N] on an amorphous silica substrate, and they study the thin film in situ in ultra high vacuum, by XPS. Cremer and co–workers found that, with a sub–monolayer coverage of the surface, the ions tend to pile up, with the anion sitting on top of the cation. The same authors studied, in a more recent work[72], sub–monolayer films produced by PVD on Au (111) surface in ultra high vacuum. The behaviour of [Dmim][Tf_2N] has been first

examined, finding that at sub–monolayer coverage, both the ions lie on the surface, with N and CF_3 groups of the anion protruding toward the vacuum. If [Omim][Tf_2N], having 8 carbons in the alkyl chain, is evaporated, until 0.4 monolayers the ions lie flat on the surface, as with the previous liquid, but when the thickness of the deposit is increased, the alkyl chains tend to orient perpendicularly to the surface toward the vacuum, as found by Conboy.

Even more interesting is the fact that the authors found that on gold if the deposition time is increased, a typical layer by layer growth is observed for both the ionic liquid studied, until a thickness around 9nm. The deposition by evaporation actually is likely to provide results similar to the drop casting technique, because the deposition rate is very low and hence the small quantities of IL deposited can restructure and develop solid–like layers. Unfortunately this study doesn't provide any information about the surface morphology so precluding the possibility of a direct comparison with my results.

The previous studies elucidate how the structure of the first IL/solid interface is influenced by the ionic composition, but also how this structure can be affected by different interfaces and different ionic liquid/solid interactions. In fact, ionic liquids can interact with the surface by hydrogen–bonding, van der Waals interaction and of course, direct coulomb forces. In particular, as also mentioned by Rollins, surface charge is thought to play a fundamental role on the behaviour of the first layers of ionic liquid.

The techniques used in the previous experiments can sense just the first ions in contact with the solid surface (SFG), or they have a very limited penetration depth (XPS).

There are some other techniques, keeping a very high resolution perpendicular to the interface, but having access to a greater portion of it, used for studying ILs in contact with solid surface.

For example Mezger and co–workers[70] performed an X-Ray reflectivity study on the behaviour of 3 ionic liquids containing FAP anion, on the surface of sapphire (0001) highlighting the presence of electron density oscillations at the solid surface, decaying exponentially into the bulk with a decay length of the order of 2nm. This oscillations have been interpreted as the signature of the formation of stacked double layers of anions and cations. The authors guess that this kind of interfacial order may be induced by the charged sapphire surface. Atkin and co-workers, as already mentioned, by means of the atomic force microscope, performed force spectroscopy local studies, highlighting the presence of solvation layers formed by different ILs on different solid surfaces[77, 76]. In particular, they found how the separation between subsequent layers is proportional to the size of the ion couples, and that on a

surface with a greater surface charge, the solvation layers become more stiff and well defined, similarly to what we found performing the same kind of experiment, as illustrated in Section 3.1.4. Furthermore, in a more recent study[78], they found that an electrified interface can promote a stronger layering, since the number of identified layers increases as the breakthrough forces. The same kind of solvation layers has been found on mica by using the surface force apparatus, by Ueno et al.[94] and Perkin et al.[95].

The studies presented above evidence the ordering of the ions at solid surfaces. Moreover strong interfacial layer has been found and reported to be related to the interaction between the ionic liquid and the solid surface. Anyway, those layers are not compatible with our solid–like layers. In fact, the solvation layers found are very fragile and furthermore they can extend just for few nanometers away from the surface, while solid–like terraces found in my work are pretty resistant to normal loads and can extend for more than 50nm. Actually the presence of solid–like terraces cannot be excluded by the previous studies, since their average lateral extension can be quite small compared to the area probed by the spectroscopic techniques like XPS and SFG, and can possibly sit underneath in the measures performed by AFM force spectroscopy, since no morphological survey has been performed.

As discussed in the previous section, the role of the solvent is presumably only that facilitating the aggregation of the ions into ordered structures. The crucial ingredient is the interaction with the substrate. In particular, as already mentioned, surface charge can be a factor inducing the ordering of the IL molecules. Kaisei et al.[85], suppose that the formation of the ordered terraces on Pt surface, is related to the electric field between the tip and the substrate, that orders the ions and induce the formation of the layers, then stable even when the electric field is turned off. The surface of the oxides in general carries a negative surface charge at ambient conditions, i.e. the conditions at which the depositions in my work have been realised. The greater surface charge of mica with respect to silica can explain the increased lateral extension of the ordered domains on the former surface respect to the latter. Defects in the surface morphology or in the physico–chemical properties, like for example charge density, can be the elements triggering the nucleation of the ordered terraces. Once a nucleation site is formed, a terrace can be formed and possibly multilayers, depending on the details of the capillary forces inside the evaporating solution, can grow. An example, in this case, could be the evidence of formation of the ordered terraces on gold surface, (see Figure 3.11, where evidence of strong layering as been found also by Cremer at al.[72]), that was deposited on highly doped silicon and was likely without fixed surface charges, while on HOPG graphite nothing could

be found. Possibly, the smooth nanostructure of the gold surfaces allow the nucleation of the terraces, while HOPG flat domains don't provide good point for ordered layers to grow. A recent study by Yokota et al.[84], performed with frequency modulation AFM where a bulk of 2 ionic liquids, [Bmim][BF_4] on the one I also used, [Bmim][TF_2N], are in contact with HOPG graphite, some ordered layers are found. In this study actually the distinction between HOPG layers and ionic liquid layers is not so statistically robust, but it is interesting because it shows the possibility of growing of ordered layers similar to what I found on other surfaces, even in bulk of pure ILs. The fact that I didn't observed layers on graphite could be due to the different experimental conditions that in the case of Yokota promote the formation of the terraces.

Along with defects, also impurities on the surface can play the role of nucleation sites. In my experiments the surface chemistry and cleanliness of the substrate is only approximatively controlled, since it is very likely that cleaned regions coexist with more contaminated parts, or parts, for example on silicon, carrying a different concentration of OH groups. Since the depositions are performed in air it is also possible that hydrocarbons could be adsorbed from the environment, locally changing the interaction between the substrate and the IL/solvent solution.

Nucleation sites can also be provided by local changes in the morphology of the substrate. For example, on the sample deposited on sub–monolayer film of silica nanoparticles on silicon, the density of ordered structures is very high and this can be due to the action of silica clusters as nucleation points. Anyway, the only nucleation is not enough to lead to the formation of an extended terrace, since the IL molecules need to have a high enough mobility to freely move and aggregate into this metastable state. The high mobility can be obtained, as previously discussed, by the presence of the solvent or by the reduction of the volume of the ionic liquid in order to have a high enough surface to volume ratio that leads the behaviour of the IL molecules to be dominated by surface interactions. This last statement can be seen in the Figure 3.19, and can also explain the presence of the sublayer seen in many AFM morphological maps (see for example Figures 3.7 and 3.18). In fact, very small droplets of ionic liquid left on the surface after evaporation of the solvent, can spontaneously undergo to the formation of this diffused layer, then in time can rearrange due to the ability of IL molecules to diffuse along the surface.

Quantitative structural analysis results, exposed in section 3.1.2, show that even if qualitative differences in shape and extension of the solid–like domains can be observed on different substrates, the same fundamental thick-

ness δ=0.6nm is found for all the surfaces analysed, i.e. amorphous silica, oxidised silicon and mica. Furthermore, statistical analysis performed on the samples produced using methanol, ethanol and chloroform, again provide the same thickness value for the fundamental layer. Some images acquired in contact mode on solid–like islands on silica, allowed to extrapolate the value of δ=0.59±0.1nm, that turned out to be fully compatible with the value measured in tapping mode. Because during several contact mode scan delamination occured, the outcome of the same δ value supports the idea that the islands behave as lamellar solids and that only multiples of the fundamental layer are removed each time.

The fact the the same δ is found for different solvents, is a further suggestion that the solvent probably acts only as a fluidiser for the IL and gives the extra–energy necessary for overcoming the barrier between the liquid and the solid–like phases. Instead finding that the heights of the terraces is an integer multiple of a molecular layer having the same thickness for different substrates, and the fact that nothing on HOPG could be found, tells that surface charge is probably an important factor inducing the ordering of IL molecules, but it is not the only player. Surface charge density on mica and silica are very different, being 1 charged site per 0.48nm^2 and per 20nm^2 respectively, as measured at neutral pH in water[77]. Nonetheless the high difference in surface charge density seems to influence more the lateral extension of the layers than the vertical packing and orientation of the ions. Other interactions with the substrate can have a role in the formation of ordered domains, acting in synergy with surface charge. For example, a simulation performed by Sieffert et al.[100], shows how when a bulk of [Bmim][TF_2N] is brought in contact with a fully hydroxylated quartz surface, the anion can form hydrogen–bonding with the surface. The same interaction between the anions and the substrate has been seen in the simulation performed by Ballone and co–workers in collaboration with our group[98], as it will be discussed later.

The value of δ extrapolated from the statistical analysis of the heights, is slightly lower than that found by SFA experiment by Ueno et al.[94], but is instead in good agreement with the periodicity of the density profile found in a simulation performed by Ballone in collaboration with our group[98], and furthermore is in accordance with the distance between solvation layers found in the measures performed in bulk [Bmim][TF_2N], even if the statistical accuracy of this value is not exceedingly high. Similar values have been obtained by Atkin et al[76]. for similar systems.

Of course, the model used for the extrapolation of the δ value, i.e. that the internal structure of the solid–like islands is composed by superimposed fundamental layers having a uniform thickness, is a simplification although

reasonable. More complex models considering a multilayer formation composed by layers having different thickness, for example two charged layers, could be develop. Nonetheless it has been thought that the last model would introduce more complications without providing a substantial improvements in the interpretation of the internal structure of solid–like layers.

3.2.3 Resistance to strong electric fields

As seen in section 3.1.3, the resistance to strong forces induce by the application of a potential difference between the tip and the substrate, has been studied. Surprisingly, since the structures are composed by ions of the ionic liquid, they are not dissolved by the exposition to such a high electric field. As underlined in Figure 3.18, if an area of the sample containing both IL in liquid and in solid–like phases, is repeatedly scanned in tapping mode, usually both the structures experience minor damages by the action of the tip, mainly located at the edges of the terraces. Anyway, after a scan applying a bias is performed, the great part of the IL droplets is removed, as expected to happen to ions in a liquid phase subjected to a strong electrostatic force. On the other hand, the solid–like layers do not leave the surface, but maintain a recognisable shape also after several scans with applied bias, even if they are eroded by the action of the electrostatic field. This behaviour means that the ions in the ordered layers are tightly bound in a solid structure. The erosion of the layers probably begins in correspondence of local defects where the bonds are looser. The marked difference respect to the behaviour of the droplets clearly supports the fact the we are dealing with 2 different phases that the ionic liquid develop once placed in contact with a solid surface. It is interesting to note the erosion in Figure 3.18 where substrate was supposed to be exposed. In fact, this observation, together with some other evidences found in other images, leads to think that a diffused molecular layer of ionic liquid is often present on the substrate surface.

Furthermore the evidence of the immobilisation of the ions into ordered structures, let us to guess that this layers behave both ionic and electrical insulators, as it has been confirmed by local measurement of the dielectric constant of ordered terraces performed by Galluzzi in our laboratory[83], leading to a relative dielectric constant ϵ_r=3–5. This observation and the measurement of the dielectric constant, could be of crucial importance for those applications in which electrons have to flow at a solid–ionic liquid interface, as in Grätzel cells.

3.2.4 Solid–like layers: mechanical resistance

The results of the section 3.1.3 show the mechanical robustness of the ordered terraces, and after that section confidently named solid–like. The scanning tip, in tapping mode or in force volume (at least until pressures lower than the breaking pressure are used), induces only a shrinkage of the solid–like layers, due to border erosion. The erosion happens at the edges of the structure because these are the most delicate parts of the terraces the ions along them interact with a lower number of nearest neighbours than the ions inside or even at the top surface. Since the borders are quite steep, in the case of tapping scans the feedback loop finite response time induce a local increasing in the lateral force applied by the tip, further promoting the erosion.

A further hint endorsing the solid–like character of ordered layers, is the possibility to perform contact mode scans on them. Figure 3.15 in the previous section in fact, show that the same structures seen in tapping mode morphologies can be found even maintaining a permanent contact between the tip and the substrate. In contact modality adhesion and, again, finite response feedback time, leads to the application of higher lateral forces respect to tapping, such that, for example layered structures formed by supported lipid bilayers in air, cannot be observed.

Even the solid–like terraces anyway, undergo to deterioration under contact mode scans, but in some cases it is possible to see that from multilayered structures, the layers are peeled off starting from top, as reported in Figure 3.15. This kind of behaviour is the typical behaviour expected for a solid composed by superimposed lamellas, as for example graphite, mica, etc...

Also observing the indentation curves on solid–like structures, it is clear a lamellar nature: in fact the highest the thickness the greatest the number of peaks in the force curve (see for example Figure 3.22). The surprising thing is that even if each set of data analysed in the structural analysis gave fundamental layer thickness of δ=0.6nm and even if also very thin layers can be found in some images, the distance between subsequent peaks in force curves always around 2.2 $\pm$ 0.1nm, never around one single fundamental layer. Furthermore, the peaks can be separated in main peaks, the highest ones, and secondary peaks, that look like shoulders on the descending part of the force curve after a main peak. The average distance between solely the main peaks is around 4.7 $\pm$ 0.2nm. When good–shaped tips are used, the heights, in force, of the main peaks in the same force curve are the same, as well as the heights of the secondary ones. A possible interpretation could be that the internal structure of the terraces is not a uniform stack of fundamental layers, but it is composed by domains possibly separated by stacking fault defects: the existence of peaks with different breakthrough

forces, can be related to the different internal ordering of the ions. It in fact possible that in the same terrace between 2 main peaks, a multiple arrangement of ions is realised.

The surprisingly well overlapping curves acquired on the same island, but also of those curves collected on different samples, means that the internal structure of solid–like islands is reproducible and consequently this tells how there is a specific ordering of the ions into the layers.

The part of the force curves before each rupture (indentation) has been interpreted as the elastic compression of the solid–like layers, whose reduced Young modulus is E*∼1.8GPa. Similar Young modulus are found for some polymeric materials like acrylonitrile butadiene styrene (ABS) plastics, acrylic, nylon, polycarbonate, etc... Observing the force curves having multiple peaks, it can be noticed that the raising part before each rupture (indentation) has almost the same slope, so compatible Young modulus, further supporting the idea that the structure of solid–like islands is made by a superposition of the same kind of layers separated by defects. Actually the interpretation of the slope before the rupture as an elastic deformation, and the fit to the simple Hertz model, is likely to be an oversimplification of the contact mechanics. Furthermore, the values of the pressures and so of the E*, is dependent on the precise calculation of the tip radius, that is particularly subjected to errors for the sharp tip used. Furthermore, has it can be observed in Figure 3.26, even small variations in the tip shape, due to the sharpness of this probes, can lead to big variations in the force curves collected. This can probably explain also why in few cases the shape of the patterns observed in the force curves don't overlap with the main group of the rest of the datasets, and also why in some cases the calculated breaking pressures can vary changing the tips. Interestingly, despite the fact that diffused layers uniformly covering the substrate have been often observe (see Figures 3.16 and 3.19), force curves performed on the area surrounding solid..like islands in PS measurements never show any indentation. Since the height of the terraces measured in tapping mode is compatible with le length of the sawtooth profile, it seems that the rigidity of this layer, if present, exceeds the pressures reached during the experiments ($\sim$ 9.5Kbar). This behaviour can be reasonable if considering that the first molecular layers could be more tightly bound due to their proximity to the substrate, as reported by Atkin et al.[76, 78].

3.2.5 Comparison with numerical simulation results

In this section the results of the numerical simulations performed by P. Ballone and M. Del Pópolo from Queen's University of Belfast and, in the second

study also with N. Manini, Università degli studi di Milano, will be discussed. In particular the discussion will be focused on similarities and differences between simulations and experiments.

In the first study[98] a simulations for a homogeneous [Bmim][Tf_2N] film 4 nm thick in contact with a Si terminated, fully hydroxylated (111) β–cristobalite surface has been performed.Samples have been equilibrated by annealing from high temperature (starting at T=600K), and production runs 5 ns long have been carried out at T=300, 350 and 400K. At these three temperatures, we observe large amplitude density oscillations arising from the IL interaction with the silica surface. At T= 350 and 400K layering is confined to the very first molecular planes, while the rest of the film appears to be liquid–like. At T=300K, however, layering extends much deeper into the IL side of the interface, up to $\sim$2.5nm. The identification of the thermodynamic state of the IL film at this temperature (T=300 K) is somewhat uncertain. On the one hand, the IL overlayer is apparently disordered, and displays some residual mobility of the ions. On the other hand, diffusion and relaxation are very slow on the simulation timescale, and several of the IL properties point to a glassy state. The periodicity (δ=0.60nm) of the density oscillations depends only weakly on temperature, and is in good agreement with interlayer separation measured by experiments.

The role of surface hydroxylation in establishing layering has been investigated by repeating the T=300K simulation for a fully de–hydroxylated, neutral silica surface, obtained by replacing each of the original OH groups by a single O atom of reduced charge. This change affects the position and shape of the first IL layer in contact with the surface, but the effect is quantitatively small. On the other hand, removing the surface altogether restores the symmetry of the slab, and restores its fluid–like character. These observations are very important, since they confirm that the melting temperature of the IL model (not quantitatively determined in this simulation) is below T=300 K, and every glassy or solid–like feature in the system structure and dynamics is due to the presence of the solid surface, apparently felt far away from the solid surface. Moreover, excluded volume effects, familiar from computational and simulation studies of simple liquids in contact with solid surfaces[105], are more important than specific adsorption, whose effect is fairly local.

First of all, it is apparent that the general properties of layered islands are far more solid–like than in the simulation results. The difference might be due to a limitation of simulation, unable to nucleate a crystal–like phase for the overlayer during the nanosecond scale of our computations. On the other hand, unaccounted for details of experiments might also be responsible for the discrepancy. Drop–casting is a rather complex process, and, in principle,

the results might depend on the deposition protocol. More importantly, impurities present on the surface might act like gelation agents able to change the state of the deposited film. The most abundant contaminant present at oxide surfaces exposed to air is likely to be water. In most cases, water is expected to enhance fluidity and diffusion of ILs[34], but, in principle and only in special cases, it might act as a gelating agent by forming an extended network of hydrogen bonds. In this respect, it is important to consider that the IL used in our experiments and simulations is relatively hydrophobic, but it is also known to be weakly hygroscopic when exposed to air[35, 36, 37]. Computer simulations[102] show that, as expected, water in bulk [Bmim][Tf_2N] tends to reside in proximity to the hydrophilic side of $[Tf_2N]^-$. In principle, one might speculate that, at precise stoichiometric composition, water and IL give rise to ordered structures whose melting temperature is higher than that of the pure and homogeneous IL. The formation of a solid–like overlayer, in any case, has to be a surface effect, since ordered water–[Bmim][Tf_2N] has never been observed in the bulk, even when the IL is equilibrated in a wet atmosphere[35, 36, 37]. In discussing the detailed comparison of experiments and simulations, however, it is essential also to consider that the silica surface described by our simulations is globally neutral, while real silica surfaces are known to acquire a small but non– negligible charge[68]. Once the validity of the computational picture is clearly assessed, and possibly brought into agreement with the experimental one, simulation can be exploited to provide a wealth of microscopic information, partly inaccessible to experiments. For instance, the analysis of simulation snapshots shows that the first IL layer in contact with silica, giving rise to a high and sharp density peak, is due primarily to the specific adsorption of the anion, hydrogen bonded to the OH groups at the solid surface. Local charge neutrality is restored by the adsorption of a nearly equivalent number of cations into this first layer, that appears depleted of butyl $[Bmim]^+$ tails. The in–plane distribution of ions in this first plane contains remarkable seeds of crystal–like ordering, probably due to the regular corrugation of the underlying solid surface.

Charge neutrality is rather effectively enforced throughout the system, as shown by the detailed analysis of the charge density profile, and of the electrostatic signature of the interface. The positional ordering of ions apparent in the wide amplitude density oscillation at the interface is complemented by considerable orientational ordering, especially for the cations. Coupled to the uneven distribution of charge on the molecular ions, this ordering might give rise to a variety of paraelectric and ferroelectric configurations. Our simulation results might already contain hints of an incipient paraelectric to ferroelectric transition taking place at interfaces before the liquid to solid transition.

In the second simulation[99], has been studied the effect of indentation the same thin slab of [Bmim][Tf_2N] seen the first in simulation, by a hard nanometric tip, on silica substrate. In particular the normal force F_z acting on the nanometric tip is monitored as a function of the distance from the silica.

At first sight, despite several qualitative similarities, the simulation results seem to differ from experimental data on solid–like layers as well as from experiments performed in bulk ionic liquids (both those performed during my PhD work and those by Atkin). First of all, the pressure under the tip required to penetrate the IL lm is estimated by the simulation at ∼5KBar. This value is likely to be much higher than the maximum pressure applied during tapping mode measurements, estimated at ∼0.2KBar. This implies that the AFM tip operated in tapping mode is unable to penetrate the lm, which therefore appears solid–like. On the other hand, the simulation results do not provide any explanation of the regular 0.6nm periodicity seen in the experiments. In the simulation sample, layering is apparently very defective, possibly as a result of the very long relaxation times of [Bmim][Tf_2N] in close contact with the silica surface. Moreover, the 0.6nm periodicity seen under tapping mode conditions (∼0.2KBar pressure under the tip) might not be present at the pressures required to penetrate the lm. Finally, ILs are known to give rise to mesophases[95, 97, 77, 76, 78], and a minimum system size larger than that in the simulated sample might be needed to reproduce the experiments quantitatively. Comparison of the simulation results with the data by Atkin and co–workers, as well as the comparison with the data I acquired in bulk [Bmim][Tf_2N] also shows similarities and differences. In particular, the comparison Figure3.44 and Figure 5 of Ref.[76], shows similar qualitative features in the Z–dependence of computed and measured F_z, both displaying an increasingly repulsive character with decreasing Z, superimposed to localised uctuations, and to low–amplitude, long wavelength oscillations. Moreover, the intensity of the normal force F_z is comparable in the two sets of data, in both cases raising up to ∼16nN. This good agreement, however, is accidental, since these forces are measured on tips of signicantly dierent radius, i.e., 2nm for the simulation, and 20nm for the experiment. The pressure under the tip, therefore, is signicantly larger in simulation than in experiment. This can be due, rst of all, to the different ionic liquid considered in the simulation and in the experiment. More importantly, however, as already emphasised, the simulation refers to a thin lm, while the experimental measurements have been carried out with the AFM tip immersed into a thick bulk–like film.

The crucial role of this last difference is confirmed by the results of the nano–mechanical analysis carried out on solid–like layers (see the second

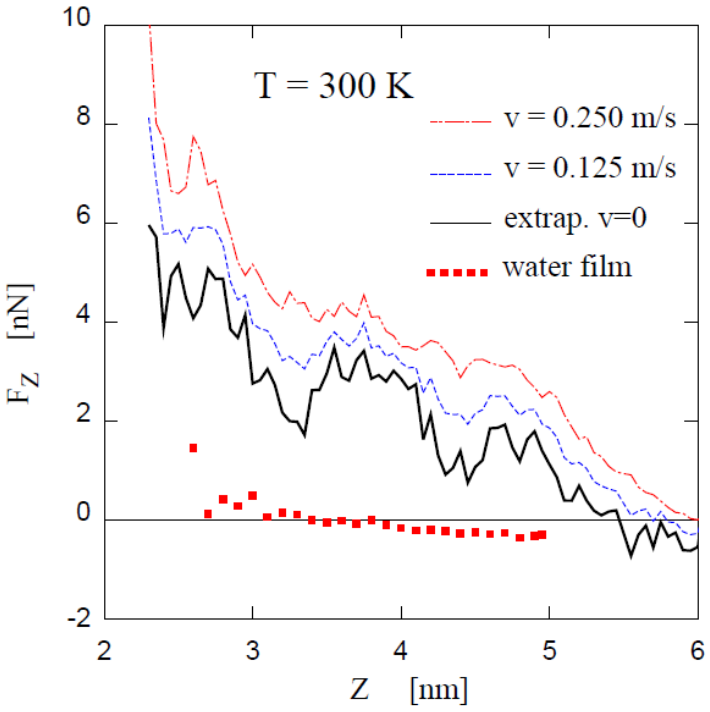

Figure 3.44: *FIG. 4: Average force on the incoming sphere as a function of distance from the silica surface. Dot-dashed line: approach velocity v=0.25m/s; dashed line: approach velocity 0.125m/s; full line: extrapolation to v=0 (see Ref.[99]). Filled squares: force required to indent a water lm of comparable thickness; single trajectory, v=0.25m/s, T=300K. Figure reproduced from Ref. [99].*

part of the section 3.1.3. These experimental results, therefore, refer to the same system that has been considered in the simulations, at comparable thermodynamical and probing conditions. The computational results are the closest to the experimental results. The breakthrough pressure to penetrate a solid–like terrace is of about 2–3KBar, fully comparable to the 5KBar estimated for the simulated system. The residual quantitative discrepancy might be due to differences in the time and size scales probed by experiments and by simulation, far beyond the range that can be approached in the computations. On the other hand, the electrostatic charge on the surface and on the tip seems to have only a minor effect on the measured normal force, at least at the pressures required to penetrate the nanometric lm. This has been indirectly veried by repeating the indentation simulation on the mica/ [Bmim][Tf_2N], taking into account the surface charge that spontaneously form at the mica surface[103]. The simulation results reveal quantitative changes with respect to the silica case, but no qualitatively new features.

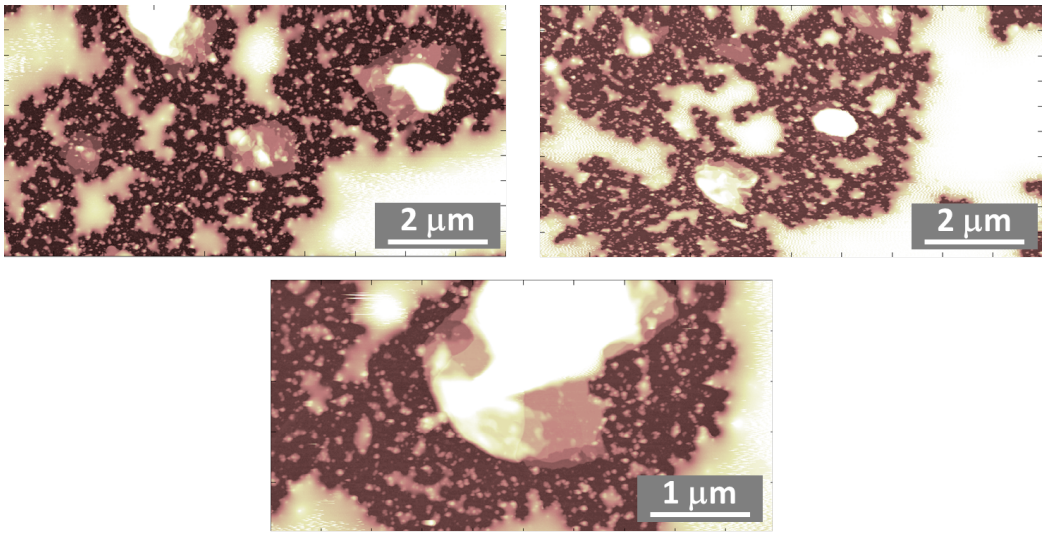

Figure 3.45: *Collection of AFM morphologies of [Bmim][Tf_2N] deposited with methanol on a sub–monolayer coating of silica nanoparticles on oxidised silicon. The images allow to appreciate the thickness and density of the terraced structures, whose formation is not prevented by the presence of silica clusters. Vertical scales 50nm.*

3.3 Preliminary results on the interaction with nanostructured materials and perspectives

As already remarked, the optimal use of nanostructured surfaces in contact with ionic liquids in many applications would requires an extensive study of the interface between the IL and the solid. During this work I have focused my attention on the interaction of ILs with model surfaces like silica and mica; preliminarily, I have also deposited ILs on ns surfaces and imaged the IL/solid interface.

The roughening of the substrate surface can be expected to lead to two opposite effects: on one hand a rougher surface introduces some degree of disorder that can inhibit the formation of well ordered structures; on the other hand, since with a nanostructured deposition the surface area is greatly increased respect to a flat substrate, if the affinity between the ionic liquid and the material composing of the nanoparticles is high, the formation of solid–like structures could be enhanced.

Figure 3.45, as well as the previously reported Figure 3.12, shows the result of a first approach to the study of a rough surface. For the AFM investigation it is of particular interest the case of a sub–monolayer deposition

of nanoparticles on a flat surface, in this case silica nanoparticles, because this represents a first step toward a nanostructured surface and also it should be easier to observe the effects of the IL/solid interaction, if any. From the figures it is possible to observe that the affinity between the silica nanoparticles and the IL is actually high. As can be noticed in fact, the shape of the liquid domains in no more that of rounded droplets, but the IL lies more flat on the surface and every droplet looks pinned to some silica nanoparticles. The morphology of the droplets remember that of a liquid experiencing dewetting for minimise its free energy, but it is not allowed to a further reduction of its interface because it is trapped on the surface be localised points acting as pinning elements, the same effect that happens when a drop of IL solution is deposited onto a small substrate and pins to the borders.

Actually the affinity of the [Bmim][Tf_2N] with the silica surface is witnessed by the low contact angle ($\sim 11°$) [Bmim][Tf_2N] on silica calculated by the shape of nano–droplets in AFM topographic map, reported in a previous work[82] (the paper is reported in App. B).

Figures 3.12 and 3.45 evidence that the presence of a dense distribution of nanoparticles on the surface of oxidised silicon actually doesn't prevent the growth of multilayered solid–like domains, that are as thick as on flat surfaces and densely distributed. The fact that, at least on substrates where it is still feasible an AFM investigation, the introduction of nanoparticles still doesn't prevent IL ordering phenomena, leads us to think that if an ionic liquid would be confined into a nanoporous matrix, where in each pore the surface to volume ratio for the IL is high, the ordered, solid–like phase, can still develop.

When considering the effect of confinement on melting point of a substance, in general a reduction in the melting temperature respect to the bulk can be observed. A simple argument can be tentatively invoked in order to predict the effect of confinement on ILs. Considering a particle, a reduction in size induces an increase in the ratio of surface atoms to volume atoms. Surface atoms have a lower number of nearest neighbours than bulk atoms and so if the surface to volume ratio increases, the cohesive energy correspondingly decreases, following the relation[87]:

$$E = E_b \left(1 - \frac{a}{d}\right) \tag{3.1}$$

where E_b is the bulk cohesive energy, a is the atomic diameter and d is the diameter of the particle. The decrease in the cohesive energy leads to a decrease in the melting point of the particle (the same reason for the decreasing in melting point going from ordinary salts to ionic liquids!). The same argument is still applicable to confined systems, in which the melting point reduction is

described by the Gibbs–Thomson equation. The Gibbs–Thomson equation analyse the behaviour of a solid confined into a nanopore in contact with its own liquid and allows to calculate the melting temperature as a function of the pore diameter as:

$$T_m(d) = T_{mb}\left(1 - \frac{4\sigma_{sl}}{d\Delta H_f \rho_s}\right) \tag{3.2}$$

where T_{mb} is the bulk melting temperature, σ_{sl} is the interfacial tension between the liquid and the solid phase of the confined material, ΔH_f is the bulk enthalpy of fusion and ρ_s is the density of the solid phase[86]. While this equation describes the behaviour of many confined liquids, i.e. in general a lowering of T_m, i.e. confinement–induced fluidification, several assumptions are made in the model such as the fact that the interfacial tension is isotropic and that ΔH_f and ρ_s retain their bulk values independently on the size. In many studies (reported in the review in Ref. [86]), ΔH_f if found to decrease with d. Furthermore, not only pore size but also pore shape influences the behaviour of T_m as a function of d.

The predicting behaviour for melting point by the Gibbs–Thomson equation is opposite to what we have seen on flat and rough surfaces as well as to that we guess can be seen into nanopores, anyway it as to be noted that the variation of melting point for immobilized or confined materials is still not fully understood and requires further investigation.

Some studies on the variation of the melting point of ILs upon confinement in nanoporous matrices, actually show that T_m follow the behaviour predicted by equation 3.2. In particular Konakubo et al.[91] studied, by density scanning calorimetry (DSC) the behaviour of the melting point for several imidazolium–based ionic liquids confined in a controlled porous glass (CPG) matrix on both the slightly hydrophilic native matrix and on a methyl–modified hydrophobic one. In both cases a marked decrease of T_m is observed for all the ILs. Liu et al.[90] studied by DSC the variation in the melting point of several imidazolium–based ILs in ILs/silica nanoparticles mixtures. They found, as Konakubo, a depression in the melting point for all the ionic liquids studied. Anyway, it is interesting to note that the authors argue that the depression in T_m is due to the immobilisation of imidazolium cations at the surface of the hydrophilic silica particles. In this confined geometry part of the ions are then freezes in an high entropic state that breaks the symmetry in the liquid and leads to a decrease in the melting point.

Despite the prediction of the Gibbs-Thomson equation, there are other studies in which the melting point seems to increase upon confinement. In particular ordering–immobilisation of ionic liquid ions at the pore interface is thought to be responsible for a decrease in conductivity in a study conducted

by Iacob et. al[53]. In this study the conductivity of the IL [Hmim][PF_6] confined in nanopores, with an average diameter around 7nm, is measured. A decrease of an order of magnitude in the conductivity respect to the bulk is observed when hydrophilic silica, i.e. with an hydroxilated surface, is used. If the internal surface of the pores is modified by silanisation, adding trimethylsilyl inert groups, the conductivity in the membrane is almost the same as in the bulk. The authors suggest that the decrease in conductivity for non–treated silica is due to the formation of a bound surface layer on the internal surface of the pores.

In another study performed by the group of Grätzel[52], silica nanoparticles are used to induce a gelation in a ionic liquid–based electrolyte for a DSSC solar cell. Only 5 wt % or 3 vol % of nanoparticles having an average diameter of 12nm added to two IL–based electrolytes (composed of 0.5M iodine and 0.45M of N–methyl–benzimidazole in either pure [Pmim][I] or a mixture of [Pmim][I] and 3–methoxypropionitrile (volume ratio 13:7), respectively) is needed to realise a gel. 3% in volume roughly means that the distance between the surface of neighbouring nanoparticles is around 20nm, but nevertheless a stable gel can be realised. This may happen because each particle is surrounded by a bonded layer of ionic liquid molecules increasing their actual diameter and leading to the gelation. The fact that the gelation influences only weakly the conductivity of the electrolyte could mean that the volume is not filled completely by immobilised layers, but some channels are formed, allowing for ionic liquid ions redox couple flowing.

Ueno et al.[88] show the formation of gels by adding to different ionic liquids hydrophilic or hydrophobic silica nanoparticles. In particular the addition of hydrophilic particles lead to the formation of stable colloidal suspension and ionogels. The authors relate this stability with the development of solvation layers that prevent the particle aggregation and lead to the formation of a stable structure.

A simulation study conducted on the ionic liquid [Dmim][Cl] confined in a nanoporous carbon material[104], shows the development of a clear surface layering and a slower dynamics of the ions than in the bulk.

In another interesting study[89], it is shown how the confinement of [Bmim][PF_6] into carbon nanotubes induces the formation of crystal, whose melting point is around 200°C, so about 200°C higher than the melting point of the bulk liquid, that is around -6°C.

3.3.1 Perspectives

Our preliminary results and the studies found in the literature, suggest the formation of immobilised, possibly solid–like, layers of ionic liquids in contact

with nanoporous matrices, is not unlikely and such structures can strongly affect the properties of the devices in which those interfaces are present. Systematic studies have to be performed on different nanostructured materials, for example on ns–carbon and ns–TiO_2. In order to better understand the behaviour of ILs in contact with those nanostructured surfaces, the studies could be conducted starting from sub–monolayer depositions and then increasing the thickness of the ns–film.

Particular attention will be devoted to the study of both the ILs and the materials directly used in photoelectrochemical applications. In this optics it will be particularly interesting the study of the interaction of ionic liquids with flat titanium dioxide covered by a monolayers of one of the dye molecules currently used in solar cells. If still solid–like layers will develop, this could be an important point to take care when assembling a solar cell adoperating an electrolyte based on that specific ionic liquid.

Interfacial phenomena occurring at the IL/ns–electrode interface of both "real"and in–silico samples will be investigated; moreover, the electric and photovoltaic performance of prototypical DSSC assembled using ns–TiO_2 films as photo–electrodes, and filled with selected ILs–based electrolytes, will be studied, in order to observe how the interfacial properties affect the behaviour of real devices. The aim is to conduct a bottom–up optimization of real devices, based on the acquired knowledge of basic interaction mechanisms occurring at the nano–scale. Diverse experimental strategies will be applied to achieve a deeper understanding of interfacial phenomena occurring within a nanoporous TiO_2 photo–electrodes impregnated by ILs. Ns–TiO_2 films with controlled porosity and granularity will be produced, exploiting novel approaches based on supersonic cluster beam deposition and suitable post–deposition treatments. The degree of impregnation of the IL–based electrolytes into the ns–TiO_2 matrices will be characterized by fluorescence optical microscopy techniques; AFM coupled to advanced surface patterning methods and Electrochemical Impedance Spectroscopy will be used to characterize the structural and electric properties of ILs confined into TiO_2 nanopores. Atomistic simulations of structural and dynamical properties of nano confined ILs will be performed in order to complement the experimental observations. Impedance and photovoltaic properties of prototypical DSSC will be characterized and correlated to the interfacial properties of nano–confined IL–based electrolytes.

Along with the studies on nanostructured materials it would be interesting to repeat, taking advantage of the experience gained, the same kind of morphological and mechanical studies using different ionic liquids. First of all it can be interesting to study ionic liquids having the same [Tf_2N] anion

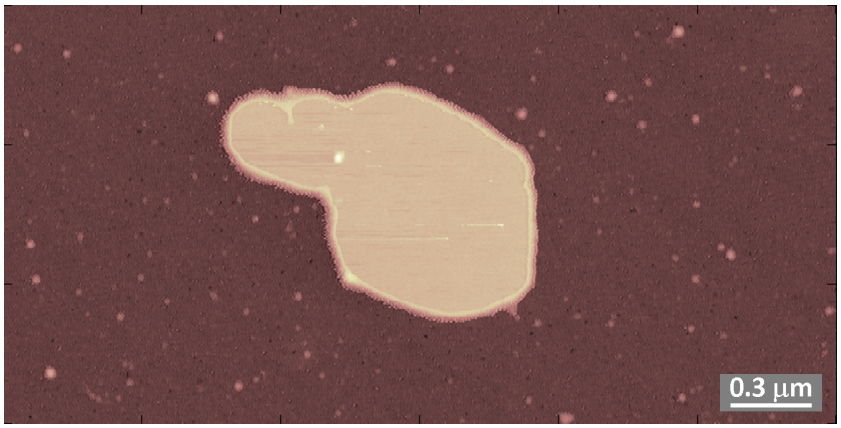

Figure 3.46: *AFM topography of [C_{12}mim][Tf_2N] deposited from a methanol solution on oxidised silicon. This preliminary result shows how the development of solid–like layers can be a characteristic common to several ionic liquids.*

and an alkyl substituent with a different number of carbons on the imidazolium cation. At the moment in our lab [C_8mim][Tf_2N] and [C_{12}mim][Tf_2N] are available for this kind of test depositions. Only few test measurements have been performed, but as it can be seen in Figure 3.46, reporting the case of [C_{12}mim][Tf_2N] on oxidised silicon, it can be argued that the formation of solid–like terraces may be a feature common to many ionic liquids, at least to the imidazolium based ionic liquids, that are widely used in applications.

Ionic liquids with the same cation and different anions can be adoperated too, in order to see for example the influence of the H–bonding capability of the anion on the formation of solid–like terraces. Furthermore, ionic liquids directly used in photoelectrochemical applications, like the [PYR14][Tf_2N] (N–butyl–N–methyl–pyrrolidinium bis(trifluoromethanesulfonyl)imide), used in electrochemical capacitors, are available and ready for the investigation.

Chapter 4

General conclusions

During my PhD work I investigated the interfacial properties of thin ionic liquid layers on solid surfaces by atomic force microscopy. Atomic force microscopy has been chosen since it allows to acquire morphological maps with a sub–Angstrom resolution along vertical direction and of the order of few nanometers in the lateral direction. Furthermore simultaneously to the topography, other maps of the physico–chemical properties can be acquired, with the same or comparative lateral resolution.

The morphological investigation of [Bmim][TF_2N] thin films on different test solid surfaces (amorphous silica, silicon covered by its native oxide, mica, HOPG and preliminarly on MgO, TiO_2 and NaCl). On all the substrates checked but HOPG, the ionic liquid exists in the form of micro- and nano--droplets and flat ordered solid–like domains behaving like solids under the AFM tip. Ordered flat layers can have an in–plane extension of several microns or even tens of microns and can be more than 50nm thick and are usually composed by superimposed terraces, in a ziggurat–like arrangement. The thickness of each single terrace ranges from fractions of nanometer to about 10 nanometers. A quantitative statistical analysis of the heigths of the terraces as been performed; interpreting the terraces as composed by stacked molecular layers with thickness δ found $\sim$0.6nm for all the substrates and all the solvents used. This observation suggests that the internal structure of the IL ordered domains is not strongly influenced by the substrate and also that the solvent acts only as a fluidising agent that allows the IL to reconstruct under the influence of surface forces. This value is in agreement with the period of density oscillations found in molecular dynamics simulation of a thin slab of [Bmim][TF_2N] on silica[98].

The mechanical resistance of the ordered domains has then been examined by nano–mechanical tests performed with the AFM. Under the influence of forces parallel to the substrate applied by scanning in contact mode, the

ordered domains are not easily removed and tend to be eroded as lamellar solids, since a terrace–by–terrace erosion can be observed. Investigating the resistance to normal loads, sawtooth profiles in nano–indentation experiments (force vs. distance curves) have been found, highlighting a sequence of ruptures, separated by 1.8–2nm, where the average rupture pressure is ∼2–3KBar, very similar to the maximum pressure found in MD simulations of a tip penetrating a 4nm thick [Bmim][Tf_2N] film on silica[99]. The first part of the sawtooth profile shows a compression that has been treated as an elastic compression of the domain. A simple Hertz model has been applied to fit the compression, leading to Young modulus E^* ∼1.8GPa, similar to that of some plastic material like nylon. Moreover, the observation that supported IL islands were not disrupted by intense electric fields up to 10^8-10^9V/m (applied biasing the AFM with respect to sample during imaging) and that Scanning Nanoscale Impedance Microscopy[14] measurements highlighted a dielectric insulating character of the ordered domains (ε_r = 3–5 was measured[83]) is consistent with the idea that IL ordered domains behave as solid materials in which the ions are tightly bound. From this observations we concluded that the ordered domains are actually solid–like structures.

Finally, some preliminary studies have been conducted on nanostructured substrates. In particular when [Bmim][Tf_2N] is drop–casted onto a sub–monolayer of silica nanoparticles on oxidised silicon (deposited by supersonic cluster beam deposition), a dense distribution of multilayered solid–like domains has been found. This observation could be possibly related to the strong affinity of [Bmim][Tf_2N] with silica, witnessed by the small contact angle, as measured on nanodroplets by AFM (for details refer to paper[82], reported in App. B). This observation is in accordance with a paper in which the addition of a small amount (5% wt) of silica nanoparticles is enough to induce gelation in an ionic liquid–based electrolyte[52].

The findings of my PhD work highlight the potentialities of scanning probe techniques for the quantitative investigation of the interfacial properties of thin ionic liquid films. In fact my AFM investigation highlights how heterogeneous can be the IL/solid interfaces and so how important is to characterise local and not only average interfacial properties.

My work shows that the behaviour of thin layers of ionic liquid is greatly modified by the influence of the substrate. In particular, I found a coexistence of liquid domains and terraces with elevated structural order. The formation of those structures, not present in the bulk liquid, is clearly induced by the contact with the solid surface. The solid–like terraces are very resistant to normal loads and to intense electric fields and, (differently with respect to liquid droplets) and they tend to behave as insulating layers.

The findings of the preliminary work on nanostructured surfaces are extremely important, because they suggest that solid–like layers can still form on rough and nanostructured surfaces. The formation of such solid–like insulating layers on the surface of a nanoporous matrix, as those used in photoelectrochemical applications, could lead to a reduction of the pores size, so affecting transport properties, and furthermore it can limit the passage of electrons; this means that solid–like formation, if present, possibly have a remarkable influence on the performances of the devices.

To further elucidate the behaviour of ILs in nanoporous matrices, in the next future it would be important to perform systematic studies on different nanostructured materials, for example on ns–carbon and ns–TiO_2. The studies could be conducted starting from sub–monolayer depositions and then increasing the thickness of the ns–film. Particular attention will be devoted to the study of both the ILs and the materials directly used in photoelectrochemical applications.

Taking advantage of the experience gained, the same kind of morphological and mechanical studies performed during my PhD work, could be replicated on different ionic liquids, to study for example the behaviour of IL having the same cation and different anions or vice–versa in order to find if some general rules could be highligthed.

Bibliography

[1] Binnig, G., Rohrer, H., Gerber, C. and Weibel, E., *Phys. Rev. Lett.* **49**, 57–61 (1982).

[2] Binnig, G., Quate, C. F. and Gerber, Ch., *Phys. Rev. Lett.* **56**, 930–933, (1986).

[3] Wiesendanger, R., *Scanning Probe Microscopy: Methods and Applications*, Cambridge University Press, Cambridge, (1994).

[4] Burnham, N. A., Chen, X., Hodges, C.S., Matei, G.A., Thoreson, E.J., Roberts, C.J., Davies, M.C. and Tendler, S.J.B., *Nanotechnology* **14**, 1–6, (2003).

[5] Butt, H. J. and Jaschke, M., *Nanotechnology* **6**, 1–7, (1995).

[6] Hutter, J. L. and Bechhoefer, J., *Review of Scientific Instruments* **64**, 1868–1873, (1993).

[7] Butt, H–J., Cappella, B. and Kappl, M., *Surf. Sci. Rep.* **59**, 1–152, (2005).

[8] Tabeta, M. F. and Urban, F. K. III, *J. Vac. Sci. Technol. B* **15**, 800–804, (1997).

[9] Radmacher, M., Cleveland, J. P., Fritz, M., Hansma, H. G. and Hansma, P. K., *Biophysical Journal* **66**, 2159–2165, (1994).

[10] Barborini, E., Piseri, P., Milani, P., *J. Phys. D: Appl. Phys.* **32**, L105–L109, (1999).

[11] Wegner, K., Piseri, P., Tafreshi, V. H. and Milani, P., *J. Phys. D: Appl. Phys.* **39**, R439–459, (2006).

[12] Tafreshi, H. V., Piseri, P., Benedek, G. and Milani, P., *J. Nanosci. Nanotechnol.* **6**, 1140–1149, (2006).

[13] Butt, H., Cappella, B. and Kappl, M., *Surf. Sci. Rep.* **59**, 1–152 (2005).

[14] Cassina, V., Gerosa, L., Podestà, A., Ferrari, G., Sampietro, M., Fiorentini, F., Mazza, T., Lenardi, C. and Milani, P., *Phys. Rev. B* **79**, 115422, (2009).

[15] Wilkis, J. S., *Green Chem* **4**, 73–80, (2002).

[16] Wasserscheid, P. and Welton, T., (editors) *Ionic Liquids in Synthesis*, Wiley-VCH Verlag GmbH & Co. KGaA (2002).

[17] Gale, R. J., Gilbert, B. and Osteryoung, R. A., *Inorg Chem* **17**, 2728–2729, (1978).

[18] Wilkes, J. S., Levisky, J. A., Wilson, R. A. and Hussey, C. L., *Inorg Chem* **21**, 1263–1264, (1982)

[19] Holbrey, J. and Seddon, K. R., Clean Prod. Process. **1**, 223, (1999).

[20] Deetlefs, M. and Seddon, K. R., *Green Chem.* **12**, 17–30, (2010).

[21] Zhang, Y., Bakshi, B. R. and Demessie, E. S., *Environ. Sci. Technol.* **42**, 1724–1730, (2008).

[22] Sheldon, R. A., *Green Chem.* **9**, 1273–1283, (2007).

[23] Rantwijk, F. and Sheldon, R. A., *Chem. Rev.* **107**, 2757–2785, (2007).

[24] Anastas, P. T. and Kirchhoff, M. M., *Acc. Chem. Res.* **35**, 686–694, (2002).

[25] Fumino, K., Wulf, A. and Ludwig, R., *Angew. Chem. Int. Ed.* **47**, 8731–8734, (2008).

[26] Sun, N., Rodríguez, H., Rahmana, M. and Rogers, R. D., *Chem. Comm.* **47**, 1405–1421, (2011).

[27] Fischer, L., Falta, T., Koellensperger, G., Stojanovic, A., Kogelnig, D., Galanski, M., Krachler, R., Keppler, B. K. and Hann, S., *Water Res.* **45**, 4601–4614, (2011).

[28] Jacquemin, J., Husson, P., Padua, A. A. H. and Majer, V., *Green Chem.* **8**, 172–180, (2006).

[29] Han, X. and Armstrong, D. W., *Acc. Chem. Res.* **40**, 1079–1086, (2007).

[30] Li, Z., Jia, Z., Luan, Y. and Mu, T., *Curr. Opin. Solid State Mater. Sci.* **12**, 1–8, (2008).

[31] Dupont, J., Fonseca, G. S., Umpierre, A. P., Fichtner, P. F. P. and Teixeira, S. R., *J. Am. Chem. Soc.* **124**, 4228–4229, (2002).

[32] Ryu, H. J., Sanchez, L., Keul, H. A., Raj, A. and Bockstaller, M. R., *Angew. Chem. Int. Ed.* **47**, 7639–7643, (2008).

[33] Endres, F., *ChemPhysChem* **3**, 144–154, (2002).

[34] Menjoge, A., Dixon, J., Brennecke, J. F., Maginn, E. J. and Vasenkov, S., *J. Phys. Chem. B* **113**, 6353–6359, (2009).

[35] Jacquemin, J., Husson, P., Padua, A. A. H. and Majer, V., *Green Chem.* **8**, 172–180, (2006).

[36] Huddleston, J. G., Visser, A. E., Reichert, W. M., Willauer, H. D., Broker, G. A. and Rogers, R. D., *Green Chem.* **3**, 156–164, (2001).

[37] Seddon, K. R., Stark, A. and Torres, M-J., *Pure Appl. Chem.* **72**, 2275–2287, (2000).

[38] Seddon, K. R., Stark, A. and Torres, M., *Pure Appl. Chem.* **72**, 2275–2287, (2000).

[39] Qu, J., Truhan, J. J., Dai, S., Luo, H., Blau, P., *J. Tribol. Lett.* **22**, 207–214, (2006).

[40] Bhushan, B., Palacio, M., Kinzig, B., *J. Coll. and Inter. Sci.* **317**, 275–287, (2008).

[41] Zhou, F., Liang, Y. and Liu, W., *Chem. Soc. Rev.* **38**, 2590–2599, (2009).

[42] Bermúdez, M., Jiménez, A., Sanes, J. and Carrión, F., *Molecules* **14**, 2888–2908, (2009).

[43] Minami, I., *Molecules* **14**, 2286–2305, (2009).

[44] Minami, I., Kamimura, H. and Mori, S., *J. Synthetic Lubrication* **24**, 135–147, (2007).

[45] Jiménez, A.E., Bermúdez , M.D., Iglesias, P. , Carrión, F.J. and Martínez–Nicolás, G., *Wear* **260**, 766–782, (2006).

[46] Suzuki, A., Shinka, Y. and Masuko, M., *Tribol Lett* **27**, 307–313, (2007).

[47] Kamimura, H., Kubo, T., Minami, I. and Mori, S., *Tribol. Int.* **40**, 620–625, (2007).

[48] Ye, C., Liu, W., Chen, Y. and Yu, L., *Chem. Commun.*, 2244–2245, (2001).

[49] Ye, C., Liu, W., Chen, Y. and Yu, L., *Chem. Lett.* **37**, 300–301, (2008).

[50] Appetecchi, G. B., Montanino, M., Carewska, M., Moreno, M., Alessandrini and F., Passerini, S., *Electrochimica Acta* **56**, 1300–1307, (2011).

[51] Grätzel, M., *Journal of Photochemistry and Photobiology A: Chemistry* **164**, 3–14, (2004).

[52] Wang, P., Zakeeruddin, S. M., Compte, P., Exnar, I. and Grätzel, M., *J. Am. Chem. Soc.*, **125**, 1166–1167, (2003).

[53] Iacob, C., Sangoro, J., R., Papadopoulos, P., Schubert, T., Naumov, S., Valiullin, R., Karger, J. and Kremer, F., *Phys. Chem. Chem. Phys.* **12**, 13798–13803, (2010).

[54] Zakeeruddin, S. M. and Grätzel, M., *Adv. Funct. Mater.* **19**, 2187–2202, (2009).

[55] Grünwald, R. and Tributsch, H., *J. Phys. Chem. B* **101**, 2564–2575, (1997).

[56] O'Regan, B. and Grätzel, M., *Nature* **353**, 737–739, (1991).

[57] Papageorgiou, N., Athanassov, Y., Armand, M., Bonhˆote, P., Pettersson, H., Azam, A. and Grätzel, M., *J. Electrochem. Soc.* **143**, 3099–3108, (1996).

[58] Yella, A., Lee, H. W., Tsao, H. N., Yi, C., Chandiran, A. K., Nazeeruddin, M. K., Diau, E. W. G., Yeh, C. Y., Zakeeruddin, S. M. and Grätzel, M., *Science* **334**, 629–634, (2011).

[59] Miller, J. R. and Burke, A. F., *Electrochem. Soc. Interf.* **17**, 53–57, (2008).

[60] Simon, P. and Gogotsi, Y., *Nature Materials* **7**, 845–854, (2008)

[61] Zhang, L. L. and Zhao, X. S., *Chem. Soc. Rev.* **38**, 2520–2531, (2009).

[62] Lazzari, M., Soavi, F. and Mastragostino, M., *Fuel Cells* **10**, 840–847, (2010).

[63] Smith, E. F., Rutten, F. J. M., Villar–Garcia, I. J., Briggs, D. and Licence, P., *Langmuir* **22**, 9386–9392, (2006).

[64] Hofft, O., Bahr, S., Himmerlich, M., Krischok, S., Schaefer, J. A. and Kempter, V., *Langmuir* **22**, 7120–7123, (2006).

[65] Santos, C. S., Baldelli, S., *J. Phys. Chem. B* **111**, 4715–4723, (2007).

[66] Romero, C. and Baldelli, S., *J. Phys. Chem. B* **110**, 6213–6223, (2006).

[67] Aliaga, C., Baldelli, S., J. Phys. Chem. C **112**, 3064–3072, (2008).

[68] Rollins, J. B., Fitchett, B. D. and Conboy, J. C., *J. Phys. Chem. B* **111**, 4990–4999, (2007).

[69] Lovelock, K. R. J., Villar-Garcia, I. J., Maier, F., Steinrück, H. and Licence, P., *Chem. Rev.* **110**, 5158–5190, (2010).

[70] Mezger, M., Schröder, H., Reichert, H., Schramm, S., Okasinski, J. S., Schöder, S., Honkimäki, V., Deutsch, M., Ocko, B. M., Ralston, J. and Rohwerder, M., *Science* **322**, 424–428, (2008).

[71] Cremer, T., Killian, M., Gottfried, J. M., Paape, N., Wasserscheid, P., Maier, F. and Steinrück, H.-P., *Chem. Phys. Chme.* **9**, 2185–2190, (2008).

[72] Cremer, T., Stark, M., Deyko, A., Steinrück, H.-P. and Maier, F., *Langmuir* **27**, 3662–3671, (2011).

[73] Smith, E. F., Rutten, F. J. M., Villar–Garcia, I. J., Briggs, D. and Licence, P., *Langmuir* **22**, 9386–9392, (2006).

[74] Hofft, O., Bahr, S., Himmerlich, M., Krischok, S., Schaefer, J. A. and Kempter, V., *Langmuir* **22**, 7120–7123, (2006).

[75] Keppler, A., Himmerlich, M., Ikari, T., Marschewski, M., Pachomow, E., Höfft, O., Maus-Friedrichs, W., Endres, F., and Krischok, S., *Phys. Chem. Chem. Phys.* **13**, 1174–1181, (2011).

[76] Hayes, R., Warr, G. G. and Atkin, R., *Phys. Chem. Chem. Phys.* **12**, 1709–1723, (2010).

[77] Atkin, R. and Warr, G. G., *J. Phys. Chem. C*, **111**, 5162–5168, (2007).

[78] Atkin, R., Borisenko, N., Drüschler, M., El Abedin, S. Z., Endres, F., Hayes, R., Huber, B. and Roling, B., *Phys. Chem. Chem. Phys.* **13**, 6849–6857, (2011).

[79] Liu, Y., Zhang, Y., Wu, G. and Hu, J., *J. Am. Chem. Soc.* **128**, 7456–7457, (2006).

[80] Zhang, F., Sha, M., Ren, X., Wu, G., Hu, J. and Zhang, Y., *Chin. Phys. Lett.* **27**, 086101, (2010).

[81] Bovio, S., Podestà, A., Lenardi, C. and Milani, P., *J. Phys. Chem. B* **113**, 6600–6603, (2009).

[82] Bovio, S., Podestà, Milani, P. N. V. Plechkova, R. D. Rogers, K.R. Seddon Editors; *Ionic Liquids: From Knowledge to Application, Vol. 1030, Chapter 19*, Pages 273-290, *ACS Symposium Series*, (2009).

[83] M. Galluzzi, *Study of morphological and dielectric properties of thin ionic liquid films by Atomic Force Microscopy*, Master Thesis, University of Milan, (2010).

[84] Yokota, Y., Harada, T. and Fukui, K., *Chem. Commun.* **46**, 8627–8629, (2010).

[85] Kaisei, K., Kobayashi, K., Matsushige, K., Yamada, H., *Ultramicroscopy* **110**, 733–736, (2010).

[86] Alcoutlabi, M. and McKenna, G. B., *J. Phys: Condens. Matter* **17**, R461–R524, (2005).

[87] Qi, W. H. and Wang, M. P., *J. Mat. Sci. Lett.* **21**, 1743–1745, (2002).

[88] Ueno, K., Imaizumi, S., Hata, K. and Watanabe, M., *Langmuir* **25**, 825–831, (2009).

[89] Chen, S., Wu, G., Sha, M. and Huang, S., *J. Am. Chem. Soc.* **129**, 2416–2417, (2007).

[90] Liu, Y., Wu, G., Fu, H., Jiang, Z., Chena, S. and Sha, M., *Dalton Trans.* **39**, 3190–3194, (2010).

[91] Kanakubo, M., Hiejima, Y., Minami, K., Aizawa, T., and Nanjo, H., *Chem. Commun.*, 1828–1830, (2006).

[92] Hu, H. and Larson, R. G., *Phys. Chem. B* **110**, 7090–7094, (2006).

[93] Deegan, R. D., Bakajin, O., Dupont, T. F., Huber, G., Nagel, S. R., Witten, T. A., *Nature* **389**, 827–829, (1997).

[94] Ueno, K., Kasuya, M., Watanabe, M., Mizukami, M. and Kurihara, K., *Phys. Chem. Chem. Phys.* **12**, 4066–4071, (2010).

[95] Perkin, S., Albrecht, T. and Klein, J., *Phys. Chem. Chem. Phys.* **12**, 1243–1247 (2010).

[96] Min, Y., Akbulut, M., Sangoro, J. R., Kremer, F., Prudhomme, R. K. and Israelachvili, J., *J. Phys. Chem. C* **37**, 16445–16449, (2009).

[97] Perkin, S., Crowhurst, L., Niedermeyer, H., Welton, T., Smith, A. M. and Gosvami, N. N., *Chem. Commun.* **47**, 6572–6574, (2011).

[98] Bovio, S., Podestà, A., Milani, P., Ballone, P. and Del Pópolo, M. G., *J. Phys. Condens. Matter* **21**, 424118, (2009).

[99] Ballone, P., Del Pópolo, M. G., Bovio, S., Podestà, A., Milani, P. and Manini, N., *Phys. Chem. Chem. Phys.* **DOI: 10.1039/C2CP23459A** (2012).

[100] Sieffert, N., and Wipff, G., *J. Phys. Chem. C* **112**, 19590–19603 (2008).

[101] Sha, M., Zhang, F., Wu, G., Fang, H., Wang, C., Chen, S., Zhang, Y., and Hu, J., *J. Chem. Phys.* **128**, 134504, (2008).

[102] Sieffert, N., and Wipff, G., *J. Phys. Chem. B* **110**, 13076–13085, (2006).

[103] Dragoni, D., *Interfacial layering of ionic liquids on solid surfaces* Master Thesis, University of Milan (2010). Available on–line at www.mi.infm.it/manini/theses/dragoni.pdf

[104] Monk, J., Singh, R. and Hung, F. R., *J. Phys. Chem. C* **115**, 3034–3042, (2011).

[105] Snook, I. K. Henderson, D., *J. Chem. Phys.* **68**, 2134–2139, (1978).

[106] Triolo, A., Russina, O., Bleif, H.–J. and Di Cola, E., *J. Phys. Chem. B* **111**, 4641–4644, (2007).

[107] Triolo, A., Russina, O., Fazio, B., Triolo, R. and Di Cola, E., *Chem. Phys. Lett.* **457**, 362–365, (2008).

[108] Canongia Lopes, J. N., Costa Gomes, M. F. and Pádua, A. A. H., *J. Phys Chem B. Letters* **110**, 16816–16818, (2006).

[109] Manini, M., Cesaratto, M., Del Pópolo, M. G. and Ballone, P., *J. Phys. Chem. B* **113**, 15602–15609, (2009).

[110] Machida, H., Takesue, M. and Smith Jr., R. L., *J. of Supercritical Fluids*, **in press**, (2011).

[111] Varma, R. S., *Green Chem.* **1**, 43–55, (1999).

[112] Simon, M. and Li, C., *Chem. Soc. Rev.* **DOI: 10.1039/c1cs15222j**, (2011).

Appendix A

X-Ray photoelectron spectroscopy

An X–ray photoelectron spectroscopy (XPS) study have been performed on pure bulk [Bmim][Tf_2N] and [Bmim][Tf_2N] microdroplets deposited from a IL/methanol solution on silicon, in order to assess whether the interaction with methanol is destructive for the ionic liquid. XPS measurements have been performed in two different apparatus. The supported [Bmim][Tf_2N] microdroplets have been characterized in a ultra high vacuum (UHV) apparatus PHI equipped with a hemispherical electron analyser and monochromatised X–ray source (Al Kα). The high resolution spectra were acquired in constant pass–energy mode Epass= 23.5eV. The overall energy resolution was 0.7eV. The pressure in the experimental chamber during experiments was below $2{\cdot}10^{-9}$mbar. The pure [Bmim][Tf_2N] liquid has been characterized in a UHV apparatus Leybold LHS 10/12 equipped with a hemispherical electron analyser and conventional X–ray source (Mg Kα). The high resolution spectra were acquired in constant pass-energy mode Epass= 30eV. The overall energy resolution was 1.0eV. The pressure in the experimental chamber during experiments was below $3{\cdot}10^{-9}$mbar. For both apparatus the spectra energy scale was scaled using as reference the Au $4f_{5/2}$ peak. In Figure A.1 we show the low–resolution XPS wide–scans of [Bmim][Tf_2N] microdroplets (top panel) and pure bulk [Bmim][Tf_2N] (bottom panel) on silicon. Both spectra show the typical [Bmim][Tf_2N] components: fluorine, oxygen, nitrogen, carbon and sulphur. Moreover, in the case of supported microdroplets, the signature of silicon is also evident due to the presence of extended non–coated areas. The contribution of silicon oxide is mirrored by the increasing of the intensity of the oxygen peak. Figure A.2 shows high resolution core level photoemission spectra of [Bmim][Tf_2N] microdroplets on silicon deposited from a [Bmim][Tf_2N]/methanol solution (solid line) and of pure bulk

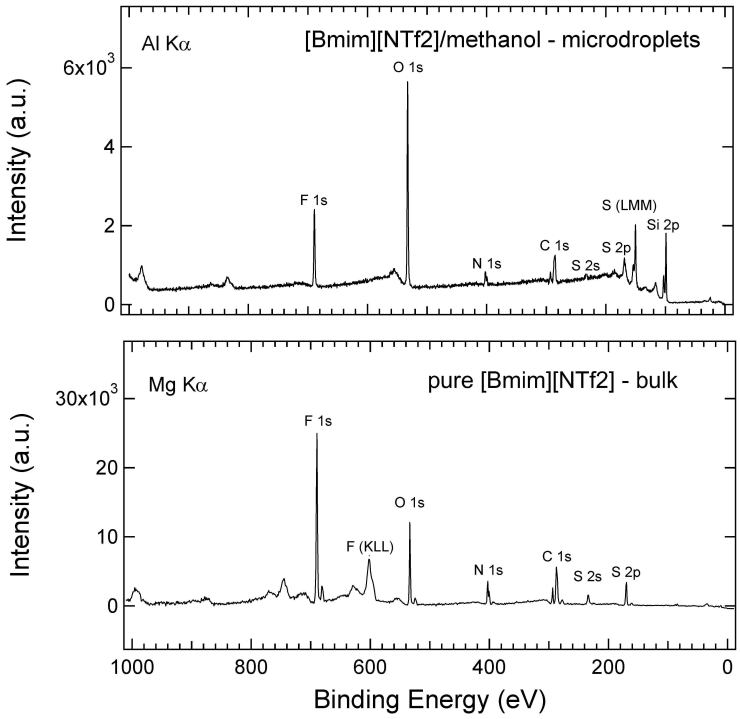

Figure A.1: *Comparison between low resolution XPS wide–scans of [Bmim][Tf_2N] micro–droplets on silicon deposited from a [Bmim][Tf_2N]/methanol solution (top panel) and pure bulk [Bmim][Tf_2N] (bottom panel).*

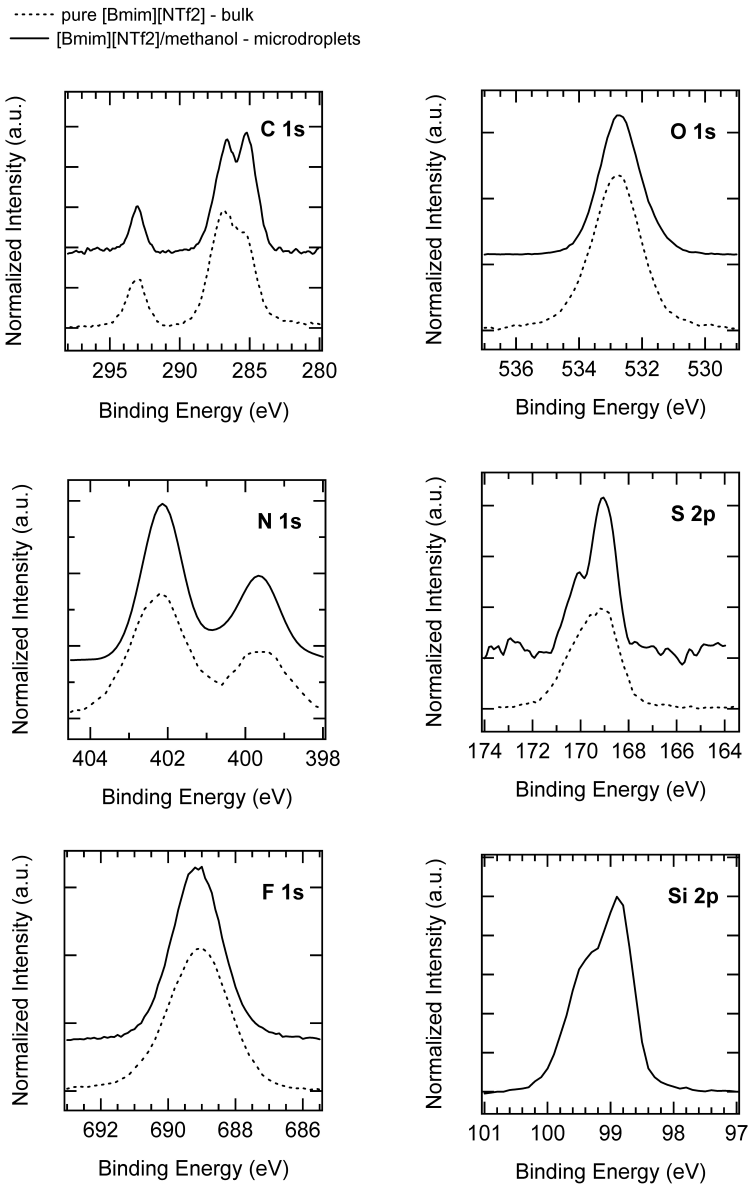

Figure A.2: *High resolution core level photoemission spectra of [Bmim][Tf_2N] micro–droplets on silicon deposited from a [Bmim][Tf_2N]/methanol solution (solid line) and of pure bulk [Bmim][Tf_2N] (dashed line).*

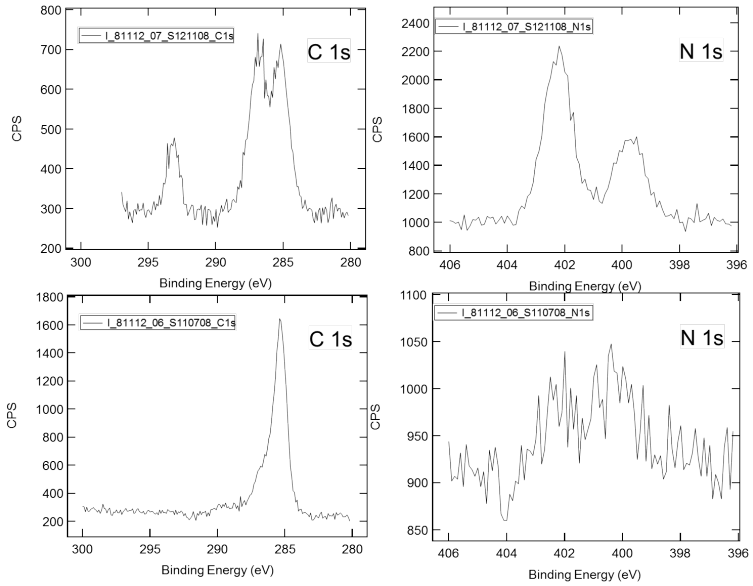

Figure A.3: *C1s and N1s spectra acquired on bulk [Bmim][Tf_2N] (top), and on a thin film deposited by drop casting (bottom).*

[Bmim][Tf_2N] (dashed line). For all the peaks a Shirley background was removed and, for the same energy region, the peak area was normalized to one. A quantitative evaluation of the surface composition of pure [Bmim][Tf_2N] provides the following ratios: F:O:N:C:S=6:4:3.5:11.2:2, in good agreement with the nominal stoichiometry of F:O:N:C:S=6:4:3:10:2. The observed spectra for pure are in good agreement with published results[63, 64]. A quantitative evaluation of the surface composition of [Bmim][Tf_2N] microdroplets deposited from a [Bmim][Tf_2N]/methanol solution provides the following ratios: F:O:N:C:S=6:4:3:11:2, again in good agreement with the nominal stoichiometry (the contribution of oxygen bound to Si in native SiO_2 has been removed in order to obtain those ratios). For each core level the peak position and the relative intensities of the constituents are comparable between the two samples. The overlapping of XPS spectra demonstrates that methanol does not interfere with the ionic liquid in the deposition process, the structure of the cation–anion pair being preserved. C1s and S2p spectra of the microdroplets show better separated peaks due to the highest resolution of the experimental apparatus. Only for [Bmim][Tf_2N] microdroplets the peak of Si2p is shown, because in the case of pure bulk [Bmim][Tf_2N] the substrate is not exposed.

Some XPS measurements have been performed on thin films of [Bmim][Tf_2N] on silicon on the PHI apparatus. High resolution spectra of carbon and ni-

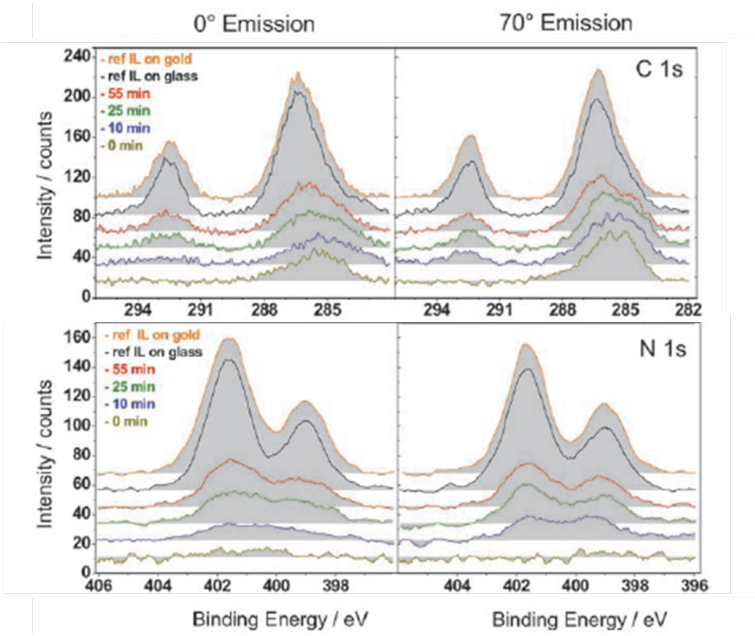

Figure A.4: *C1s and N1s spectra acquired on evaporated films of [Emim][Tf_2N] on silica, with increasing thickness going from bottom to top. The two topmost spectra have been acquired on a thick evaporated film on silica and non–evaporated thick sample on gold. Only two spectra of the Figure 1 of Ref. [71] have been reported here.*

trogen can be seen in Figure A.3, along with the spectra acquired on the same elements on the bulk IL. As it can be noticed, even if the N1s spectrum is very noise due to the low signal, the double peak feature related to the presence of N in both the ions is still preserved, but the relation between the intensities of the two peaks is greatly modified, form 2:1 to almost 0.8:1. The effect on the C1s spectrum is even more evident: in fact the peak around 293eV, referred to the CF_3 groups in the [Tf_2N] cannot be found, even if the ratio of the intensities between the carbon peaks found in the bulk would in principle allow the peak detection.

A similar behaviour of the spectra on thin ionic liquid films has been found by Cremer et al.[71] analysing thin films of [Emim][Tf_2N] evaporated on a silica substrate. In Figure A.4, taken from cited paper, is reported the evolution of the spectra of N1s and C1s (in this case measurements were carried out at 0°and 70°respect to the surface normal) with the deposition time (in the Figure from bottom to top). The tow topmost spectra of the series reported in Figure A.4 were respectively acquired on a thick evaporated film on silica and on a reference thick film of the same IL casted (not evaporated)

on gold.

The comparison of these two spectra show that the deposition process seems preserve the structure of the ionic liquid. The authors suggest a layer–by–layer growth on the substrate, at least for the first two molecular layers. In the paper then the evolution of the spectra with increasing deposition time is ascribed to an ordering of the ionic liquid ions in contact with the silica surface, with the the anion sitting on top of the cation.

The N1s spectrum showed by Cremer agrees with the spectrum in Figure A.3. Instead the spectrum of C1s acquired by Cremer show the expected anion peak once the intensity of the signal is high enough to allow the peak to effectively rise from the background. In any case, the picture depicted by Cremer is not in accordance with the morphology found on thins films deposited by drop coating from IL/solvent solutions. In fact, as shown in Chapter 3, the thin film is not organised as a uniform coverage of the substrate, but shows a coexistence of micro- to nano- -droplets and solid–like flat domains. In another study[72], the same author shows that ordered layers of ionic liquids on gold can grow up to 9nm in thickness. Anyway Cremer only speculates about the morphology of the evaporated film, but does not provide any topography of the samples, so even if the calculation of the film thickness and growth mechanism (layer–by–layer on gold) is very accurate, it always relates to measurements performed on a large area, so an average measurement, that do not completely exclude the possibility of a 3D film developing on the surface.

Since on drop coated samples the IL coexist in different phases and it doesn't uniformly cover the surface, the interpretation of the XPS spectra cannot be as simple as that provided by Cremer and collaborators and further measurements are required in order to clarify the picture.

A.1 Radiation–induced degradation

It is already know from the literature that XPS analysis is potentially harmful for ionic liquids[75]. In particular the study shows that the switch on a non–monochromated X-Ray source, induces the rupture of some ions, as revealed by an increase in the pressure of the chamber and by mass spectroscopy of ion fragments, as well as by a visual inspection of the IL sample, that turns from transparent to yellowish. After such a sever irradiation some new peaks appear in the XPS spectra and stoichiometry changes are detected. The IL degradation is ascribed by the authors mainly to the effect of electrons, both the secondary electrons injected in the IL sample from the grounded substrate and those emitted during the irradiation by non–monocromated source. In

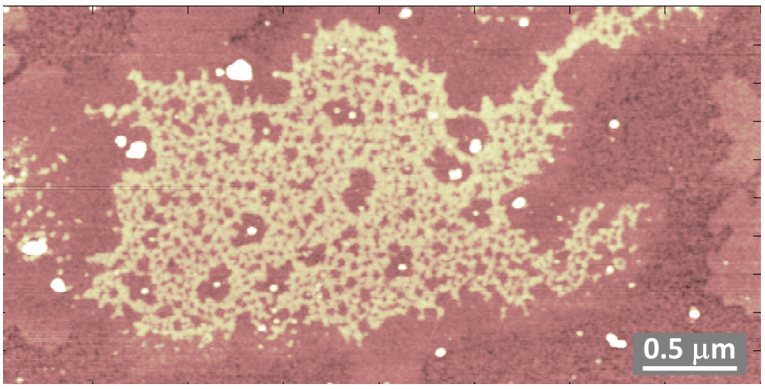

Figure A.5: *Beam damages on a solid–like island deposited from a [Bmim][Tf_2N/ chloroform solution. The network structure is probably the remnant of a solid–like terrace eroded by the beam (vertical scale 6nm).*

fact, they report the same colour change in samples of IL exposed to high–energy electron beam, as we have directly seen during the SEM investigation of thin layers.

It is interesting to look at the effect of XPS analysis onto the solid–like domains. Figure A.5 reports an example of the effect of an ionic liquid island exposed to XPS irradiation. As can be seen, in the figure, on top of a domain recognisable as a thin IL ordered layer, there is a network structure never encountered in samples that have not been exposed to XPS. The network structure, as can be appreciate from Figure A.5 is a 2D structure, i.e. is topmost part is flat. Our interpretation is that the structure is the remnant of a terrace whose has been pierced during the beam exposure. Probably, in some points the degradation of the ions produced more volatile structures that evaporated in the UHV chamber (as reported in [75] study).

The XPS analysis performed showed that ionic liquids can be analysed by X–Ray photoelectron spectroscopy in UHV because they easily dissipate the accumulated charges and because of their low volatility. A pure sample of [Bmim][Tf_2N] as well as a sample previously mixed with methanol have been examined, both providing compatible spectra, in accordance with the literature[64, 63]. A quantitative analysis shows that the stoichiometry is in agreement with the nominal one for both the samples. An XPS investigation has been performed also on [Bmim][Tf_2N] thin films deposited by drop-casting on oxidised silicon. The low coverage causes a low number of counts, so noisy spectra, that do not resemble the spectra of the bulk, because the ratio between the intensity of anions and cations peaks in N1s and C1s do not fit with that found in the bulk. The modification of the spectra reducing

the thickness of the films has been already reported in the literature[71, 72], although our results are only in partial agreement, possibly because of the different morphology of the deposit.

Finally the beam effect on solid–like islands has been preliminarily investigated. As also reported in the literature[75], XPS measurements induce fragmentation of some ions, that is likely due to the effect of incident electrons coming from the X-Ray source and on those coming from the grounded substrate (evaporation of the solid–like islands under the electron beam in SEM measurements have been actually seen during my PhD work). On solid–like terraces, the beam effect seems to be that of piercing the islands, leading to network structure.

Appendix B

List of published papers

THE JOURNAL OF PHYSICAL CHEMISTRY B

Article

Evidence of Extended Solidlike Layering in [Bmim][NTf2] Ionic Liquid Thin Films at Room-Temperature

Simone Bovio, Alessandro Podesta#, Cristina Lenardi, and Paolo Milani

J. Phys. Chem. B, **2009**, 113 (19), 6600-6603• Publication Date (Web): 17 April 2009

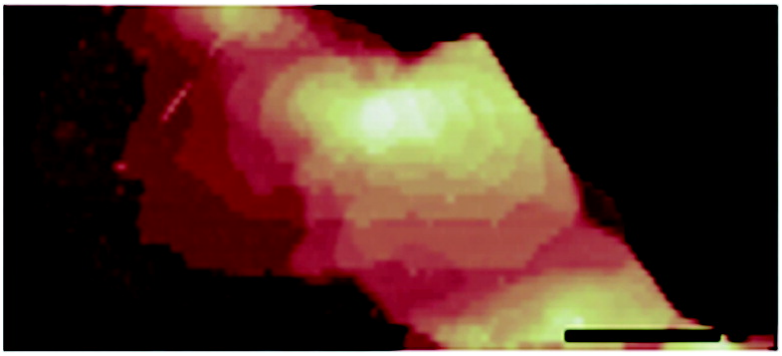

ARTICLES

Evidence of Extended Solidlike Layering in [Bmim][NTf2] Ionic Liquid Thin Films at Room-Temperature

Simone Bovio,[†] Alessandro Podestà,*[,†] Cristina Lenardi,[‡] and Paolo Milani[†]

C.I.Ma.I.Na. and Dipartimento di Fisica, Università degli Studi di Milano, via Celoria 16, 20133, Milano, Italy, and C.I.Ma.I.Na. and Istituto di Fisiologia Generale e Chimica Biologica, Università degli Studi di Milano, via Trentacoste 2, 20134, Milano, Italy

Received: January 26, 2009

We report the direct observation of solidlike ordering at room temperature of thin films of [Bmim][NTf2] ionic liquid on mica, amorphous silica, and oxidized Si(110). A statistical quantitative analysis of atomic force microscopy topographies shows that on these surfaces [Bmim][NTf2] forms layered structures, characterized by a perpendicular structural periodicity of ∼0.6 nm. Remarkably, even the highest structures, up to 50 nm high, behave solidlike against the AFM probe. Conversely, on highly oriented pyrolitic graphite the ionic liquid forms nanometer-sized, liquidlike domains. The results of this study are directly relevant for those applications where ILs are employed in form of thin films supported on solid surfaces, such as in microelectromechanical or microelectronic devices. More generally, they suggest that at the liquid/solid interface the structural properties of ILs can be far more complex than those depicted so far, and prompt new fundamental investigations of the forces that drive supported ILs through a liquidlike-to-solidlike transition.

Introduction

Room-temperature ionic liquids (ILs)[1,2] are receiving a rapidly increasing interest as alternatives to conventional electrolytes that can boost the performances of photoelectrochemical devices used for energy storage and energy production such as supercapacitors[3] or Graetzel solar cells.[4] Moreover, ILs are considered as a promising new class of lubricants in miniaturized as well as in macroscopic mechanical systems.[5,6] In all these cases, the most relevant processes determining the performance of the devices take place at the liquid/solid interface between ILs and solid surfaces: this is a region only a few nanometers thick where the properties of ILs can be significantly different from those of the bulk. The investigation of the interfacial properties of ILs is therefore of primary importance for their technological exploitation.

To date, the (bulk)liquid−vapor and solid−(bulk)liquid ILs interfaces have been studied, mostly by sum-frequency generation spectroscopy,[7−11] by X-ray photoemission spectroscopy, [12,13] and by a combination of these and other surface science techniques,[14−18] including atomic force microscopy (AFM).[19,20] For imidazolium-based ILs, ordering of the cations at the solid/liquid or liquid/vapor interface has been inferred from vibrational spectroscopy data. Sloutskin et al.[15] inferred from X-ray reflectivity data of imidazolium-based ILs the existence of an ordered surface layer at the liquid/vapor interface, about 0.6−0.7 nm thick, composed by both cations and anions. Very recently, Mezger et al. performed a similar study of the (bulk)liquid/solid interface between a negatively charged sapphire substrate and imidazolium and pyrrolidinium-based ILs.[21] They found strong interfacial layering, with repeated spacing of 0.7−0.8 nm, decaying exponentially into the bulk liquid. Moreover, the existence of periodically ordered layers of ILs, including an imidazolium-based, at the (bulk)liquid/solid interface with mica and silica, has been recently reported by Atkin et al.,[20] and interpreted as solvation layers. Despite these interesting results, the knowledge of the structural properties of ILs at interfaces, in particular with solid surfaces, is still very poor and important questions are still waiting to be answered. Researchers still do not know whether, and how far, the ordered layers extend into the bulk of the liquid, nor do they know how the cation−anion pairs are organized within each layer, and what is the phase (liquid, solidlike) of the IL in the ordered region. A better understanding of the behavior of ILs at interfaces can be achieved studying systems where the surface to volume ratio is very large, as in very thin supported films. To date, this is a largely unexplored field, since all the above-mentioned studies were conducted on systems where a bulk amount of IL was present right above, or below, the interface.

In this communication, we report on the direct observation by tapping-mode AFM of nanoscale morphological and structural properties of very thin coatings of 1-butyl-3-methylimidazolium bis(trifluoromethylsulfonyl)imide, [Bmim][NTf2], on different surfaces of technological interest. Our work significantly expands the preliminary work of Liu et al., who recently reported about the layering at room-temperature of an imidazolium-based IL, [Bmim][PF6], on mica.[22] Using AFM, we have visualized nanoscale structures of [Bmim][NTf2] on a variety of surfaces: mica, amorphous silica, polished, oxidized p-doped Si(110), and highly oriented pyrolitic graphite (HOPG). Applying a rigorous protocol for the statistical analysis of AFM images we have characterized the structural properties of IL

* To whom correspondence should be addressed. E-mail: alessandro.podesta@mi.infn.it.
[†] C.I.Ma.I.Na. and Dipartimento di Fisica.
[‡] C.I.Ma.I.Na. and Istituto di Fisiologia Generale e Chimica Biologica.

10.1021/jp9022234 CCC: $40.75
Published on Web 04/17/2009

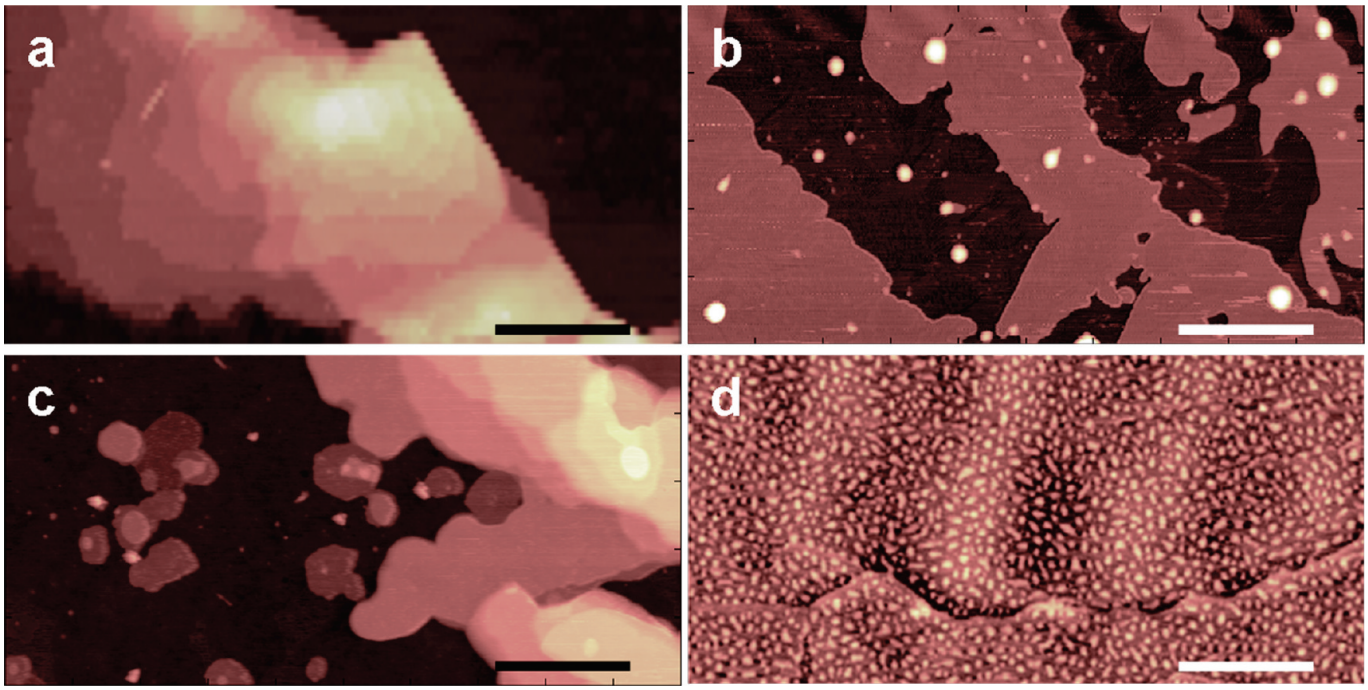

Figure 1. AFM topographies of thin [Bmim][NTf2] coatings on different substrates: (a) polished oxidized Si(110); (b) mica; (c) amorphous silica; (d) HOPG. Vertical scales: (a,b) 50; (c) 90; (d) 10 nm. Scale bars: 1 μm.

films, validating a structural model where [Bmim][NTf2] forms layered solidlike structures at room-temperature on mica and silica surfaces, with a basic periodicity in the perpendicular direction of ~0.6 nm. In contrast, on HOPG [Bmim][NTf2] segregates in nanometer-sized domains.

Experimental Methods

[Bmim][NTf2] thin films are prepared by spotting a 20 μL droplet of [Bmim][NTf2]-methanol solution on mica, highly oriented pyrolitic graphite (HOPG), amorphous silica, and polished, oxidized p-doped Si(110) substrates, and allowing methanol to completely evaporate in air, leaving behind IL layers and/or droplets. Methanol with 99.8% (HPLC) purity grade was used. The IL concentration in the deposition solution was typically kept below 1×10^{-3} mg/ml. To make the methanol evaporation process slower and obtain more uniform coatings and thicker structures, the specimens were cured in a saturated methanol atmosphere during evaporation. A comparative X-ray photoelectron spectroscopy analysis of pure and methanol-mixed [Bmim][NTf2] confirmed that the solvent used in the deposition process does not react with [Bmim][NTf2] (see Supporting Information, Figures S1 and S2).

Substrates were freshly prepared immediately before deposition of the [Bmim][NTf2]-methanol solution. Mica and HOPG were stripped with adhesive tape in order to obtain atomically smooth, clean surfaces. Discs (13 mm-diameter) of amorphous silica (glass coverslips) and squared specimens of polished, oxidized Si(110) were cured in aqua-regia solution ($HCl-HNO_3$ from, respectively, 37% and 69.5% solutions at ratio 3:1) before use, to remove organic contaminants and rehydroxilyze the surface.

A Bioscope II−Nanoscope V AFM from Veeco Instruments was used. The AFM was operated in tapping mode in air with standard single-crystal silicon cantilevers (resonance frequency between 200 and 300 kHz, nominal radius of curvature of the tip, 5−10 nm). Typically, image scan size was between 5 μm $\times$ 5 μm and 20 μm $\times$ 20 μm, with scan rates in the range 0.5−1.5 Hz. Stable imaging conditions could be achieved and maintained for hours as if scanning on a solid surface. We did not observe significant changes in the imaging conditions when imaging in a dry nitrogen atmosphere. AFM raw data have been analyzed according to the statistical protocol described in the Supporting Information.

Results and Discussion

Figure 1 shows a collection of representative AFM topographies of thin coatings of [Bmim][NTf2] on polished oxidized Si(110), mica, amorphous silica, and HOPG. Figure 1a−c show layered structures, characterized by lateral dimensions in the 1−20 μm range, and height above 50 nm in some cases. While the average height of terraces is similar on the three substrates, on silica substrates [Bmim][NTf2] shows a more pronounced tendency to grow three-dimensionally than on mica. No evidence of ordered extended structures could be found on HOPG substrates (Figure 1d). On HOPG only nanometer-sized, rounded domains (nanodroplets) of IL spontaneously form upon evaporation of methanol. Coexistence of submicrometer droplets and layers is observed occasionally on amorphous silica and mica, and very rarely on oxidized Si(110) surfaces. No changes in the shape of layered features were typically observed after repeated scanning of the same areas, if not occasionally, when working with high forces. When imaged by AFM, such structures, even the highest, behave like solid surfaces. AFM phase-imaging (Figure S3 in the Supporting Information) also suggests that the phase of IL in layered structures and droplets is different. The observed layers have been imaged also after several months, and no changes in their average structure and morphology have been observed, demonstrating that such structures are extremely stable even in ambient (humid) conditions.

A statistical analysis of the AFM images provided quantitative information on the structural properties of [Bmim][NTf2] films (see Supporting Information for the details). We investigated whether the layers observed in Figure 1a−c could result from

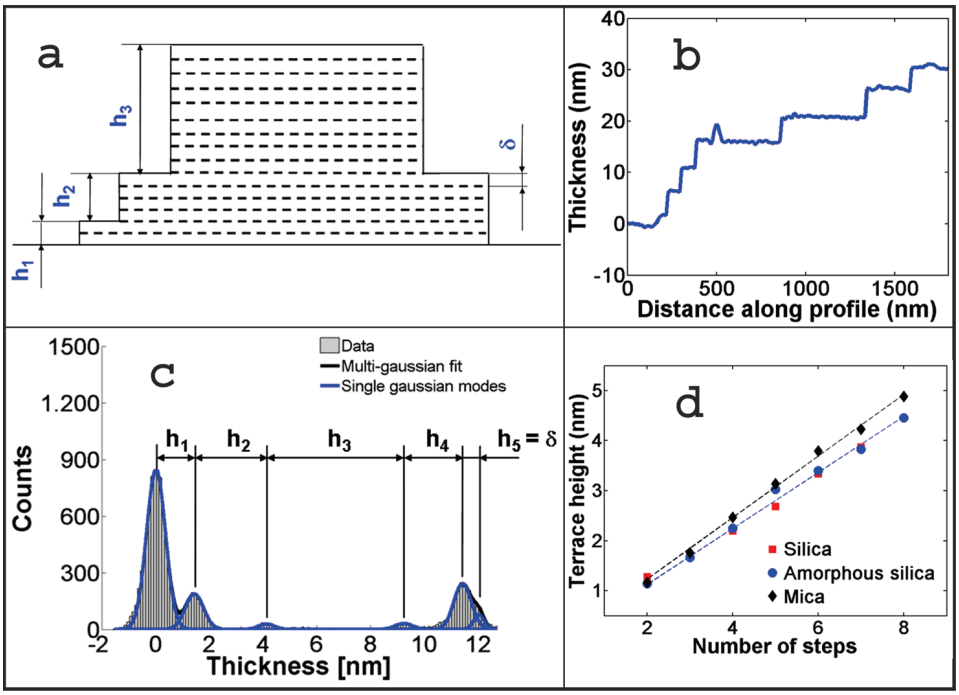

Figure 2. (a) Structural model of layered structures, consisting in the stacking of a molecular layer with thickness δ resulting in terraces with different heights *h*1, *h*2,... (b) Representative AFM topographic profile of a layered structure. (c) Typical height histogram of a layered structure. Peak-to-peak distances represent terrace heights. (d) Correlation between average terrace heights measured on different surfaces and the number of basic steps in each terrace, obtained by fitting structural data (error bars are comparable to marker size).

the regular vertical arrangement of a molecular layer with thickness δ. According to the structural model shown in Figure 2a, we made the hypothesis that each terrace consists of several basic layers, and terraces with different heights are stacked one on top of the other. This model well represents the typical AFM profiles of layered structures (one is shown in Figure 2b). To characterize statistically and accurately the heights of the observed terraces, we considered the histograms of the heights in AFM topographies of layered structures. Figure 2c shows a typical height histogram of a layered structure. Such histograms consist of a series of peaks, each corresponding to a plateau in the AFM image. The peak-to-peak distances represent the average heights of piled-up terraces. We performed an optimization procedure on terrace heights data in order to find the best value of δ for the different substrates. We found $\delta = 0.61 \pm 0.01$, 0.56 ± 0.02, and 0.56 ± 0.02 nm for mica, polished oxidized Si(110), and amorphous silica, accordingly. Figure 2d shows the curves obtained plotting the average heights of the terraces versus the ratio of these heights to δ, approximated to the closest integer; this ratio representing the number of basic steps in each terrace. The good linear correlation of data reflects the good vertical structural order of [Bmim][NTf2] films on mica and silica substrates. Remarkably, these results are in good agreement with the results of numerical simulations of thin [Bmim][NTf2] and [Bmim][PF6] films on silica.[23]

Nanometer-sized heterogeneities have been observed in the bulk liquid phase of imidazolium-based ILs,[24,25] and interpreted as the result of the segregation of the nonpolar alkyl chains, separated by thin layers of cations paired to anions (a sort of micellization). The size of these locally ordered domains turned out to be roughly twice the length of the alkyl tail plus the cation−anion pair, scaling linearly with the number of CH_2 units in the alkyl chain. This scheme however is not appropriate to explain what we have observed on silica and mica surfaces, where the presence of the surface likely plays a fundamental role. The (bulk)liquid/solid interface of imidazolium and pyrrolidinium-based ILs on a negatively charged sapphire surface recently studied by Mezger et al. represents a system that is closer to our case.[21] The authors explained the observed extended interfacial layering of ILs as due to the combined effect of a net surface charge and the absence of screening of charged ions, which drive the self-assembling of charged double layers. On noncharged, nonpolar surfaces, like graphite, the alkyl tails of the cations very likely interact with the surface, hampering the stable ordering of correlated positively and negatively charged layers, therefore favoring the liquid phase. Similar arguments are invoked by Atkin et al. for explaining the observation by AFM of solvation force profiles of ILs, including an imidazolium-based, at the (bulk)liquid/solid interface with mica, silica, and graphite.[20] Similarly to the charged sapphire surface, the silica and mica surfaces used in our study have a negative charge. It is worth noting however that none of the works cited above provide information about the lateral extension of the ordered domains at the solid/liquid interface, while we have observed on silica and mica surfaces that the lateral dimensions of the layered domains are finite, typically in the $1-20$ μm range. Moreover, we have shown that solidlike, ordered terraces typically a few nanometers thick grow on top of each other, forming ziggurat-like structures, more than 50 nm tall, despite the fact that with the same amount of IL deposited it would be possible to cover uniformly the substrate with a single terrace. This experimental evidence requires a more complex interpretation scheme than the one presented above and stimulate new investigations of the solid/liquid interface of supported ILs.

Conclusions

We have shown that when a few monolayers of [Bmim][NTf2] are deposited on a variety of surfaces, the whole ionic liquid rearranges in a solidlike phase, characterized by the stacking of a basic layer with thickness compatible to the size of the

cation−anion pair. Structural order is maintained up to distances corresponding to much more than the single or the few molecular layers recently observed at the interface between a bulk amount of IL and a solid surface,[20,21] or air.[15] With respect to what was reported by Liu et al. for [Bmim][PF6] on mica,[22] where only the molecularly thin layers appeared to be solidlike, we have observed in the case of [Bmim][NTf2] that even the highest structures behave solidlike against the AFM probe on all the substrates.

Our findings highlight the potentialities of atomic force microscopy for the quantitative investigation of the interfacial properties of thin ILs coatings. The results of this study are directly relevant for those applications where ILs are employed in the form of thin films supported on solid surfaces, such as in microelectromechanical or microelectronic devices. More generally, they suggest that at the (bulk)liquid/solid interface the structural properties of ILs can be far more complex than those depicted so far and prompt new fundamental investigations of the forces that drive supported ILs through a liquidlike-to-solidlike transition.

Acknowledgment. We thank P. Ballone and M. Del Pópolo for discussions and suggestions, K. Seddon and M. Deetlefs for having provided the ILs used in this study, and M. Perego for the XPS analysis of our samples. This work has been supported by Fondazione Cariplo under grant "Materiali e tecnologie abilitanti 2007".

Supporting Information Available: X-ray photoelectron spectroscopy of [Bmim][NTf2]; statistical analysis of AFM data; AFM phase imaging of layers and droplets. This material is available free of charge via the Internet at http://pubs.acs.org.

References and Notes

(1) Welton, T. *Chem. Rev.* **1999**, *99*, 2071–2083.
(2) Holbrey, J. D.; Seddon, K. R. *Clean Products and Processes* **1999**, *1*, 223–236.
(3) Frackowiak, E.; Lota, G.; Pernak, J. *Appl. Phys. Lett.* **2005**, *86*, 164104−1/3.
(4) Kuang, D.; Wang, P.; Ito, S.; Zakeeruddin, S. M.; Grätzel, M. *J. Am. Chem. Soc.* **2006**, *128*, 7732–7733.
(5) Qu, J.; Truhan, J. J.; Dai, S.; Luo, H.; Blau, P. J. *Tribol. Lett.* **2006**, *22*, 207–214.
(6) Nainaparampil, J. J.; Eapen, K. C.; Sanders, J. H.; Voevodin, A. A. *J. Microelectromech. Syst.* **2007**, *16*, 836–843.
(7) Fitchett, B. D.; Conboy, J. C. *J. Phys. Chem. B* **2004**, *108*, 20255–20262.
(8) Romero, C; Baldelli, S. *J. Phys. Chem. B* **2006**, *110*, 6213–6223.
(9) Santos, C. S.; Baldelli, S. *J. Phys. Chem. B* **2007**, *111*, 4715–4723.
(10) Romero, C.; Moore, H. J.; Lee, T. R.; Baldelli, S. *J. Phys. Chem. C* **2007**, *111*, 240–247.
(11) Rollins, J. B.; Fitchett, B. D.; Conboy, J. C. *J. Phys. Chem. B* **2007**, *111*, 4990–4999.
(12) Caporali, S.; Bardi, U.; Lavacchi, A. *J. Electron Spectrosc. Relat. Phenom.* **2006**, *151*, 4–8.
(13) Gottfried, J. M.; Maier, F.; Rossa, J.; Gerhard, D.; Schulz, P. S.; Wasserscheid, P.; Steinrück, H.-P. *Z. Phys. Chem.* **2006**, *220*, 1439–1453.
(14) Iimori, T.; Iwahashi, T.; Kanai, K.; Seki, K.; Sung, J.; Kim, D.; Hamaguchi, H.-o; Ouchi, Y. *J. Phys. Chem. B* **2007**, *111*, 4860–4866.
(15) Sloutskin, E.; Ocko, B. M.; Tamam, L.; Kuzmenko, I.; Gog, T.; Deutsch, M. *J. Am. Chem. Soc.* **2005**, *127*, 7796–7804.
(16) Hofft, O.; Bahr, S.; Himmerlich, M.; Krischok, S.; Schaefer, J. A.; Kempter, V. *Langmuir* **2006**, *22*, 7120–7123.
(17) Krischok, S.; Eremtchenko, M.; Himmerlich, M.; Lorenz, P.; Uhlig, P.; Neumann, A. *J. Phys. Chem. B* **2007**, *111*, 4801–4806.
(18) Smith, E. F.; Rutten, F. J. M.; Villar-Garcia, I. J.; Briggs, D.; Licence, P. *Langmuir* **2006**, *22*, 9386–9392.
(19) Nainaparampil, J. J.; Phillips, B. S.; Eapen, K. C.; Zabinski, J. S. *Nanotechnology* **2005**, *16*, 2474–2481.
(20) Atkin, R.; Warr, G. G. *J. Phys. Chem. C* **2007**, *111*, 5162–5168.
(21) Mezger, M.; Schröder, H.; Reichert, H.; Schramm, S.; Okasinski, J. S.; Schöder, S.; Honkimäki, V.; Deutsch, M.; Ocko, B. M.; Ralston, J.; Rohwerder, M. *Science* **2008**, *322*, 424–428.
(22) Liu, Y.; Zhang, Y.; Wu, G.; Hu, J. *J. Am. Chem. Soc.* **2006**, *128*, 7456–7457.
(23) Del M., Pópolo. Ballone, P. Private communication, 2009.
(24) Triolo, A.; Russina, O.; Bleif, H.-J.; Di Cola, E. *J. Phys. Chem. B* **2007**, *111*, 4641–4644.
(25) Triolo, A.; Russina, O.; Fazio, B.; Triolo, R.; Di Cola, E. *Chem. Phys. Lett.* **2008**, *457*, 362–365.

JP9022234

Supporting Information

Evidence of extended solid-like layering in [Bmim][NTf2] ionic liquid thin films at room-temperature

S. Bovio[1], A. Podestà[1,], C. Lenardi[2], P. Milani[1]*

[1] C.I.Ma.I.Na. and Dipartimento di Fisica, Universita' degli Studi di Milano, via Celoria 16, 20133, Milano, Italy.

[2] C.I.Ma.I.Na. and Istituto di Fisiologia Generale e Chimica Biologica, Universita' degli Studi di Milano, via Trentacoste 2, 20134, Milano, Italy.

* Corresponding author. E-mail: alessandro.podesta@mi.infn.it

X-ray photoelectron spectroscopy.

We have studied by X-ray photoelectron spectroscopy (XPS) pure bulk [Bmim][NTf2] and [Bmim][NTf2] microdroplets deposited from a [Bmim][NTf2]/methanol solution, both on silicon, in order to assess whether the interaction with methanol is destructive for the ionic liquid.

XPS measurements have been performed in two different apparatus. The supported [Bmim][NTf2] microdroplets have been characterized in a UHV apparatus PHI equipped with a hemispherical electron analyzer and monochromatized X-ray source (Al Kα). The high resolution spectra were acquired in constant pass-energy mode E_{pass}= 23.5 eV. The overall energy resolution was 0.7 eV. The pressure in the experimental chamber during experiments was below $2 \cdot 10^{-9}$ mbar. The pure [Bmim][NTf2] liquid has been characterized in a UHV apparatus Leybold LHS 10/12 equipped with a hemispherical electron analyzer and conventional X-ray source (Mg Kα). The high resolution spectra were acquired in constant pass-energy mode E_{pass}= 30 eV. The overall energy resolution was 1.0 eV. The pressure in the experimental chamber during experiments was below $3 \cdot 10^{-9}$ mbar. For both apparatus the spectra energy scale was scaled using as reference the Au $4f_{5/2}$ peak.

In Figure S1 we show the low-resolution XPS wide-scans of [Bmim][NTf2] microdroplets (top panel) and pure bulk [Bmim][NTf2] (bottom panel) on silicon. Both spectra show the typical [Bmim][NTf2] components: fluorine, oxygen, nitrogen, carbon and sulphur. Moreover, in the case of supported microdroplets, the signature of silicon is also evident due to the presence of extended non-coated areas. The contribution of silicon oxide is mirrored by the increasing of the intensity of the oxygen peak.

Figure S2 shows high resolution core level photoemission spectra of [Bmim][NTf2] microdroplets on silicon deposited from a [Bmim][NTf2]/methanol solution (solid line) and of pure bulk [Bmim][NTf2] (dashed line). For all the peaks a Shirley background was removed and, for the same energy region, the

peak area was normalized to one. A quantitative evaluation of the surface composition of pure [Bmim][NTf2] provides the following ratios: F:O:N:C:S=6:4:3.5:11.2:2, in good agreement with the nominal stoichiometry of F:O:N:C:S=6:4:3:10:2. The observed spectra for pure are in good agreement with published results [Smith06, Hofft06]. A quantitative evaluation of the surface composition of [Bmim][NTf2] microdroplets deposited from a [Bmim][NTf2]/methanol solution provides the following ratios: F:O:N:C:S=6:4:3:11:2, again in good agreement with the nominal stoichiometry (the contribution of oxygen bound to Si in native SiO_2 has been removed in order to obtain those ratios).

For each core level the peak position and the relative intensities of the constituents are comparable between the two samples. The overlapping of XPS spectra demonstrates that methanol does not interfere with the ionic liquid in the deposition process, the structure of the cation-anion pair being preserved. C1s and S2p spectra of the microdroplets show better separated peaks due to the highest resolution of the experimental apparatus. Only for [Bmim][NTf2] microdroplets the peak of Si2p is shown, because in the case of pure bulk [Bmim][NTf2] the substrate is not exposed.

Statistical analysis of AFM data.

This analysis is based on the study of height histograms, rather than of single representative topographic profiles (sections). This approach permits to consider in the analysis a huge amount of topographic data (order of 10^6-10^7 data points), avoiding the questionable manual choice of the analysis areas by the operator. Custom routines have been developed to this purpose in Matlab environment. AFM topographic maps are first flattened by line-by-line subtraction of 0th to 3th order polynomials evaluated on flat substrate regions, in order to get rid of distortions introduced by the scanning piezos and of the tilt of the sample in the sample holder of the AFM. Height histograms are then calculated, in the case merging data from AFM images containing homogeneous features. Terraces, that are constant-

height regions, produce sharp peaks in the histograms. Peak-to-peak distances represent terrace heights. The corresponding error is calculated summing in quadrature the statistical error, related to the width of the histogram peaks, and an instrumental error that reflects the accuracy of the calibration of the vertical piezo (~2% of average terrace height).

Each terrace height h_i is supposed to be an integer multiple of the same basic monolayer height δ (the latter being in principle different on different surfaces). In order to find the best divider of terrace heights, and the series of best integers, we minimize the following chi-square with respect to δ in the region $0.5 < \delta < 0.9$:

$$\chi^2 = \sum w_i (h_i - \delta \cdot \mathrm{round}(h_i / \delta))^2$$

where $w_i = (\sigma_i^2 \delta^2)^{-1}$, σ_i is the error associated to h_i, and $\mathrm{round}(h_i / \delta)$ represents the closest integer N_i such that $\delta N_i \sim h_i$. The extra weight δ^{-2} avoid privileging the small dividers, which systematically provide a smaller quadratic error ($(h_i - \delta N_i)^2 < \delta^2$) and therefore would bias the chi-square.

Terrace heights corresponding to the same N are averaged, and the average height is plotted against N (Figure 2d) to check the goodness of the structural model.

AFM phase imaging of layers and droplets.

Phase imaging is routinely performed simultaneously to intermittent-contact –mode (tapping-mode) in most of commercial AFMs. Phase imaging consists in recording the phase lag between the sinusoidal driving force and the oscillation of the AFM tip [Garcia02]. Qualitatively, a phase contrast can be associated to different visco-elastic properties of the sample surface, and more generally to different tip-surface interactions, which makes the interpretation of phase maps rather complicated. Figure S3 shows simultaneously recorded topographic and phase maps of a region of a thin [Bmim][NTf2] coating on amorphous silica where the substrate, the layered IL and the liquid droplets coexist. It can

be noticed a contrast between the IL droplets and the IL layers, which suggests that the IL is present in different phases. While it is straightforward to compare the phase lags of different forms of the same material (the IL in the droplets and in the layers), the comparison of phase signal of different materials (substrate and IL, both layered or in droplets), in particular the interpretation of the absence of phase contrast between the silica substrate and the IL droplets, is not obvious, and would require less qualitative application of phase imaging technique and models.

References.

[Smith06] Smith, E.F.; Rutten, F.J.M.; Villar-Garcia, I.J.; Briggs, D.; Licence, P. *Langmuir* **2006**, *22*, 9386-9392.

[Hofft06] Hofft, O.; Bahr, S.; Himmerlich, M.; Krischok, S.; Schaefer, J.A.; Kempter, V. *Langmuir* **2006**, *22*, 7120-7123.

[Garcia02] García, R.; Pérez, R. *Surf. Sci. Reports* **2002**, *47*,197-301.

Figures

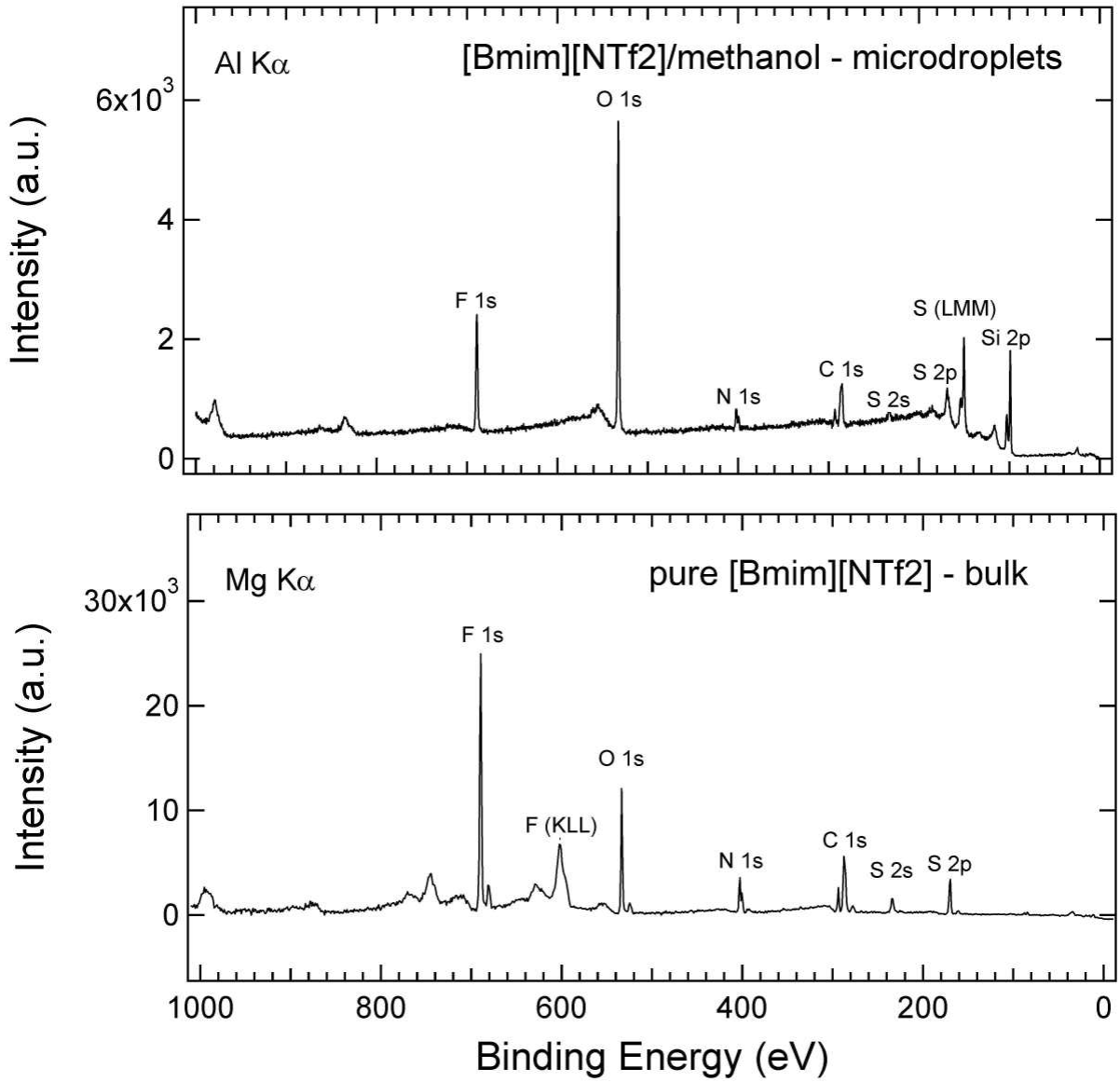

Figure S1. Comparison between low resolution XPS wide-scans of [Bmim][NTf2] microdroplets on silicon deposited from a [Bmim][NTf2]/methanol solution (top panel) and pure bulk [Bmim][NTf2] (bottom panel).

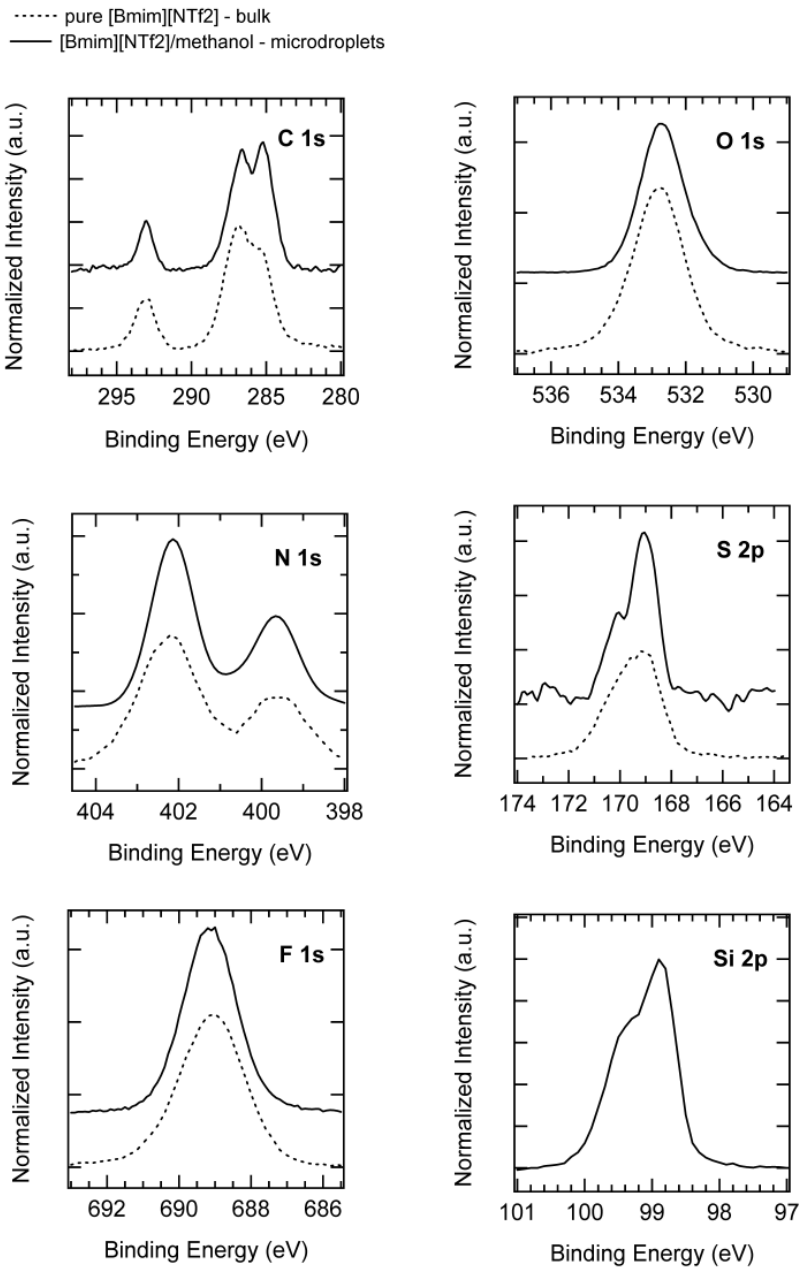

Figure S2. High resolution core level photoemission spectra of [Bmim][NTf2] microdroplets on silicon deposited from a [Bmim][NTf2]/methanol solution (solid line) and of pure bulk [Bmim][NTf2] (dashed line).

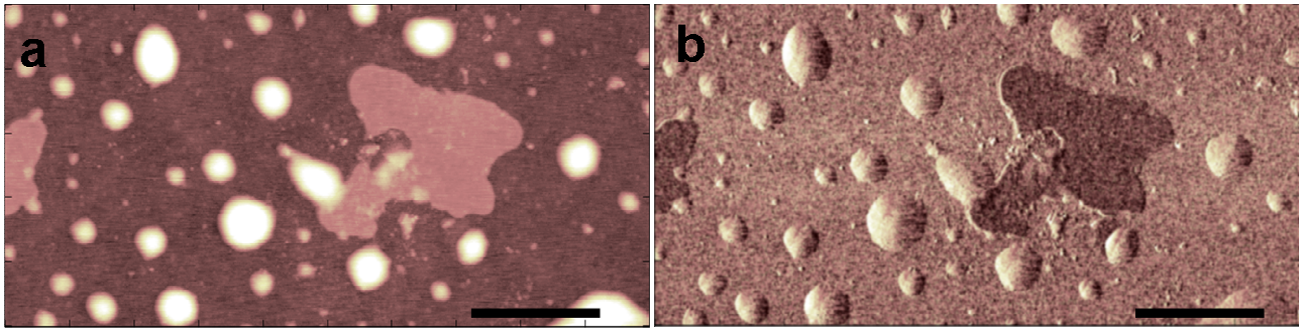

Figure S3. AFM (a) topography and (b) phase maps of a region of a thin [Bmim][NTf2] coating on amorphous silica where the substrate, the layered IL and the liquid droplets coexist. Scale bar is 1 μm.

Chapter 19

Investigation of Interfacial Properties of Supported $[C_4mim][NTf_2]$ Thin Films by Atomic Force Microscopy

Simone Bovio, Alessandro Podestà,* and Paolo Milani

C.I.Ma.I.Na. and Dipartimento di Fisica, Universita' degli Studi di Milano, via Celoria 16, 20133, Milano, Italy.

We report the results of an atomic force microscopy investigation of the morphological and structural properties of thin films of $[C_4mim][NTf_2]$ ionic liquid on mica, amorphous silica, oxidised Si(110), and highly-oriented pyrolytic graphite. We show that $[C_4mim][NTf_2]$ forms solid-like ordered structures on these surfaces at room temperature, with a vertical structural periodicity of ~0.6 nm. Moreover, we analyse the contact angles of nano-scale $[C_4mim][NTf_2]$ droplets on the different surfaces and show that they are sensitive to the chemical and morphological environment. Our findings highlight the potentialities of atomic force microscopy for the quantitative investigation of the interfacial properties of thin ionic liquid coatings. The results of this study suggest that at the liquid-solid interface, the structural properties of ionic liquids can be far more complex than those depicted so far, and indicate new fundamental investigations of the forces that drive supported ionic liquids through a liquid-to-solid-like transition.

Introduction

The thermophysical bulk properties of room-temperature ionic liquids have been thoroughly investigated in the last two decades - see for example *(1-6)* - due to their promising application as more environment-friendly solvents, as an alternative to conventional organic solvents *(7,8)*. In several applications, however, the interfacial rather than the bulk properties of ionic liquids are determinant. Indeed, there is increasing evidence that the use of ionic liquids as replacements for conventional electrolytes can boost the performance of several photoelectrochemical devices used for energy storage and energy production, such as Grätzel cells *(9)* or supercapacitors *(10)*. Moreover, ionic liquids have been successfully employed as a new class of lubricants in miniaturised as well as in macroscopic mechanical systems *(11,12)*. In all these cases, the most relevant processes determining the operation of the device take place at the liquid-solid interface between the ionic liquid and some relevant surfaces. This is a region extending only a few nanometers into the bulk of the liquid, yet its properties can be dramatically different from those of the bulk. The investigation of the interfacial properties of ionic liquids is therefore of primary importance for their technological exploitation.

To date, the (bulk)liquid-vapour and solid-(bulk)liquid ionic liquid interfaces have been studied, mostly by sum-frequency generation spectroscopy *(13-17)*, by X-ray photoemission spectroscopy *(18,19)*, and by a combination of these and other surface science techniques *(20-24)*, including atomic force microscopy *(25,26)*. For imidazolium-based ionic liquids, ordering of the cations at the solid-liquid or liquid-vapour interface has been inferred from vibrational spectroscopic data. Sloutskin *et al. (21)* inferred from X-ray reflectivity data of imidazolium-based ionic liquids the existence of an ordered surface layer at the liquid-vapour interface, about 0.6-0.7 nm thick, composed of both cations and anions. Moreover, the existence of periodically ordered layers of ionic liquids, including imidazolium-based, at the (bulk)liquid-solid interface with mica and silica, has been recently reported by Atkin *et al. (26)*, and interpreted as solvation layers. Despite these interesting results, still the knowledge of the structural properties of ionic liquids at interfaces, in particular with solid surfaces, is very poor. For example, it is not known whether, and how far, the ordered layers extend into the bulk of the liquid, nor it is known how the cation-anion pairs are organised within each layer, and what is the phase (liquid, solid-like) of the ionic liquid in the ordered region. A better understanding of the behaviour of ionic liquids at interfaces can be achieved studying systems where the surface-to-volume ratio is very large, as in very thin supported films. To date, this is a largely unexplored field, since all the above-mentioned studies were conducted on systems where a bulk amount of ionic liquid was present right above, or below, the interface.

Despite their great potential, scanning probe microscopy techniques are still not widely used in the community of ionic liquid-related surface scientists. In particular, atomic force microscopy (AFM), when suitable characterisation and data analysis protocols are employed, can provide extremely valuable information about the interfacial properties of supported thin ionic liquid coatings. On one hand, thanks to the in-plane nanometer resolution and vertical sub-nanometer resolution, AFM can quantitatively and non-invasively

characterise the nano-scale structural and morphological properties of ionic liquids films; on the other hand, the AFM probe could be used to map several interfacial properties, simultaneously to topography, such as interfacial electric impedance *(27)*, friction, and adhesion *(28)*, with nanometer resolution. AFM can therefore valuably contribute, together with the other surface-sensitive techniques, like sum-frequency generation spectroscopy or X-ray photoemission spectroscopy, as well as numerical simulations, to the understanding of the basic mechanisms driving the reorganisation of ionic liquids on solid surfaces.

We report here on the application of atomic force microscopy to the study of nanoscale morphological and structural properties of very thin coatings of 1-butyl-3-methylimidazolium bis(trifluoromethylsulfonyl)amide, $[C_4mim][NTf_2]$, on different surfaces of technological interest.

Following the work of Liu *et al. (29)*, who recently reported about the layering at room-temperature of $[C_4mim][PF_6]$ on mica, we have visualised nanoscale structures of $[C_4mim][NTf_2]$ on a variety of surfaces: mica, amorphous silica, polished, oxidised *p*-doped Si(110), and highly oriented pyrolytic graphite (HOPG). Applying a rigorous protocol for the statistical analysis of AFM images, we have characterised the structural properties of ionic liquids films, validating a structural model according to which $[C_4mim][NTf_2]$ forms layered solid-like structures at room-temperature on mica and silica surfaces, with a basic periodicity in the perpendicular direction of ~0.6 nm. In contrast, on HOPG, $[C_4mim][NTf_2]$ segregates in nanometer-sized domains. Exploiting the capability of AFM of detecting and controlling nanoscale surface forces, we have qualitatively tested the mechanical properties of solid-like $[C_4mim][NTf_2]$ films, showing that the layered structures respond like lamellar solids to vertical and lateral stresses. Moreover, we have studied the local wettability of $[C_4mim][NTf_2]$ on different substrates, analysing the contact angles of nanoscale droplets in AFM topographies. The comparative study of morphology and wettability of these ionic liquid films provided some more hints on the surface organisation of liquid and solid-like phases.

Material and methods

Chemicals and substrates

Two samples of the ionic liquid $[C_4mim][NTf_2]$ from Sigma Aldrich and from the Queen's University Ionic Liquids Laboratories (QUILL) were used, both with purity grade greater than 98.0%.

Methanol, from Fluka, with 99.8% (HPLC) purity grade was further distilled two times and used for preparation of solutions with the ionic liquid.

Hydrochloric (HCl) and nitric (HNO_3) acids (Carlo Erba), with concentrations of 37% and 69.5%, respectively, and ratio 3:1 were used to prepare *aqua regia* solutions for cleaning silica substrates.

Ruby-muscovite mica and highly oriented pyrolytic graphite (HOPG) sheets were acquired from Ted Pella and Assing.

Standard 13mm-diameter discs of amorphous silica (glass coverslips) from Assing and squared, single-side polished specimens of oxidised Si(110) were

used. In the text, the words 'silica surfaces' will be used to refer to amorphous and ordered silica surfaces together.

Sample preparation

Samples suitable for the investigation by AFM of the solid-liquid-air interface of $[C_4mim][NTf_2]$ have been obtained by drop-casting 20 μl of highly diluted solutions of $[C_4mim][NTf_2]$ in methanol (concentrations lower than 10^{-2} - 10^{-3} mg cm^{-3}) on the substrates, allowing them to dry in ambient conditions. A comparative X-ray photoelectron spectroscopy analysis of pure and methanol-mixed $[C_4mim][NTf_2]$ confirmed that the solvent used in the deposition process does not react with $[C_4mim][NTf_2]$ (data not shown).

All substrates were freshly prepared immediately before deposition of the $[C_4mim][NTf_2]$-methanol solution. Mica and HOPG were typically freshly cleaved using an adhesive tape in order to obtain clean and atomically-smooth substrates. 13 mm-diameter discs of amorphous silica (glass coverslips) and squared specimens of polished, oxidised Si(110) were cured in *aqua regia* solution before deposition in order to remove organics and re-hydroxylise their surfaces.

AFM measurements

A Bioscope II AFM from Veeco Instruments was used. The AFM was operated in tapping mode in ambient conditions with standard single-crystal silicon cantilevers (resonance frequency between 200 and 300 kHz, nominal radius of curvature of the tip 5-10 nm). Typically, image scan size was 5 μm x 5 μm and 15 μm x 15 μm, with scan rates in the range 0.5-1.5 Hz. Stable imaging conditions could be achieved and maintained for hours as if scanning on a solid surface. We did not observe significant changes in the imaging conditions when imaging in a dry dinitrogen atmosphere.

The AFM was also operated in force-spectroscopy mode, using force modulation tips with typical force constant $k = 4$ N m^{-1}. When force-spectroscopy is coupled to contact-mode imaging, several force-*vs.*-distance curves are acquired along a raster pattern spanning a finite area, and built on a previously-acquired AFM image. Each force curve is obtained recording the cantilever deflection (which is converted into a force, upon suitable calibration of the lever) as a function of the relative tip-surface distance *(30)*.

Statistical analysis of AFM data

This analysis is based on the study of height histograms. This approach permits consideration in the analysis of a huge amount of topographic data (order of 10^6-10^7 data points). Terraces, that are constant-height regions, produce sharp peaks in the histograms. Peak-to-peak distances represent terrace heights. A multi-Gaussian fit provides the peak positions, as well as the corresponding width. The error associated to the height of a terrace is calculated summing in quadrature the statistical error, related to the width of the histogram peaks, and an instrumental error that reflects the accuracy of the calibration of the vertical piezo (~2% of average terrace height).

Each terrace height h_i is supposed to be an integer multiple of the same basic monolayer height δ (the latter being in principle different on different surfaces). In order to find the best divider of terrace heights, and the series of best integers, we minimise the following chi-squared function with respect to δ in the region 0.5 nm < δ < 0.9 nm:

$$\chi^2 = \sum w_i (h_i - \delta \cdot \mathrm{round}(h_i / \delta))^2$$

where $w_i = (\sigma_i^2 \delta^2)^{-1}$, σ_i is the error associated with h_i, and $round(h_i/\delta)$ represents the closest integer N_i such that $\delta N_i \sim h_i$. The extra weight δ^{-2} avoids weighting the small dividers, which systematically provide a smaller quadratic error ($(h_i - \delta N_i)^2 < \delta^2$) and therefore would bias the chi-squared term.

Contact angle measurements

A suitable analysis of three-dimensional AFM topographies allows a statistical evaluation of the morphological parameters of nanodroplets needed to calculate the contact angles (the droplet radius and height, see later). To calculate the morphological properties of each object (droplet) in an image, a filtering procedure was used. To analyse separately the contact angles of the droplets sitting on the substrate, and of those sitting on top of solid-like layers, the images were cropped in such a way that all the heights are calculated starting from the correct flat background. The droplets were separated from their backgrounds masking the data using manually-set height thresholds. Using the Image Processing Toolbox of Matlab (Mathworks) in conjunction with these masks, each object was labelled separately, and several morphological parameters were calculated, such as the area, the volume, the radius, the height, the eccentricity, *etc*. Then, automatic filters were applied, in order to select only the desired objects (the round droplets), discarding all the others (remnants of layers, elongated liquid-like patches, *etc.*). The first constraint applied is that the logarithm of the heights and the volumes must be linearly correlated (as for spherical-like objects): all those data were rejected that were more than one or two standard deviations from the best straight line fitting the data. Only those objects having a ratio between major and minor axes of the best-fitting ellipse smaller than 1.2 were then kept. The few non-droplet-like objects that survived the previous filtering procedures (actually a negligible fraction of the total) were eventually rejected manually. Of the remaining (good) objects, the contact angles were calculated, along with their average value for each substrate, with the associated standard deviation of the mean.

Results and Discussion

Surface morphology of [C_4mim][NTf_2] films

Figure 1 shows a collection of representative AFM topographies of thin coatings of [C_4mim][NTf_2] on polished oxidised Si(110), mica, amorphous silica, and HOPG. These AFM images have been acquired in tapping-mode, with the exception of Figure 1c, which has been acquired in contact-mode.

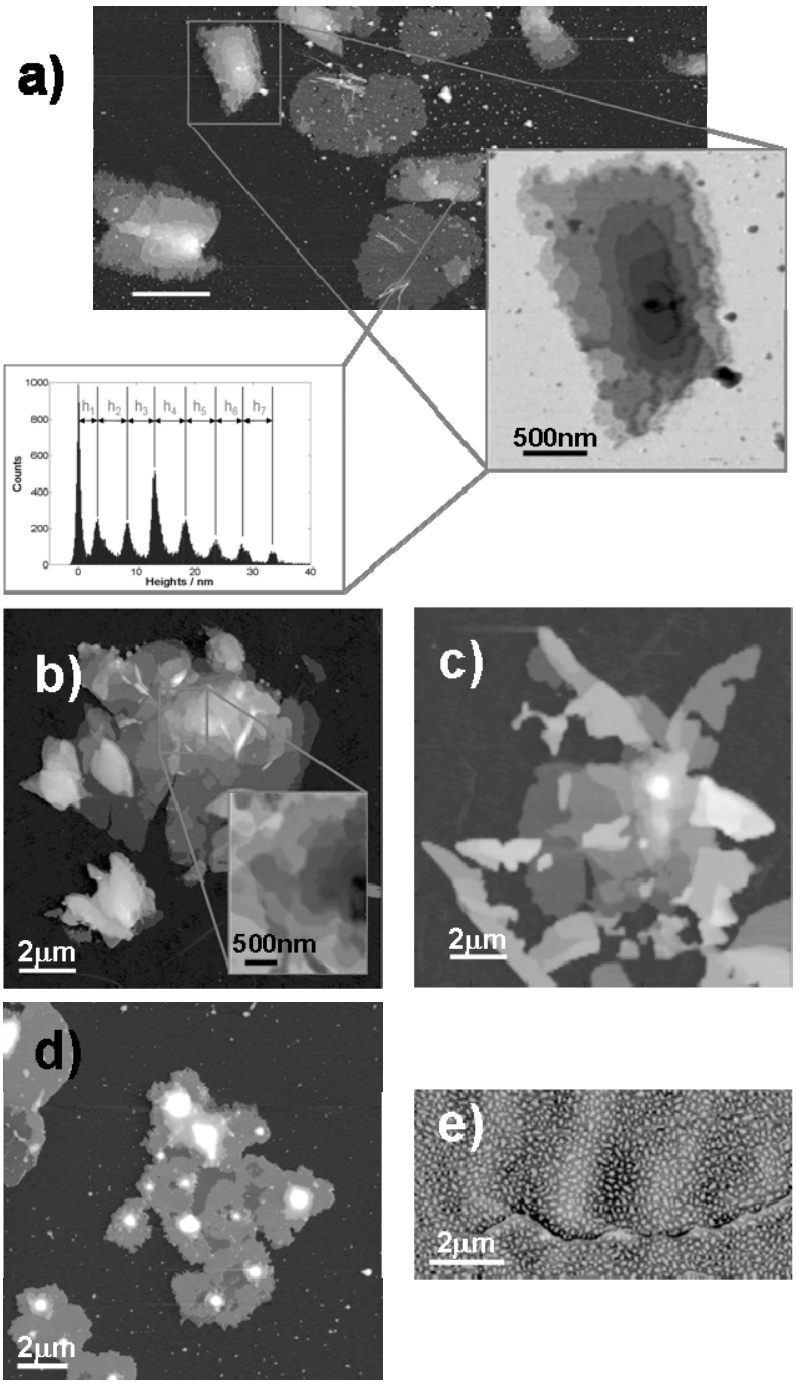

Figure 1. AFM topographic maps of thin [C_4mim][NTf_2] films on a) Polished oxidised Si(110); b,c) Amorphous silica; d) Mica; e) HOPG. All images acquired in tapping-mode, except c), which has been acquired in contact-mode. In a) it is shown the histogram of heights of the layered structure in the inset. Peak-to-peak distances represent the heights h_1, h_2,... of single terraces. Vertical scales: a) 50 nm; b) 100 nm (inset 70 nm); c) 50 nm; d) 35 nm; e) 10 nm.

Figures 1(a-d) show isolated layered structures, whose width is in the 1-20 μm range, and whose heights are well above 50 nm in some cases. Each layer has well defined edges, and height distributed typically between 2 nm and 6 nm. It is remarkable that also the layered structures that extend up to 50 nm away from the substrate behave like solid surfaces against the AFM probe. In particular, even during contact-mode imaging, no evidence of scratching or invasive tip/sample interaction was observed, Figure 1(c), despite the fact that the applied normal pressures and lateral forces are at least one order of magnitude larger than in tapping-mode. No changes in the shape of layered features were typically observed after repeated scanning of the same areas, if not occasionally, when working with high forces (see later). On silica substrates, a more pronounced tendency of $[C_4mim][NTf_2]$ to grow three-dimensionally than on mica was observed. No evidence of ordered extended structures could be found on HOPG substrates, Figure 1(e). On HOPG, only nanometre-sized, rounded domains (nanodroplets) of ionic liquid spontaneously form upon evaporation of methanol. Coexistence of sub-micrometer droplets and layers is observed occasionally on amorphous silica and mica, and very rarely on oxidised Si(110) surfaces. The observed structures were extremely stable, even in ambient (humid) conditions: layers have been imaged also after several months, and no changes in their average structure and morphology have been observed, demonstrating that such structures are extremely stable.

Structural characterisation

AFM three-dimensional topographies allow to extract quantitative information about the structure of $[C_4mim][NTf_2]$ films. In particular, AFM images suggest that the layered structures result from the regular vertical arrangement of a molecular layer with thickness δ, Figure 2(a). Several basic layers arrange to form terraces, whose heights are typically in the range 1-6 nm. Terraces are typically observed growing on top of each other, each being delimited by a sharp step clearly observable in the AFM topographies. In order to characterise statistically and accurately the heights of the observed terraces, we considered the histograms of the heights in AFM topographies of layered structures. In the inset of Figure 1a is shown a typical height histogram of a layered structure. Such histograms consist in a series of peaks, each corresponding to a plateau in the AFM image. The peak-to-peak distances represent the average heights of piled-up terraces. These heights are supposed to be integer multiples of the height δ of the basic layer. We performed an optimisation procedure on terrace heights data in order to find the best value of δ for the different substrates. We found $\delta = 0.61 \pm 0.01$ nm, 0.56 ± 0.02 nm,

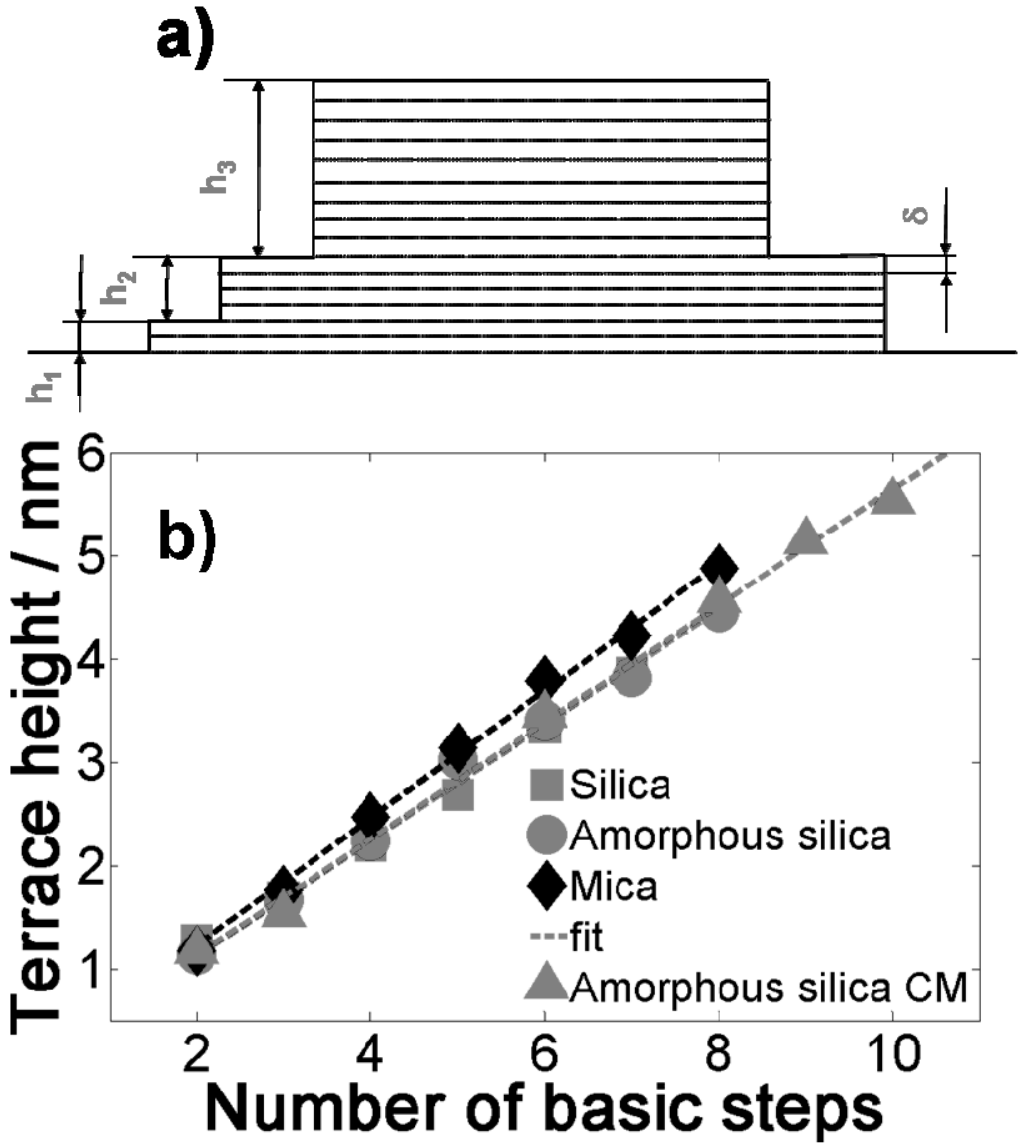

Figure 2. a) Structural model of solid-like [C_4mim][NTf_2] films: a basic layer with thickness δ is stacked in terraces with different heights h_1, h_2,...b) Correlation between average terrace heights measured on different surfaces and the number of basic steps in each terrace, obtained by fitting structural data (error bars are comparable to marker size). In the case of amorphous silica, data from both tapping- and contact-mode AFM images are reported.

0.56 ± 0.02 nm for mica, amorphous silica, and polished oxidised Si(110), accordingly. Figure 2(b) shows the curves obtained plotting the ratio of terrace heights to δ, approximated to the closest integer N_i (this ratio represents the number of basic layers stacked in a terrace) as abscissa, the average heights of the terraces with the same N_i as ordinate. The good linear correlation of data reflects the good vertical structural order of [C_4mim][NTf_2] films on mica and silica substrates. Remarkably, the analysis of AFM images acquired in contact-mode on amorphous silica provided the same result as that of tapping-mode images: the average terrace heights measured on amorphous silica in contact-mode show the same correlation with the number of repeated layers than the

heights measured in tapping-mode {Figure 2(b), circles and triangles}, with similar slope $\delta = 0.56$ nm. This is a further confirmation that these structures are solid-like. These results are in remarkably good agreement with the results of numerical simulations of thin $[C_4mim][NTf_2]$ and $[C_4mim][PF_6]$ films on silica *(31)*.

Test of the solid-like character of $[C_4mim][NTf_2]$ films

The force that the AFM probe exerts on the sample surface can be controlled. During imaging, the force is typically minimised, while in force-spectroscopy experiments it can be made large in order to test the mechanical resistance of the surface. Evidence has been collected that the layered structures oppose a strong mechanical resistance to the AFM tip. As already mentioned, there was no observation of any scratch or penetration of the tip into the structures, even after repeated scans, even when imaging in contact-mode (in contact-mode normal forces are typically 10-100 times larger than in tapping-mode, the contact pressure being of the order of 10-100 MPa). This proves that the layered structures are very compact, and in particular possess a strong mechanical resistance against vertical compression. The applied lateral force is expected to play a major role in disrupting the ordered $[C_4mim][NTf_2]$ films. In fact, erosion of the terraces has been occasionally observed along the borders, in both tapping- and contact mode, as shown in Figure 3. In correspondence of the edges, the mechanical strength of the solid-like films is expected to be reduced, and therefore the lateral force exerted by the AFM tip can be enough to break the arrangement of the molecules. Noticeably, the applied lateral force is larger when the tip climbs the steep edges of the higher terraces, because the feedback loop of the AFM react with some delay to the quick changes of the topography. A stronger erosion is observed when imaging in contact-mode, Figure 3(a), because lateral force are greatly increased with respect to tapping-mode. Erosion observed in tapping-mode, Figure 3(b), is negligible. However, it is clear that erosion is localised only at the edges of the structures. When imaging in contact-mode at higher forces, delamination of a layered structure can also be observed. In Figures 4(a and b) AFM images of the same terrace before and after repeated scans in contact-mode at high force are shown. It can be seen by comparing Figure 4(a and b) that a complete stack of basic layers has been removed from the top of the terrace. Comparison of the height histograms before and after the scan, Figure 4(c), shows that the height of the removed layer is ten times the height δ of the basic layer. This layer has been delaminated by high lateral forces during the first two scans. In fact, the strong peak at $h \sim 15$ nm grows at the expense of the peak at $h \sim 20$ nm, corresponding to the topmost terrace that has been swept away. AFM images and height analysis suggest that this structure behaves like a lamellar solid, which can be cleaved along preferential directions.

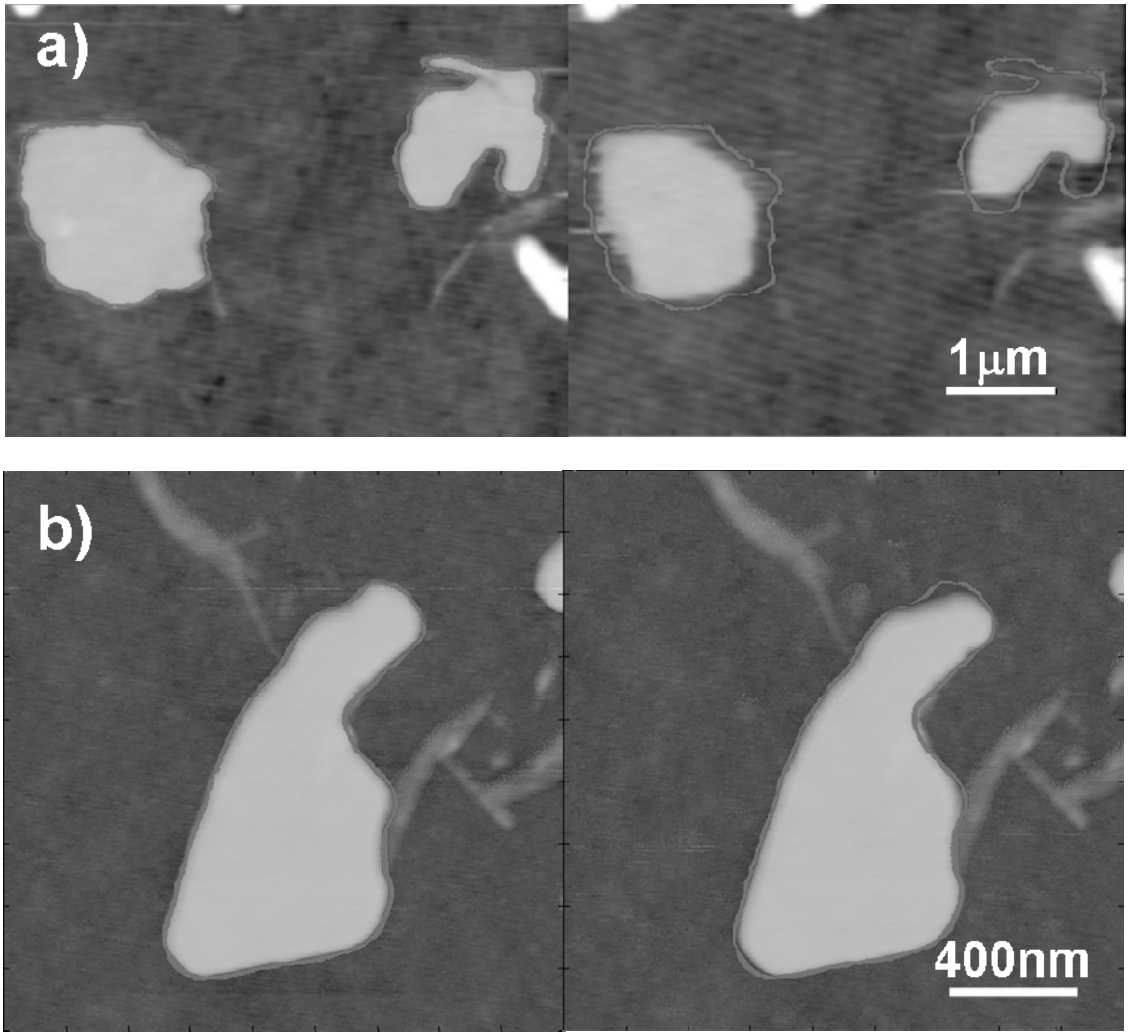

Figure 3. Evidence of erosion at the edges of [C_4mim][NTf_2] terraces on amorphous silica after repeated scans in a) Contact-mode AFM, 4 scans; b) Tapping-mode AFM, 10 scans. The continuous line highlights the terrace border before erosion. Vertical scales: a) 10 nm; b) 20 nm.

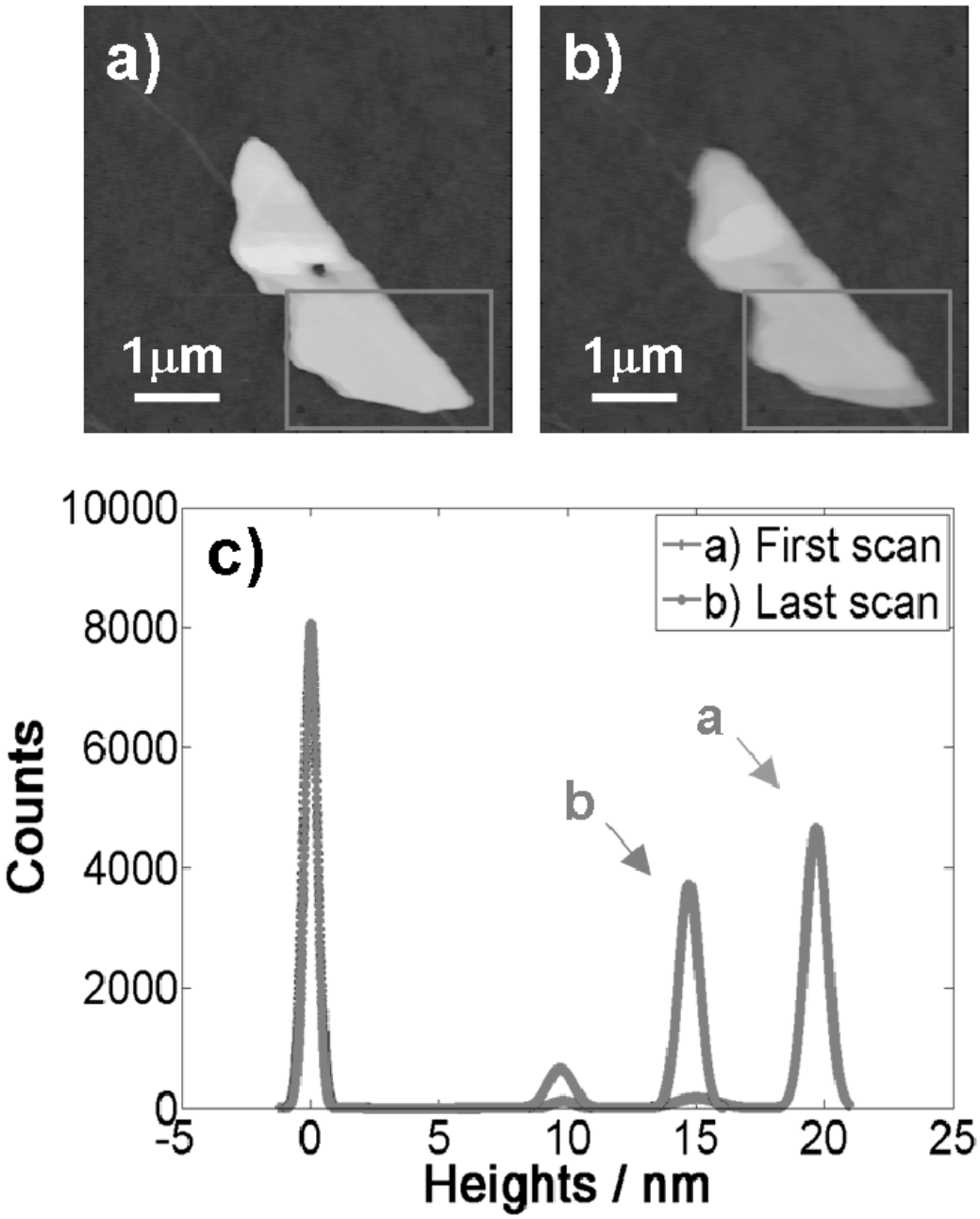

Figure 4. Delamination of [C_4mim][NTf_2] layers on amorphous silica after three scans in contact-mode. a,b) AFM topographies before and after delamination (vertical scales: 35 nm); c) Multi-Gaussian -fitted height histograms of the boxed regions in a) and b), showing that a stack of basic layers is swept away from the top.

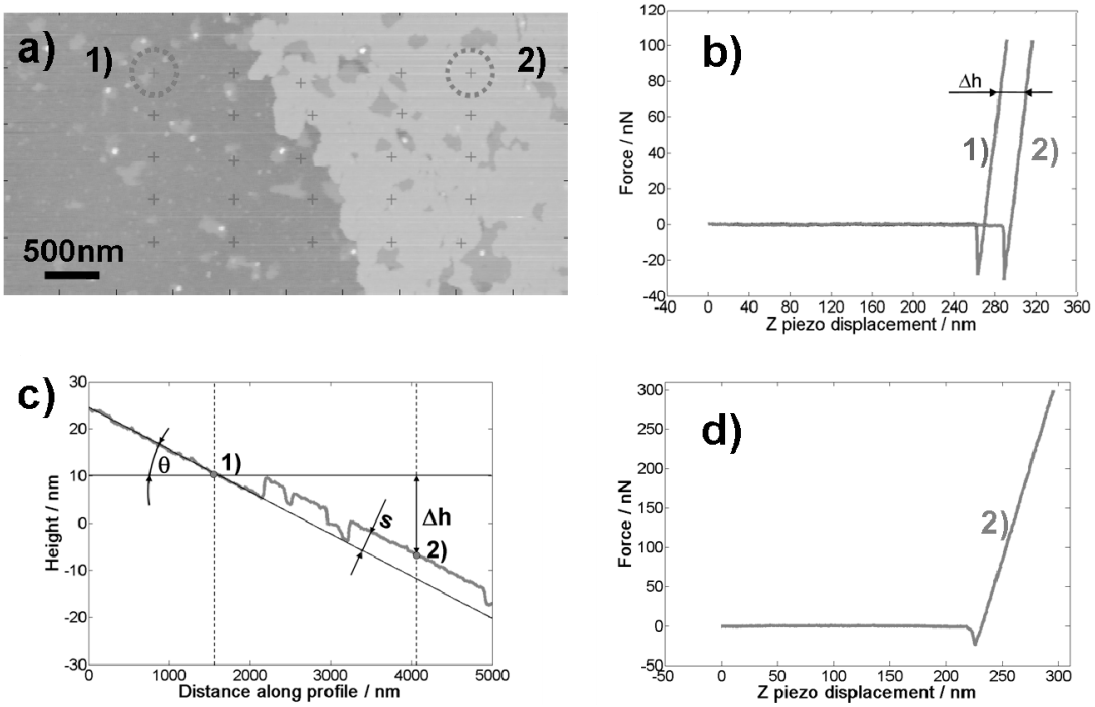

Figure 5. Test of the normal hardness of solid-like [C_4mim][NTf_2] layers on oxidized Si(110). a) AFM contact-mode topography (Vertical scale: 15 nm). A force-distance curve has been acquired in each point marked by a cross; b)Two representative force curves acquired in the circled locations, on the bare substrate (1), and on top of the ionic liquid layer (2); c) The topographic profile from the non-flattened AFM image passing through points (1) and (2), highlighting the overall tilt of the sample; d) A force curve acquired in (2) with a higher normal force set point.

The perpendicular hardness of [C_4mim][NTf_2] layered structures has been qualitatively tested by using the AFM in force-spectroscopy–mode. A topographic map of a terrace on polished oxidised Si(110) has been acquired, Figure 5(a), and several force-distance curves along a grid, on the substrate as well as on the film, have been collected. Figure 5(b) shows two approaching force curves, acquired on the silica substrate and on the film, in locations (1) and (2) (the circled spots). The slopes of these curves in the contact region are the same. This suggests that the film behaves upon loading exactly as the hard silica substrate, that is like an impenetrable, solid surface. If deformation of the [C_4mim][NTf_2] film occurred during contact, a different slope would be observed, together with discontinuities and irregularities in the first part of the linear region, witnessing the penetration of the film. The possibility that a sudden and traceless film penetration of [C_4mim][NTf_2] occurs right after contact could not be completely excluded. In this case the silica substrate, and not the film would be actually loaded, providing the same slopes in the two curves. The observation that the two curves are horizontally shifted by an amount Δh corresponding to the thickness of the film {plus exactly the tilt of the sample! – see Figure 5(c)} allows elimination of this unlikely event. In the case of complete film penetration, only the displacement due to the tilt of the sample

would be present. The surface of the film is actually loaded, not the substrate. Similar slopes and displacements were observed when much higher than normal pressures (up to 1 GPa) are applied to $[C_4mim][NTf_2]$ films, Figure 5(d). These topography-related local force measurements provided a direct proof that the $[C_4mim][NTf_2]$ layered structures are solid-like.

Analysis of the contact angles of $[C_4mim][NTf_2]$ nanodroplets

The coexistence of solid-like ordered layers and nanodroplets has been observed in samples deposited on mica and amorphous silica. On oxidised Si(110) only a very few droplets have been observed.

The contact angle of a droplet at equilibrium on a smooth surface is related to the surface energies by the Young equation:

$$cos(\theta) = (\sigma_{sv} - \sigma_{sl})/\sigma_{lv}$$

where σ_{sv}, σ_{sl}, σ_{lv} are the solid-vapour, solid-liquid, and liquid-vapour surface energies, accordingly. While σ_{lv} of $[C_4mim][NTf_2]$ is known, σ_{sl} is not (as often is the case for σ_{sv}). Analysis of the contact angles of nanodroplets on the different substrates can therefore provide some insights into the chemistry of the interface, in particular on the effective surface energy $\Delta\sigma_{sl} = \sigma_{sv} - \sigma_{sl}$.

For droplets as small as those in our samples, gravity effect can be ignored, and it is possible to demonstrate that their shape is that of a spherical cap, with radius r, height h, Figure 6(c) *(32)*. The contact angle of a spherical cap can be expressed in terms of the droplet aspect ratio $A = 2r/h$ only:

$$tan(\theta) = 4A^2/(A^2 - 4)$$

Figure 6(a) shows a region of $[C_4mim][NTf_2]$ on amorphous silica where droplets and layers coexist. In particular, droplets have been observed sitting on the silica substrate and $[C_4mim][NTf_2]$ layer. Figure 6(b) shows a three-dimensional view of a droplet sitting on a layer. Typical size of droplets is well below 1 μm, with the height typically between 20 nm and 50 nm.

Table 1 reports the values of the contact angles measured on mica, amorphous silica, and HOPG. On HOPG, the droplets are very small, typically 20-50 nm large and only a few nanometers tall, and this makes the calculation of

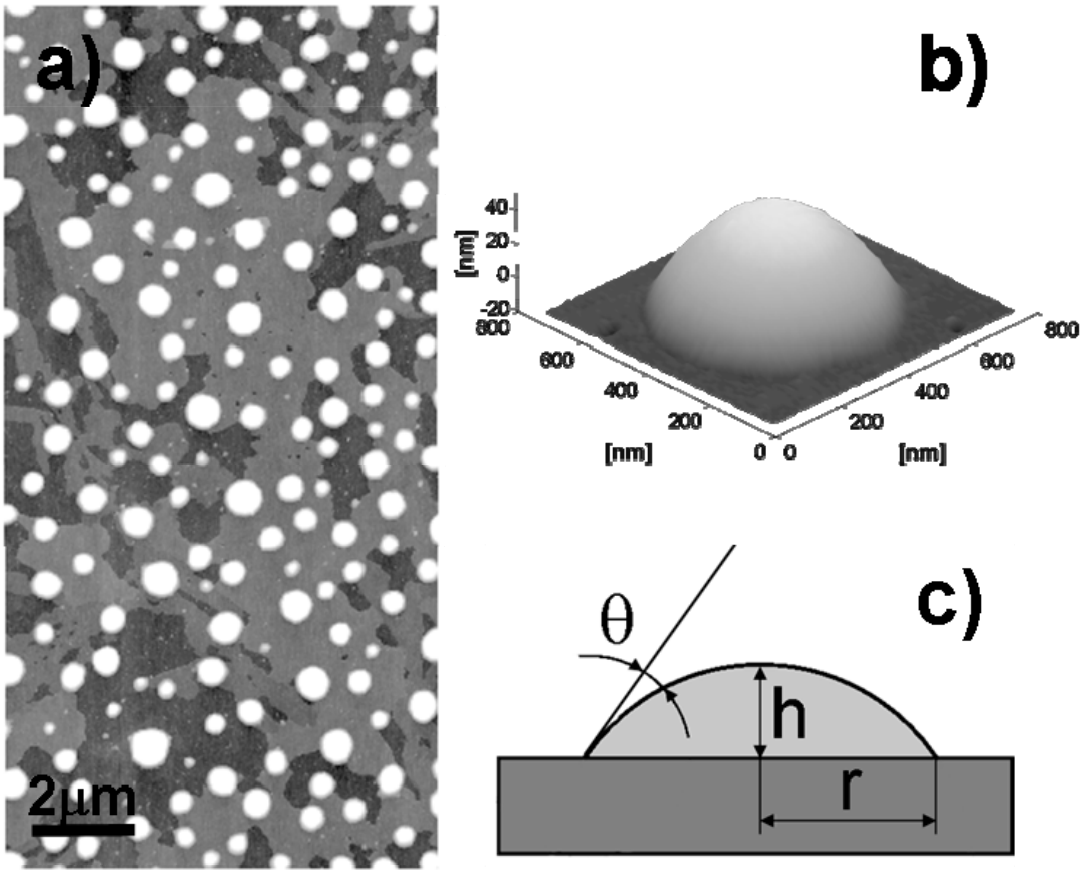

Figure 6. a) AFM tapping-mode topography of a [C_4mim][NTf_2] film on amorphous silica, showing coexistence of layers and nanodroplets (Vertical scale 20 nm). b) A three-dimensional view of a nanodroplet sitting on top of a layer; c) The spherical cap model assumed for the droplets. θ, h, and r are the contact angle, height, and radius of the droplet, accordingly.

the contact angle less reliable, because convolution effects and tip-induced deformation of the droplets have a stronger impact on the imaging process.

Table 1. Contact angles and effective surface energies of nano-droplets

Substrate	*Contact angle / °*	$\Delta\sigma_{sl}$ / (mJ m^{-2}) [a]
Mica	41.7 ± 5.6	24.78 ± 2.16
Terraces on mica	45.7 ± 6.0	23.20 ± 2.48
Amorphous silica	12.2 ± 1.0	32.45 ± 0.28
Terraces on am. silica	27.0 ± 5.2	29.57 ± 1.38
HOPG	19.7 ± 2.2	31.25 ± 0.48

[a] σ_{lv} = 33.20 ± 0.25 mJ m^{-2} from *(4)*.

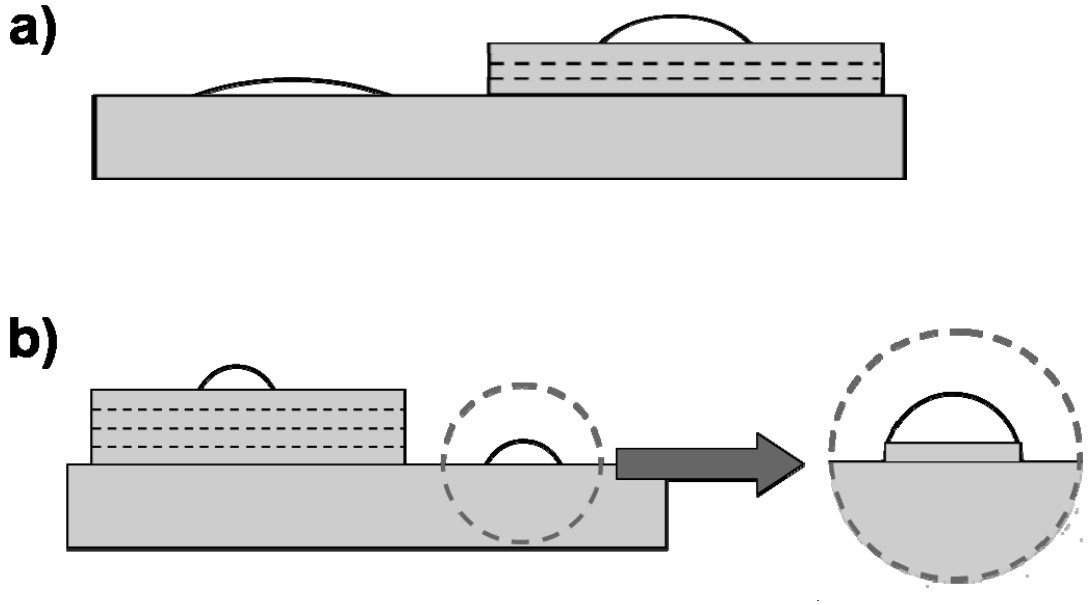

Figure 7. Schematic view of [C_4mim][NTf_2] nanodroplets sitting on the substrate or on top of solid-like layers, in the case of a) Amorphous silica; b) Mica. A thin solid-like layer, not detectable by AFM, could be present below the droplets sitting on mica, explaining the similarity of contact angles found on the substrate and on top of layers.

From Table 1, the measured contact angles show some variability, which deserves some consideration. The different situations have been summarised and represented in Figure 7. Firstly, the contact angles of [C_4mim][NTf_2] droplets on different surfaces are different, as expected. In particular, [C_4mim][NTf_2] wets better on amorphous silica, HOPG, and mica (in this order). On amorphous silica, Figure 7(b), the contact angle on the substrate is different from that on top of a solid-like layer, with the somewhat unexpected detail that the ionic liquid wets the silica substrate better than its solid-like phase. This represents a further confirmation that the phases of contacting [C_4mim][NTf_2] volumes are actually different. Other interesting observations can be made from Table 1 and Figure 7. [C_4mim][NTf_2] wets the solid-like layers that form on amorphous silica better than those on mica. This can suggest that, despite the strong structural similarity, some fine differences in the chemical surface properties of solid-like layers exist. Remarkably, a small (but still statistically significant) difference in the basic spacing of the solid-like phases which form on mica and silica was found. Eventually, it was noticed that, in the case of mica, there is no difference between the contact angles on the substrate and on the solid like layer (within statistical error). The intuitive explanation for this is sketched in Figure 7(b): a molecularly thin, solid-like layer, not detectable by the AFM, could be hidden below the droplet.

Conclusions

When a few monolayers of $[C_4mim][NTf_2]$ are deposited on a variety of surfaces, the whole ionic liquid rearranges in a solid-like phase, characterised by the stacking of a basic layer with thickness compatible to the size of the cation-anion pair ($\delta \sim 0.6$ nm). Structural order is maintained up to distances corresponding to much more than the single or the few molecular layers recently observed at the interface between a bulk amount of ionic liquid and a solid surface, or air. The solid-like character of these films has been qualitatively tested by exploiting the capability of the AFM of acting as a controlled local force transducer. Moreover, it has been shown that AFM allows characterising the contact angles of ionic liquids nanodroplets, providing information about the chemical heterogeneity of different interfaces, as well as quantitative data about the surface energies.

The potential of atomic force microscopy for the quantitative investigation of the interfacial properties of thin ionic liquids coatings was highlighted. The results of this study are directly relevant for those applications where ionic liquids are employed in form of thin films supported on solid surfaces, such as in micro-electromechanical or micro-electronic devices. More generally, they suggest that at the (bulk)liquid-solid interface the structural properties of ionic liquids can be far more complex than those depicted so far, and prompt new fundamental investigations of the forces that drive supported ionic liquids through a liquid-to-solid-like transition. Finally, it is concluded that the possibility of comparing the results of AFM investigations to those of numerical simulations will be extremely interesting.

Acknowledgements

We thank P. Ballone and M. Del Pópolo for discussions and suggestions, K.R. Seddon and M. Deetlefs for providing the ionic liquid used in this study, and C. Lenardi and M. Perego for the XPS analysis of our samples. This project has been financially supported by Fondazione Cariplo under grant “Materiali e tecnologie abilitanti 2007”.

References

1. Jin, H.; O'Hare, B.; Dong, J.; Arzhantsev, S.; Baker, G.A.; Wishart, J.F.; Benesi, A.J.; Maroncelli, M. *J. Phys. Chem. B* **2008**, *112*, 81–92.
2. Singh, T.; Kumar, A. *J. Phys. Chem. B* **2008**, *112*, 12968–12972.
3. Troncoso, J.; Cerdeirina, C.A.; Sanmamed, Y.A.; Romani, L.; Rebelo, L.P.N. *J. Chem. Eng. Data* **2006**, *51*, 1856–1859.
4. Deetlefs, M.; Seddon, K.R.; Shara, M. *Phys. Chem. Chem. Phys.* **2006**, *8*, 642-649.
5. de Azevedo, R.G.; Esperança, J.M.S.S.; Najdanovic-Visak, V.; Visak, Z.P.; Guedes, H.J.R.; da Ponte, M.N.; Rebelo, L.P.N. *J. Chem. Eng. Data* **2005**, *50*, 997.
6. de Azevedo, R.G.; Esperança, J.M.S.S.; Szydlowski, J.; Visak, Z.P.; Pires, P.F.; Guedes, H.J.R.; Rebelo, L.P.N. *J. Chem. Thermodyn.* **2005**, *37*, 888-899.
7. Welton, T. *Chem. Rev.* **1999**, *99*, 2071-2083.
8. Holbrey, J.D.; Seddon, K.R. *Clean Products and Processes* **1999**, *1*, 223-236.
9. Kuang, D.; Wang, P.; Ito, S.; Zakeeruddin, S.M.; Grätzel, M. *J. Am. Chem. Soc.* **2006**, *128*, 7732–7733.
10. Frackowiak, E.; Lota, G.; Pernak J. *Appl. Phys. Lett.* **2005**, *86*, 164104-1/3.
11. Qu, J.; Truhan, J. J.; Dai, S.; Luo, H.; Blau, P. J. *Tribology Letters* **2006**, *22*, 207-214.
12. Nainaparampil, J.J.; Eapen, K.C.; Sanders, J.H.; Voevodin, A.A. *J. Microelectromech. Syst.* **2007**., *16*, 836-843.
13. Fitchett, B.D.; Conboy, J.C. *J. Phys. Chem. B* **2004**, *108*, 20255-20262.
14. Romero, C; Baldelli, S. *J Phys Chem B* **2006**, *110*, 6213-6223.
15. Santos, C.S.; Baldelli, S. *J. Phys. Chem. B* **2007**, *111*, 4715-4723.
16. Romero C.; Moore, H.J.; Lee, T.R.; Baldelli, S. *J. Phys. Chem. C* **2007**, *111*, 240-247.
17. Rollins, J.B.; Fitchett, B.D.; Conboy, J.C. *J. Phys. Chem. B* **2007**, *111*, 4990–4999.
18. Caporali, S.; Bardi, U.; Lavacchi, A. *J. Electr. Spectr. Rel. Phen.* **2006**, *151*, 4–8.
19. Gottfried, J.M.; Maier, F.; Rossa, J.; Gerhard, D.; Schulz, P.S.; Wasserscheid, P.; Steinrück, H.-P. *Z. Phys. Chem.* **2006**, *220*, 1439-1453.
20. Iimori, T.;, Iwahashi, T.; Kanai, K.;, Seki, K.;, Sung, J.; Kim, D.; Hamaguchi, H.-o; Ouchi, Y. *J. Phys. Chem. B* **2007**, *111*, 4860–4866.
21. Sloutskin, E.; Ocko, B.M.;Tamam, L.; Kuzmenko, I.; Gog, T.; Deutsch M. *J. Am. Chem. Soc.* **2005**, *127*, 7796−7804.
22. Hofft, O.; Bahr, S.; Himmerlich, M.; Krischok, S.; Schaefer, J.A.; Kempter, V. *Langmuir* **2006**, *22*, 7120-7123.
23. Krischok, S.; Eremtchenko, M.; Himmerlich, M.; Lorenz, P.; Uhlig, P.; Neumann, A. *J. Phys. Chem. B* **2007**, *111*, 4801-4806.
24. Smith, E.F.; Rutten, F.J.M.; Villar-Garcia, I.J.; Briggs, D.; Licence, P. *Langmuir* **2006**, *22*, 9386-9392.

25. Nainaparampil, J.J.; Phillips, B.S.; Eapen, K.C.; Zabinski, J.S. *Nanotechnology* **2005**, *16*, 2474–2481.
26. Atkin, R.; Warr, G.G. *J. Phys. Chem. C* **2007**, *111*, 5162-5168.
27. Gomila, G.; Toset, J.; Fumagalli, L. *J. Appl. Phys.* **2008**, *104*, 024315.
28. Dedkov, G.V.; *Phys. Status Solidi A* **2000**, *179*, 3-75.
29. Liu, Y.; Zhang, Y.; Wu, G.; Hu, J. *J. Am. Chem. Soc.* **2006**, *128*, 7456-7457.
30. Butt, H.-J.; Cappella, B.; Kappl, M. *Surf. Sci. Rep.* **2005**, *59*, 1–152.
31. M. Del Pópolo, P. Ballone, Queen's University, Belfast, private communication.
32. de Gennes, P. G. *Rev. Mod. Phys.* **1985**, *57*, 827-863.

J. Phys.: Condens. Matter **21** (2009) 424118 (11pp) doi:10.1088/0953-8984/21/42/424118

Nanometric ionic-liquid films on silica: a joint experimental and computational study

S Bovio[1,2], A Podestà[1,2], P Milani[1,2], P Ballone[3] and M G Del Pópolo[3]

[1] C.I.Ma.I.Na, Università degli Studi di Milano, via Celoria 16, 20133, Milano, Italy
[2] Dipartimento di Fisica, Università degli Studi di Milano, via Celoria 16, 20133, Milano, Italy
[3] Atomistic Simulation Centre, Queen's University, Belfast, BT7 1NN Belfast, UK

E-mail: m.del-popolo@qub.ac.uk

Received 24 April 2009, in final form 27 June 2009
Published 29 September 2009
Online at stacks.iop.org/JPhysCM/21/424118

Abstract

Atomic force microscopy images for [bmim][Tf_2N] films deposited at ambient conditions by drop-casting show a population of terraced islands of mesoscopic area (1–100 μ^2) and ∼50 nm height. The regularity of terraces and steps, stiff mechanical properties and a fragile fracture mode all suggest that the islands are solid-like, even though bulk [bmim][Tf_2N] is liquid at the temperature of the experiment. Molecular dynamics simulations for a homogeneous [bmim][Tf_2N] film 4 nm thick on silica also display marked layering in proximity to silica of periodicity closely matching the experimental estimate of the step height. The density modulation of the simulated sample, however, decays into an approximatively homogeneous and fluid-like density distribution ∼2 nm from the solid surface. The detailed comparison of experiments and simulations is contained in the closing section of the paper.

(Some figures in this article are in colour only in the electronic version)

1. Introduction

A wide potential for applications coupled to favourable environmental properties have made room temperature ionic liquids (ILs) one of the most extensively investigated subjects in chemical physics of the last few years [1]. The viability and eventual impact of several among the proposed applications, including electrochemistry and heterogeneous catalysis, strictly depend on the properties of ILs at the interface with solid phases. Interfacial properties play an even larger role in applications such as lubrication [2], in which ILs are confined in a narrow space in between solid surfaces.

Despite these reasons for interest, the exploration of IL–solid interfaces is still in its infancy. To be sure, several experimental and computational studies of surface and interfacial properties of ILs have been published in recent years, and new contributions are appearing at an ever quickening rate [3]. Nevertheless, surfaces and interfaces are more diverse and more challenging than bulk systems, and the pace of progress is, by necessity, correspondingly slower. More importantly, the number of possible combinations arising from all different ILs, solid surfaces, and experimental conditions make the exploration of these systems a virtually open-ended task.

To enlarge our knowledge of interfacial properties of ILs, we undertook an extensive investigation of thin IL films deposited on solid surfaces, using a combination of experimental and computational methods. Preliminary results obtained by atomic force microscopy (AFM) on the morphology of 1-butyl-3-methylimidazolium bis-trifluoromethanesulfonylimide ([bmim][Tf_2N]) films deposited on the surface of silica, mica, and highly oriented pyrolytic graphite (HOPG) have been published recently in [4] and [5]. Here we focus on the case of [bmim][Tf_2N] on silica, and we discuss in detail the comparison of experimental data with the results of computer simulations carried out for the same system at comparable thermodynamic conditions.

In our experiments the solid substrate is represented by either an ordered silica surface, obtained by oxidizing a Si(110) layer, or by the surface of amorphous silica. At

the conditions of our experiments, both surfaces are expected to be largely hydroxylated, with comparable densities of OH groups. The ionic-liquid film is obtained by drop-casting, i.e. by first dissolving [bmim][Tf_2N] in methanol, and then spotting a few microlitres of solution onto the silica surface. Evaporation of the solvent leaves a thin IL deposit on the surface, whose structure, in principle, might depend on the deposition protocol. The chemical composition of the film, however, is free from appreciable contamination from the deposition solvent, as verified by x-ray photoelectron spectroscopy [4]. The resulting interface, analysed by AFM imaging, consists mainly of IL islands randomly distributed on the silica surface. Measurements of the surface topography emphasizes the regularity in the vertical organization of the islands, made of wide terraces and sharp steps, that persists throughout the entire thickness of the overlayer, in some cases exceeding 50 nm. The lateral size of the islands extends up to a few μm. In the case of amorphous silica, more rounded liquid droplets sometimes are seen to coexist with the thin, layered IL islands, uniformly spread on the islands themselves, or on the original silica surface [4, 5].

Simulations are carried out by molecular dynamics based on an atomistic force field model, and concern a fairly idealized interface made of a nanometric [bmim][Tf_2N] film ~4 nm thick, homogeneously spread over a fully hydroxylated β-cristobalite(111) surface.

Comparison of experimental and computational results reveals clear similarities between the two sets of data, as well as important differences. At all temperatures the simulation results display an apparent layering of the IL density in the direction z perpendicular to the surface. At room temperature the wide amplitude modulation of the IL density extends well into the liquid side of the interface, and is apparently reminiscent of the layering seen in the AFM images of thin IL islands. Moreover, the interlayer separation is very similar in the experimental ($\delta = 0.56$ nm) and in the simulated ($\delta = 0.60$ nm) samples.

Layering, however, appears to be far more marked in the experimental than in the simulation samples. The sequence of terraces and steps characterizing the shape of the islands seen in AFM images extends up to nearly 100 layers. Even at $T = 300$ K, four molecular layers at most are clearly defined in the IL density profile computed by simulation, and density appears to be nearly uniform beyond ~2.5 nm from the interface.

Moreover, the strict regularity of the step height, and the remarkable time stability of the structures seen by AFM, extending up to several months, suggest that [bmim][Tf_2N] islands on silica are solid-like, and perhaps crystalline, at ambient conditions. This conclusion is supported by AFM measurements of mechanical properties, showing that the basic framework of IL islands is surprisingly stiff, and even displays a fragile character upon fragmentation. This observation is particularly remarkable, since bulk [bmim][Tf_2N] is fluid at the temperature of the experiment, and even for a molecular system such as [bmim][Tf_2N] the thickness of the layered islands is already well within the mesoscopic range. On the other hand, the simulated IL films appear to be liquid-like down to $T = 350$ K. Their thermodynamic state is less certain at $T = 300$ K, since relaxation mechanisms and dynamics are very slow on the simulation timescale, and the IL film shares properties of liquid and glassy systems. Nevertheless, the simulated system is apparently not solid-like, and much less crystalline.

A second remarkable feature revealed by simulation is represented by an apparent density peak in the uppermost portion of the IL layer. This density anomaly, already seen in previous simulations for the free surface of IL [6], has been confirmed by x-ray reflectivity measurements [7] and by sum frequency vibrational spectroscopy (SFVS) [8] for systems closely related to the one considered in the present simulations. This feature, however, is not apparent on the scale of our AFM measurements for the thin [bmim][Tf_2N] film on silica, showing that the height of all IL planes is virtually the same across the entire width of the layered islands.

The reasons underlying these apparent differences between computations and experiments are discussed in section 4 of our paper. Understanding and possibly extending the validity and reliability limits of the computational model is clearly a very important target for our study, since, once validated, simulations could provide a wealth of microscopic information on the structure and dynamics of the interface. Examples reported in section 3 include the computation of the diffusion coefficient for anion and cation, the determination of the electrostatic properties of the interfacial double layer, and the analysis of correlation functions and orientational ordering for all species of interest.

The results of our investigations largely agree with those of previous studies whenever a comparison is possible. Layering and solid-like ordering in [$C_n$mim][X] ([X]$^-$ = [PF_6]$^-$, [BF_4]$^-$, [$PdCl_4$]$^-$) thin films on Si(111) covered with native oxide have been inferred from x-ray reflectivity measurements reported in [9]. In recent years, SFVS has been the method of choice to characterize the interface between ILs and solid phases. SFVS measurements on [bmim][Tf_2N] on silica and on closely related systems have been reported in the literature (see, for instance [10, 11]), documenting, in most cases, an apparent layered structure at the interface. Layering of the IL density has also been observed in [bmpy][FAP] on sapphire(0001) [12]. The fit of the experimental data with relatively simple models, however, suggests that in these cases the density modulation induced by the interface does not extend more than a few layers away from the solid surface. The difference from the experimental results reported here and from those of [9] might be due to the macroscopic width of the IL side of the interface, in contrast with the thin film configuration considered here and in [9].

Computer simulations for [bmim][Tf_2N] on ordered quartz surfaces have been reported recently in [13]. The simulation conditions and the results are closely related to our own computations. The simulations of [13], however, are meant to model an extended IL phase in contact with the solid surface. The thin IL slab, therefore, is enclosed in between two equivalent and parallel hydroxylated quartz surfaces, while in our computation we consider a thin film, deposited on silica and exposing a free surface towards vacuum. The

influence of the thin film geometry on the IL properties is in fact an important issue for our study. Moreover, the simulations of [13] are limited to fairly high temperature ($T \geqslant 400$ K). The results of our study, however, show that the most dramatic manifestations of layering take place at around room temperature.

Large amplitude layering of the IL density was also predicted on the basis of molecular dynamics simulations for [bmim][NO_3] on rutile (110) [14], and for [bmim][PF_6] on graphite [15]. The [bmim][NO_3] on rutile computations have close similarities with the simulations reported in the present paper. The computations of [15], although very interesting, rely on a model whose validity is somewhat more uncertain than in the oxide case, because of the semi-metal character of graphite, introducing, among other things, image charge interactions at the interface.

2. The experimental picture

2.1. Materials and methods

Two samples of the ionic liquid [bmim][Tf_2N] from Sigma Aldrich and from Queens University Ionic Liquids Laboratories (QUILL) were used, both with purity grade greater than 98.0%. Methanol, from Fluka, with 99.8% (HPLC) purity grade, was further distilled twice and used for preparation of solutions with the ionic liquid. Standard 13 mm diameter discs of amorphous silica (glass cover-slips) from Assing and squared, single-side polished specimens of Si(110) were used. Samples suitable for the investigation by AFM of the solid–liquid interface of [bmim][Tf_2N] have been obtained by drop-casting 20 μl of highly diluted solutions of [bmim][Tf_2N] in methanol (concentrations lower than $1 \times 10^{-2}/1 \times 10^{-3}$ mg ml^{-1}) on the substrates, allowing them to dry in ambient conditions. A comparative x-ray photoelectron spectroscopy analysis on a bulk of pure [bmim][Tf_2N] and on drops obtained by casting a concentrated methanol–IL solution confirmed that the solvent used in the deposition process does not react with the ionic liquid. All substrates were freshly prepared immediately before deposition of the [bmim][Tf_2N]–methanol solution. Amorphous silica and Si(110) substrates were cured in aqua regia solution (3 parts HCl–1 part HNO_3) before deposition in order to remove organics and re-hydroxylate their surfaces.

A Bioscope II AFM from Veeco Instruments was used. The AFM was typically operated in tapping mode in ambient conditions with standard single-crystal silicon cantilevers (resonance frequency between 200 and 300 kHz, nominal radius of curvature of the tip 5–10 nm). Typically, image scan size was between 5 μm $\times$ 5 μm and 20 μm $\times$ 20 μm, with scan rates in the range 0.5–1.5 Hz. Stable imaging conditions could be achieved and maintained for hours as if scanning on a solid surface. We did not observe significant changes in the imaging conditions when imaging in a dry nitrogen atmosphere. The AFM was also operated in force-spectroscopy mode, using force modulation tips with typical force constant $k = 4$ N m^{-1} and standard contact-mode tips with force constants in the range 0.06–0.6 N m^{-1}. When force spectroscopy is coupled to contact-mode imaging, several force-versus-distance curves are acquired along a raster pattern spanning a finite area, and built on a previously acquired AFM image. Each force curve is obtained recording the cantilever deflection (which is converted into a force, upon suitable calibration of the lever) as a function of the relative tip–surface distance [4].

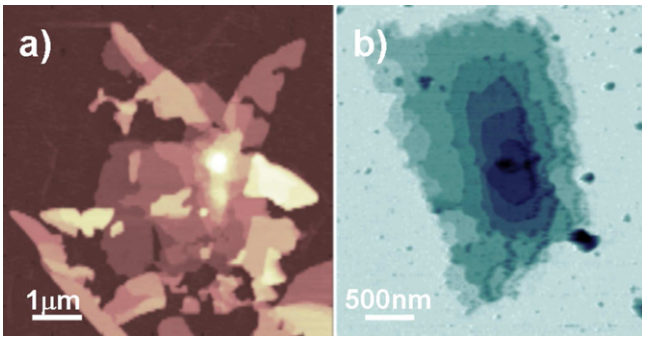

Figure 1. AFM topographic maps of thin [bmim][Tf_2N] films on (a) amorphous silica and (b) polished oxidized Si(110). The first map has been acquired in contact mode and the second one in tapping mode. Vertical colour scales 50 nm.

All depositions and measurements have been carried out in air at ambient conditions, i.e. at a nominal temperature of $T = 298$ K.

2.2. Statistical analysis of the heights of solid-like layers

Wide area scans of the silica surfaces following deposition show a population of randomly distributed and partly overlapping islands of ~1–10 μm lateral size (see figure 1(a)). Detailed topographic measurements on single islands (see figure 1(b)) reveal a layered structure, with wide flat terraces and sharp steps, extending throughout the entire island thickness, sometimes exceeding 50 nm. As discussed in detail below, islands appear solid-like under AFM measurements of their mechanical properties.

In a previous paper [4] we analysed the height of these solid-like layers by means of histograms of the heights calculated from the AFM topographies; this analysis has been performed to understand if the observed structures result from the regular vertical arrangement of a molecular layer with thickness δ. According to the schematic structural model shown in figure 2(a), we made the hypothesis that each terrace consists of several basic layers, and terraces with different heights are stacked one on top of the other. Figure 2(b) shows a typical height histogram of a layered structure. Such histograms consist of a series of peaks, each corresponding to a plateau in the AFM image. The peak-to-peak distances represent the average heights of piled-up terraces. Using an optimization procedure on terrace height data we find the best value of $\delta = 0.56 \pm 0.02$ nm for polished oxidized Si(110) and amorphous silica.

2.3. Test of the solid-like character of [bmim][Tf_2N] films

The force that the AFM probe exerts on the sample surface can be controlled. During imaging, the force is typically

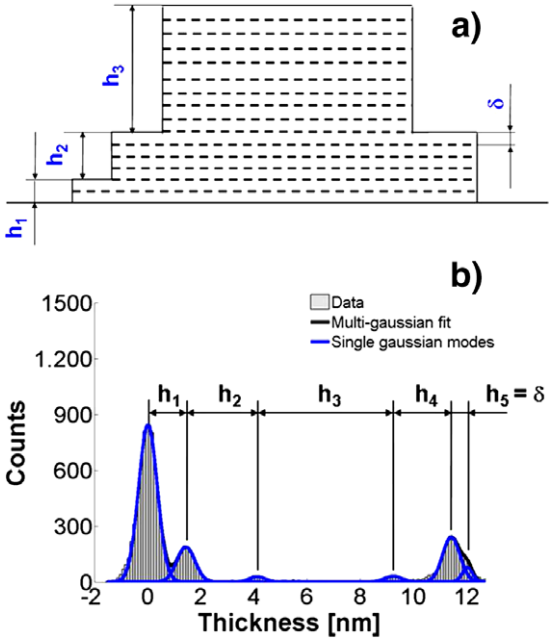

Figure 2. (a) Schematic representation of a layered structure. (b) Typical histogram of the heights of an AFM topography where terraces are present.

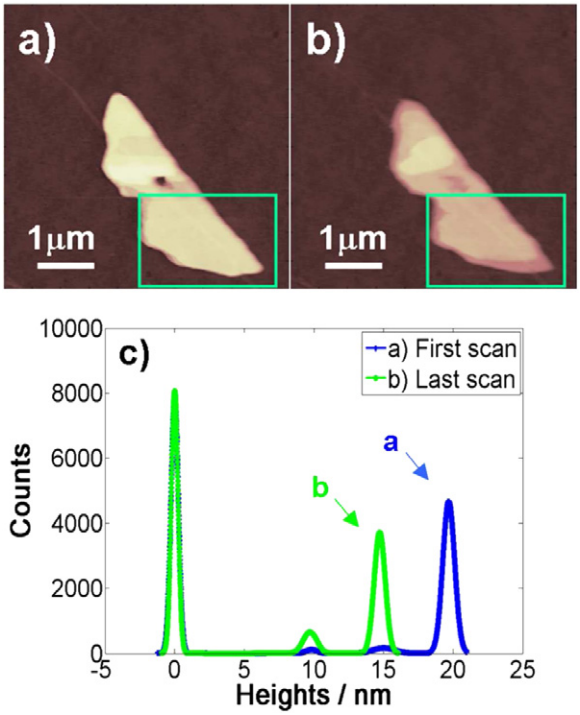

Figure 3. Delamination of [bmim][Tf_2N] layers on amorphous silica after three scans in contact mode. (a), (b) AFM topographies before and after delamination (vertical colour scales: 35 nm); (c) multi-Gaussian-fitted height histograms of the boxed regions in (a) and (b), showing that a top stack of basic layers disappears.

minimized, while in force-spectroscopy experiments it can be made large in order to test the mechanical resistance of the surface. We have collected evidence that the layered structures oppose a strong mechanical resistance to the AFM tip. We typically did not observe any scratch or penetration of the tip into the structures, even after repeated scans, and even when imaging in contact mode (in contact mode normal forces can be 10–100 times larger than in tapping mode, the contact pressure being of the order of 10–100 MPa). This proves that the layered structures are very compact, and in particular possess a strong mechanical resistance against vertical compression. The applied lateral force is expected to play a major role in disrupting the ordered [bmim][Tf_2N] films. Corresponding to the edges, the mechanical strength of the solid-like films is expected to be reduced, and therefore the lateral force exerted by the AFM tip can be enough to break the arrangement of the molecules. Noticeably, the applied lateral force is larger when the tip climbs the (steep) edges of the (higher) terraces, because the feedback loop of the AFM reacts with some delay to the quick changes of the topography. Stronger erosion is observed when imaging in contact mode because lateral forces are greatly increased with respect to tapping mode. Erosion observed in tapping mode is negligible. When imaging in contact mode at higher forces, delamination of a layered structure can also be observed. In figures 3(a) and (b) we show AFM images of the same terrace before and after repeated scans in contact mode at high force. It can be seen by comparing figures 3(a) and (b) that a complete stack of basic layers has been removed from the top of the terrace. Comparison of the height histograms before and after the scan (figure 3(c)) shows that the height of the removed layer is 10 times the height δ of the basic layer. This layer has been delaminated by high lateral forces during the first three scans. In fact, the strong peak at $h \sim 15$ nm grows at the expense of the peak at $h \sim 20$ nm, corresponding to the topmost terrace that has been swept away. AFM images and height analysis suggest that this structure behaves like a lamellar solid, which can be cleaved along preferential directions.

We have qualitatively tested the perpendicular hardness of [bmim][Tf_2N] layered structures by using the AFM in force-spectroscopy mode. We have acquired a topographic map of a terrace on polished oxidized Si(110) (figure 4(a)) and collected several force–distance curves along a grid, on the substrate as well as on the film. Figure 4(b) shows two approaching force curves, acquired on the silica substrate and on the film. The slopes of these curves in the contact region are the same. This suggests that the film behaves upon loading exactly as the hard silica substrate, which is like an impenetrable, solid surface. If deformation of the [bmim][Tf_2N] film occurred during contact, different slopes would be observed, together with discontinuities and irregularities in the first part of the linear region, witnessing the penetration of the film. We could not exclude however the possibility that a sudden and traceless penetration of [bmim][Tf_2N] film occurs immediately after contact. In this case the silica substrate, and not the film, would be loaded, and the slopes in the two force curves would be the same. We could rule out the occurrence of this event by observing that the two curves are horizontally shifted by an amount Δh corresponding to the thickness of the film (minus a height difference due to the presence of a clockwise tilt of the sample). In the case of penetration, this offset would be exactly equal to the height difference due to the tilt, and this

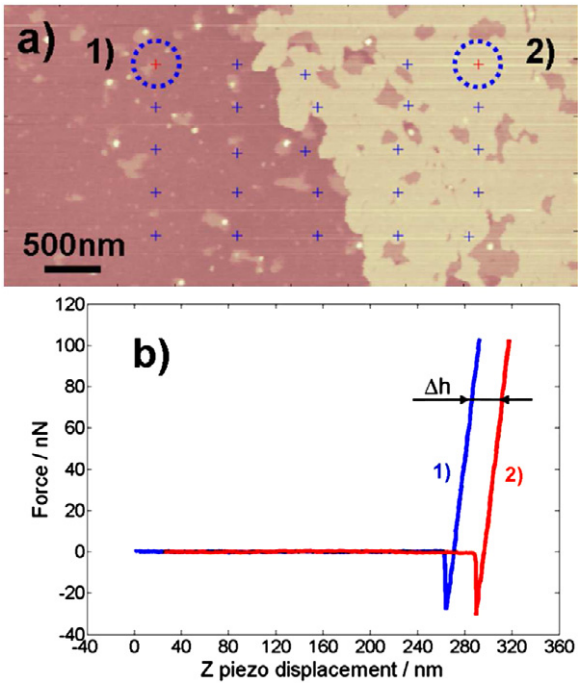

Figure 4. Test of the normal hardness of solid-like [bmim][Tf_2] layers on oxidized Si(110). (a) AFM contact-mode topography. A force–distance curve has been acquired in each point marked by a cross. (Vertical colour scale: 15 nm.) (b) Two representative force curves acquired in the circled locations, on the bare substrate (1), and on top of the IL layer (2).

is not the case. Same slopes and displacements are observed when much higher normal pressures (up to 1 GPa) are applied to the [bmim][Tf_2N] film (data not shown). These topography-related local force measurements provided a direct proof that the [bmim][Tf_2N] layered structures are solid-like.

3. Computer simulations

3.1. Model and simulation parameters

Computer simulations for an idealized but still realistic model of the experimental system have been carried out by molecular dynamics based on an atomistic force field, expressing the potential energy of the system as the sum of intra- and intermolecular terms. Intramolecular contributions account for bond stretching, bending and torsion, while intermolecular terms include dispersion and Coulomb interactions. The parameters proposed in [17] have been used for [bmim][Tf_2N], while the solid side of the interface is modelled using the potential of [18]. Intermolecular cross interactions are accounted for by combining the parameters of the IL and of silica using Berthelot's rule. All simulations are performed using the DL-POLY package [19].

A minimal representation of the solid side of the interface has been adopted for reasons of computational expediency. More precisely, the silica surface is represented by an oxygen and a silicon plane only, whose atoms reproduce the geometry of the Si terminated (111) surface of the β-cristobalite polymorph. Moreover, each Si ion in the terminal plane is decorated with one OH group, leading to an OH surface density of 4.1 OH groups nm^{-2}.[4] The stability of the solid surface is enforced by keeping fixed the positions of all the Si and O atoms in the simulated system, while the H atoms of the hydroxyl groups are mobile. This drastic simplification of the solid surface is justified by the fact that at room temperature the dynamics of the silica atoms is nearly completely frozen out because of strong covalent interactions and of quantum mechanical effects. Test computations for a single ion pair on a hydroxylated SiO_2 slab of increasing thickness have shown that atomic layers below the two top ones do not affect significantly either the adsorption energy and geometry, or the mobility of the ions on the surface. The simulated surface has a cross section of 54.9×52.8 $Å^2$.

The IL film is represented by 250 ion pairs, corresponding, at equilibrium, to a thickness of ∼4 nm. The orthorhombic simulation cell, of sides $54.9 \times 52.8 \times 170$ $Å^3$, is periodically replicated in 3D to mimic an extended system. The periodicity along z, in particular, is such that the IL film is separated by more than 130 Å from the closest repetition of the silica layer, thus ensuring a fair decoupling of replicated interfaces. Not surprisingly, given the relatively low temperature and the low vapour pressure of ILs, we never observe the evaporation of ions or ion pairs into the empty space in between periodic replicas. Coulomb interactions are dealt with using 3D Ewald sums. Constant temperature is enforced using a Nosé–Hoover thermostat.

3.2. Simulation results

A simulation sample consisting of 250 ion pairs in contact with an hydroxylated silica surface has been first prepared at $T = 600$ K, and then progressively annealed down to $T = 300$ K in steps of 50 K. At each temperature the system was equilibrated for 2 ns and we verified that no drift is apparent in running averages of computed properties after the equilibration stage. At $T = 300$ K, however, the system relaxation is very slow, and we cannot exclude the presence of a long term drift, undetectable by our statistical analysis. Production runs lasting 5 ns have been carried out at $T = 300$, 350 and 400 K.

The primary result of the simulation is the determination of the density profile for cations and anions along the direction z perpendicular to the interface. The ionic character of the system suggests to analyse the simulation trajectories representing each molecular ion by a single particle, carrying the full formal charge of the corresponding species. In what follows, the representing particle is located at the centre of the imidazolium ring for cations, while its centre coincides with the position of the N atom of the [Tf_2N] anion. Needless to say, this representation neglects the contribution of the butyl tails to the equilibrium structure of the IL film, that, however, will be discussed in more detail below. The total (anion + cation) density profiles for the representative ionic particles is shown in figure 5 for the three temperatures considered in our simulations.

[4] The experimental estimate of the OH density for fully hydroxylated amorphous silica surfaces is 4.9 ± 0.5 OH nm^{-2}, see [20].

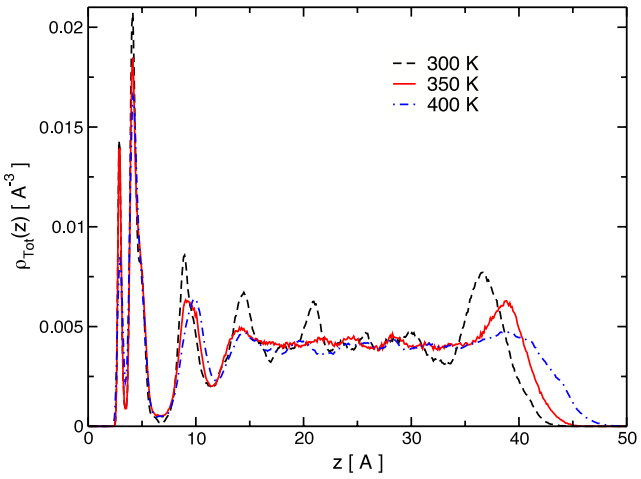

Figure 5. Total density profiles (cation plus anion centres) at 300, 350 and 400 K obtained from MD simulations of a [bmim][Tf_2N] film adsorbed on a hydroxylated SiO_2 surface. The surface area of the substrate is 2898.72 $Å^2$ and the OH concentration is 0.041 $Å^{-2}$.

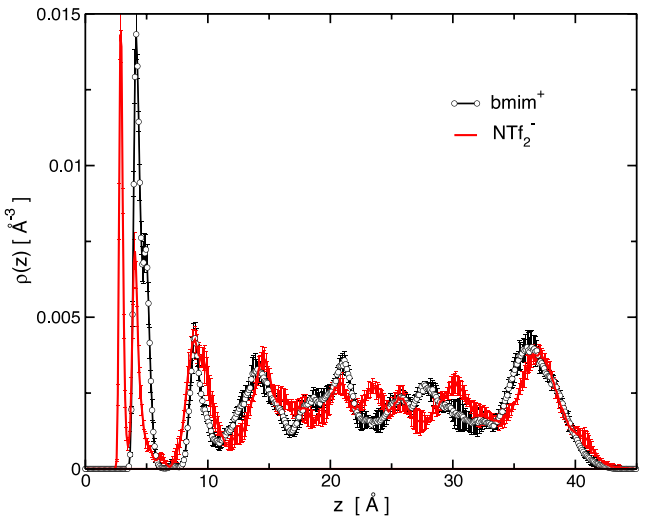

Figure 6. Cation (black with circles) and anion (red) density profiles at 300 K obtained from MD simulations of a [bmim][Tf_2N] film supported on hydroxylated SiO_2. Error bars calculated from five independent 1 ns trajectories.

First of all, the plot of figure 5 shows that the equilibrated IL film is ∼4 nm thick, and displays an apparent and sizeable thermal expansion with increasing T. In comparing our simulation results to the experimental data of section 2, it is important to consider that the simulated IL film is one order of magnitude thinner than the thickness of the solid-like islands imaged by AFM.

At all temperatures 300 K $\leqslant T \leqslant$ 400 K, the total density of ions displays a prominent double peak in close contact with the silica surface, followed by a regular succession of large amplitude density oscillations extending well into the IL film. Excluding the first two peaks, whose sharp profile is directly affected by the interaction with hydroxylated silica, the periodicity of the density oscillations turns out to be $\delta =$ 0.60 nm, independent of temperature to within the estimated error bar.

A second remarkable feature of the density profiles is apparent at the IL/vacuum interface, represented by a broad density maximum, overshooting the average density by more than a factor of two at $T = 300$ K.

As expected, the amplitude of the density oscillations induced by the silica surface increases with decreasing temperature. At $T = 300$ K, in particular, the wide density modulation of the first few IL layers is reminiscent of the apparent layering seen in the experimental images of terraced islands. Even at this temperature, however, oscillations do not extend more than 2.5 nm into the IL side of the simulated sample, whose central portion displays a nearly constant density, as expected in the case of fluid systems.

A slightly different picture, however, is suggested by the analysis of the total density in terms of cation and anion contributions, shown in figure 6 for $T = 300$ K. As apparent from this figure, the narrow region of nearly constant density at the centre of the slab results from the mutual cancellation of out-of-phase oscillations of the anion and cation densities, whose individual profiles display instead relatively sharp features, more characteristic of the glassy state than of a genuinely fluid system. The characterization of the system state as a glass is supported by the analysis of dynamical properties (see below). The distinction between a fluid and a glass, however, relies on the quantitative evaluation of properties such as the viscosity coefficient that are difficult to obtain by simulation, especially for an inhomogeneous system close to its melting point such as [bmim][Tf_2N] at $T = 300$ K. The precise identification of the thermodynamic state of the IL thin film, therefore, is rather uncertain at the lowest simulation temperature.

In parallel with the trend shown by layering at the silica–IL interface, also the height of the density anomaly at the IL–vacuum interface increases rapidly with decreasing T, while its width shrinks slightly. By contrast, the position and the shape of the double peak directly in contact with silica does not change appreciably over the 300 K $\leqslant T \leqslant$ 400 K temperature range.

Analysis of simulation snapshots, and of the density profiles for anions and cations, reveals that the sharp feature closest to silica in the prominent density doublet seen at low z in figure 5 is due to the $[Tf_2N]^-$ anion, whose oxygen atom accepts an H-bond from the OH groups at the silica surface. We estimated that, on average, only 60% of the OH groups available at the surface are engaged in a H-bond with $[Tf_2N]^-$, the saturation of the remaining hydroxyl groups apparently being prevented by steric constraints. The accumulation of surface charge due to the specific OH–anion bonding is compensated by the adsorption of a nearly equivalent number of positively charged imidazolium groups, giving rise to the second sharp peak in the doublet. As a result, and despite the fairly different interaction of anions and cations with the OH groups passivating the solid surface, the first IL layer in contact with silica turns out to be remarkably neutral.

The in-plane structure of the first layer in contact with silica has been visualized by identifying all ions whose distance from the reference surface plane is less than 4 Å.

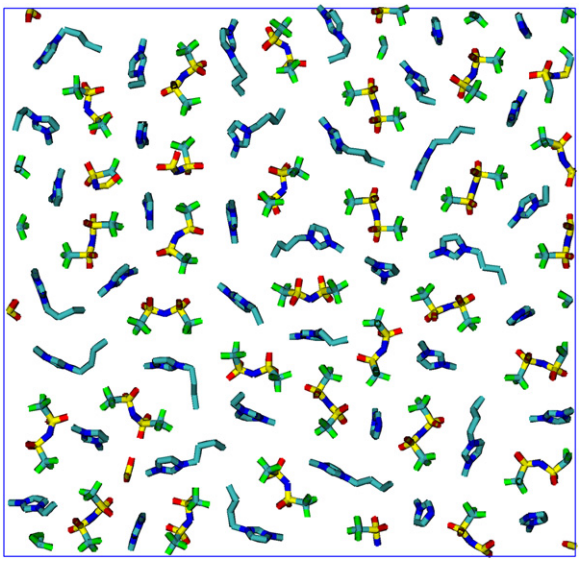

Figure 7. Snapshot of the first IL layer in contact with silica. Only ions separated by less that 4 Å from the silica surface are represented.

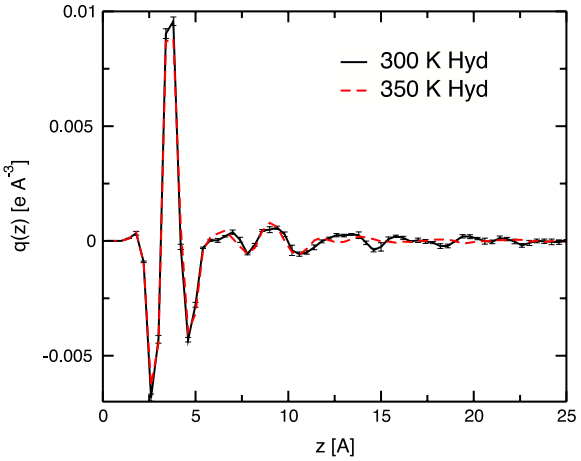

Figure 8. Charge density profiles, $q(z)$, calculated at 300 and 350 K.

Simulation snapshots (see figure 7 for the $T = 300$ K sample) highlight three major features: (i) a clear tendency to charge alternation, driven by strong Coulomb forces, responsible also for the near electrostatic neutrality of the first IL layer; (ii) apparent geometric regularities, hinting at crystal-like ordering for the in-plane distribution of ions, only marginally concealed by a sizeable concentration of defects; (iii) the depletion of the inner layer of cation tails. The distribution of ions on the surface appears to be in registry with the underlying surface lattice, even though the periodicity of the solid and IL layers appears to be different. Therefore, the in-plane regularity of the ion positions is likely to result mainly from specific interactions with the OH groups at the surface, introducing a sizeable corrugation of the xy potential felt by the ions. It is tempting to classify the motifs of positional disorder seen in figure 7 into localized (mainly substitutional) and extended (dislocation) surface defects, but the relatively small size of the 2D sample prevents an unambiguous identification. The study of crystal-like ordering, of defects, and, even more, of long-range interfacial correlations in the IL structure is an important and fascinating subject, whose investigation, however, requires coarse grained models and sophisticated statistical mechanics methods. The imidazolium rings in close proximity of silica tend to be oriented perpendicular to the surface, in qualitative agreement with the structural data extracted in [10] from sum frequency vibrational spectroscopy. Finally, the butyl tail depletion of the inner plane is apparently due to the preferential bonding of OH groups to the anion, and to the competing drive of the cations, due to local charge neutrality considerations. However, entropy might also play a role, since the solid silica surface limits the orientation and isomerization freedom of the hydrocarbon chain, effectively pushing it outwards.

The clear tendency of the IL to form neutral planes, already apparent from the structure of the first IL layer in contact with silica, is a dominant motif also for the few additional layers following the first one. The plot of figure 6 for the individual anion and cation probability distributions shows that, as expected, the two densities tend to vary in phase whenever the amplitude of the oscillation is sizeable, turning to charge alternation far from the surface, where the amplitude of the oscillations is small. The effectiveness of short-range screening at the interface, however, is somewhat remarkable for ions whose structure is so apparently different from each other. The strict enforcement of local neutrality is reflected in the plot of the charge profile (ρ_Q) along z (see figure 8), showing that the charge density is fairly small nearly everywhere. The oscillating character of $\rho_Q(z)$, however, still points to strong electrostatic and steric interactions, in apparent contradiction with the basic assumptions and results of simple theoretical approaches such as Gouy–Chapmann.

The numerical solution of Poisson's equation for $\rho_Q(z)$ shows that the inside of the IL slab tends to be at higher electrostatic potential than either the surface or vacuum. The total electrostatic potential drop across the interface (i.e. from silica to vacuum) turns out to be $\phi = 0.12$ V at $T = 300$ K, $\phi = -0.24$ V at $T = 350$ K and at $T = 400$ K, corresponding to an average dipole $d_z = 0.32$ Debye nm^{-2} at $T = 300$ K, and $d_z = -0.64$ Debye nm^{-2} at $T = 350$ and 400 K. The temperature dependence of ϕ and d_z is easily interpreted in terms of the relative displacement with changing T of the centre of mass R_z^+ and R_z^- of the cation and anion density distributions, respectively. A marked temperature dependence of all these quantities could have been expected, given the sizeable thermal expansion shown by the anion and cation density distributions. Nevertheless, the sudden change of sign in between $T = 300$ and 350 K is an intriguing observation, that might point to an incipient phase transition, either solid–liquid or para- to ferroelectric, taking place at about room temperature. Phenomena of this kind have already been detected in experiments for the surface of organic systems ([21]). In comparing simulation and experimental data, however, it is necessary to consider that in reality silica surfaces tend to be slightly charged [10], while the hydroxylated silica slab included in our simulations is strictly neutral.

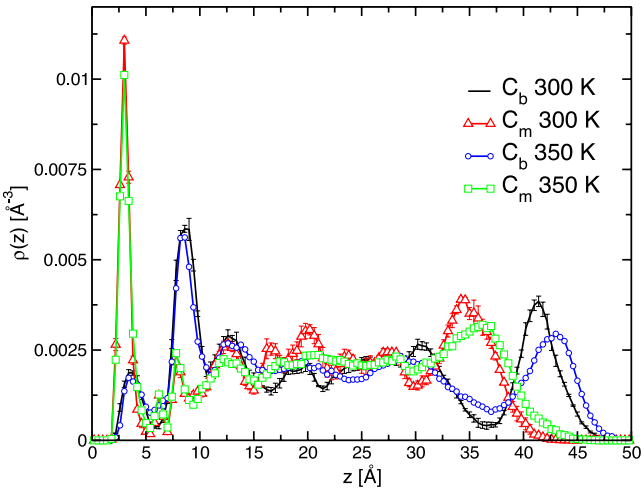

Figure 9. Density distribution of the methyl (C_m) and terminal butyl (C_b) carbon atoms of $[bmim]^+$.

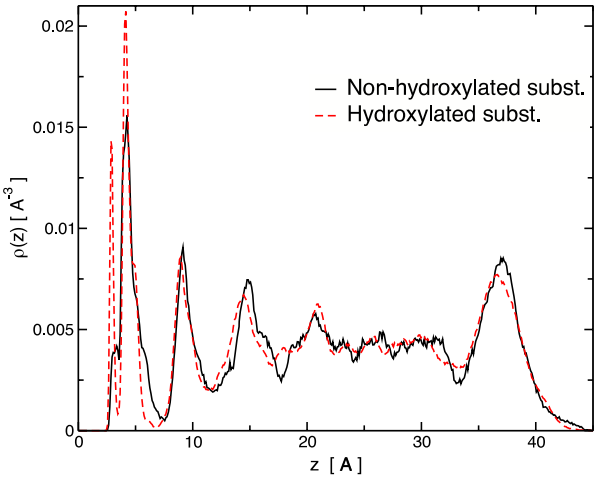

Figure 10. Density profiles for [bmim][Tf_2N] adsorbed on hydroxylated and non-hydroxylated SiO_2.

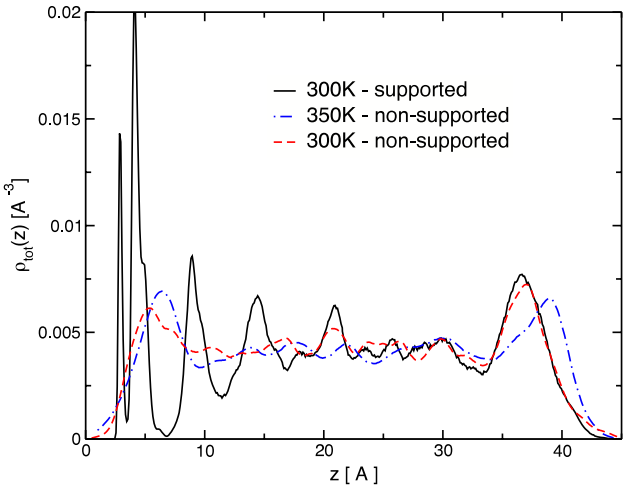

Figure 11. Total ionic densities for supported and non-supported films. Black continuous line: density profile for a [bmim][Tf_2N] film supported on hydroxylated silica at 300 K. Dashed coloured lines: density at 300 and 350 K for a free standing [bmim][Tf_2N] slab.

As already anticipated, the density profile at the IL–vacuum interface represents a second major feature of the simulated sample. As can be seen in figure 6, anions and cations contribute nearly equally to the broad density peak. Analysis of the spatial distribution of the butyl tails of $[bmim]^+$ show that they tend to segregate into a fairly thick external layer, extending up to 5 Å beyond the maximum of the ions density. The segregation of the hydrocarbon tails does not depend significantly on temperature, suggesting that potential energy and entropy both play a relevant role. These two thermodynamic potentials, in fact, might reinforce each other at the IL/vacuum surface. First of all, tails tend to stick out to enhance their rotational freedom, thus increasing their entropy. On the other hand, the depletion of tails in the immediate surface sub-layer allows a tighter packing of ions, giving rise to the density anomaly seen in figures 5 and 6, at the same time decreasing potential energy. The thickening of ILs at their surface predicted by simulations [6] has been confirmed by experiments [7, 8].

A more systematic view of the $[bmim]^+$ orientation relative to the surface is obtained by separately plotting the density distribution of the methyl (C_m) and outermost butyl (C_b) carbon atoms. The results shown in figure 9 for the $T = 300$ K simulated sample confirm the depletion of butyl tails in the first layer in contact with silica, and emphasize their enrichment on the vacuum side of the interface. The clear layering seen in between suggests that, at $T \sim 300$ K, the positional ordering already seen in the density profile is complemented by a sizeable degree of orientational ordering of cations (and presumably anions) throughout the entire interface. Once again, the simulation results agree at least qualitatively with the experimental data reported in [10].

The role of the OH groups in promoting layering at the solid-IL interface has been investigated by simulating the same IL slab in contact with a fully de-hydroxylated, oxygen terminated silica surface, meant to represent a prototypical hydrophobic surface. Starting from the thin silica slab used in the previous simulations, this second model of a neutral solid silica surface was obtained by replacing each terminal OH group with a single oxygen atom, whose charge is equal to the sum of the O and H charges in OH. As expected, the IL density peak closest to silica reduces upon this change, but the effect is quantitatively small (see figure 10), showing that IL layering is primarily due to the excluded volume effect represented by the solid surface [22], while the specific adsorption due to the OH–anion hydrogen bond mainly determine the height and detailed shape of the first peak.

On the other hand, removing completely the solid substrate restores both the symmetry of the slab and the fluid-like state of the IL (see figure 11). This observation is very important, because it confirms that the basic IL model is indeed liquid at $T = 300$ K (the experimental melting point of [bmim][Tf_2N] is $T_m = 267$ K, see [24, 25]) and, therefore, any glassy or even solid-like feature seen in the supported film must arise from the interaction between silica and the IL.

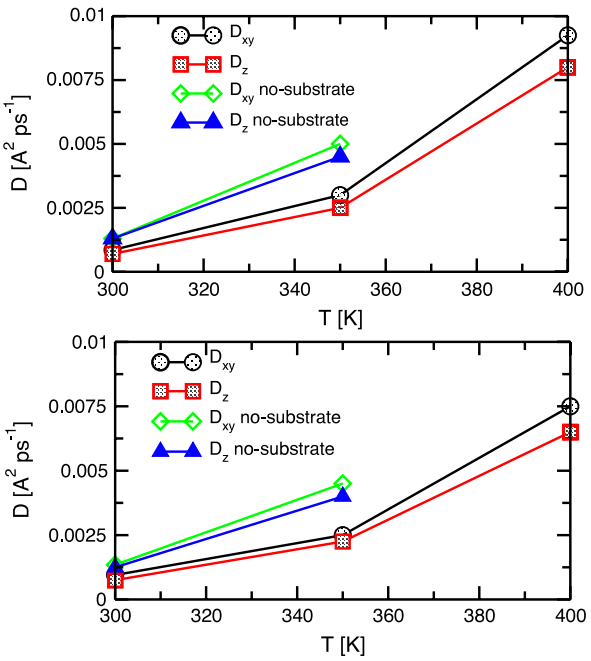

Figure 12. In-plane (D_{xy}) and out-of-plane (D_z) diffusion coefficients of cations (upper panel) and anions (lower panel) as a function of temperature for the solid-supported and the free standing [bmim][Tf_2N] slabs.

The in-plane (D_{xy}) and out-of-plane (D_z) diffusion constants[5] of cations and anions have been estimated from the asymptotic slope of the mean square displacement of ions as a function of time (i.e. using Einstein's relation). The temperature dependence of the anion and cation diffusion constants is displayed in figure 12). Diffusion is non-negligible down to $T = 350$ K, while at $T = 300$ K is at the limit of what we can estimate from simulations on the ∼5 ns timescale. Above $T = 300$ K, the diffusion constant of anions and cations is fairly similar, and, somewhat surprisingly, it is fairly isotropic. Moreover, removing the substrate enhances diffusion, supporting the conclusion that any glassy or solid-like feature shown by the system at $T = 300$ K is due to the interaction with the solid surface.

As a further characterization of the IL dynamics, we estimated the average time τ_R that ions in the inner region of the interface spend on each of the molecular layers identified by the density oscillations, before migrating to another one by thermal diffusion. The residence time of ions in the first layer in contact with silica turns out to be much longer than our simulations, and, therefore, it cannot be determined to any acceptable level of confidence. The residence times in neighbouring layers are also very long, in the several nanosecond range, and therefore they are also rather uncertain. By way of comparison, we computed the residence time τ_R of ions in a $\delta z = 4$ Å range located at the centre of the slab. The results, $\tau_R = 9$ ns at $T = 300$ K and $\tau_R = 3.2$ ns at $T = 350$ K are similar for cations and anions, and give a quantitative measure of the sluggish dynamics of ions at relatively low temperature. To the best of our knowledge, no experimental data have been reported for this quantity, whose measurements might be beyond the reach of present techniques.

[5] The different dimensionality of the motion along z and in the xy plane has been taken into account by selecting the dimensionality d that appears in the Einstein relation for the diffusion constant (see, for instance [23]).

4. Summary and concluding remarks

Experimental results for thin IL films deposited on silica surfaces have been compared to simulation data for an idealized but still realistic atomistic model of the same interface.

AFM, in particular, has been used to image the topography and to estimate mechanical properties of thin [bmim][Tf_2N] films deposited by drop-casting on ordered and amorphous hydroxylated silica surfaces at ambient conditions. The collected images show a population of layered IL islands uniformly distributed on the solid surface. The islands' height reaches up to, and sometimes exceeds, ∼50 nm, while their lateral size extends up to a few μm. On amorphous silica, islands sometimes coexist with nanometric IL droplets, lying on top of the islands themselves, or directly in contact with the original silica surface.

The vertical organization of the islands consists of a regular succession of wide terraces delimited by sharp steps. Statistical analysis of the steps' height shows that layering has an underlying periodicity of $\delta = 0.56$ nm, virtually independent of the island shape and thickness. The geometric structure of the islands turns out to be surprisingly stable for a material whose bulk equilibrium phase is liquid at the temperature of our experiments, and AFM images are fully reproducible over times of several months, even when kept unprotected in contact with atmospheric air. The determination of mechanical properties confirms that the basic framework of islands is solid-like and remarkably rigid, even displaying a fragile fracture pattern.

Of course, the only conceivable reason for solid-like behaviour for the overlayer at a temperature at which ILs are, as their name implies, liquid ($T_m = 267$ K) is the interaction with the underlying solid substrate. Nevertheless, this observation is still particularly remarkable, given the fact that the height of the layered islands seen in our AFM images extends up to nearly 100 molecular layers, i.e. well into the mesoscopic range.

Simulations for a homogeneous [bmim][Tf_2N] film 4 nm wide in contact with a Si terminated, fully hydroxylated (111) β-cristobalite surface provide a microscopic view complementing the topographic images obtained by AFM. Samples have been equilibrated by annealing from high temperature (starting at $T = 600$ K), and production runs 5 ns long have been carried out at $T = 300$, 350 and 400 K. At these three temperatures, we observe large amplitude density oscillations arising from the IL interaction with the silica surface. At $T = 350$ and 400 K layering is confined to the very first molecular planes, while the rest of the film appears to be liquid-like. At $T = 300$ K, however, layering extends much deeper into the IL side of the interface, up to ∼2.5 nm. The identification of the thermodynamic state of the IL film at this temperature ($T = 300$ K) is somewhat uncertain. On the one hand, the IL overlayer is apparently disordered, and

displays some residual mobility of the ions. On the other hand, diffusion and relaxation are very slow on the simulation timescale, and several of the IL properties point to a glassy state. The periodicity ($\delta = 0.60$ nm) of the density oscillations depends only weakly on temperature, and closely matches the interlayer separation measured by experiments.

The role of surface hydroxylation in establishing layering has been investigated by repeating the $T = 300$ K simulation for a fully de-hydroxylated, neutral silica surface, obtained by replacing each of the original OH groups by a single O atom of reduced charge. This change affects the position and shape of the first IL layer in contact with the surface, but the effect is quantitatively small. On the other hand, removing the surface altogether restores the symmetry of the slab, and restores its fluid-like character. These observations are very important, since they confirm that the melting temperature of the IL model (not quantitatively determined in our study) is below $T = 300$ K, and every glassy or solid-like feature in the system structure and dynamics is due to the presence of the solid surface, apparently felt far away from the solid surface. Moreover, excluded volume effects, familiar from computational and simulation studies of simple liquids in contact with solid surfaces [22], are more important than specific adsorption, whose effect is fairly local.

While the similarities between the experimental and simulation results are encouraging, their differences might turn out to be more interesting. First of all, it is apparent that the general properties of layered islands are far more solid-like than in the simulation results. The difference might be due to a limitation of simulation, unable to nucleate a crystal-like phase for the overlayer during the nanosecond scale of our computations. On the other hand, unaccounted for details of experiments might also be responsible for the discrepancy. Drop-casting is a rather complex process, and, in principle, the results might depend on the deposition protocol. More importantly, impurities present on the surface might act like gelation agents able to change the state of the deposited film[6]. The most abundant contaminant present at oxide surfaces exposed to air is likely to be water. In most cases, water is expected to enhance fluidity and diffusion of ILs [27], but, in principle and only in special cases, it might act as a gelating agent by forming an extended network of hydrogen bonds. In this respect, it is important to consider that the IL used in our experiments and simulations is relatively hydrophobic, but it is also known to be weakly hygroscopic when exposed to air [28]. Computer simulations [29] show that, as expected, water in bulk [bmim][Tf_2N] tends to reside in proximity to the hydrophilic side of [Tf_2N]$^-$. In principle, one might speculate that, at precise stoichiometric composition, water and IL give rise to ordered structures whose melting temperature is higher than that of the pure and homogeneous IL. The formation of a solid-like overlayer, in any case, has to be a surface effect, since ordered water–[bmim][Tf_2N] has never been observed in the bulk, even when the IL is equilibrated in a wet atmosphere [28].

On the other hand, x-ray spectroscopy seems to exclude sizeable changes in the chemical composition of the film due to the methanol solvent used in the deposition, or due to decomposition of the IL [16].

In discussing the detailed comparison of experiments and simulations, however, it is essential also to consider that the silica surface described by our simulations is globally neutral, while real silica surfaces are known to acquire a small but non-negligible charge [10].

At present we are unable to unambiguously attribute the apparent difference in the overlayer self-organization to one or the other among the reasons proposed above. Further experimental and computational investigations, already partly under way, are needed to clarify this issue. The results might have a sizeable impact on applications such as lubrication, and perhaps electrochemistry and heterogeneous catalysis. On the other hand, they might point to important limitations of the computational model or of the simulation method, thus offering a useful opportunity to improve them.

Once the validity of the computational picture is clearly assessed, and possibly brought into agreement with the experimental one, simulation can be exploited to provide a wealth of microscopic information, partly inaccessible to experiments.

For instance, the analysis of simulation snapshots shows that the first IL layer in contact with silica, giving rise to a high and sharp density peak, is due primarily to the specific adsorption of the anion, hydrogen bonded to the OH groups at the solid surface. Local charge neutrality is restored by the adsorption of a nearly equivalent number of cations into this first layer, that appears depleted of butyl [bmim]$^+$ tails. The in-plane distribution of ions in this first plane contains remarkable seeds of crystal-like ordering, probably due to the regular corrugation of the underlying solid surface.

Charge neutrality is rather effectively enforced throughout the system, as shown by the detailed analysis of the charge density profile, and of the electrostatic signature of the interface. The positional ordering of ions apparent in the wide amplitude density oscillation at the interface is complemented by considerable orientational ordering, especially for the cations. Coupled to the uneven distribution of charge on the molecular ions, this ordering might give rise to a variety of paraelectric and ferroelectric configurations. Our simulation results might already contain hints of an incipient paraelectric to ferroelectric transition taking place at interfaces before the liquid to solid transition.

An additional interesting effect shown by simulations is the formation of a dense layer at the free IL surface. This is due to the tendency of the butyl tails to orient outwards, enhancing their orientational and rotational isomerization entropy. The depletion of hydrocarbon tails in the immediate sub-layer allows the tight packing of ions, that further decrease potential energy of the free surface.

The results obtained until now suggest several directions for further investigations. First of all, it is important to extend the close comparison of simulation and experiments to other interfaces, including both different ILs and different solid substrates. This might provide a very useful playground to validate, develop and improve computational models. In this respect, we point out that, while models for ILs in contact

[6] The formation of so-called ionogels obtained by mixing ILs with relatively small third species has been reported in [26].

with oxide surfaces might represent a fairly simple extension of present force field models already used for ILs, the modelling of interfaces with metals or semi-metals such as graphite is virtually unexplored or severely untested.

Acknowledgment

This project has been financially supported by Fondazione Cariplo under the grant 'Materiali e tecnologie abilitanti 2007'.

References

[1] Welton T 1999 *Chem. Rev.* **99** 2071
Holbrey J and Seddon K R 1999 *Clean Prod. Process.* **1** 223
[2] Liu X, Zhou F, Liang Y and Liu W 2006 *Wear* **261** 1174
Mu Z, Zhou F, Zhang S, Liang Y and Weimin L 2005 *Tribol. Int.* **38** 725
Liu W, Ye C, Gong Q, Wang H and Wang P 2002 *Tribol. Lett.* **13** 81
[3] See for instance the review in Aliaga C, Santos C S and Baldelli S 2007 *Phys. Chem. Chem. Phys.* **9** 3683
[4] Bovio S, Podestà A, Lenardi C and Milani P 2009 *J. Phys. Chem.* B **113** 6600
[5] Bovio S, Podestà A and Milani P 2009 *Ionic Liquids: From Knowledge to Application* (*ACS Symposium Series*) ed R D Rogers, N V Plechkova and K R Seddon (Washington, DC: American Chemical Society) at press
[6] Lynden-Bell R M and Del Pópolo M G 2006 *Phys. Chem. Chem. Phys.* **8** 949
Yan T, Li S, Jiang W, Gao W, Xiang W and Voth G A 2006 *J. Phys. Chem.* B **110** 1800
Bhargava B L and Balasubramanian S 2006 *J. Am. Chem. Soc.* **128** 10073
[7] Sloutskin E, Ocko B M, Tamam L, Kuzmenko I, Gog T and Deutsch M 2005 *J. Am. Chem. Soc.* **127** 7796
Bowers J and Vergara-Gutierrez B M 2004 *Langmuir* **20** 309
[8] Romero C, Moore H J, Lee T R and Baldelli S 2007 *J. Chem. Phys.* C **111** 240
Rivera-Rubero S and Baldelli S 2006 *J. Phys. Chem.* B **110** 15499
Rivera-Rubero S and Baldelli S 2006 *J. Phys. Chem.* B **110** 4756
[9] Carmichael A J, Hardacre C, Holbrey J D, Nieuwenhuyzen M and Seddon K R 2001 *Mol. Phys.* **99** 795
[10] Rollins J B, Fitchett B D and Conboy J C 2007 *J. Phys. Chem.* B **111** 4990
Fitchett B D and Conboy J C 2004 *J. Phys. Chem.* B **108** 20255
[11] Romero C and Baldelli S 2006 *J. Phys. Chem.* B **110** 6213
[12] Mezger M *et al* 2008 *Science* **322** 424
[13] Seifert N and Wipff G 2008 *J. Chem. Phys.* C **112** 19590
[14] Liu L, Li S, Cao Z, Peng Y, Li G, Yan T and Gao X-P 2007 *J. Phys. Chem.* C **111** 12161
[15] Maolin S *et al* 2008 *J. Chem. Phys.* **128** 134504
[16] Butt H-J, Cappella B and Kappl M 2005 *Surf. Sci. Rep.* **59** 1
[17] Canongia Lopes J N and Pádua A A H 2004 *J. Phys. Chem.* B **108** 16893
[18] Giovambattista N, Rossky P J and Debenedetti P G 2006 *Phys. Rev.* E **73** 041604
Giovambattista N, Debenedetti P G and Rossky P J 2007 *J. Phys. Chem.* B **111** 9581
[19] Smith W, Leslie M and Forester T R 2003 *DL-POLY, Version 2.14* Daresbury Laboratories, Daresbury, Warrington, UK
[20] Zhuravlev L T 1987 *Langmuir* **3** 316
[21] Halka V, Tsekov R and Freyland W 2005 *J. Phys.: Condens. Matter* **17** S3325
[22] Snook I K and Henderson D 1984 *J. Chem. Phys.* **68** 2134
[23] Hansen J P and MacDonald I R 1976 *Theory of Simple Liquids* (London: Academic)
[24] Dzyuba S V and Bartsch R A 2002 *Chem. Phys. Chem.* **3** 161
[25] Arce A, Rodrigues O and Soto A 2004 *J. Chem. Eng. Data* **49** 514
[26] Kimizuka N and Nakashima T 2001 *Langmuir* **17** 6759
Kubo W, Kitamura T, Hanabusa K, Wada Y and Yanagida S 2002 *Chem. Commun.* 374–5
[27] Menjoge A, Dixon J N, Brennecke J F, Maginn E J and Vasenkov S 2009 *J. Phys. Chem.* B **113** 6353
[28] Jacquemin J, Husson P, Padua A A H and Majer V 2006 *Green Chem.* **8** 172
Huddleston J G, Visser A E, Reichert W M, Willauer H D, Broker G A and Rogers R D 2001 *Green Chem.* **3** 156
Seddon K R, Stark A and Torres M-J 2000 *Pure Appl. Chem.* **72** 2275
[29] Sieffert N and Wipff G 2006 *J. Phys. Chem.* B **110** 13076

PCCP

View Online / Journal Homepage
Dynamic Article Links

Cite this: DOI: 10.1039/c2cp23459a

www.rsc.org/pccp

PAPER

Nano-indentation of a room-temperature ionic liquid film on silica: a computational experiment

P. Ballone,*[a] M. G. Del Pópolo,[a] S. Bovio,[bc] A. Podestà,*[bc] P. Milani[bc] and N. Manini[c]

Received 3rd November 2011, Accepted 13th December 2011
DOI: 10.1039/c2cp23459a

We investigate the structure of the [bmim][Tf_2N]/silica interface by simulating the indentation of a thin (4 nm) [bmim][Tf_2N] film by a hard nanometric tip. The ionic liquid/silica interface is represented in atomistic detail, while the tip is modelled by a spherical mesoscopic particle interacting *via* an effective short-range potential. Plots of the normal force (F_z) on the tip as a function of its distance from the silica surface highlight the effect of weak layering in the ionic liquid structure, as well as the progressive loss of fluidity in approaching the silica surface. The simulation results for F_z are in near-quantitative agreement with new AFM data measured on the same [bmim][Tf_2N]/silica interface under comparable thermodynamic conditions.

I. Introduction

Room-temperature ionic liquids (RTILs[1]) represent a vast class of organic ionic systems actively investigated for their potential role as versatile and environmentally friendly solvents.[2] In recent years, several other applications have been proposed, most notably in catalysis,[3] lubrication,[4,5] electrochemistry,[6] and photovoltaic power generation.[7] The successful development of these applications, however, depends on the properties of RTIL interfaces with solid surfaces, which are still poorly understood. To be precise, several experimental and a few computational studies have been carried out to characterise these interfaces, but, because of their complexity and of the huge number of different RTIL and solid surface choices, the combined effort of several experimental and computational groups has until now at most scratched the surface of this gargantuan research field.

Sum frequency generation spectroscopy,[8] X-ray[9] and neutron[10] scattering are among the most relevant experimental techniques that have been used to characterise the structure of RTIL/solid interfaces. Most experiments have been carried out for RTILs in contact with silica, mica and graphite, mainly because of the relatively inert character of these solid substrates, but measurements on TiO_2, noble- and near-noble metal surfaces have been carried out as well. Almost without exception, the results for samples close to room temperature reveal strong molecular layering close to the surface.

Mechanical and, in particular, rheological properties have been investigated using the surface force apparatus (SFA), probing the RTIL/mica interface[11–13] down to nanometric length scales. The results for very thin RTIL films in between mica layers point, first of all, to a very low shear viscosity of RTILs at the interface, thus emphasising the interest of ionic fluids as lubricants. Moreover, the measurement of the normal force F_z as a function of the distance z separating the two approaching surfaces in the SFA displays apparent oscillations, consistently with the RTIL layering seen in structural experiments. The periodicity, amplitude and phase of the oscillations strictly depend on the RTIL under investigation, reflecting the competing role of Coulomb forces and excluded volume effects.[11,12]

Atomic force microscopy (AFM) could represent a decisive tool to characterise RTIL/solid interfaces, able, in principle, to provide a direct view of the structure, and to map local mechanical properties at the nm scale. Early AFM measurements[5,14] for RTILs of the imidazolium, pyrrolidinium and pyridinium families deposited as thin films on the oxidised silicon surface revealed a surprising variety of different behaviours, depending on the surface hydroxylation and charge, on the water content, on the electric bias of the tip, and on the velocity of the surface scanning. More importantly, these measurements provided evidence of solid-like behaviour for RTILs in confined geometries, even under conditions such that the bulk equilibrium phase is the liquid. This observation, in turn, might explain the remarkable stability of ionogels made of inorganic nanoparticles solvated into RTILs, that could find applications in electrochemical and photovoltaic devices.[15]

Recently, the debate on structural, dynamical and mechanical properties of RTIL/solid interfaces has been revived by new AFM measurements carried out by two groups, investigating different

[a] *Atomistic Simulation Centre, Queen's University Belfast, Belfast BT7 1NN, UK. E-mail: p.ballone@qub.ac.uk*
[b] *C.I.Ma.I.Na, Università degli Studi di Milano, via Celoria 16, 20133, Milano, Italy*
[c] *Dipartimento di Fisica, Università degli Studi di Milano, via Celoria 16, 20133, Milano, Italy. E-mail: alessandro.podesta@mi.infn.it*

but related systems. In the first case,[16] the interface separating a solid support from a thick, bulk-like RTIL slab has been considered, while in the second case[17,18] thin sub-micron RTIL films on the same or similar solid surfaces have been prepared and characterised.

In ref. 16, the solvation force (F_z) on a 20 nm AFM tip immersed in a thick, bulk-like RTIL has been measured as a function of distance from a solid surface for a variety of ammonium- and imidazolium-based RTILs supported on mica, silica, graphite and gold. Room temperature data for mica display a sequence of regular jumps, each corresponding to the puncturing of a discrete layer, whose separation is comparable to the diameter of the molecular ions. The sharp discontinuities in the force at regularly spaced distances from the surface do not conform to the idea of a fluid film, suggesting instead solid-like ordering of the RTIL in proximity of the solid support. As expected, the precise details of the force *versus* distance relation depend somewhat on the RTIL. More important is the dependence on the substrate, the strong layering apparent in the case of mica being progressively attenuated in going to silica, graphite and gold. On all substrates, only a few layers (five or six at most) can be identified by steps in the force. This picture is consistent with the X-ray data shown in ref. 9*b*.

Topographic AFM images of [bmim][Tf_2N] nanometric droplets on mica, silica and graphite have been reported in ref. 17. Measurements have been carried out in tapping mode, reaching a contact pressure under the tip ($\sim$0.2 kbar) presumably lower than that of the force–distance measurements reported in ref. 16. In the case of mica and silica, the AFM images reveal layered structures, consisting of the stacking of up to 100 RTIL planes, raising more than 50 nm above the substrate terraces. The measured local mechanical properties and the long persistence time of the observed structures are fully consistent with the properties of solid-like RTIL islands. Even though solid-like layering of liquids wetting solid surfaces has been seen at several other interfaces, the wide extension (up to 100 planes) of the solid-like structures is indeed unusual, taking into account that in the bulk the deposited compound is liquid at the ambient temperature and pressure of experiment. The solid-like character, therefore, has to result from the in-plane perturbation due to the substrate, which, however, is localised 50 nm below the topmost solid-like RTIL layers. Also in these measurements, layering is greatly attenuated in the case of graphite and gold. The results reported in ref. 17 are qualitatively consistent with those reported in ref. 19.

Similarities in the results reported in ref. 16 and 17 are apparent in the strong layering observed in both experiments for mica, and in the common trends seen when going from mica to silica, graphite and gold. Differences are present as well, since the layering reported in ref. 17 extends far beyond the few molecular planes observed in ref. 16.

Strict comparison of the results reported in ref. 16 and 17, however, is prevented by the difference in the RTIL under consideration, and by the different system configuration (*i.e.*, a thick, bulk-like film in ref. 16, a distribution of nanometric droplets in ref. 17) adopted in the two experiments. More importantly, the two sets of experiments do not measure the same quantities, since ref. 16 reports primarily the normal force F_z on the AFM tip immersed in the RTIL, and approaching the solid substrate, while ref. 17 focuses on the topography of thin RTIL films. Moreover, the pressure under the AFM tip is expected to reach a significantly higher value in the force–distance measurements reported in ref. 16 than in the topographic imaging in ref. 17.

New AFM experiments,[18] briefly discussed in Section IV, clarify the connection between the data reported in ref. 16 and 17, and show that the mechanical response of thin films is significantly different from that of contact layers in thick, bulk like RTIL slabs. This result, together with the computational study detailed in the next two sections, provides support and insight on the unusual stability of solid-like [bmim][Tf_2N] islands on insulating, solid oxide surfaces.

II. Model and simulation method

To investigate local mechanical properties of thin RTIL films deposited on solid surfaces, we resort to computational approaches, simulating the indentation process of a nanometric film by a hard AFM tip, represented as a rigid sphere of nanometric diameter.

In the present study we focus on the [bmim][Tf_2N]/silica interface, *i.e.*, one of the systems considered in ref. 17. The same interface has been investigated by atomistic simulations,[20,21] modelling either a bulk liquid/solid termination, or a thin [bmim][Tf_2N] film deposited on silica, exposing a free surface to vacuum. This last configuration, in particular, was considered in a series of computations carried out in our group,[21] simulating a $\sim$4 nm film on silica at temperatures $300 \leq T \leq 400$ K.

A plot of the [bmim][Tf_2N] density profile in the direction perpendicular to the surface is shown in Fig. 1. Layering is apparent at the interface, but its amplitude decreases quickly on moving away from silica. Another remarkable feature is the density peak at the [bmim][Tf_2N] free surface, due to the pile-up of cations lowering the surface energy and increasing entropy by exposing their alkane tails towards the vacuum side of the interface.

Analysis of the ion mobility[21] shows that diffusion is slow at all temperatures, and practically vanishes on the simulation

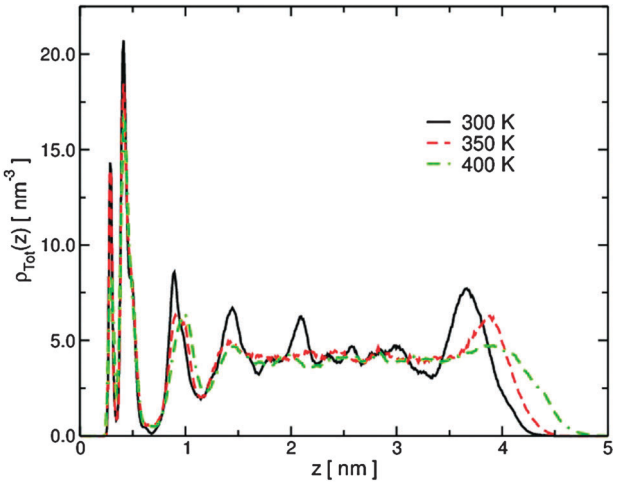

Fig. 1 Ion density profile as a function of distance from the silica surface. Ions are represented as point particles, located at their centre of charge (see ref. 21).

time scale (~10 ns) in the first [bmim][Tf_2N] ionic layers. Ion diffusion is negligible across the entire film at $T = 300$ K, a temperature at which at least four [bmim][Tf_2N] layers are clearly identified at the interface. At this temperature, the decay of the density oscillations away from silica appears to be due more to the defective stacking of solid-like planes than to a genuine fluid-like dynamics of the ions. In other terms, at least up to the film thickness (~4 nm) and time scale (~10 ns) covered by our simulations, the properties of the [bmim][Tf_2N] film appear to be more glassy than liquid-like.

Despite the detailed description provided by the atomistic simulations reported in ref. 21, it is difficult to infer from these results whether the film will appear solid-like or fluid-like under probing by an AFM tip. To fill this gap, we carried out a molecular dynamics (MD) simulation of a nanometric tip penetrating into a thin [bmim][Tf_2N] film on silica. We adopted simulation protocols similar to those used by other authors[22] for simpler solid/liquid interfaces.

The atomistic model of the RTIL film deposited on silica is described in detail in ref. 21 and 23. The validity, reliability and accuracy of the interatomic potentials for [bmim][Tf_2N], that represents the main portion of our system, are extensively discussed in ref. 23.

Experimental tips typically are made of a ceramic material (Si_3N_4 in the experiments reported in ref. 17), with a radius of ~20–50 nm, corresponding to a few million atoms. In general, the tip carries a charge, that could be controlled by a suitable external bias. In our computations we consider smaller, neutral tips. The simulated tip size, in particular, will range from 1.6 nm to 2.0 nm, corresponding to ~1000–3000 atoms. Within this range, the atomistic structure of the tip could affect the results for the normal force felt by the tip in proximity of the surface. However, we aim at comparing our data to experimental results obtained for much larger tips (~20 nm), whose atomistic structure is likely to have only a minor effect. For this reason, we adopt a very idealised model of the tip, while we briefly discuss the possible role of its electrostatic charge in Section IV.

In what follows, the tip is represented by a spherical particle of infinite mass (nano-sphere, NS) interacting with all real atoms *via* a short-range potential. The radial dependence is given by:

$$V(r) = \frac{4\varepsilon}{\alpha^2}\left\{\frac{1}{\left[\left(\frac{r}{\sigma}\right)^2-1\right]^6} - \alpha\frac{1}{\left[\left(\frac{r}{\sigma}\right)^2-1\right]^3}\right\} \quad r>\sigma \qquad (1)$$

This functional form of $V(r)$ has been proposed in ref. 24 to model colloids and nanoparticles. The parameters chosen for our simulation (σ = 1.6–2 nm, ε = 0.7 kJ mol^{-1}, α = 10) are such that to describe a nanometric excluded volume, with a thin (sub-nanometric) attractive well outside the sphere. It is apparent from eqn (1) that no atom can enter the sphere of radius σ centred on the NP. Since atoms are ~1000 times smaller (in volume) than the smallest NP we considered, it is easy to verify that the length σ represents in this case the *radius* of the NP. This is at variance from the case of equi-sizes LJ particles, for which the corresponding σ_{LJ} parameter represents the particle's diameter. This consideration will be relevant when estimating the pressure under the tip during the indentation process.

III. Simulation results

MD simulations have been carried out using a version of the DL_POLY package[25] slightly modified to account for the potential of eqn (1).

The simulations reported in ref. 21 provided well equilibrated starting configurations for the present study. The simulated surface, lying parallel to the xy plane, is nearly square, with a cross section of $L_x \times L_y = 5.5 \times 5.3$ nm^2. The solid side of the interface is represented by one oxygen plane and one silicon plane, whose atoms reproduce the geometry of the Si-terminated (111) surface of β-cristobalite. Each silicon atom carries an OH group, corresponding to a coverage of 4.1 OH per nm^2. All Si and O atoms in the system are kept fixed, while the H atoms of the hydroxyl terminations are mobile. The RTIL film is represented by 250 [bmim]$^+$, [Tf_2N]$^-$ ion pairs, corresponding to a thickness of 4.5 nm at $T = 300$ K. The basic simulation box is replicated in 3D with periodicity $L_x \times L_y \times L_z = 5.5 \times 5.3 \times 17$ nm^3, sufficient to accommodate a mesoscopic spherical tip interacting with the free surface of the RTIL, and still well separated from the periodic image of the silica surface. In what follows, the position of the meso-particle is identified by the z coordinate (Z) of its centre with respect to the topmost Si plane in the SiO_2 slab. The in-plane periodicity of the (111) cristobalite surface is much shorter than the NS diameter, and therefore the precise location of the contact point in the xy plane is relatively unimportant. Long-range Coulomb interactions are accounted for using 3D Ewald summation, with a relative convergence parameter of 10^{-5}. The NVT conditions of our simulations are enforced by a Nosé–Hoover thermostat.[25] The equations of motion are integrated using the velocity Verlet algorithm with a time step of 1 fs.

A schematic view of the system, showing the orientation of the reference axes, is given in Fig. 2. Each simulation of an indentation event starts with the NS far above the free RTIL surface. The NS–surface distance is reduced, until when a

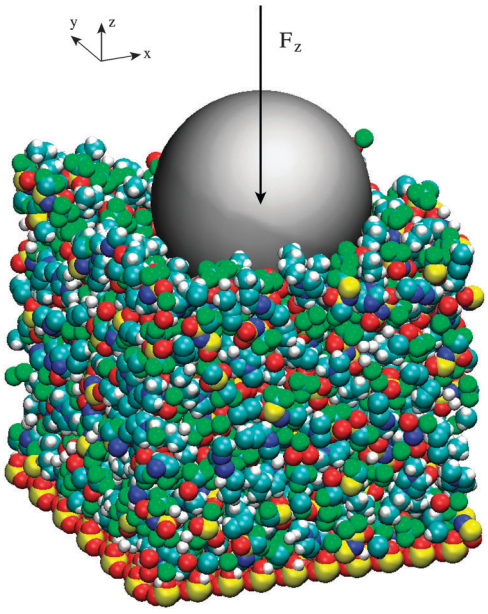

Fig. 2 Schematic view of the simulated system, showing the orientation of the reference axes.

sizable interaction is felt at the probing tip. At first the interaction is attractive, pulling the tip towards the liquid. The force becomes repulsive at $Z \approx 6$ nm, roughly equal to the film thickness plus the NS radius, marking the beginning of the *contact* range for our simulated AFM measurement. From this point of first contact, the tip is lowered towards silica through the RTIL in discontinuous steps of regular amplitude. At each distance, the system configuration is relaxed and then statistics is accumulated keeping fixed the relative position of the tip with respect to the silica plane. The primary result of our simulations is the average force F_z on the meso-particle along the direction z perpendicular to the silica surface.

Simulations have been carried out at two temperatures, *i.e.*, $T = 300$ K and $T = 350$ K. Four trajectories have been generated at $T = 300$ K simulating the indentation by a particle of $\sigma = 1.6$ nm. The relative size of the $\sigma = 1.6$ nm NS and of the surface area can be appreciated in Fig. 2 and 3. Independent starting configurations for the four distinct simulations were obtained by equilibrating at $T = 300$ K four configurations selected at 1 ns time separation along an equilibrium run at $T = 350$ K, temperature at which we do observe diffusion of the RTIL ions.

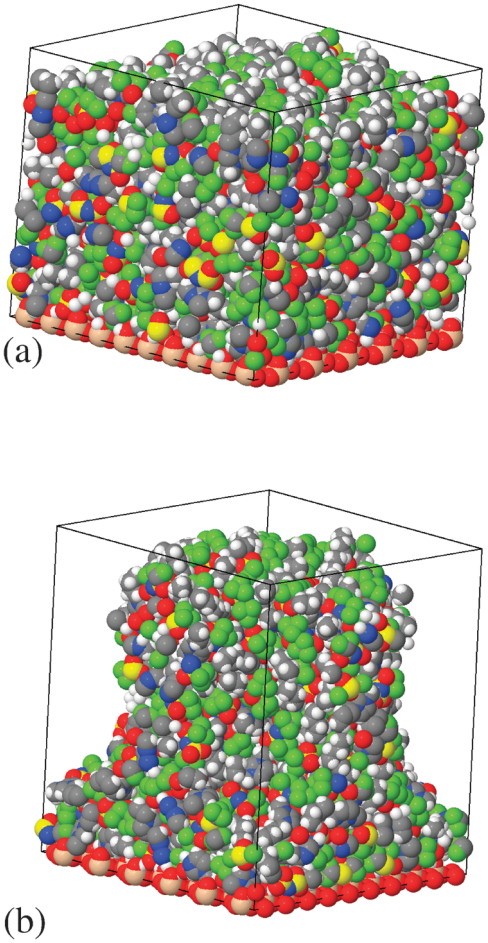

Fig. 3 Two simulation snapshots, (a) before and (b) during the indentation process. The origin of the simulation box has been displaced by (L_x/2; L_y/2,0) with respect to Fig. 2 to show the hole produced by the incoming nanoparticle. Periodic boundary conditions are applied.

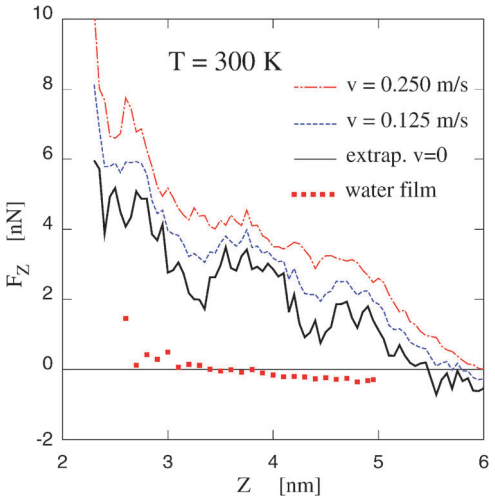

Fig. 4 Average force on the incoming sphere as a function of distance from the silica surface. Dot-dashed line: approach velocity $v = 0.25$ m s^{-1}; dashed line: approach velocity 0.125 m s^{-1}; full line: extrapolation to $v = 0$ (see text). Filled squares: force required to indent a water film of comparable thickness; single trajectory, $v = 0.25$ m s^{-1}, $T = 300$ K.

For each trajectory, the $2.1 \leq Z \leq 6.0$ nm range has been covered in steps 0.05 nm wide, relaxing the system at each distance during 0.1 ns, and collecting statistics during another 0.1 ns simulation. Each simulation of the film indentation covers 16 ns, and requires $\sim$10 days running in parallel on 8 octuple-core Xeon E5530 2.4 GHz nodes. The average force F_z as a function of distance Z estimated during the simulation at $T = 300$ K, $\sigma = 1.6$ nm, is shown in Fig. 4. The data refer to the average over time and over the four simulated trajectories. The average force is repulsive for $Z \leq 5.9$ nm, and its modulus tends to increase with decreasing separation, reaching a region of very high stiffness for $Z \leq 2.2$ nm. Even at the lowest separation and highest force, there remains one residual layer in between the tip and the surface.

The F_z dependence on Z is not monotonic, but displays both localised irregularities and longer-wavelength small-amplitude oscillations. As discussed below, the longer wavelength oscillations reflect the defective but still apparent layering at the interface, while the irregularities are due to activated molecular displacements representing rare events on the rather short time scale of our simulations. In principle, the role of these last events could be reduced at will by increasing the number of trajectories over which F_z is averaged, or by increasing the time scale of the simulation.

To provide a comparison, we simulate the penetration of a 2 nm water film on silica, using the same NS and the same time progression. The results, represented by squares in Fig. 4, show that the response of [bmim][Tf_2N] is, as expected, qualitatively different from that of water over most of the film thickness. Only at the shortest separations do the computed forces become comparable in both cases determined by the NS contact with a residual molecular layer pinned at the silica surface.

The average approach velocity in our simulations is $v = 0.25$ m s^{-1}, that, although modest on a macroscopic scale, it is still orders of magnitude faster than that in AFM experiments, whether in tapping mode, and, even more, in force–distance mode. More importantly, the simulation time is still relatively

short compared to the long relaxation times estimated in ref. 21 for [bmim][Tf_2N] at room temperature. The $F_z(Z)$ force measured in our simulation, in particular, is expected to contain a friction contribution $F_z^f(Z)$, proportional to the approach velocity v, plus an equilibrium contribution, accounting for the Z-dependence of the system free energy. To compare our data with experiments, therefore, it is important to estimate and subtract the friction contribution $F_z^f(Z)$ to $F_z(Z)$. To this aim, we repeated the simulation at half the approaching speed, increasing from 0.1 + 0.1 ns to 0.2 + 0.2 ns the equilibration and averaging time spent at each distance. The total simulation time is now 32 ns per trajectory, and, because of the fairly high number of atoms, and of the long-range interactions, it represents a sizable computation. The new $F_z(Z)$, resulting from averaging over two independent trajectories, is shown in Fig. 4. Since the friction contribution is proportional to v, the difference between the two curves at v and at $v/2$ represents 50% of $F_z^f(Z)$ measured at v, or 100% of $F_z^f(Z)$ measured at $v/2$. These simple considerations allow us to extrapolate our data to zero velocity, see the full line in Fig. 4. The relatively short time scale of our simulations does not allow us to exclude that highly activated events corresponding to the migration of ions from underneath the tip, rarely seen in our simulations, and thus not fully accounted for in our extrapolation, could reduce the average force below the limit estimated by the relaxation on a short time scale. However, simulations at intermediate values of Z extended for a few ns beyond the standard relaxation time provided an estimate of the long-time value of F_z consistent with the extrapolation, enhancing our confidence in the results.

The in-plane forces (F_x, F_y) acting on the tip average to zero because of symmetry. The average of their fluctuating modulus increases monotonically from $6 \geq Z \geq 4$ nm, reflecting the increasing contact area between the incoming sphere and [bmim][Tf_2N]. The contact area stops increasing for $Z \lesssim 4$ nm, and also the average modulus of F_x, F_y remains nearly constant. A similar behaviour is displayed by the fluctuations of F_z around its average value. More interesting is the evolution of the instantaneous value of F_z following a discontinuous decrease of Z by 0.05 nm, showing the superposition of rapid thermal fluctuations with a slow downward drift. A few discrete processes followed by exponential relaxation are also seen from time to time, as exemplified in Fig. 5. Analysis of simulation snapshots shows that these jumps in the force are due to the large-amplitude motion of single ions, being displaced by the increased pressure under the tip. These displacements represent rare activated events, and their random occurrence is likely to be the main cause of the short-length noise seen in the Z dependence of F_z.

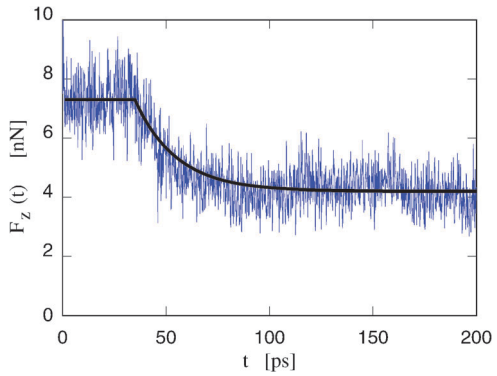

Fig. 5 Time dependence of the force on the tip following the discontinuous displacement at $t = 0$ of the incoming NS from $Z = 2.7$ nm to $Z = 2.65$ nm. The thick line is a guide to the eye.

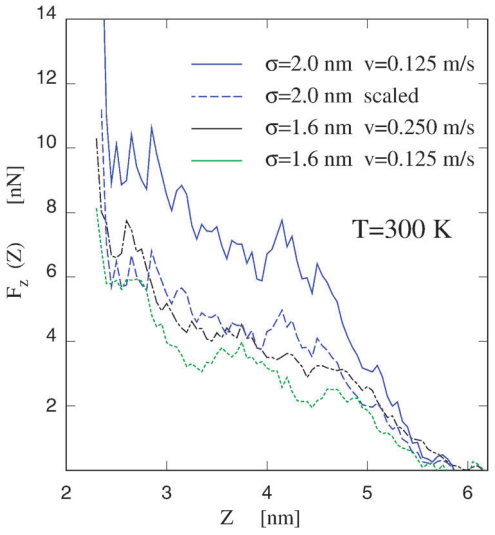

Fig. 6 Verification of the F_z scaling with the tip radius σ. Full line, blue: average force on the $\sigma = 2.0$ nm tip, shifted by $\Delta Z = -0.4$ nm. Single trajectory at $v = 0.125$ m s^{-1}, $T = 300$ K. Dashed line, blue: average force on the $\sigma = 2.0$ nm tip, shifted by $\Delta Z = -0.4$ nm and multiplied by the ratio $(1.6/2.0)^2$ to highlight the scaling of F_z with the contact area. Green dotted line: average force on the $\sigma = 1.6$ nm tip, single trajectory at $v = 0.125$ m s^{-1}, $T = 300$ K. Black dash-dotted line: average force on the $\sigma = 1.6$ nm tip, averaged over four trajectories at $v = 0.25$ m s^{-1}, $T = 300$ K.

The scaling of the force F_z with the tip radius σ is expected to be $F_z \propto \sigma^2$. To verify this relation, we carried out simulations with a penetrating sphere of $\sigma = 2$ nm. To account for the longer time needed to relax a larger perturbed volume, the indentation has been carried out at the slowest speed 0.125 m s^{-1}, and, because of cost considerations, only one trajectory has been generated in this case. As expected, the force on the tip is systematically higher than in the simulations with $\sigma = 1.6$ nm, as can be verified in Fig. 6, where the results for $\sigma = 2$ nm are compared to those for $\sigma = 1.6$ nm at $v = 0.125$ m s^{-1} and at $v = 0.250$ m s^{-1}. Multiplication of the $\sigma = 2$ nm results by $(1.6/2.0)^2$ brings them in between the two curves obtained with the $\sigma = 1.6$ nm tip, thus confirming the expected size scaling. On average, the rescaled data for $\sigma = 2$ nm, $v = 0.125$ m s^{-1} are somewhat closer to the $\sigma = 1.6$ nm results obtained at the higher velocity $v = 0.250$ m s^{-1}, probably because of the larger residual effect of relaxation for the $\sigma = 2$ nm probe with respect to the $\sigma = 1.6$ nm case.

The observation that the average force scales with the expected $F_z \propto \sigma^2$ law provides an indirect test of convergence with respect to the lateral periodicity L_x and L_y. Spurious effects due to the finite size of the simulation cell have no reason to follow the same $\propto \sigma^2$ relation. The verification of $F_z \propto \sigma^2$, therefore, indirectly confirms that the finite-size error on F_z is relatively small.

To assess the effect of temperature, we carried out a simulation using a sample equilibrated at $T = 350$ K. No extrapolation of

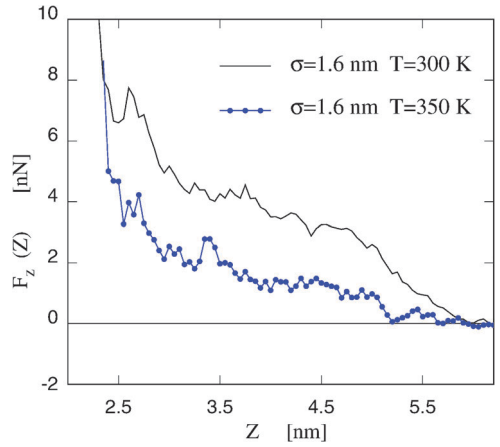

Fig. 7 Full line: average force on the $\sigma = 1.6$ nm tip, averaged over four trajectories at $v = 0.25$ m s^{-1}, $T = 300$ K. Full line with dots (blue): average force on the $\sigma = 1.6$ nm tip, single trajectory at $v = 0.25$ m s^{-1}, $T = 350$ K.

$F_z(Z)$ to $v = 0$ has been done in this case. A comparison with the raw data at $T = 300$ K at the same approach velocity $v = 0.25$ m s^{-1} shows that the film resistance to penetration decreases rapidly with increasing T (see Fig. 7). At $T = 350$ K, however, it is still much higher than the force estimated at $T = 300$ K for the most prototypical liquid of comparable melting point, *i.e.*, water.

As a final point, we verified that at $T = 300$ K (but not at $T = 350$ K) the deformation of the RTIL film due to the indentation is permanent on the simulation time scale, since the hole made by the approaching sphere remains practically unchanged during 4 ns after removing the NS potential, providing further evidence of the glassy state of the thin film. Moreover, at $T = 300$ K, the MD simulation of retracting the sphere, reversing the regular progression described above, invariably gives rise to small and negative forces, pointing to a large hysteresis in F_z. This effect is much attenuated at $T = 350$ K.

IV. Comparison with experimental results

The conditions of our simulations are close to those of the measurements reported in ref. 17 on thin [bmim][Tf_2N] films deposited on the silica surface, while they differ somewhat from those in ref. 16, carried out for different ionic liquids, and for thick, bulk-like RTIL films.

At first sight, despite several qualitative similarities, the simulation results seem to differ from both sets of experimental data. However, as discussed below, new AFM results reconcile the simulation picture with the results reported in ref. 17, and explain the discrepancy with the F_z measurements reported in ref. 16.

We first discuss the comparison with the results reported in ref. 17. First of all, the pressure under the tip required to penetrate the RTIL film is estimated by the simulation at ~5 kbar. This value is likely to be much higher than the maximum pressure applied during tapping mode measurements, estimated at ~0.2 kbar. This implies that the AFM tip operated in tapping mode is unable to penetrate the film, which therefore appears solid-like. On the other hand, the simulation results do not provide any explanation of the regular 0.6 nm periodicity seen in the experiments. In the simulation sample, layering is apparently very defective, possibly as a result of the very long relaxation times of [bmim][Tf_2N] in close contact with the silica surface. Moreover, the 0.6 nm periodicity seen under tapping mode conditions (~0.2 kbar pressure under the tip) might not be present at the pressures required to penetrate the film. Finally, RTILs are known to give rise to mesophases,[11,12,26] and a minimum system size larger than our simulated sample might be needed to reproduce the experiments quantitatively.

Comparison of the simulation results with the data shown in ref. 16 also shows similarities and differences. In particular, the comparison of our Fig. 4 with Fig. 5 of ref. 16*a* shows similar qualitative features in the Z-dependence of computed and measured F_z, both displaying an increasingly repulsive character with decreasing Z, superimposed to localised fluctuations, and to low-amplitude, long wavelength oscillations. Moreover, the intensity of the normal force F_z is comparable in the two sets of data, in both cases raising up to ~16 nN. This good agreement, however, is accidental, since these forces are measured on tips of significantly different radii, *i.e.*, 2 nm for the simulation, and 20 nm for the experiment. The pressure under the tip, therefore, is significantly larger in simulation than in experiment. This can be due, first of all, to the different ionic liquid considered in the simulation and in the experiment. More importantly, however, as already emphasised, the simulation refers to a thin film, while the measurements reported in ref. 16 have been carried out with the AFM tip immersed into a thick bulk-like film.

The crucial role of this last difference is confirmed by the results of a new set of AFM measurements,[18] carried out by the same team of ref. 17. Data for the normal force $F_z(Z)$ measured by AFM on a [bmim][Tf_2N] thin film deposited on silica are shown in Fig. 8. At variance from the conditions reported in ref. 17, the force on the tip is sufficiently large to penetrate the [bmim][Tf_2N] layers. These experimental results, therefore, refer to the same system that has been considered in the simulations, under comparable thermodynamical and probing conditions. Encouragingly, the data shown in ref. 18 are the closest to the computational results.

More in detail, the results for F_z in Fig. 8 show a few broad peaks of width ~2 nm, possibly corresponding to the tip penetration into successive molecular or ionic layers. In the case of a 10 nm [bmim][Tf_2N] overlayer, four successive rupture events can be clearly recognised, and some other sub-structures

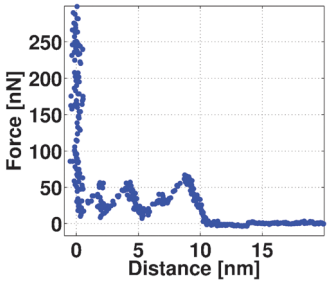

Fig. 8 Normal force F_z on a ~20 nm tip penetrating a 10 nm [bmim][Tf_2N] film deposited on an oxidised silicon surface. AFM force–distance measurements at room pressure and temperature.[18]

could be hidden by noise. The indentation behaviour of [bmim][Tf_2N] islands is very reproducible, and curves acquired on different islands of similar height tend to overlap, including sub-structures. Remarkably, under these experimental conditions no 0.6 nm regularity is apparent, even though the analysis of the topographic data shown in ref. 17 suggests that solid-like islands consist of stacks of layers 0.6 nm thick.

A simple geometric estimate of the contact area shows that the peaks of the $F_z(Z)$ in Fig. 8 correspond to a critical pressure of about 3.5 kbar, fully comparable to the 5 kbar estimated for the simulated system. The residual quantitative discrepancy might be due to differences in the time and size scales probed by experiments and by simulation, far beyond the range that we can approach in our computations.

On the other hand, the electrostatic charge on the surface and on the tip seems to have only a minor effect on the measured normal force, at least at the pressures required to penetrate the nanometric film. This has been indirectly verified by repeating the indentation simulation on the mica/[bmim][Tf_2N], taking into account the surface charge that spontaneously form at the mica surface.[27] The simulation results reveal quantitative changes with respect to the silica case, but no qualitatively new features.

As a further check, experimental measurements of the F_z force have been carried out on a bulk-like slab of [bmim][Tf_2N] on the mica surface.[18] The results, not shown here, do reproduce those reported in ref. 16, and confirm, in particular, that local mechanical properties at the interface are different for thin and thick [bmim][Tf_2N] layers on a solid support.

V. Summary and conclusive remarks

Our results can be summarised as follows. We have simulated the indentation of a [bmim][Tf_2N] thin film deposited on an ordered silica surface by a structureless sphere of nanometric diameter. MD simulations have been carried out at $T = 300$ K and at $T = 350$ K, based on an atomistic empirical potential model. The main result of our computation is the determination of the average force F_z on the tip as a function of distance Z from the planar silica surface. The effect of different (and relatively high) approaching velocities has been estimated, and used to extrapolate the simulation results to conditions close to the experimental ones. Systematic errors in the extrapolation of the simulation data to zero approach velocity cannot be excluded and might be due to non-linear viscoelastic effects. These, however, are unlikely to change qualitatively the results, and a limited series of test supports the reliability of our extrapolation.

The scaling with the tip radius σ has been verified to match the expected $F_z \propto \sigma^2$.

We verified by additional simulations for the unperturbed slab (*i.e.*, no nanosphere) that an extra charge on the silica surface does not affect much the periodicity and amplitude of the RTIL density oscillations (see also ref. 28). However, it might have a larger effect on the regularity and persistence of *charge* oscillations.[21,29] These, in turn, could give rise to regularly oscillating forces on a charged tip, extending up to fairly long distances from the silica surface. While too weak to affect the result of AFM force–distance measurements, reaching pressures of the order of a few kbar, these oscillating forces might become relevant on the $\sim$0.2 kbar pressure scale that is the norm for topographic measurements in tapping or contact mode, and could possibly explain the regular, solid-like layered features reported in ref. 17.

Our results for the normal force F_z differ from those reported in ref. 16. However, the systems considered in these experiments and in our simulation differ for the choice of the ionic liquid, and for the conditions of the measurements. Our simulations concern the indentation of a thin [bmim][Tf_2N] layer on silica, while the measurements reported ref. 16 have been carried out with the tip immersed into a bulk-like ionic liquid layer. The crucial difference between these two situations is confirmed by new AFM measurements,[18] whose results most relevant for our study are being anticipated in Fig. 8.

Needless to say, quantitative differences remain between simulation and experimental results. Both experiments and simulations are likely to be responsible for the discrepancy. For instance, the elasticity of the silica surface, neglected in our simulation, is likely to affect the force measured on the tip. Differences in the response could also be due to a different quality and purity of the silica surface, including its hydroxylation coverage. Unfortunately, these parameters are difficult to control in experiment, and to include in simulation models. The technique to prepare and distribute droplets, relying on dissolving [bmim][Tf_2N] in methanol, and then letting the solvent to evaporate, might also play a role.

In conclusion, we have shown that simulations can provide a nearly quantitative description of the indentation of RTILs in contact with an insulating oxide surface, despite major technical limitations that still affect the computational approach.[30] The resolution, time and length scales of the present simulations are not sufficient to reproduce and explain the solid-like features seen in the topography of thin [bmim][Tf_2N] films on oxide surfaces, but the gap between simulations and experiments is not very wide, and could be reduced with only incremental changes of the simulation capability.

The observation of solid-like features in RTIL films on solid surfaces is, at the same time, conceptually intriguing and potentially very relevant for applications. Hints of similar phenomena in thin RTIL films have been reported a few times without a clearcut explanation. Further evidence on these effects and phenomena has been provided by measurements carried out on RTILs confined to carbon[31] and silica[32] matrices, whose porosity amplifies the role of RTIL/solid interfaces. Layering and slow relaxation times might cause the solid-like properties of iono-gels made of oxide nanoparticles dissolved into RTILs.[15] Clarification of their stability and properties could greatly help their usage in electrochemistry and photovoltaic applications.

Acknowledgements

The CIMaINa group has been financially supported by Fondazione Cariplo under the grant "Materiali e tecnologie abilitanti 2007". The collaboration has been made possible by an International Joint Project Grant of the Royal Society.

References

1 T. Welton, *Chem. Rev*., 1999, **99**, 2071.
2 S. G. Cull, J. D. Holbrey, V. Vargas-Mora, K. R. Seddon and G. J. Lye, *Biotechnol. Bioeng*., 2000, **69**, 227.
3 V. I. Parvulescu and C. Hardacre, *Chem. Rev*., 2007, **107**, 2615.
4 C. Ye, W. Lui, Y. Chen and L. Yu, *Chem. Commun*., 2001, 2244.
5 J. J. Nainaparampil, K. C. Eapen, J. H. Sanders and A. A. Voevodin, *J. Microelectromech. Syst*., 2007, **16**, 836.
6 S. Z. El Abedinand and F. Endres, *Acc. Chem. Res*., 2007, **40**, 1106; F. Endres, *ChemPhysChem*, 2002, **3**, 144; S. Z. El Abedinand, E. Mustafa, R. Hempelmann, H. Natter and F. Endres, *ChemPhysChem*, 2006, **7**, 1535.
7 M. Gratzel, *Nature*, 2001, **414**, 338.
8 J. B. Rollins, B. D. Fitchett and J. C. Conboy, *J. Phys. Chem. B*, 2007, **111**, 4990; C. R. Romero and S. Baldelli, *J. Phys. Chem. B*, 2006, **110**, 6213.
9 (*a*) E. Sloutskin, B. M. Ocko, L. Tamam, I. Kuzmenko, T. Gog and M. Deutsch, *J. Am. Chem. Soc*., 2005, **127**, 7796; (*b*) A. J. Carmichael, C. Hardacre, J. D. Holbrey, M. Nieuwenhuyzen and K. R. Seddon, *Mol. Phys*., 2001, **99**, 795.
10 J. Bowers, M. C. Vergara-Gutierrez and J. R. P. Webster, *Langmuir*, 2004, **20**, 309.
11 S. Perkin, L. Crowhurst, H. Niedermeyer, T. Welton, A. M. Smith and N. N. Gosvami, *Chem. Commun*., 2011, **47**, 6572.
12 S. Perkin, T. Albrecht and J. Klein, *Phys. Chem. Chem. Phys*., 2010, **12**, 1243.
13 K. Ueno, M. Kasuya, M. Watanabe, M. Mizukami and K. Kurihara, *Phys. Chem. Chem. Phys*., 2010, **12**, 4066.
14 J. J. Nainaparampil, B. S. Phillips, K. C. Eapen and J. S. Zabinsli, *Nanotechnology*, 2005, **16**, 2474.
15 P. Wang, S. M. Zakeeruddin, P. Compte, I. Exnar and M. Grätzel, *J. Am. Chem. Soc*., 2003, **125**, 1166; K. Ueno, S. Imaizumi, K. Hata and M. Watanabe, *Langmuir*, 2009, **25**, 825.
16 (*a*) R. Hayes, G. G. Warr and R. Atkin, *Phys. Chem. Chem. Phys*., 2010, **12**, 1709; (*b*) R. Atkin and G. G. Warr, *J. Phys. Chem. C*, 2007, **111**, 5162; (*c*) D. Wakeham, R. Hayes, G. G. Warr and R. Atkin, *J. Phys. Chem. B*, 2009, **113**, 5961.
17 S. Bovio, A. Podestà, C. Lenardi and P. Milani, *J. Phys. Chem. B*, 2009, **113**, 6600.
18 S. Bovio, A. Podestà and P. Milani, unpublished.
19 Y.-D. Liu, Y. Zhang, G.-Z. Wu and J. Hu, *J. Am. Chem. Soc*., 2006, **128**, 7456.
20 N. Seifert and G. Wipff, *J. Phys. Chem. C*, 2008, **112**, 19590.
21 S. Bovio, A. Podestà, P. Milani, P. Ballone and M. G. Del Pópolo, *J. Phys.: Condens. Matter*, 2009, **21**, 424118.
22 L. D. Gelb and R. M. Lynden-Bell, *Chem. Phys. Lett*., 1993, **211**, 328; L. D. Gelb and R. M. Lynden-Bell, *Phys. Rev. B: Condens. Matter*, 1994, **49**, 2058; D. L. Patrick and R. M. Lynden-Bell, *Surf. Sci*., 1997, **380**, 224.
23 J. N. Canongia Lopes, J. Deschamps and A. A. H. Padua, *J. Phys. Chem. B*, 2004, **108**, 2038; J. N. Canongia Lopes and A. A. H. Padua, *J. Phys. Chem. B*, 2004, **108**, 16893. see also (additions and corrections): J. N. Canongia Lopes, J. Deschamps and A. A. H. Padua, *J. Phys. Chem. B*, 2004, **108**, 11250.
24 P. R. ten Wolde and D. Frenkel, *Science*, 1997, **277**, 1975; M. H. J. Hagen and D. Frenkel, *J. Chem. Phys*., 1994, **101**, 4093.
25 W. Smith, M. Leslie and T. R. Forester, *DL-POLY v.2.14*, Daresbury Laboratories, Daresbury, Warrington, WA4 4AD, UK, 2003.
26 J. N. A. Canongia Lopes and A. A. H. Padua, *J. Phys. Chem. B*, 2006, **110**, 3330; A. Triolo, O. Russina, H.-J. Bleif and E. Di Cola, *J. Phys. Chem. B*, 2007, **111**, 4641; N. Manini, M. Cesaratto, M. G. Del Pópolo and P. Ballone, *J. Phys. Chem. B*, 2009, **113**, 15602.
27 Daniele Dragoni, *Master Thesis*, University of Milano, 2011. Available on-line at www.mi.infm.it/manini/theses/dragoni.pdf.
28 The same conclusion is supported by the simulation of a tip approaching the [bmim][Tf_2N]/mica interface, see ref. 27.
29 M.-L. Sha, G.-Z. Wu, Q. Dou, Z.-F. Tang and H.-P. Fang, *Langmuir*, 2010, **26**, 12667.
30 J. Tamayo and R. Garcia, *Langmuir*, 1996, **12**, 4430; R. Garcia and R. Perez, *Surf. Sci. Rep*., 2002, **47**, 197.
31 J. Monk, R. Singh and F. R. Hung, *J. Phys. Chem. C*, 2011, **115**, 3034.
32 B. Coasne, L. Viau and A. Vioux, *J. Phys. Chem. Lett*., 2011, **2**, 1150.

Appendix C

List of publications and congresses

Publications/in press papers

S. Bovio, , A. Podestà, C. Lenardi, P. Milani, *Evidence of extended solid–like layering in [Bmim][NTf2] ionic liquid thin films at room–temperature* J. Phys. Chem. B, 113 (19), pp 66006603 (2009).

S. Bovio, A. Podestà, P. Milani, *Investigation of interfacial properties of supported [Bmim][NTf2] thin films by atomic force microscopy* Vol. 1030, Chapter 19, Pages 273-290, N.V. Plechkova, R.D. Rogers, K.R. Seddon Editors; Ionic Liquids: From Knowledge to Application, ACS Symposium Series , (2009).

S. Bovio, A. Podestà, P. Milani, P. Ballone, M. G. Del Pópolo, *Nanometric ionic–liquid films on silica: a joint experimental and computational study* J. Phys.: Condens. Matter 21, 424118 (2009).

G. Bongiorno, C. Semprebon, A. Podestà, P. Scopelliti, S. Bovio, et al. *Cluster–assembled nanostructured titanium oxide films with tailored wettability* J. Phys. Chem. C 113, 18264 (2009).

P. Ballone, M. G. Del Pópolo, S. Bovio, A. Podestà, P. Milani, N. Manini, *Nano-indentation of a room–temperature ionic liquid film on silica: a computational experiment*, Phys. Chem. Chem. Phys., (DOI: 10.1039/C2CP23459A), (2012).

A. V. Singh, A. Rahman, N.V.G. Sudhir Kumar, A.S. Aditi, M. Galluzzi, S. Bovio, S. Barozzi, E. Montani, D. Parazzoli, *Bio–inspired approaches to design smart fabrics*, Materials & Design, In press, corrected proof (doi:10.1016-/j.matdes-.2011.-01.061), (2011).

S. Bovio et al., *Investigation of nano–mechanical properties of thin [Bmim]-[Tf_2N] films by atomic force microscopy*, in preparation.

M. Galluzzi et al., *Study of the electrical properties of thin [Bmim][Tf_2N] films by scanning probe microscopies*, in preparation.

Contributions at international congresses

1^{st} Winter Meeting on Functional SPM in Bio and Chemical Physics, CNR-INFM S3, Modena, 2009-12-10; *Production and characterization of epoxy-free colloidal probes for SPM studies*, Simone Bovio and M. Indrieri, A. Podestà, G. Bongiorno, D. Marchesi, P. Milani

XII International Symposium on Polymer Electrolytes, Padova, 2010-08-29; *Investigation of interfacial properties of supported [Bmim][NTf2] ionic liquid layers by Scanning Probe Microscopy*, Simone Bovio and A. Podestà, M. Galluzzi, C. Lenardi, G. Losacco, M. Del Pópolo, P. Ballone, P. Milani

Ionic Liquids: Faraday Discussion 154, Belfast 2011-08-22; *Investigation of morphological and mechanical properties of [bmim][Tf2N] thin layers on solid surfaces by Scanning Probe Microscopy*, S. Bovio, M. Galluzzi, A. Podestà, C. Lenardi, P. Milani

Ionic Liquids: Faraday Discussion 154, Belfast 2011-08-22; *Characterization of electrical properties of thin films of [bmim][Tf2N] using Atomic Force Microscopy*, M.Galluzzi, A. Podestà, S. Bovio

Acknowledgements

Prima di tutto vorrei ringraziare Alessandro Podestà per questi 4 anni (tesi + PhD). Grazie al suo sostegno, sia in campo scientifico e professionale che umano, che mi ha permesso di portare avanti la mia ricerca. Un sentito grazie va anche a Paolo Milani, il boss, che ha avuto il coraggio di darmi fiducia quando mi ha preso presso il suo laboratorio per la laurea magistrale, e ha continuato a darmene anche durante questi 3 lunghi (ma anche brevi) anni di dottorato. Vorrei ringraziare anche Pietro Ballone, della Queen's University di Belfast, per la sua disponibilità e per le sue immense conoscenze scientifiche, che mi hanno notevolmente aiutato durante i miei anni di studi sui liquidi ionici; lo vorrei ringraziare anche per i periodi vissuti a Belfast in cui, oltre ad ampliare le mie conoscenze fisiche, ho avuto l'opportunnit di conoscere una bella città e soprattutto tante belle persone. Oltre a Pietro ringrazio anche Mario Del Pópolo (QUEEN'S) e Nicola Manini (UNIMI), per le interessanti discussioni e le loro consulenze sui liquidi ionici. Ringrazio anche Franco Camera, che mi ha dato l'opportunità di fare la bella esperienza di assistente in laboratorio studenti.

Un doveroso grazie va anche a Davide Marchesi e Gero Bongiorno, Fondazione Filarete, per le misure SEM che mi hanno consentito di acquisire le splendide immagini riportate nella tesi e molte altre ancora; li vorrei ringraziare molto sia per la loro competenza che per la loro impagabile simpatia! Un grazie anche a Cristina Lenardi, Matteo Amati e Gabriele Losacco per le misure XPS eseguite presso il nostro laboratorio, e a Michele Perego per quelle eseguite presso il laboratorio MDM.

Vorrei anche ringraziare tutti i colleghi, passati e presenti, del laboratorio LGM, a cominciare da Marco che mi ha sempre dato una mano, soprattutto con Matlab, ed è sempre stato un buon amico (anche se ha bidonato il bungee jumping!); e poi Massimiliano, per il suo costante buon umore e le sue battute, e per aver condiviso con me gioie e dolori della ricerca sui liquidi ionici; ancora Valeria e Varun, due ex del box AFM con cui ho vissuto i miei primi anni da afmista, e Francesca, l'ultima arrivata nel gruppo SPM. Un sentitissimo grazie va anche a Michele, perché quando ne ho avuto bisogno mi ha sempre dato tutto il supporto informatico necessario, anche all'ultimo secondo. Vorrei ringraziare anche Roberto, per la sua irruenza e il suo stile di vita, anche se averlo come compagno d'ufficio è stata dura! A proposito di compagni d'ufficio, come non ringraziare Claudio, con cui abbiamo fatto delle gran belle risate! Un grazie anche a tutte le segretarie del CIMaINa, in particolare a Barbara e a Giulia.

Oltre ai compagni di ventura, un doveroso grazie va ai miei genitori, che con i loro sacrifici mi hanno consentito di studiare ed arrivare fino ad un dottorato di ricerca, e a mio fratello Franco, che mi ha convinto a buttarmi nel campo della fisica! Vorrei dire grazie anche a tutta la mia numerosa famiglia, anche se a volte qualcuno fa confusione tra un fisico ed un ingegnere! Dopo la famiglia non posso non ringraziare anche tutti gli amici della mia compagnia di Bellinzago, per tutti gli anni che abbiamo passato assieme e per tutte le feste che abbiamo fatto e che ancora faremo! Soprattutto grazie a Sola, per la sua vicinanza e per le sue birre di prima qualità! Grazie anche a Daria, preziosa compagna delle lunghe ore passate in treno! Grazie anche ad Alessandra, per essere un'ottima amica e per la sua faccia di bronzo clamorosa. Infine, vorrei ringraziare Olivia per la sua preziosissima amicizia e perché, pur vivendo lontani fisicamente, si è sempre adoperata in modo che non ci allontanassimo con lo spirito: grazie!